U.S. Nuclear Regulatory Commission

Research Information Letter 12-01

Confirmatory Analysis of Seismic Hazard at the Diablo Canyon Power Plant from the Shoreline Fault Zone

September 2012

Table of Contents

Figures

Tables

Executive Summary

On November 14, 2008, the Pacific Gas & Electric (PG&E) Company informed the U.S. Nuclear Regulatory Commission (NRC) that it had identified a zone of seismicity that may indicate a previously unknown fault located offshore of the Diablo Canyon Power Plant (DCPP). The potential fault was identified as a result of a collaborative research program between PG&E and the U.S. Geological Survey (USGS).

Shortly after PG&E notified the NRC of the potential for a new fault, it provided the agency with sets of initial scientific data and information related to the hypothesized fault, which PG&E subsequently named the "Shoreline fault." In discussions with the NRC staff, PG&E described the results from its preliminary assessment that indicated that the hazard potential of the Shoreline fault is bounded by the current review ground motion spectrum for the facility, indicating that the plant has been designed to safely withstand the effects from ground motions or shaking levels larger than the Shoreline fault is capable of producing.

Based on the initial information PG&E provided, the NRC staff immediately performed a preliminary review of possible implications of the Shoreline fault to the DCPP to determine if an immediate safety concern existed. The staff subsequently issued Research Information Letter (RIL) 09-001 entitled, "Preliminary Deterministic Analysis of Seismic Hazard at Diablo Canyon Nuclear Power Plant from Newly Identified 'Shoreline Fault'" (NRC, 2009). RIL 09-001 described the staff's preliminary review, including assessment of the data available at that time, the parameters used, and the basis for the staff's initial conclusions. Although RIL 09-001 discussed all relevant aspects to the extent possible, the work was based on the limited preliminary information available at the time. Over the next 2 years, the NRC continued to review information as the USGS and PG&E obtained new data emerging from their collaborative work.

In January 2011, PG&E submitted to the NRC, "Report on the Analysis of the Shoreline Fault Zone, Central Coastal California: Report to the U.S. Nuclear Regulatory Commission." This report (hereafter called the "Shoreline Fault Report") provides new geological, geophysical, and seismological data to assess the potential seismic hazard of the Shoreline fault. This new information supplements or improves the geological, geophysical, and seismological information near the DCPP site documented in the PG&E Long-Term Seismic Program (LTSP). The Shoreline Fault Report provides sufficient data on the Shoreline fault to allow the NRC to perform a confirmatory analysis.

In reviewing the complete set of seismological, geological, and geophysical data, the NRC staff worked with independent experts from the Center for Nuclear Waste Regulatory Analyses in the fields of paleoseismology, tectonics, and structural geology to assess the quality and reliability of the data, to address the broader questions related to the regional tectonics, and to develop the five principal scenarios used in the analyses. The NRC staff and its team of experts also visited the site in October 2011 to view firsthand the geologic and tectonic features. The assessment of the interpretations of the Shoreline fault, the deterministic analyses, the site response analyses, and the review of the risk from secondary faulting were performed by NRC staff.

Based on a review of the Shoreline Fault Report, insights gained from the site visit, and the report to the NRC provided by the independent experts, the NRC staff developed an assessment of the seismic source characteristics of the Shoreline fault and performed a deterministic seismic hazard assessment (DSHA). In this review of the hazard from the Shoreline fault, the NRC compared the resulting deterministic seismic ground motions to loading levels for which the plant has been previously reviewed, specifically the Hosgri Earthquake (HE) ground motion response spectrum as described in NUREG-0675, "Safety Evaluation Report Related to the Operation of Diablo Canyon Power Plant, Units 1 and 2," Supplement No. 7 (NRC, 1978), and the LTSP ground motion response spectrum as detailed in NUREG-0675, Supplement No. 34 (NRC, 1991). The results indicate that deterministic seismic-loading levels predicted for all the Shoreline fault earthquake scenarios developed and analyzed by the NRC are at, or below, those levels for the HE ground motion and the LTSP ground motion. The HE ground motion and the LTSP ground motion are those for which the plant was evaluated previously and demonstrated to have reasonable assurance of safety.

This RIL presents results from a conservative deterministic (scenario-based) viewpoint and is intended to allow the NRC staff to determine if a safety concern exists as a result of the identification of the Shoreline fault. By their nature, deterministic approaches do not explicitly account for the likelihood of a particular earthquake scenario occurring, or the rate at which earthquakes can occur on known seismic sources. Therefore, deterministic results cannot be used for a quantitative assessment of the overall risk to the plant from the Shoreline fault. Instead, deterministic approaches focus only on the safety margin that exists for a specific earthquake scenario, in this case for the Shoreline fault. Current NRC guidance uses a probabilistic seismic hazard assessment (PSHA) approach, as described in Regulatory Guide (RG) 1.208, "A Performance-Based Approach to Define the Site-Specific Earthquake Ground Motion" (NRC, 2007); NUREG/CR-6372, "Recommendations for Probabilistic Seismic Hazard Analysis: Guidance on Uncertainty and Use of Experts" (NRC, 1997); and NUREG-2117, "Practical Implementation Guidelines for SSHAC Level 3 and 4 Hazard Studies" (NRC, 2012). A detailed PSHA is currently being undertaken at DCPP, the results of which will strengthen the understanding of the relative importance of the Shoreline fault to the seismic hazard at this site.

The following are the principal findings from the NRC review of the Shoreline Fault Report:

1. The Shoreline fault was discovered from relocated microearthquakes in 2008. Further data collection confirmed the existence of the Shoreline fault as a potential seismic source.
2. The geologic and geophysical information, including geologic mapping and the earthquake database, can be used to develop reasonable interpretations of fault geometry, activity, maximum magnitude, and proximity of earthquakes to the DCPP.
3. Geologic evidence for recent surface fault displacement along the Shoreline fault is not evident in the newly acquired data.
4. The NRC's conservative estimates for the potential ground motions from the Shoreline fault are at or below the ground motions for which the DCPP has been evaluated previously and demonstrated to have reasonable assurance of safety (i.e., the HE and LTSP ground motion response spectra). This analysis confirms the earlier conclusions of RIL 09-001.

5. The NRC also analyzed the risk to the DCPP from secondary surface fault rupture associated with the Shoreline fault and found no evidence of significant secondary surface faulting.
6. The Shoreline fault has a low slip rate that is estimated to be an order of magnitude less than the Hosgri fault, which implies that its overall contribution to the hazard is relatively limited. An understanding of the relative importance of the Shoreline fault to the hazard at DCPP is best demonstrated from a PSHA, which considers the likelihood of earthquake activity from all the seismic sources.
7. Evaluation of the current dataset indicates that it is sufficient to move forward with the new Senior Seismic Hazard Analysis Committee (SSHAC) Level 3 PSHA.

Acknowledgements

This report was developed by NRC staff with the assistance of a team of consultants from the Center for Nuclear Waste Regulatory Analyses, Southwest Research Institute. Annie Kammerer led the NRC team and John Stamatakos led the Southwest Research Institute team. Annie Kammerer was the Project Technical Lead.

The Shoreline Fault Report Review Team consisted of the following people:

- Annie Kammerer, Rasool Anooshehpoor, and Scott Stovall (NRC)
- John Stamatakos (Center for Nuclear Waste Regulatory Analyses, Southwest Research Institute)
- James McCalpin (GEO-HAZ Consulting, Consultant to Center for Nuclear Waste Regulatory Analyses, Southwest Research Institute)
- Larry Anderson (Consulting Geologist to Center for Nuclear Waste Regulatory Analyses, Southwest Research Institute)

The RIL also benefitted from the NRC internal peer review performed by Tianqing Cao, Cliff Munson, Andrew Murphy, Vladimir Graizer, Kamal Manoly and Jon Ake.

Acronyms and Parameters

A	rupture area
ACRS	Advisory Committee on Reactor Safeguards
ADAMS	Agencywide Documents Access and Management System
ASLB	Atomic Safety and Licensing Board
ca.	approximately (circa)
CBR	center, body, and range
CCSN	Central California Seismic Network
CDF	core damage frequency
CFR	Code of Federal Regulations
cm	centimeter
CRADA	Cooperative Research and Development Agreement
1D	one dimensional
2D	two dimensional
3D	three dimensional
DE	Design Earthquake (ground motion)
DDE	Double Design Earthquake (ground motion)
DCPP	Diablo Canyon Power Plant
DEM	digital elevation model
DSHA	deterministic seismic hazard assessment
ε	number of standard deviations from the logarithmic mean
f	frequency
FSAR	final safety analysis report
g	acceleration of gravity
GIS	global information system
GMPE	ground motion prediction equation (also known as an attenuation relationship)
GMC	ground motion characterization
HE	Hosgri Earthquake (ground motion)
HID	hazard input document
hypoDD	double-difference hypocenter
Hz	hertz
ISFSI	independent spent fuel storage installation

κ_o	high-frequency, hard-rock ground motion attenuation parameter
ka	kilo-annum (thousand years ago)
kHz	kilohertz
km	kilometer
λ	annual rate at which the target PGA value is exceeded
LiDAR	Light Detection and Ranging
LTSP	Long-Term Seismic Program
μ	rigidity of the crust (usually taken as 3.3×10^{10} N.m^{-2})
μ	median expected value
M	magnitude
MBES	multibeam echo sounding
M_i	magnitude of interest in a magnitude recurrence curve
MIS	marine isotopic stage (or marine oxygen-isotopic stage)
M_{max}	largest earthquake that is considered possible within a particular seismic source (also shown as m_{max})
M_{min}	lower limit of magnitude (generally considered to reflect the smallest earthquake considered of engineering significance)
M_o	seismic moment
M_w	moment magnitude
M_s	surface-wave magnitude
n	number of earthquakes in a Gutenberg-Richter relationship
υ_i	annual rate of earthquakes of M_i and greater in a seismic source
$\upsilon_{m_{min}}$	annual rate of earthquakes of magnitude m_{min} and greater
NCEDC	Northern California Earthquake Data Center
NGA	Next Generation Attenuation
NPP	nuclear power plant
NRC	U.S. Nuclear Regulatory Commission
NUREG	U.S. NRC Nuclear Regulation Report
NUREG/CR	U.S. NRC Nuclear Regulation Contractor's Report
OBE	Operating Basis Earthquake (ground motion)
PGA	peak ground acceleration
PG&E	Pacific Gas & Electric
PGV	peak ground velocity
PPRP	Participatory Peer Review Panel
PRA	probabilistic risk assessment

PSHA	probabilistic seismic hazard analysis (or assessment)
RG	regulatory guide
RIL	research information letter
r_{epi}	epicentral distance
r_{hyp}	hypocentral distance
r_{JB}	Joyner-Boore distance
r_{rup}	rupture distance
r_x	horizontal distance to the top edge of the rupture perpendicular to strike
σ	standard deviation
σ_σ	standard deviation of the standard deviation
σ_{ss}	single station uncertainty (sigma)
σ_μ	standard deviation of the median
S_a	spectral acceleration
SMA	seismic margins assessment
SPRA	seismic probabilistic risk assessment
SSC	seismic source characterization
SSE	Safe Shutdown Earthquake ground motion
SSER	supplemental safety evaluation report
SSHAC	Senior Seismic Hazard Analysis Committee
TDI	technically defensible interpretations
TI	technical integrator
t_{max}	duration of an earthquake recording
tomoDD	double-difference tomography
u	average slip on the fault plane
USGS	U.S. Geological Survey
USNRC	U.S. Nuclear Regulatory Commission
UTM	Universal Transverse Mercator
V_S	shear-wave velocity
V_{S30}	average shear-wave velocity over the uppermost 30 meters of a geologic column
Z_{TOR}	depth-to-top-of-rupture

1 Introduction

On November 14, 2008, the Pacific Gas & Electric (PG&E) Company informed the U.S. Nuclear Regulatory Commission (NRC) that it had identified a zone of seismicity that may indicate a previously unknown fault located offshore of the Diablo Canyon Power Plant (DCPP). Figure 1-1 shows the relative location of the fault and DCPP. The potential fault was identified as a result of a collaborative research program between PG&E and the U.S. Geological Survey (USGS). This research program (the PG&E-USGS Cooperative Research and Development Agreement (CRADA)) focuses on increasing understanding of the tectonic setting in the region around the DCPP. The current phase of this long-standing program includes both new geophysical and geological field studies and the application of advanced seismological techniques to small-magnitude recorded earthquakes.

Shortly after PG&E notified the NRC of the potential for a new fault, it provided the agency with sets of initial scientific data and information related to the hypothesized fault (Agencywide Documents Access and Management System (ADAMS) Accession Nos. ML090690193, ML090690218), which PG&E subsequently named the "Shoreline fault." In discussions with the NRC staff, PG&E described the results from its preliminary assessment that indicated that the hazard potential of the Shoreline fault is bounded by the current review ground motion spectrum for the facility, indicating that the plant has been designed to safely shut down following a ground motion or shaking level larger than the Shoreline fault is capable of producing.

Based on the initial information PG&E and the USGS provided, the NRC staff immediately performed a preliminary review of possible implications of the Shoreline fault to the DCPP to determine if an immediate safety concern existed. The staff subsequently issued Research Information Letter (RIL) 09-001 entitled, "Preliminary Deterministic Analysis of Seismic Hazard at Diablo Canyon Nuclear Power Plant from Newly Identified 'Shoreline Fault'" (NRC, 2009). RIL 09-001 described the staff's preliminary review, including assessment of the available data, the parameters used, and the basis for the staff's initial conclusions. Although RIL 09-001 discussed all relevant aspects to the extent possible, the work was based on the limited preliminary information available at the time. Over the next 2 years, the NRC continued to review information as the USGS and PG&E obtained new data emerging from the ongoing CRADA field work.

In January 2011, PG&E submitted to the NRC, "Report on the Analysis of the Shoreline Fault Zone, Central Coastal California: Report to the U.S. Nuclear Regulatory Commission" (ADAMS Accession No. ML110140431). This report (hereafter called the "Shoreline Fault Report") provides new geological, geophysical, and seismological data to assess the potential seismic hazard of the Shoreline fault. This new information supplements or improves the geological, geophysical, and seismological information near the DCPP site documented in the PG&E Long-Term Seismic Program (LTSP). The Shoreline Fault Report provides sufficient data on the Shoreline fault to allow the NRC to perform a confirmatory analysis.

In reviewing the complete set of seismological, geological, and geophysical data, the NRC staff worked with consultants from the Center for Nuclear Waste Regulatory Analyses in the fields of paleoseismology, tectonics, and structural geology to assess the quality and reliability of the data, to address the broader questions related to the regional tectonics, and to develop the five principal scenarios described in Section 4. The NRC staff and its team also visited the site in October 2011 to view firsthand the geologic and tectonic features. The assessment and weighting of interpretations of the Shoreline fault, the deterministic analyses, the site response

analyses, and the review of the risk from secondary faulting were performed by NRC staff. Contributors to this document are listed in the Acknowledgements Section.

Based on a review of the Shoreline Fault Report, insights gained from the site visit, and the report to the NRC provided by the consultants, the NRC staff developed an assessment of the seismic source characteristics of the Shoreline fault and performed a deterministic seismic hazard assessment (DSHA). In this review of the hazard from the Shoreline fault, the NRC compared the resulting deterministic seismic ground motions to loading levels for which the plant has been previously reviewed, specifically the Hosgri Earthquake (HE) ground motion response spectrum as described in NUREG-0675, "Safety Evaluation Report Related to the Operation of Diablo Canyon Power Plant, Units 1 and 2," Supplement No. 7 (NRC, 1978), and the LTSP ground motion response spectrum as detailed in NUREG-0675, Supplement No. 34 (NRC, 1991). The results indicate that the 84th-percentile deterministic seismic-loading levels predicted for all the Shoreline fault earthquake scenarios developed and analyzed by the NRC are at or below those levels for the HE ground motion and the LTSP ground motion. The HE ground motion and the LTSP ground motion are those for which the plant was evaluated previously and demonstrated to have reasonable assurance of safety.

This RIL presents results from a deterministic (scenario-based) viewpoint and is intended to allow the NRC staff to determine if a safety concern exists as a result of the identification of the Shoreline fault. However, current NRC guidance endorses a probabilistic seismic hazard assessment (PSHA) approach, as described in Regulatory Guide (RG) 1.208, "A Performance-Based Approach to Define the Site-Specific Earthquake Ground Motion" (NRC, 2007); NUREG/CR-6372, "Recommendations for Probabilistic Seismic Hazard Analysis: Guidance on Uncertainty and Use of Experts" (NRC, 1997); and NUREG-2117, "Practical Implementation Guidelines for SSHAC Level 3 and 4 Hazard Studies" (NRC, 2012).

Over the last year, PG&E initiated a new project to use the NRC's current regulatory guidance (RG 1.208) in the development of a new PSHA model that includes both a new seismic source characterization model and a new ground motion characterization model. This project is being conducted using the Level 3 process from the Senior Seismic Hazard Analysis Committee (SSHAC) guidance as detailed in NUREG/CR-6372 (NRC, 1997) and NUREG-2117 (NRC, 2012). This process is more commonly known as a "SSHAC Level 3" process and is laid out in practical terms in NUREG-2117. A summary of the SSHAC process is also provided in Appendix A of this document. PG&E initially stated that its objective for conducting the SSHAC Level 3 project was to apply a state-of-the-art process to the full set of newly acquired data to develop a new PSHA model consistent with NRC requirements for new reactors. However, on March 12, 2012, the NRC issued a letter to all operating reactor licensees entitled, "Request for Information Pursuant to Title 10 of the *Code of Federal Regulations* 50.54(f) Regarding Recommendations 2.1, 2.3, and 9.3 of the Near-Term Task Force Review of Insights from the Fukushima Dai-ichi Accident" (hereafter called the "10 CFR 50.54(f) Request for Information Letter," ADAMS Accession No. ML12056A046). The letter requested updated seismic hazard information to be submitted to the NRC. This updated information for DCPP would be developed through the site-specific SSHAC Level 3 study that PG&E has already initiated.

Section 2 of this RIL summarizes the history of DCPP licensing as it relates to seismic hazard. In Section 3 of this report, the NRC reviews the datasets and discusses PG&E's interpretation of the datasets. Section 4 provides the NRC's interpretation of the data in the Shoreline Fault Report. Section 5 and Appendix B discuss the parameters and results of the DSHA performed by the NRC staff. A discussion of the PSHA method is provided in Section 6 and Appendices A and D provide a summary of the SSHAC Level 3 process for PSHA studies and the use of constraints on PSHA inputs respectively. Section 7 provides a summary of a confirmatory analysis of the potential for risk from secondary rupture, which is discussed in detail in Appendix C. Section 8 is a summary of the key findings of the staff's review.

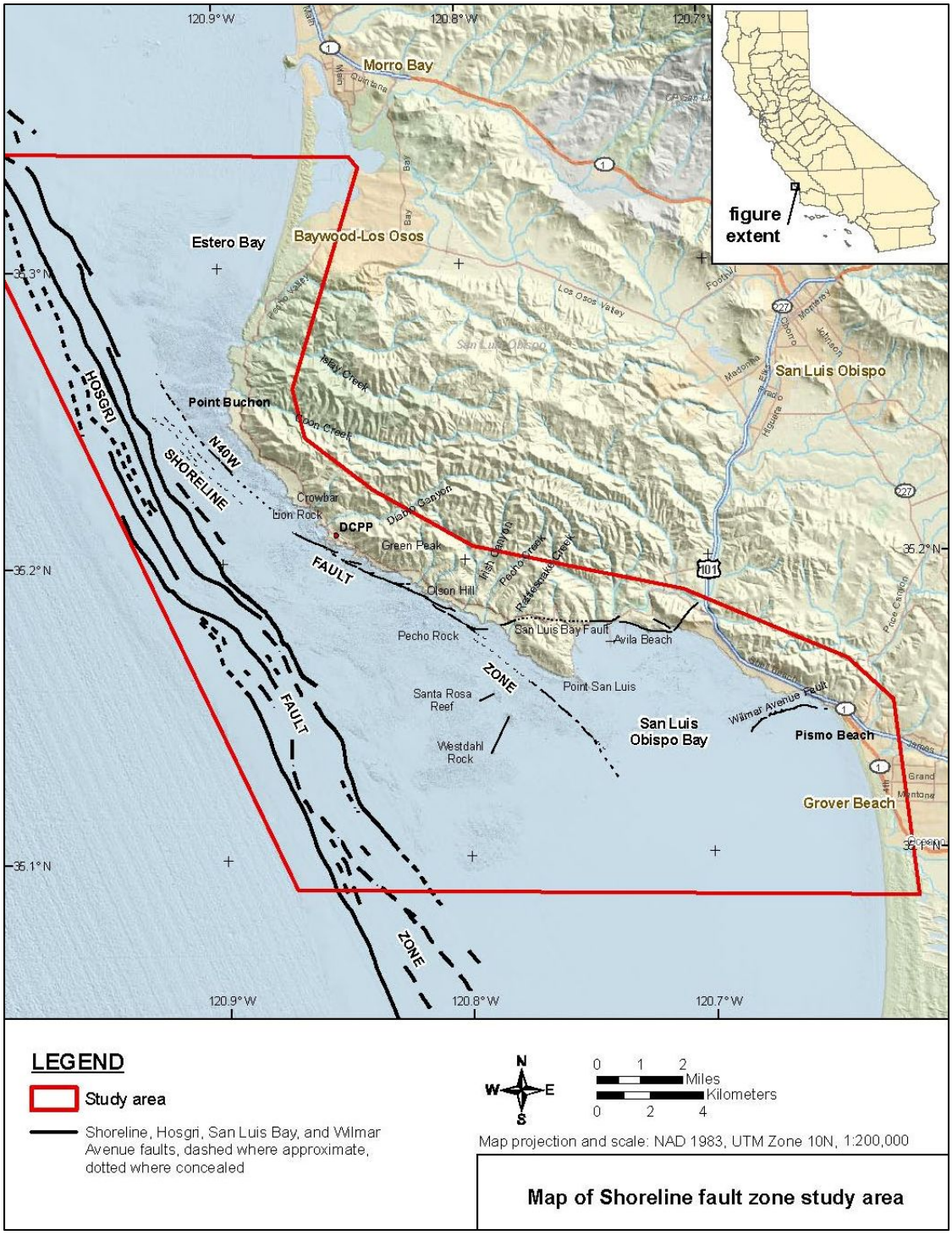

Figure 1-1 The location of DCPP and the Shoreline fault (Figure 1.1 from the PG&E Shoreline Fault Report).

2 Background (Historical Context and Recent Events)

The DCPP has unique and complex seismic design and licensing bases. A brief review of the history of the DCPP is provided to explain both the basis for the NRC assessment of the new fault and the context of the research program that identified the fault. The Atomic Energy Commission originally issued construction permits to PG&E for DCPP Units 1 and 2 in 1968 and 1970, respectively. These construction permits included a "Double Design Earthquake" (DDE) ground motion response spectrum with a horizontal peak ground acceleration (PGA) of 0.4g and a "Design Earthquake" (DE) ground motion response spectrum with a horizontal PGA of 0.2g. The DDE ground motion and the DE ground motion were similar to the regulatory ground motion levels that the NRC subsequently developed as the "Safe Shutdown Earthquake (SSE)" ground motion and the "Operating Basis Earthquake (OBE)" ground motion. Development of the DDE and DE for DCPP is described in Section 3.8.5.2, "Ground Response Spectra," in Supplement No. 7 to NUREG-0675 (NRC, 1978). Both the DE and the DDE ground motions were determined using a "scenario-based" DSHA. Later, as the plant was under construction and the operating license applications were under development (about 1971), proprietary oil company studies describing a significant and previously unknown seismic zone offshore near the DCPP were made public. PG&E included a brief discussion of this seismic zone in the Diablo Canyon final safety analysis report (FSAR) submitted in 1973. PG&E called the zone the East Boundary Fault Zone in the FSAR, but it is now known as the Hosgri Seismic Zone.

In the years following the FSAR submittal, PG&E investigated the Hosgri Seismic Zone in response to NRC requests for additional information. At the same time, the USGS performed an independent investigation of the fault zone for the NRC. Based on USGS recommendations and on requirements contained in Appendix A, "Seismic and Geologic Siting Criteria for Nuclear Power Plants," to 10 *CFR* Part 100, "Reactor Site Criteria" (which was newly issued at that time), the NRC required a significant increase in the ground motion used for the seismic design basis of the plant to what is now known as the Hosgri Earthquake (HE) ground motion. The HE ground motion has a horizontal PGA of 0.75g, consistent with the scenario of a M7.5 earthquake on the Hosgri Fault, which is located 5 kilometers (km) (3 miles) from the DCPP. PG&E performed a reevaluation, including reanalysis of designated safety-related structures, systems, and components in a safe-shutdown path, and using the higher HE ground motion, reanalyzed and upgraded the plant design to accommodate the new seismic design basis. Necessary hardware upgrades were implemented where components exceeded their acceptance limits. As a result, DCPP is currently the only U.S. nuclear power plant (NPP) with three ground motion levels incorporated into its license. These are the DE, DDE, and HE ground motions levels (quantitatively described as response spectra), as shown in Figure 2-1. Each ground motion level has a different set of analysis assumptions (e.g., damping values) and different performance criteria. This is discussed in NUREG-0675, Supplement No. 7 (NRC, 1978).

In addition to defining the new HE ground motion and the associated reevaluation and retrofit required before licensing, the Diablo Canyon Unit 1 full-power license DPR-80 also has a license condition (2.C.(7)) that required a future reevaluation of the seismic design basis of the plant. This was included in response to the Advisory Committee on Reactor Safeguards (ACRS) recommendation that "…the seismic design of Diablo Canyon be re-evaluated in about 10 years taking into account applicable new information." To meet this requirement, PG&E developed the LTSP.

The license condition reads as follows:

> 2.C.(7) Seismic Design Bases Reevaluation Program (SSER 27 Section IV.5)
>
> PG&E shall develop and implement a program to reevaluate the seismic design bases used for the Diablo Canyon Nuclear Power Plant.
>
> The program shall include the following Elements:
>
> (1) PG&E shall identify, examine, and evaluate all relevant geologic and seismic data, information, and interpretations that have become available since the 1979 Atomic Safety and Licensing Board (ASLB) hearing in order to update the geology, seismology and tectonics in the region of the Diablo Canyon Nuclear Power Plant. If needed to define the earthquake potential of the region as it affects the Diablo Canyon Plant, PG&E will also reevaluate the earlier information and acquire additional new data.
>
> (2) PG&E shall reevaluate the magnitude of the earthquake used to determine the seismic basis of the Diablo Canyon Nuclear Plant using the information from Element 1.
>
> (3) PG&E shall reevaluate the ground motion at the site based on the results obtained from Element 2 with full consideration of site and other relevant effects.
>
> (4) PG&E shall assess the significance of conclusions drawn from the seismic reevaluation studies in Elements 1, 2 and 3, utilizing a probabilistic risk analysis and deterministic studies, as necessary, to assure adequacy of seismic margins.
>
> PG&E shall submit for NRC staff review and approval a proposed program plan and proposed schedule for implementation by January 30, 1985. The program shall be completed and a final report submitted to the NRC three years following the approval of the program by the NRC staff.
>
> PG&E shall keep the staff informed on the progress of the reevaluation program as necessary, but as a minimum will submit quarterly progress reports and arrange for semi-annual meetings with the staff. PG&E will also keep the ACRS informed on the progress of the reevaluation program as necessary, but not less frequently than once a year.

To meet this condition, as part of the LTSP, PG&E performed a full seismic reevaluation of the DCPP between 1985 and 1988. Both a seismic margins assessment (SMA) and a seismic probabilistic risk assessment (SPRA) were performed as detailed in the "Final Report of the Diablo Canyon Long-Term Seismic Program" (PG&E, 1988) and as summarized in the Seismic Safety Evaluation Report, NUREG-0675, Supplement No. 34 (NRC, 1991). During that reevaluation, PG&E determined that the Hosgri fault was still the fault capable of producing the largest ground motion at DCPP and therefore it remained the fault with the highest deterministic hazard (i.e., the "controlling fault"). However, the NRC staff came to believe that the faulting may have a larger component of reverse-slip than previously accounted for, leading to higher review shaking levels over some ground motion frequencies. As a result of NRC staff comments, PG&E increased the review spectrum over part of the frequency range and undertook a reevaluation of the plant with this new LTSP spectrum. The LTSP response spectrum has been used as a review spectrum for the plant and is used as a point of

comparison in this study, along with the HE response spectrum. Figure 2-1 shows each of the DCPP seismic response spectra.

Because the science and tools available to study the seismic zone continue to evolve over time, PG&E committed, in letters dated April 17, 1991, and May 29, 1991 (PG&E, 1991a and 1991b), to continue to study seismic issues and to perform periodic seismic reviews of the DCPP. This commitment to ongoing research and review led to the development of the CRADA program, which identified the Shoreline fault.

Although the CRADA is a long-term program that has been in place since 1997, the USGS identified the lineament called the Shoreline fault during a new phase of the CRADA that was recently implemented. The NRC staff and members of the broader seismic community are aware of the work being undertaken through the CRADA program and will continue to monitor any results as they become available. This work performed through the CRADA, which has typically been published by the USGS, has increased understanding of the tectonics in the region around the DCPP and includes both a large set of new field studies and the application of new advanced seismological techniques to a catalog of small-magnitude recorded earthquakes. The data produced as a result of the CRADA will be used in the SSHAC Level 3 PSHA study currently ongoing and will, in turn, be used to address the 10 CFR 50.54(f) Request for Information Letter (see Section 1).

The USGS has undertaken both field studies and analyses of each of the data sets as information was obtained. The “Action Plan for the Study of the Shoreline Fault” (ADAMS Accession No. ML090720505) describes the field work that was focused specifically on characterization of the Shoreline fault. The CRADA program has now moved back to a broader regional characterization focus. A description of the currently available datasets is provided in the following Section.

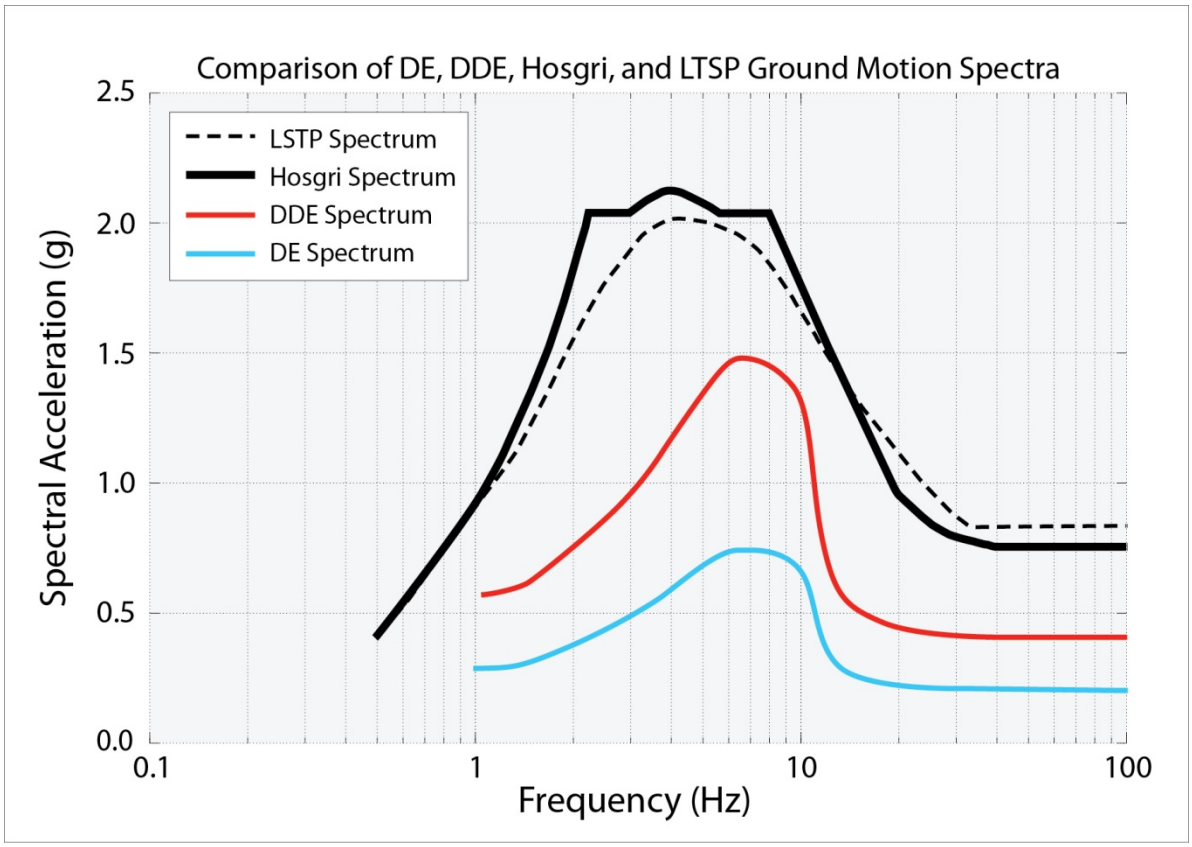

Figure 2-1 Ground motion response spectra for the DCPP.

3 Available Data and Information for Hazard Assessment

3.1 Data and Information Overview

In the Shoreline Fault Report, PG&E provided new geological, geophysical, and seismological data to assess the potential seismic hazard from the Shoreline fault. This new information supplements or improves the data and information documented in the PG&E LTSP. The data set currently developed for the region around the DCPP as part of the USGS/PG&E CRADA is of significantly higher quality than the data available at the time of the earlier LTSP study (PG&E, 1988), although that LTSP dataset was state-of-the-art at its time. The new data include observations from both terrestrial and marine studies, including two aeromagnetic surveys—one acquired by fixed-wing airplane and another by helicopter—and highly detailed bathymetric data. PG&E used these new data, interpretations, and analyses with existing information in the LTSP to support its characterization of the Shoreline fault as a potential seismic source that could produce strong ground shaking at the DCPP. This new information is also being used to evaluate the Shoreline fault hazard within the existing licensing basis ground motion for the plant. The NRC also reviewed each of the datasets provided, and they are discussed below.

The NRC reviews provided in Section 3 (data) and Section 4 (interpretations) are focused on the datasets, analysis, and interpretations important to describing the characteristics of the Shoreline fault as a possible seismic source. These are (1) the potential that the fault is capable of producing significant ground motions at the plant, (2) the style of faulting: reverse, thrust, or strike-slip (see Figure 3-1), (3) fault geometry defined by the fault's trace length, down-dip width, and orientation, and (4) the maximum magnitude earthquake that slip on the fault could produce based on this geometry.

3.2 Geologic Setting

As described in the Shoreline Fault Report, the DCPP is located on the southwestern edge of the Irish Hills, the northwestern-most portion of the San Luis Range. The Shoreline fault, as mapped by PG&E in the Shoreline Fault Report, is an approximately 16-23 km-long fault that bounds most of the western margin of the Irish Hills. At its closest approach, the fault is located approximately 600 meters from the plant (Figure 3-2). The San Luis Range is one of many northwest to north-northwest trending ranges that make up the central Coast Ranges of California. According to PG&E (1988, 1991, and 2011) and Lettis et al. (2004), "this region of California is characterized by transpressional deformation[1] between the San Andreas fault zone to the east and the San Gregorio-San Simeon-Hosgri system of near-coastal faults to the west." As shown in Figure 3-3, the transpressional deformation is responsible for the series of uplifted blocks and subsiding basins that make up what is termed the "Los Osos domain." The San Luis Range and the Irish Hills are one uplifted portion or structural block (termed the San Luis-Pismo block) within the Los Osos domain that is characterized by block bounding northwest-striking reverse, oblique, and strike-slip faults. The San Luis-Pismo block is bounded on the north by Moro Bay and the Los Osos Valley and on the south by the Santa Maria basin. Figure 3-4

[1] Transpressional deformation occurs when a region experiences both compression and shear forces.

shows focal mechanisms and recorded seismicity for the DCPP region. The rocks exposed in the vicinity of DCPP range from the Jurassic Franciscan complex to the Pliocene Pismo Formation (Plate 1 of the PG&E Shoreline Fault Report). The structure of the Irish Hills is a syncline, with older rocks of the Franciscan complex and Cretaceous sedimentary rocks forming the exposed limbs of the syncline and younger late Tertiary rocks of the Obispo, Monterey, and Pismo formation forming the core.

Structurally, the San Luis-Pismo block is bounded on the west by the strike-slip Hosgri fault zone, on the northeast by the reverse-oblique slip Los Osos fault, and on the south-southwest by what has been termed the Southwest Boundary fault zone. The Southwest Boundary zone is believed to include the north-dipping San Luis Bay fault zone (which includes the Olson and Rattlesnake faults), as well as the Wilmer Avenue, Pecho, Los Berros, and Oceano faults. Lettis and Hall (1994) and Lettis et al. (2004) believe that the San Luis-Pismo block is being uplifted as a relatively rigid crustal block. Studies of late Quaternary[2] deformation (Hanson et al., 1994, 2004) indicate that the uplift rate for the block is about 0.1 to 0.2 mm/yr.

The major structural and tectonic feature in the area of the DCPP is the north-northwest-striking Hosgri fault. This fault zone, located approximately 5 km southwest from DCPP, was not identified until the early 1970s with the availability of seismic reflection profiles. Since its discovery, this fault has been the subject of controversy, speculation, and study. Disagreements over the fault have centered on its length, segmentation, relationship to other faults, age, cumulative displacement, sense of slip (thrust/reverse versus strike-slip), and activity. Studies conducted by and for DCPP consider the Hosgri fault to be the southern-most part of the 410-km-long San Gregorio-San Simeon-Hosgri fault system. These studies characterize the 110-km-long Hosgri fault to be a transpressional, convergent right-slip fault. The Hosgri fault has been mapped along its entire length using seismic reflection data (PG&E, 1991, 1988) and was remapped as part of the Shoreline fault investigation using single-channel, high-resolution sparker data (PG&E, 2011, Appendix H). In the immediate vicinity of DCPP, the Hosgri trends about N 25° to N 30° W and is characterized by multiple fault traces up to 18 km long in a zone up to 2.5 km wide (PG&E, 2011, Plate 1). Fault traces appear vertical to steeply dipping in the upper most sedimentary section but some of the traces dip steeply to the east below about 1 km depth. Given its location offshore, no direct data are available on the slip rate for the Hosgri fault. The slip rate is estimated to be 1 to 3 mm/yr, based primarily on studies and data collected on the on-land San Simeon fault, which PG&E characterizes as a separate section or segment within the San Gregorio-San Simeon-Hosgri fault system. This major conclusion within their characterization is based on an apparent right step-over of 3 to 5 km between the northern Hosgri and the San Simeon fault immediately south of San Simeon, CA.

The Los Osos fault, located about 10 km north of DCPP, is believed to be a southwest-dipping, reverse right-oblique fault. Extensive studies, including detailed geologic mapping and paleoseismic trenching, were conducted on this fault in the late 1980s (PG&E, 1988 and 1991). In the Shoreline Fault Report, PG&E characterizes the Los Osos fault as dipping between 45° and 70° to the southwest and capable of producing a maximum earthquake magnitude of 6.8.

The Southwest Boundary zone is believed to include the north-dipping San Luis Bay fault zone (which includes the Olson and Rattlesnake faults), as well as the Wilmer Avenue, Pecho, Los Berros, and Oceano faults. In the Shoreline Fault Report, the San Luis Bay fault is modeled as a 50° to 80° north-dipping fault with a maximum magnitude of 6.3. The source modeling for the San Luis Bay is complicated because of its possible interaction with the Shoreline fault.

---

[2] We are currently in the Quaternary period of the Cenozoic Era in terms of geologic time. Therefore, late Quaternary deformations are of importance because they are recent.

3.3 Geology of the Diablo Canyon Power Plant Site

As shown in Figure 3-5, the DCPP is located on a relatively broad Quaternary terrace surface near the mouth of Diablo Canyon Creek. Bedrock at the site consists of the Miocene Obispo Formation, a 400-meters-thick sequence of thin to thickly-bedded marine volcanic and volcaniclastic deposits. Near the site, the Obispo Formation has been subdivided into three basic subunits: a tuff or tuffaceous sandstone, fine-grained sandstone and claystone, and an intrusive diabase. In the Shoreline Fault Report, PG&E reported an age of the tuff unit at 15.5 to 15.3 million years. Within the DCPP site, the Obispo Formation has been both faulted and folded and typically dips 35° to 75° to the north (Hall, 1973). Overlying the Obispo Formation bedrock is a thin veneer, typically 1- to 2-meters thick, of marine sands and gravels underlain by a relatively thick sequence (1-meter thick to several 10s of meters thick) of nonmarine, fluvial sands and gravels and colluvium. The basal contact between the overlying marine sands and gravels and the underlying Obispo Formation is a gently southwest-sloping eroded marine terrace platform. This eroded platform can be very sharp and planar or have considerable relief, depending on the resistance of the beds within the Obispo Formation. In Appendix I of the Shoreline Fault Report, PG&E concludes that at the site, this platform was eroded during the last interglacial marine high-stand, which is referred to as marine isotope stage 5e (MIS 5e). MIS 5e occurred about 120 ka. The shoreline angle for this platform (i.e., the former sea cliff) at the site is at an elevation of 30±1 to 34±1 meters (Hanson et al., 1994; PG&E, 2011, Appendix I).

3.4 Onshore-Offshore Geologic Mapping

In the Shoreline Fault Report, PG&E developed new and more detailed maps of the surface exposures in the vicinity of the DCPP, especially along the outcrop exposures in sea cliffs and bedrock surface exposed on wave-cut platforms (at low tide). Mapping of the rock formations and geologic features, such as faults and folds, was enhanced beyond what was compiled for the LTSP (PG&E, 1991, 1988), because the mapping teams used Light Detection and Ranging (LiDAR) and orthophoto maps—technology that was not available during the development of the LTSP in the 1970s and 1980s. The new maps are largely consistent with earlier geologic mapping and add additional information and constraints to the overall geologic and tectonic setting of the DCPP.

The geology mapped onshore was projected offshore using much of the new data in the Shoreline Fault Report, including bathymetry data from new multibeam echo soundings (MBES), magnetic and gravity anomaly maps, seismic reflection data, and diver-collected rock samples. Fifty new diver samples were collected in July 2010 to complement the existing suite of samples obtained for the LTSP (PG&E, 1991, 1988). The sample locations were picked from areas where the MBES data revealed distinct bathymetric textures and at locations where the revised geologic mapping indicated different geologic interpretations from those in the LTSP (PG&E, 1991, 1988). The new samples were also taken to support interpretations of the potential field maps, by providing direct measurements of density, magnetic susceptibility, and magnetic remanence. However, these results were not included in the Shoreline Fault Report because the laboratory measurements of the 2010 dive samples were not yet completed.

One of the most important geological datasets used to make interpretations of the recent tectonic and seismic history of the DCPP site is the mapping and analyses of both raised and submerged marine terraces and their associated wave-cut platforms and paleoshorelines (see Figure 3-6). Marine terraces develop at the shoreline impact zone as waves cut into the rocks at the elevation of the current sea level. Because this process takes time, discrete observable

terraces require that the sea level remain stable over a long period of time. This process can be seen occurring along the California coastline today. The identification and dating of marine terraces in the DCPP region, coupled with the known chronology of sea level elevations during different sea level "stands" (periods of time when the sea level was stable long enough for a platform to be developed), allow for a long-term estimate of how fast the landmass has moved upward or downward. The chronology and naming of sea level stands follows a global protocol tied to the climatic conditions that cause the melting or creation of the global ice mass that directly affects the elevation of the oceans. The term MIS is part of the naming approach and is followed by a number identifying the stage. For example, we currently are in MIS 1 (11 ka to present). The last glacial maximum was MIS 2 (ca. 24 ka), and the DCPP sits on the MIS 5e terrace. The stages move backward in time with increasing numbers. Table I-1-1 of the Shoreline Fault Report provides definitions helpful to the reader unfamiliar with this important technique.

As noted, the identification and dating of marine terraces in the local coastal region provides important data for evaluating uplift rates of the Irish Hills and the DCPP site. The rate of uplift is an important constraint and provides input to understanding the overall kinematics and tectonic movements in the region. The location, elevation, geomorphic characteristics, and ages of these features were mapped in detail by Hanson et al. (1994) and by PG&E as part of the LTSP (PG&E, 1991, 1988). In the Shoreline Fault Report, PG&E updates the original mapping by Hanson et al. (1994) and LTSP (PG&E, 1991; 1988), enhancing the original work with the addition of improved topographic maps based on LiDAR. In addition, because of the detailed bathymetric data acquired as part of the MBES and the high-resolution seismic reflection data, PG&E was better able to identify and map submerged paleoshoreline features in the shallow marine environment offshore.

The updated marine terrace information supports the earlier interpretations of Hanson et al. (1994) and the LTSP (PG&E, 1991; 1988) that the uplift rate for the Irish Hills is approximately 0.2 mm/yr compared to a lower uplift rate of less than 0.1 mm/yr for areas south of the DCPP, including San Luis Bay. The boundary separating the differentially uplifting blocks is the offshore projection of the San Luis Bay fault zone, which also includes the Rattlesnake fault and the Olson Hill zone of deformation. An important observation provided in the Shoreline Fault Report from these new data is that the San Luis Bay fault zone appears to cross, and perhaps truncate, the Shoreline fault, with as much as 8 meters of down-to-the-north displacement, before continuing westward to intersect the Hosgri fault. If correct, this observation constrains the southern extent of the Shoreline fault, limiting its trace length to approximately 16 km. In the Shoreline Fault Report, PG&E also concludes that there is no observable vertical offset across the Shoreline fault, within the 1-to 2-meter uncertainty of the bathymetric data, where wave-cut platforms about 75 ka cross the mapped trace of the Shoreline fault.

PG&E (2011) also concludes that there are no site-specific data with which to constrain a slip rate for the Shoreline fault. PG&E's analyses rely primarily on comparisons of the geomorphic and geologic features of the Shoreline fault relative to the Hosgri fault. The Hosgri fault has an estimated horizontal slip rate between 0.5 and 6 mm/yr (preferred rate of 1 to 3 mm/yr; Hall et al., 1994; Hanson et al., 1994, 2004). PG&E estimates that the slip rate for the Shoreline fault is probably at least an order of magnitude lower than that for the Hosgri. Thus, PG&E estimates the slip rate of the Shoreline fault to range from 0 to a maximum horizontal rate of 0.2 to 0.3 mm/yr. In the seismic source characterization of the Shoreline Fault Report (PG&E, 2011, Section 5), the horizontal slip rate is considered to be between 0.05 and 1.0 mm/yr, with the highest weights given to 0.1 and 0.3 mm/yr.

The NRC agrees with PG&E that it can be very difficult to determine the slip rate for a strike-slip fault; however, a more careful look at the available offshore data to better constrain the slip rate

for the Shoreline fault may be beneficial, especially given PG&E's current efforts to update its assessment of earthquake risk at the DCPP with a new PSHA. Specifically, detailed mapping of the tectonic geomorphology of the fault trace, similar to that done for onshore strike-slip faults, may be beneficial to document and measure the presence (or absence) of lateral offsets of piercing points (discrete features in the landscape, such as streams, that cross a fault and help to quantify slip over time).

3.5 Seismic (Earthquake) Data

3.5.1 Earthquake Locations

As noted in Section 1, the alignment of relocated earthquake hypocenters was the original piece of information that led to the discovery of the Shoreline fault. Although seismic recordings were available from a few stations in central California before the 1980s, consistent recordings of local earthquakes began with the installation of the USGS National Earthquake Hazard Reduction Program system in 1981. The system was enhanced in 1987, following the installation of the Central California Seismic Network (CCSN) by PG&E. The minimum magnitude threshold for the CCSN is approximately M1.0 to M1.5. Since 1987, the network has recorded more than 23,500 events, many considered to be aftershocks from the 2003 San Simeon M6.5 earthquake. The epicenter of the San Simeon Earthquake was approximately 10 km north of San Simeon, CA, and approximately 40 km north of the DCPP. According to McClaren et al. (2008), the San Simeon mainshock was located on a 30-km-long thrust fault that projects to the surface near or to the west of the mapped trace of the Oceanic fault.

Precisely locating the earthquakes in the CCSN catalog, especially microearthquakes with magnitudes of M3.0 or less, is not straightforward because earthquakes in the offshore region are recorded by stations only on land. Having earthquake recordings on only one side of the fault challenges traditional triangulation techniques normally used to locate earthquake epicenters and leads to increased uncertainty. Additionally, the time it takes for the earthquake wavefront to travel from the earthquake source (hypocenter or focus) to the seismographs in the seismic networks is affected by the physical and material properties of the earth's crust, especially impedance contrasts between strata or by discontinuities in the rock layers, such as fractures and faults. PG&E obtained the initial locations in the CCSN database using a simple one-dimensional (1D) crustal velocity model (e.g., McClaren and Savage, 2001). The 1D model assumes the velocity structure of the crust is essentially composed of horizontal velocity layers.

In 2008 (published in 2010), a USGS study by Dr. J. L. Hardebeck reprocessed a large subset of these earthquakes with other geophysical data using an advanced technique called double-difference tomography (tomoDD) to develop a three-dimensional (3D) crustal velocity model (Hardebeck, 2010). TomoDD methods perform an inversion of datasets of seismic recordings, which provides both a 3D velocity model of the region that the seismic waves travel through and highly improved estimates of earthquake location related to each other. Not all earthquakes in the original USGS or CCSN catalogs were included in the analyses; aftershocks to the 2003 San Simeon event were excluded, as were those with poorly recorded P-wave and S-wave arrival times. However, 8,050 earthquakes from the dataset were used to develop the new crustal velocity model. Because both horizontal and vertical variations in crustal structure were included, this revised crustal model allowed earthquakes to be more accurately positioned, thereby permitting seismic features to be imaged more sharply. Plots of hypocenters from the Northern California Earthquake Data Center (NCEDC) and Hardebeck (2010) are shown in Figure 3-7 and Figure 3-8. It can be seen that the NCEDC dataset in Figure 3-7 is a regional dataset that does not well define the Shoreline fault. By contrast, the data from Hardebeck

(2010) shown in Figure 3-8 clearly defines a linear feature offshore of DCPP. Figure 3-9 and Figure 3-10 show the relocated hypocenters in plan view and in cross section, respectively.

Within the relocated database, Hardebeck (2010) noted the alignment of earthquakes on the Hosgri-San Simeon fault zone and along other features in the offshore area. The data appear to show that most of these faults are very steeply dipping to vertical and extend downward into the crust to at least a 12-km depth. As seen in Figure 3-11, focal mechanisms from most of these earthquakes show right-lateral horizontal motion. The vertical geometry and hypocenter data further support the conclusion that these faults are essentially strike-slip. In addition, Hardebeck (2010) noted an approximately 25-km-long alignment of relocated microearthquakes along and subparallel to the coast in the vicinity of the DCPP. As reported in the Shoreline Fault Report, this alignment consists of 49 relocated earthquakes. The 49 earthquakes occurred between 1988 and 2008 with magnitudes between M0.8 and M3.5. The depth range of these microearthquakes is between 2 and 15 km. The alignment of microearthquakes also coincides with linear magnetic anomalies revealed as part of the high-resolution aeromagnetic data (Langenheim et al., 2009, Watt et al., 2009). As can be seen in Figure 3-12, this alignment of microearthquakes, coincident with a strong magnetic anomaly (discussed in Section 3.6.1), constitutes the primary basis for identifying the Shoreline fault and considering it a potential seismic source.

In 2009, PG&E contracted two independent technical reviews to verify Hardebeck's relocation methodology and results. Dr. C.H. Thurber and Dr. F. Waldhauser conducted the two reviews, each using different but comparable approaches to verify Hardebeck's results. Thurber relied on the TomoDD program of Zhang and Thurber (2003). Waldhauser used the hypoDD double-difference hypocenter location program of Waldhauser and Ellsworth (2000). Both reviews confirmed Hardebeck's relocations, except that when using Thurber's preferred velocity model, his Shoreline lineament is shifted approximately 500 meters seaward. This is not surprising given that these techniques refine the relative locations of earthquake hypocenters, rather than the absolute location of any individual event. The location of the fault in this case is confirmed through the magnetic and multibeam data. The results of all three studies are shown in map view in Figure 3-9 and in cross section in Figure 3-10.

Based on differences in the geologic and geomorphic expressions of the fault trace and variations in the continuity of the trend of microearthquakes, PG&E (2011) subdivides the Shoreline fault into three segments of nearly equal length, referred to as the north, central, and south segments, as shown in Figure 3-2. The north segment is 8 km long with a strike of N 40° W. It intersects the Hosgri fault at its northern end. Its southern end is buried beneath a 0.5- to 1-km-wide sand sheet coincident with a gap in the microearthquakes lineament. The central segment is also 8-km long, strikes approximately N 50° W, and coincides with a strong magnetic anomaly. Its southern end is also buried beneath a sand sheet. The south segment is 7-km long and strikes approximately N 40° W and is also associated with a magnetic anomaly. The southern terminus is drawn where the microearthquake lineament ends.

In contrast, Hardebeck et al. (2011) suggest that the best fit of the relocated microearthquake data shows just two distinct fault planes, one corresponding to the Hosgri and one to the Shoreline fault. The best-fit Shoreline fault is a 25-km-long, nearly vertical fault plane while the Hosgri dips 70° to the northeast and intersects the Shoreline fault with an angle of 30°. According to Hardebeck et al. (2011), there is no evidence that the Shoreline fault is segmented at depth and there is no gap between the Shoreline and Hosgri fault zones.

The NRC staff incorporated these differing interpretations of segmentation into the five deterministic Shoreline fault earthquake scenarios discussed in Section 4 and analyzed in Section 5.

3.5.2 Hypocenters and Earthquake Focal Mechanisms

Based on the algorithm by Hardebeck and Shearer, 2002, single-event, first-motion focal mechanisms were computed for 836 earthquakes and 34 composite mechanisms in the CCSN catalog (Hardebeck, 2010). Hardebeck's results show predominantly right-lateral strike-slip mechanisms on a vertical fault plane for the Hosgri-San Simeon fault zone, supporting the conclusion that the Hosgri is a near-vertical strike-slip fault. Aftershocks from the 2003 San Simeon earthquake show a more complex pattern, with reverse focal mechanisms at depth that transition to right-lateral strike-slip focal mechanisms along the fault at shallower depths.

As shown in Figure 3-11, focal mechanisms along the Shoreline fault are also dominated by right-lateral strike-slip events aligned on a vertical fault plane. Near the junction of the Shoreline fault with the Hosgri, the pattern is diffuse and the focal mechanisms include both pure strike-slip and reverse-oblique motions. The strikes of the focal mechanisms also appear rotated in alignment with the strike of the Hosgri fault. In the Shoreline Fault Report, PG&E proposes several explanations, including a hypothesis that the Shoreline merges with and is part of the Hosgri fault system. However, based on its interpretation of the microearthquake patterns, PG&E's preferred interpretation is that the Shoreline fault is a distinct fault and near its northern terminus, the fault plane is subvertical with oblique reverse and strike-slip motions.

Similar to PG&E, the NRC concluded that the Shoreline fault is a vertical or nearly vertical strike-slip fault over most of its length, although it possibly dips 70 degrees to the northeast near its intersection with the Hosgri fault near Point Buchon. The NRC assumed a vertical strike-slip fault for its DSHA characterization.

3.6 Potential Field Data

3.6.1 Magnetic Data

New high-resolution magnetic surveys of the DCPP site area were recently conducted as part of the CRADA: a high-resolution survey using a fixed-wing airplane in 2008, a supplemental helicopter survey in 2009, and marine magnetic surveys conducted in 2008 and 2009. The USGS obtained all three new surveys, and they are provided in Langenheim et al. (2009). The composite magnetic anomaly map reveals a number of linear magnetic anomalies, including several well-defined curvilinear anomalies that trend subparallel to the coastline just offshore of the DCPP. As shown in Figure 3-12 and Figure 3-13, the most prominent of these anomalies is coincident with the alignment of the 49 microearthquakes (PG&E, 2011) along the Shoreline fault as described in Section 3.5.1.

The USGS also processed the data and developed a series of two-dimensional (2D) forward models to test various interpretations of the resulting magnetic anomaly maps. Based on forward modeling, the USGS concluded the most favored interpretation is that the anomalies result from a nearly vertical source body with a width of approximately 200 meters and extending to a depth of at least 200 to 300 meters below the surface. In these models, the USGS assumes that the dominant source of magnetization in these rocks is an induced magnetization (present earth's field) with variable magnetic susceptibilities. Remanent magnetizations of the source bodies were presumed to be too weak compared with the induced component to contribute significantly to the observed anomalies. Appendix D of the Shoreline Fault Report also notes that, because of possible variation in the magnetic susceptibility of the source body, it is permissible to extend the source to a termination depth of 4 km into the subsurface and still fit the observed magnetic trends. PG&E interprets the magnetic anomaly as serpentine or greenstone lenses commonly associated with the Franciscan mélange bedrock.

In its interpretation, the magnetic anomalies arise due to the juxtaposition of the highly magnetic serpentine against nonmagnetic Tertiary sandstone.

The NRC agrees with the present interpretation by PG&E regarding the source of magnetic anomalies. In the Shoreline Fault Report, PG&E indicates that laboratory measurements of the 2010 dive samples are yet to be completed. The NRC concurs that acquisition of this data may better constrain the forward models and improve their reliability.

3.6.2 Gravity Data

The USGS compiled nearly 30,000 gravity measurements of the region. The resulting isostatic gravity map reveals a positive gravity anomaly coincident with denser Franciscan basement rocks. The gravity signature reveals first-order crustal features, such as the Pismo Syncline and the Hosgri fault. However, PG&E does not rely on these data for its interpretations of the Shoreline fault. The NRC agrees that, because of the low resolution, the current gravity maps do not reveal any additional details about the structures associated with the Shoreline lineament and therefore are not useful in further characterizing the Shoreline fault.

3.7 Bathymetry

New MBES and sidescan data from the Estero Bay to San Luis Obispo Bay nearshore region were acquired using a combination of several sonar systems (400 kHz Reson 7125, 240 kHz Reson 8101, SEA SwathPlus) aboard the Research Vessel R/V Ven Tresca by the Seafloor Mapping Lab at California State University, Monterey Bay, during 2007, 2009, and 2010. The new bathymetric data provided a substantially improved image of the seafloor and allowed PG&E to recognize features within the seafloor with a resolution of 1 meter or less. The new bathymetric data, in combination with high-resolution seismic reflection data, were used by PG&E to develop new detailed geologic maps of the seafloor and to identify the surface expressions of offshore geologic features, including the traces of the Shoreline and Hosgri faults. In addition, the new bathymetry data were used to identify paleoshoreline features in the near shore environment. It is not clear from the discussion in Appendix F of the Shoreline Fault Report if PG&E included sidescan sonar as part of the new MBES data acquisition. According to Goldfinger (2009), “sidescan sonar offers detailed imagery that is generally superior for mapping of tectonic features, and when combined with multibeam bathymetry, yields a 3D surface map that images both morphology and material properties in the area of interest.” Therefore, while the addition of the new MBES data greatly improved resolution of the seafloor bathymetry, resolution limits of the digital elevation models (DEM) produced by these data are on the order of 1 to 2 meters. Additional processing of this data in combination with the sidescan backscatter data could refine the imagery to obtain resolution of less than 1 meter.

3.8 High-Resolution Marine Seismic Reflection Data

The USGS collected high-resolution single-channel seismic reflection data in 2008 and 2009 between Pismo Beach and Piedras Blancas. The surveys were orthogonal to the beach, spaced 800 m apart, and extended from near shore to about 5 km offshore. Details about data acquisition and processing are published in Sliter et al. (2009). According to PG&E, the high-resolution seismic profiles data and interpretations were used to support other mapping methods offshore and to provide a complementary dataset to deeper-penetrating common-depth point seismic-reflection profiles evaluated during the LTSP (PG&E, 1988 and 1991). In particular, the new high-resolution seismic data were used to support new interpretations of the continuity and relative altitudinal spacing of strandlines in the mid- to

upper-continental shelf regions offshore and to refine near-surface resolution of the fault traces of the Hosgri fault zone.

However, the high-resolution seismic data were of marginal value to the analysis of the Shoreline fault, particularly for imaging small displacements, because of the lack of coherent reflectors in the bedrock. In Appendix B of the Shoreline Fault Report, PG&E concluded that this data "provided limited interpretations of structures in the areas covered by marine deposits and mobile sand sheets." The NRC concurs that available seismic reflection data are not especially useful for characterizing the structure of the Shoreline fault.

3.9 NRC Evaluation of the Data

The NRC concludes that the PG&E Shoreline Fault Report provides a comprehensive summary and assessment of the available geologic, geophysical, and seismological data used to evaluate the seismic hazard levels of the DCPP site and region. Most of the information is used to develop and support the interpretation of a regional tectonic model and thereby constrain the ranges of reasonable interrelations of the seismic sources that could affect the seismic hazard of the DCPP. However, several new lines of data are also germane specifically to the identification and characterization of the Shoreline fault. These include the alignment of relocated microearthquakes from Hardebeck (2010) and the linear magnetic anomalies coincident with these aligned microearthquakes (Langenheim et al., 2009; Watt et al., 2009). Together, these two datasets provide the best evidence supporting the identification of the Shoreline features as a fault and as a potential seismic source.

Based on this review, the NRC staff concludes that the information in the Shoreline Fault Report is a significant improvement over earlier studies. It is based on well-established scientific methods and practices. The data and methods are described in sufficient detail to permit objective evaluation of the new information by the NRC. The information is sufficient to allow PG&E to develop reasonable and defensible technical conclusions to support its seismic hazard evaluation of the Shoreline fault. The two independent reviews of the Hardebeck (2010) analysis PG&E provided in the Shoreline Fault Report offer additional assurance that the technique was applied properly and the relative locations of the hypocenters are supported.

The newly acquired datasets also provide important information for understanding the regional tectonics. Important constraints related to the size, geometry, style of faulting, and capability of the fault to generate earthquakes capable of producing strong ground motions at the DCPP can be developed from the larger body of information PG&E provided in the report. The geologic and geophysical information, including geologic mapping and the earthquake database, can be used to develop reasonable interpretations of fault geometry, activity, maximum magnitude, and proximity of earthquakes to the DCPP. Based on this information, the parameters in the following section have been identified as the NRC's best estimates of deterministic fault parameters for the Shoreline fault.

However, the NRC review noted several areas in which additional data collection, data processing, data integration, and more detailed interpretations could improve the PG&E (2011) results and reduce existing uncertainties in these interpretations of the Shoreline fault. These areas are discussed below. Data needs and critical issues are identified within a SSHAC Level 3 framework as part of the Workshop #1 activities (see Section 1) and these could be considered during that phase of the project.

- PG&E could improve the resolution of the bathymetric maps by combining the MBES data with the sidescan radar data to develop even greater resolution images of the sea floor.

- PG&E could constrain uncertainties on its slip rate estimates with more detailed mapping of the tectonic geomorphology along the entire fault trace—similar to what is done for onshore strike-slip faults—to document and measure the presence (or absence) of lateral offsets of landforms perpendicular to the fault. The Shoreline Fault Report included some efforts to document vertical separations across the mapped fault trace, but because the report concluded that the Shoreline feature is essentially a vertical strike-slip fault, future efforts should focus on delineating piercing points to document any such evidence of horizontal offset.
- Forward 2D models of the magnetic anomalies could be improved and better constrained by measuring the magnetic properties of the source rocks, especially accurate measurements of magnetic susceptibility and natural remanent magnetization.

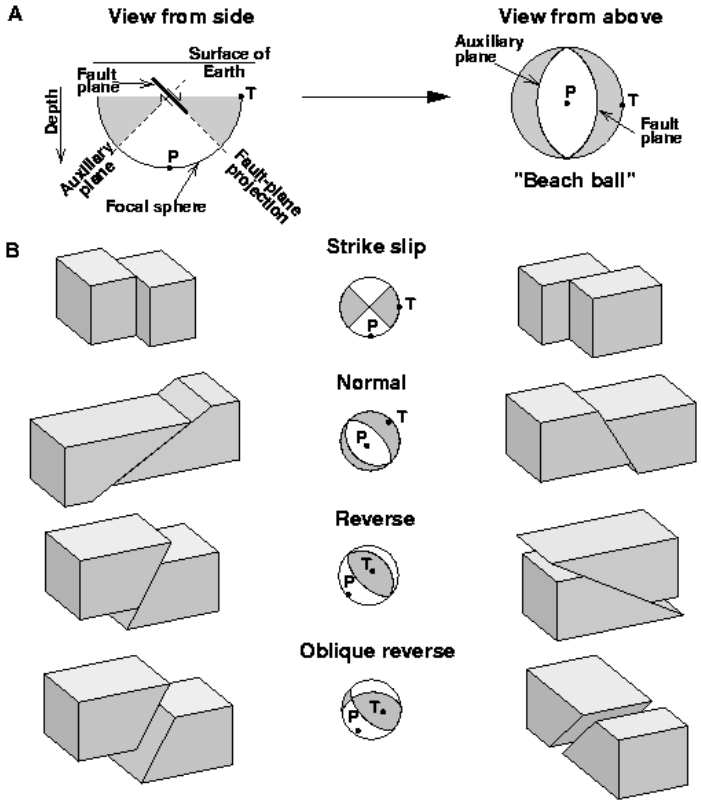

Figure 3-1 Illustration of faulting mechanisms and focal mechanisms by the USGS.

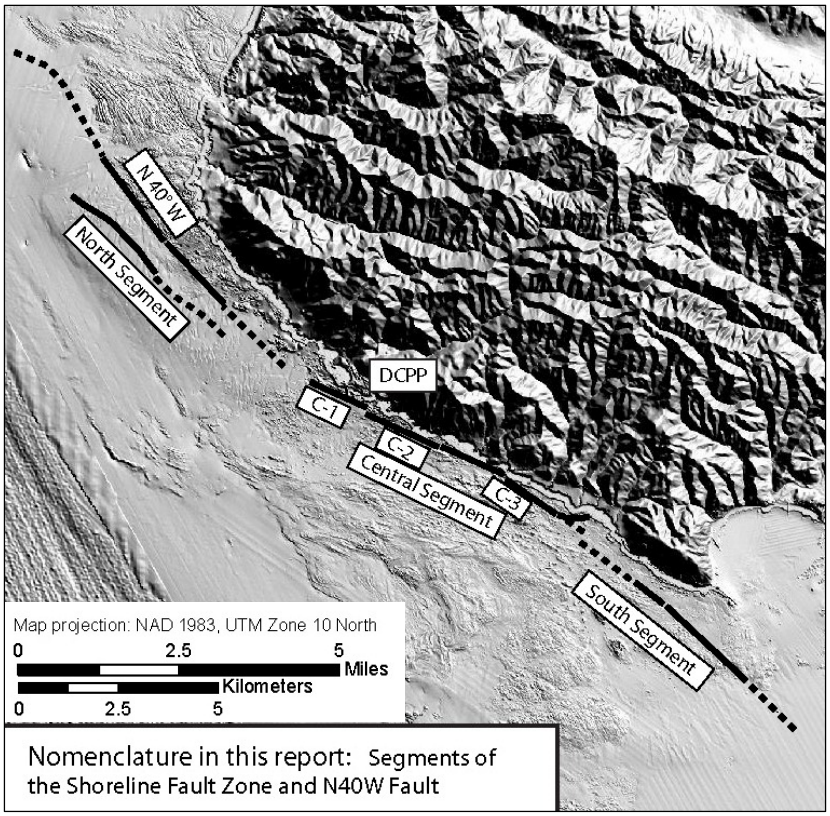

Figure 3-2 Shoreline fault location and segments (from Figure 4-1 of the PG&E Shoreline Fault Report).

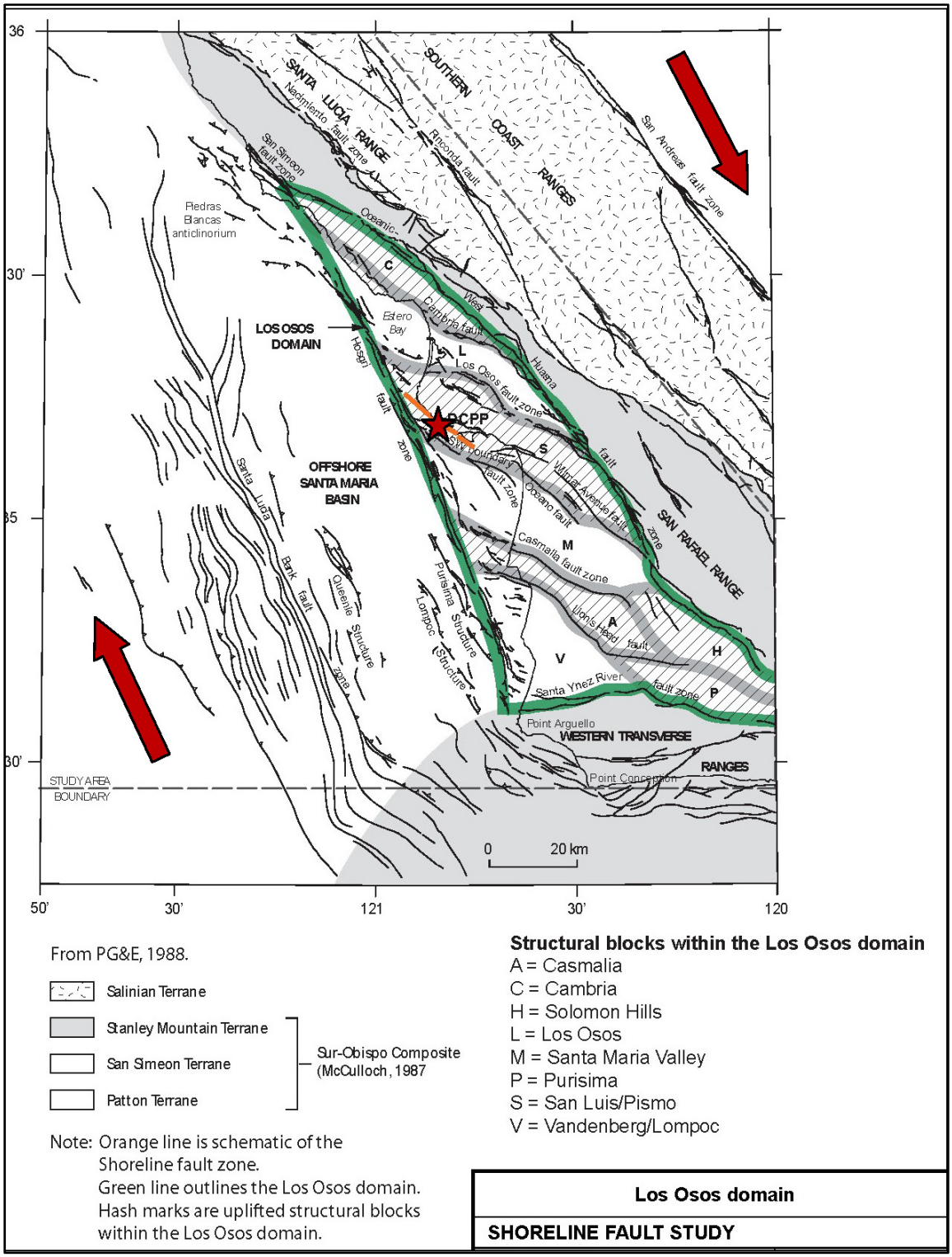

Figure 3-3 Regional tectonics and seismic setting of the DCPP (Figure 3-1 of the PG&E Shoreline Fault Report, annotated by the NRC).

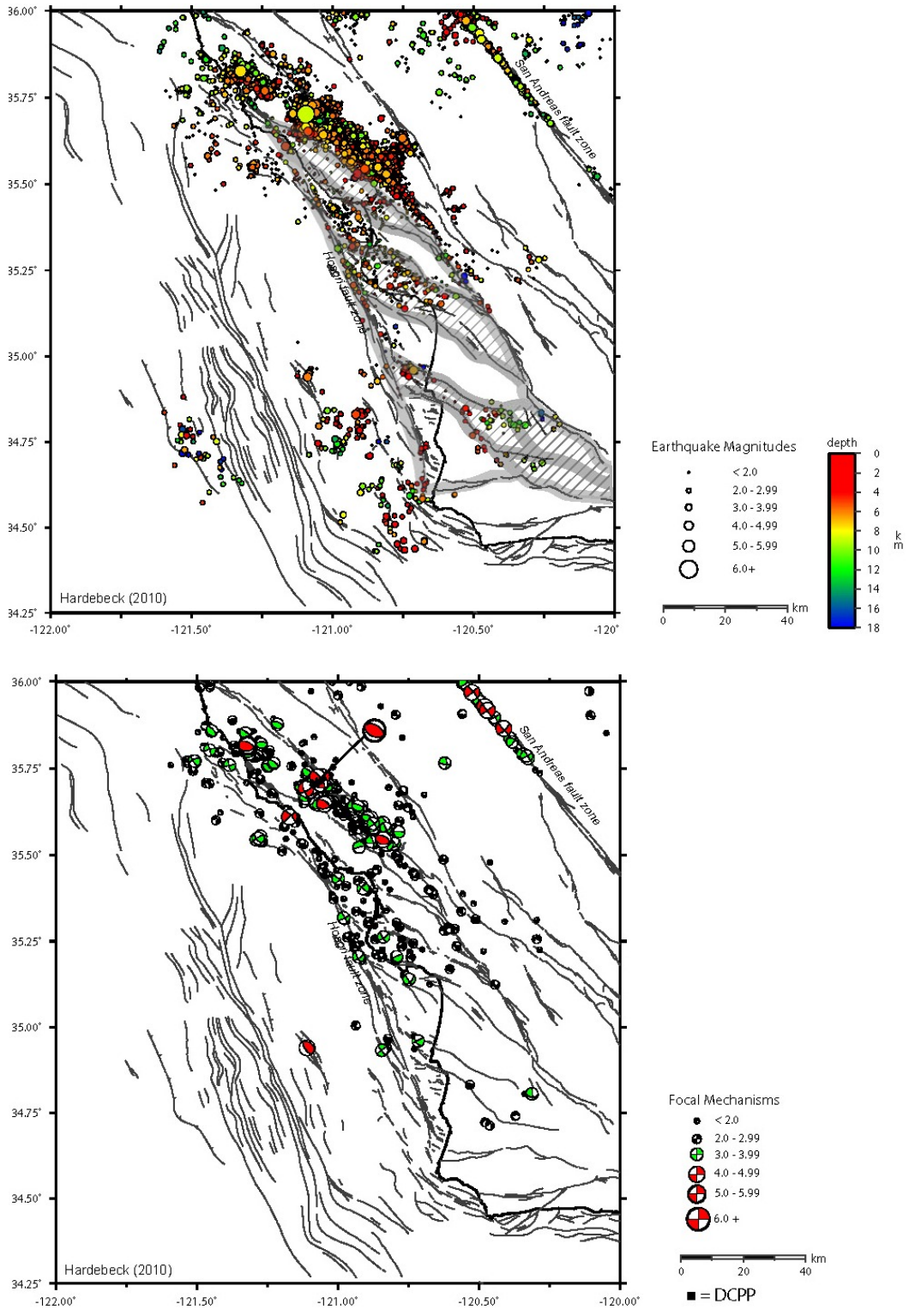

Figure 3-4 Seismicity patterns and focal mechanisms of the DCPP region from 1987 through 2008 (extracted from Figure 3-2 of the PG&E Shoreline Fault Report).

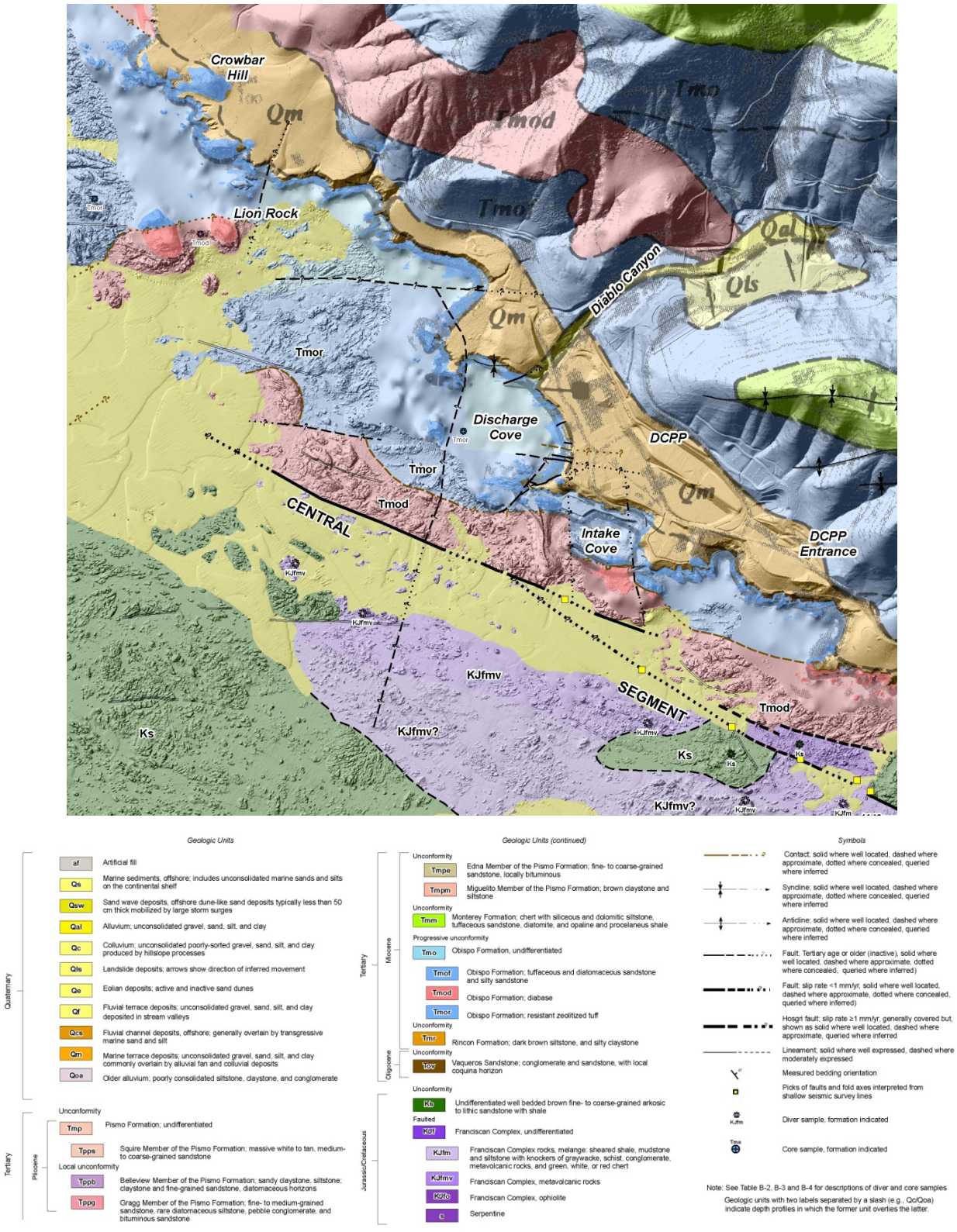

Figure 3-5 Geology underlying DCPP (extracted from Plate B-1B of the PG&E Shoreline Fault Report).

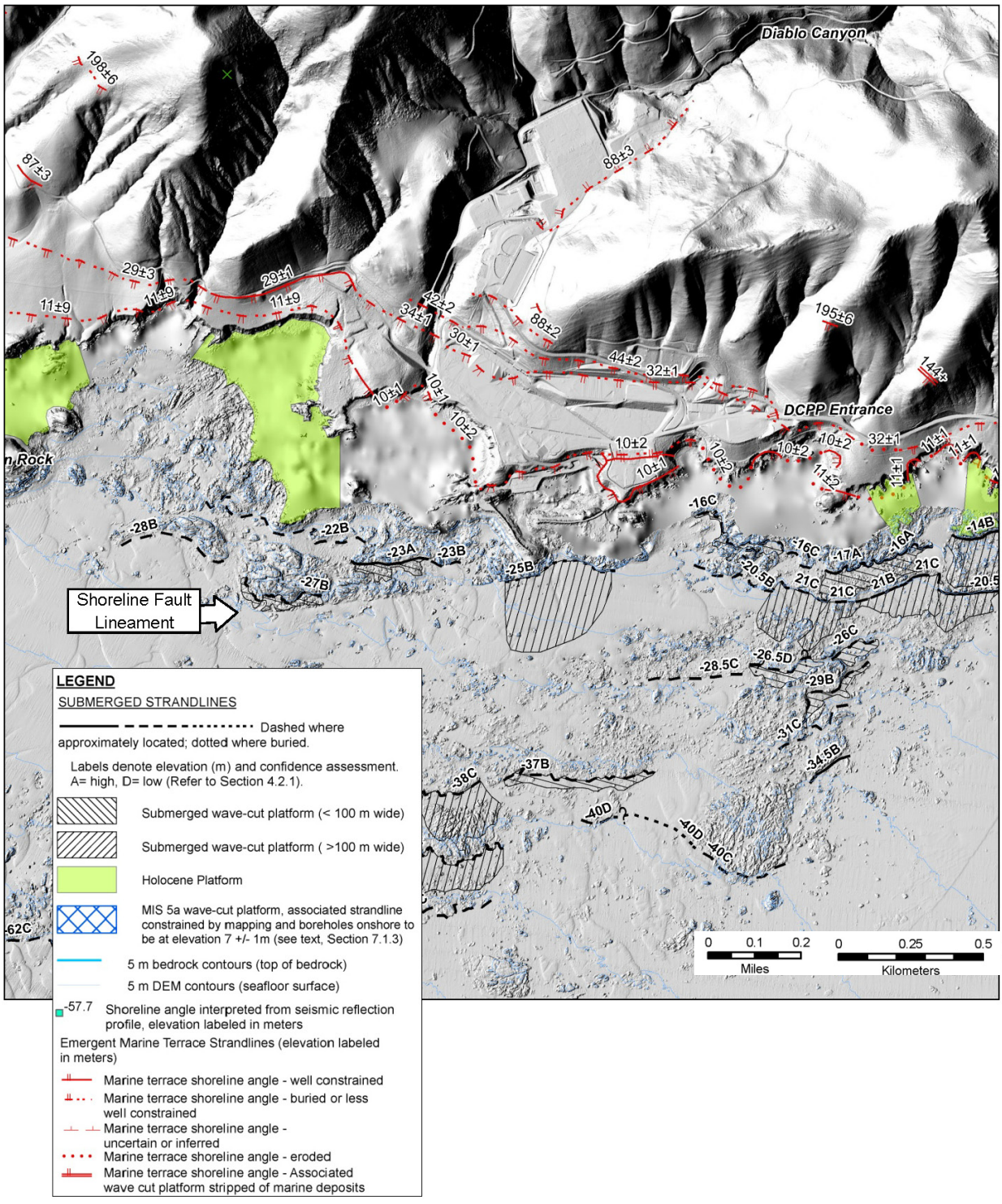

Figure 3-6 Paleostrandlines in the DCPP region (extracted from Plate I-1b of the PG&E Shoreline Fault Report).

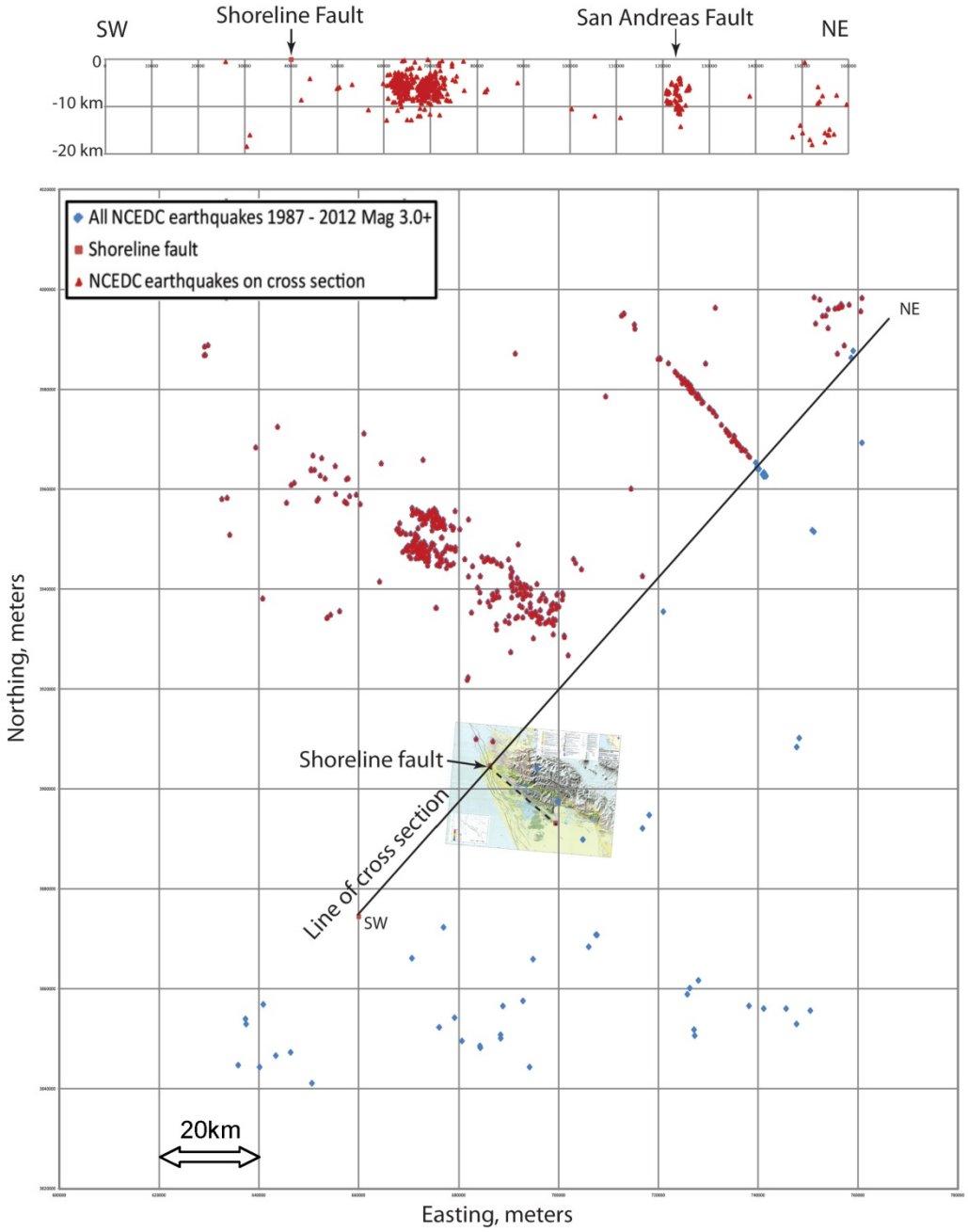

Inset map is the geologic map in PG&E's Shoreline Fault Report. The cross-section plot above shows the hypocenters located from the Line of Cross Section up to the northwest (also shown in red). The cluster between the Shoreline Fault and the San Andreas Fault indicates the San Simeon Fault Zone earthquakes.

Figure 3-7 Northern California Earthquake Data Center earthquakes, 1987 through 2011, plotted in plan view and in cross section.

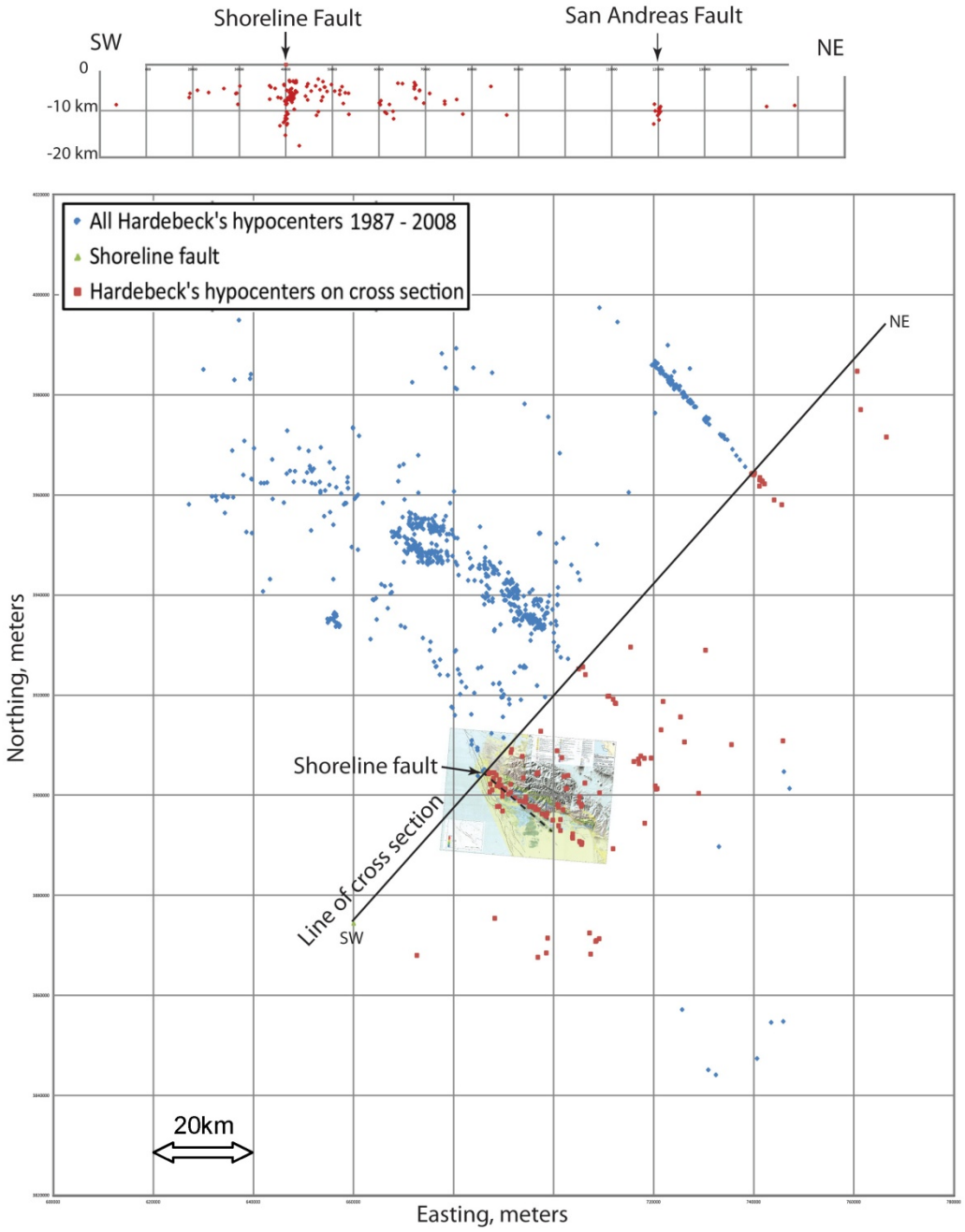

Inset map on the plan view plot is the geologic map in PG&E's Shoreline Fault Report. The cross-section plot above shows the hypocenters located from the Line of Cross Section down to the southeast (also shown in red).

Figure 3-8 Earthquake data from Hardebeck (2010) plotted in plan view and in cross section.

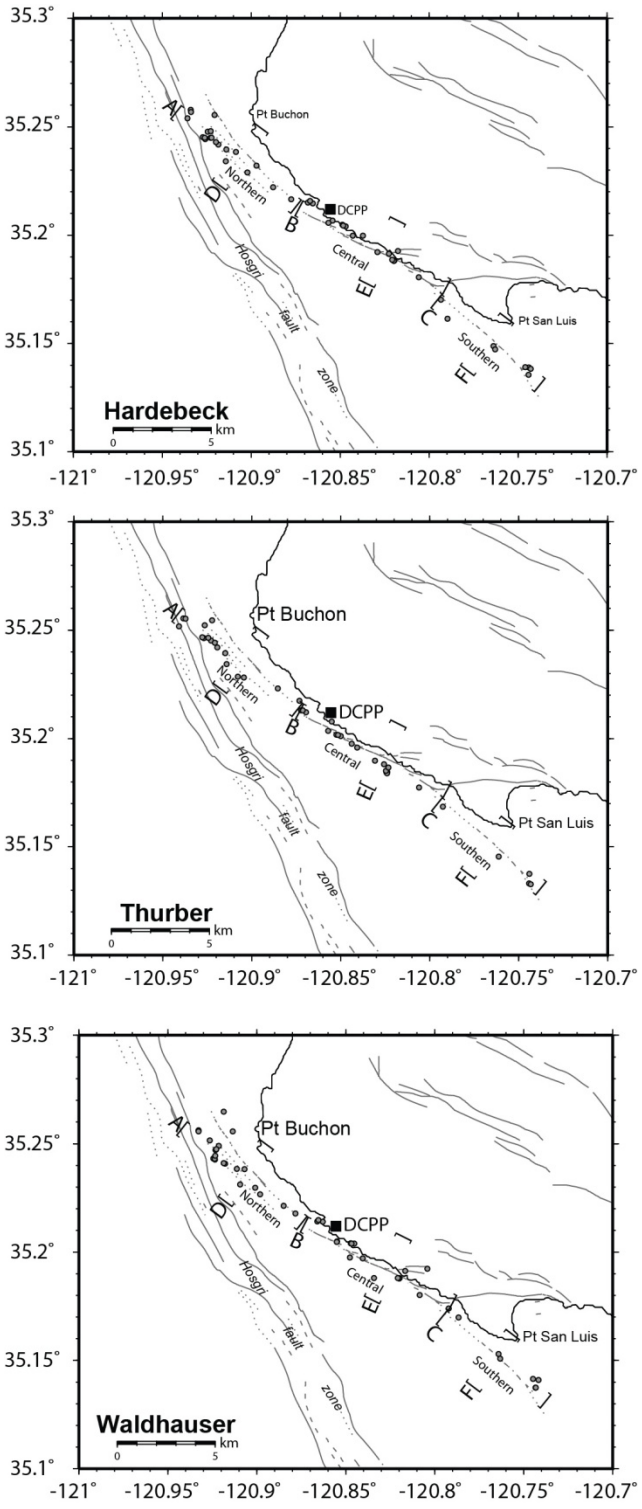

Figure 3-9 Comparison of reanalysis of hypocenters by Hardebeck, Thurber, and Waldhauser in plan view (Figure 4-2 of Shoreline Fault Report).

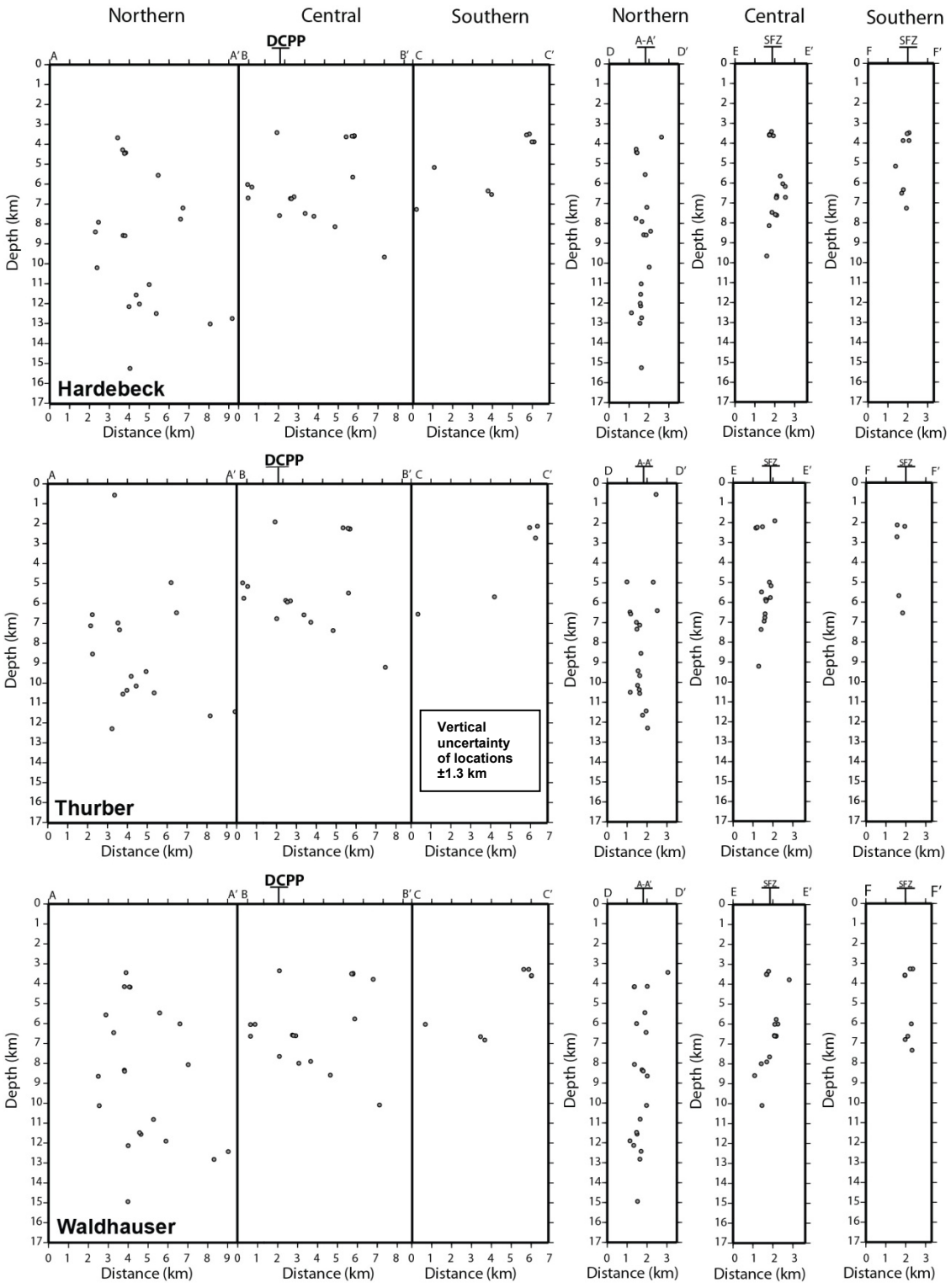

Figure 3-10 Comparison of result from reanalysis of hypocenters by Hardebeck, Thurber, and Waldhauser in cross section (Figure 4-2 of Shoreline Fault Report).

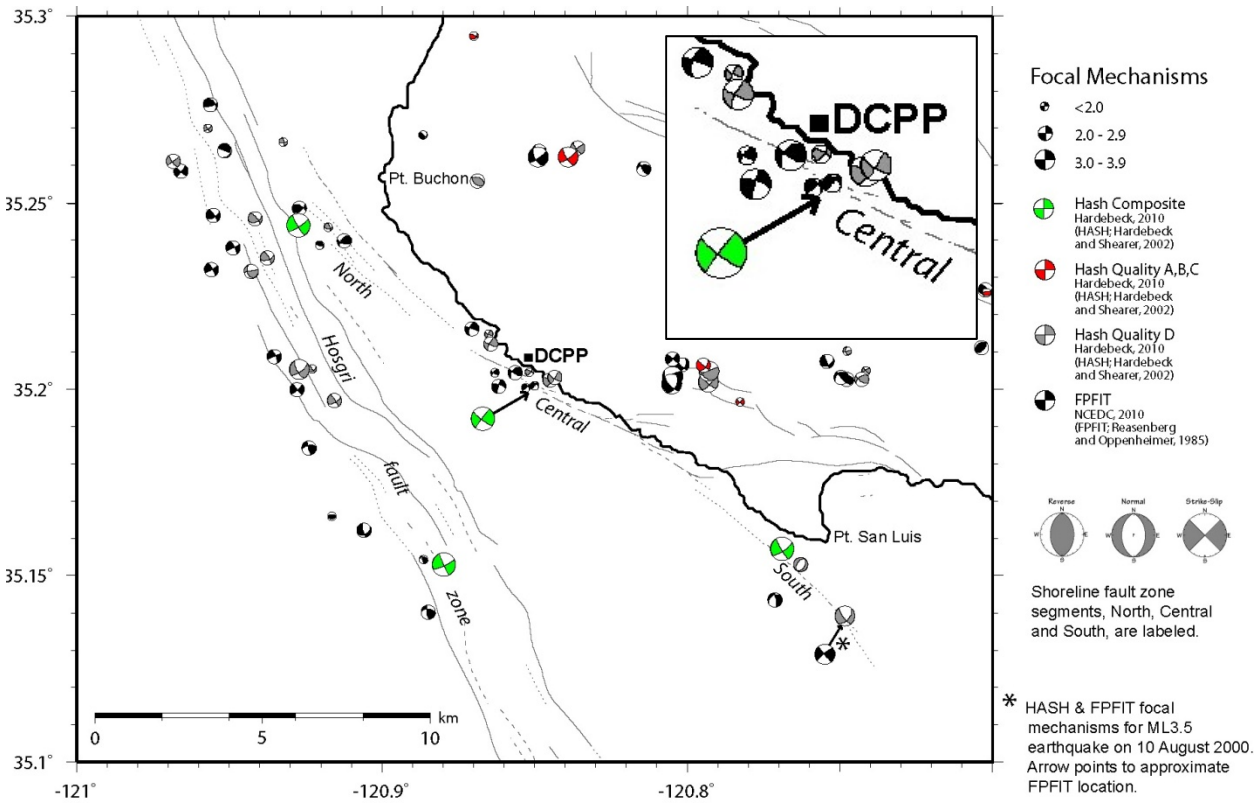

Figure 3-11 Focal mechanisms recorded in the vicinity of DCPP (Figure 4-7 from Shoreline Fault Report).

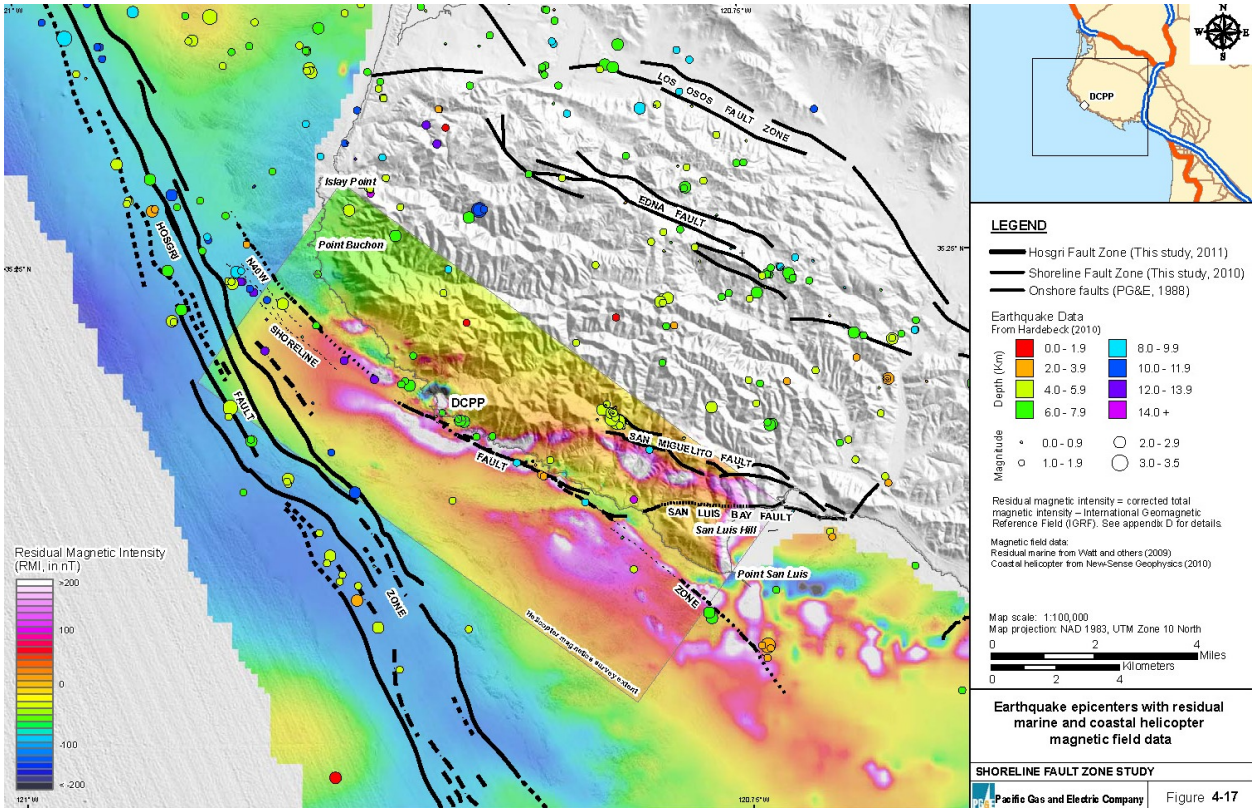

Figure 3-12 Earthquake epicenters recorded in vicinity of DCPP plotted with magnetic field data and the local faults (Figure 4-17 from Shoreline Fault Report).

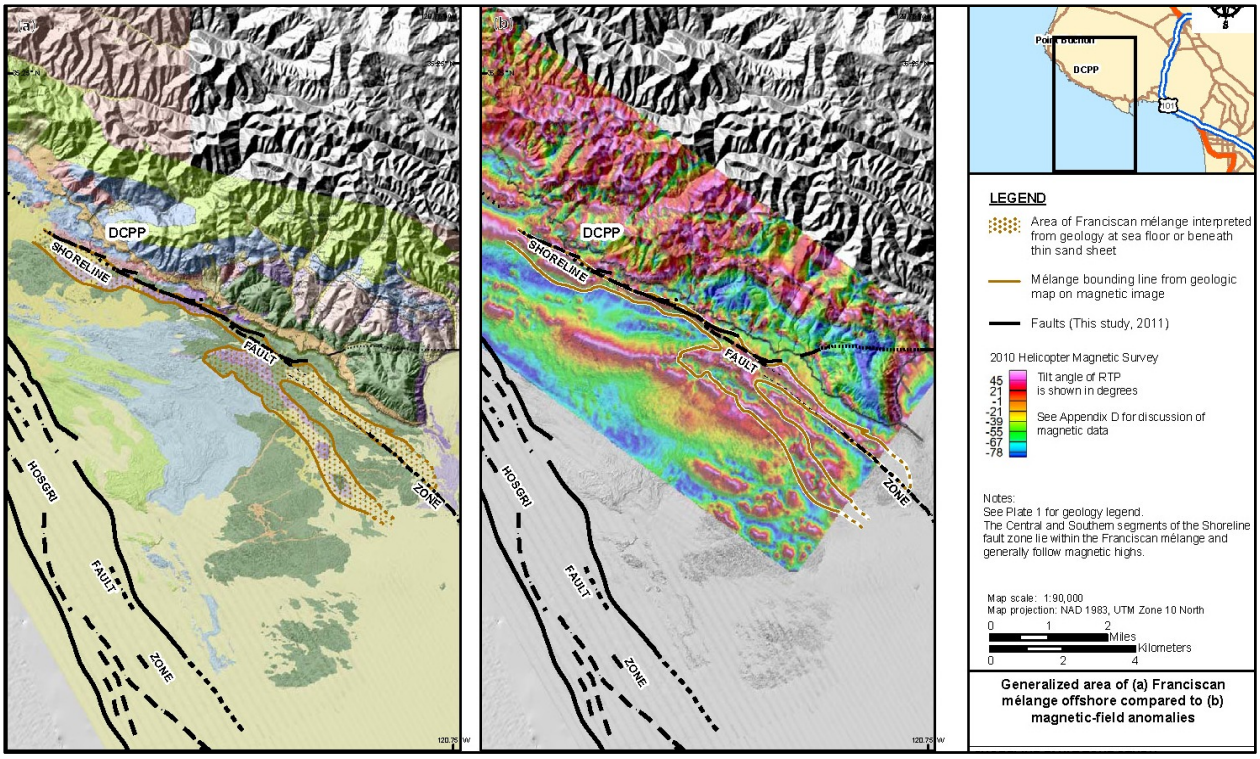

Figure 3-13 Franciscan mélange plotted with magnetic field data and local faults (Figure 4-18 from Shoreline Fault Report).

4 Data Interpretation and Determination of Scenario Earthquakes for Deterministic Analysis

The NRC's assessment of PG&E's conclusions on the characteristics of the Shoreline fault and the determination of fault characteristics used in the NRC's confirmatory DSHA were developed by considering the following questions.

- Does the available geologic and seismologic evidence support the interpretation that the Shoreline feature is a fault or potential seismic source?
- If so, is there evidence that the fault is capable of producing significant earthquakes that could affect the DCPP site?
- Assuming the Shoreline fault is an active and capable fault, what are the best estimates (and reasonable upper bounds) of fault zone characteristics (length, width, dip, slip rate, and magnitude) that should be used to evaluate the fault in comparison to the existing seismic hazard analyses for the DCPP?

Because the NRC analysis was deterministic, it was performed assuming that the Shoreline fault is active and capable. The NRC staff notes that, based on information discussed in the next section, there is considerable evidence that the fault may not be capable of producing large earthquakes (i.e., greater than magnitude 6).

4.1 Geologic and Seismologic Evidence in Support of the Existence of the Shoreline Fault

The NRC review started with the basic question of whether or not the lineament that is being called the Shoreline fault is actually an active fault or some other feature. The most definitive evidence in support of the Shoreline fault is the relocated microearthquakes from Hardebeck (2010) coincident with the mapped linear magnetic anomalies (Langenheim et al., 2009; Watt et al., 2009). The exception to this pattern is along the northernmost part of the microearthquake lineament, which trends seaward of the line of magnetic anomalies and the mapped N 40° W fault where it intersects the Hosgri fault near Point Buchon.

As noted in the Shoreline Fault Report and modeled by the USGS in Appendix D to that document, the source of the magnetic anomalies is most likely serpentine or greenstone lenses within the Franciscan mélange caused by the juxtaposition of highly magnetic serpentine against less magnetic pre-Tertiary sandstones. According to the LTSP (PG&E, 1988, 1991), faulting within the Franciscan mélange probably occurred during a mid-Miocene to early-Pliocene period of transtensional deformation or during a later middle-to-late-Pliocene period of transpressional deformation; therefore, it is not related to present-day tectonics. In addition, several other prominent linear magnetic anomalies are evident in the magnetic anomaly maps (e.g., a nearly east-west curvilinear trend of high magnetization between the Shoreline fault trace and the Hosgri fault near the UTM 389500 northing line in Figure D-12 of the PG&E Shoreline Fault Report) that are not associated with recent microseismicity or other evidence of active seismicity. PG&E interprets these observations to conclude that, at least along the central and southern segments, the Shoreline fault is a reactivated older Pliocene or late Miocene fault. PG&E has alternatively interpreted the northernmost section of aligned microearthquakes as an extension of Shoreline faulting beyond the northern tip of the

reactivated segments or microearthquakes associated with the Hosgri fault and not part of the Shoreline fault at all.

With few exceptions, strong geologic or geomorphic expressions of displacement along the Shoreline structure are lacking. PG&E (2011) notes several possible vertical offsets of Tertiary strata near the fault trace in the reprocessed high-resolution seismic-reflection images, and parts of the central and southern segments coincide with prominent and subdued bathymetric lineaments. However, these lineaments could also reflect differential erosion of ultramafic rocks within the Cretaceous sandstones and may represent buried relict sea cliffs rather than direct evidence of fault offset. Although the geologic maps show what appear to be offsets across the faults that juxtapose Obispo diabase, Cretaceous sandstones, and Franciscan mélange, the offsets are not systematic in a way that clearly delineates a consistent sense and amount of cumulative slip and certainly provide no clear evidence for late Quaternary slip.

Based on a detailed review of this information in the Shoreline Fault Report, the NRC concludes that the feature identified as the Shoreline fault is very likely a fault or fault zone, at least in the sense that the geologic and geophysical data show it to be a fracture or series of fractures with some evidence for displacement of the adjacent blocks on either side of the fault relative to one another.

4.2 Evidence for Large Magnitude Earthquakes

Evidence that the Shoreline fault can produce large magnitude earthquakes is equivocal. Several observations suggest that the Shoreline fault could be capable of producing large magnitude earthquakes. Where presently mapped, the fault traces align with the magnetic anomalies and microearthquake alignment. In several places the fault traces also appear to align with small vertical scarps or scarp-like features. However, other lines of evidence do not support this interpretation. For example, the hypocenter data from Hardebeck (2010) show recent motions are dominated by purely strike-slip fault mechanisms, so it is not clear to the NRC why this faulting would produce vertical scarps. Several sections of the Shoreline fault traces in the MBES bathymetry images were viewed in detail by the NRC, but there appeared to be no evidence of systematic offset geologic or geomorphic features indicative of strike-slip faulting. PG&E (2011) also finds “no definitive evidence for late Quaternary displacement anywhere along the Shoreline fault zone” (PG&E, 2011 pp. 4-17). Similarly, in Figure 4-22 of the Shoreline Fault Report, PG&E shows that the Shoreline fault does not appear to displace the north-south fault of Discharge Cove, at least to within the 1-to 2-meter resolution of the data. The resolution of these images is 1 to 2 meters per pixel scale, so it is possible that small displacements, on the order of several meters, are present but remain undetected.

Given these uncertainties in the data and the interpretations, the Shoreline fault may be capable of generating earthquakes that need to be evaluated within the seismic hazard framework of the DCPP because of their potential to contribute to the overall hazard at the site. Within the context of a deterministic analysis, which does not consider the rate of earthquake occurrence, the NRC review determined that there is a reasonable likelihood, but no certainty, that the Shoreline feature is an active fault in terms of its ability to produce significant earthquakes. Fault characteristics needed for a DSHA are provided in the next section of this report.

4.3 Fault Characteristics Needed for Deterministic Seismic Hazard Assessment

To assess the potential ground motions associated with the Shoreline fault, a reasonable estimate of the range of earthquake maximum magnitudes (M_{max}) that the Shoreline fault could produce must be estimated for input to the DSHA. Estimates of these magnitudes are often derived from observations from recent earthquakes (e.g., Wells and Coppersmith, 1994), which scale fault length or fault area to magnitude. Different relationships exist for the various styles of faulting: dip-slip normal, dip-slip reverse, and strike-slip.

Using this approach, the required fault characteristics for an estimate of magnitude are as follows:

- Fault segmentation; whether the fault is composed of a single strand or of two or more segments that could rupture independently of each other
- Faulting style and fault geometry: normal, reverse, strike-slip, or oblique
- Fault length or maximum surface or subsurface rupture length
- Fault area based on fault length and down-dip width of the fault

The method PG&E (2011) used to estimate maximum magnitudes for the Shoreline fault relied on a statistical approach based on a number of alternative rupture scenarios. The Shoreline Fault report identified three segments of the Shoreline fault (i.e., the north, central, and south segments), as shown in Figure 4-1. PG&E used a probabilistic model of all these possible scenarios (expressed as a fault tree) to develop a cumulative probability distribution function (Figure 6-17 of PG&E Shoreline Fault Report). PG&E selected the 90th percentile of the characteristic magnitude distribution based on what it deemed "a reasonably conservative value for use in the deterministic analysis." Using this approach, PG&E estimates the median M_{max} is M6.2 and the 90th percentile M_{max} is M6.5.

The NRC's approach is more straightforward. Based on data in the Shoreline Fault Report, the NRC also interprets the Shoreline fault as a vertical strike-slip fault over most of its length. It possibly dips 70 degrees to the northeast near its intersection with the Hosgri fault near Point Buchon. The depth of the fault plane is limited to between 12 and 15 km, based on the maximum depth of the microearthquakes. However, several other important aspects of the Shoreline fault remain poorly characterized and therefore subject to uncertainty. These uncertainties include (1) the surface or subsurface rupture length of the fault, (2) structural relationships of the Shoreline fault to other faults, in particular the faults of the San Luis Bay fault zone, and (3) whether the Shoreline fault is capable of producing large enough earthquakes to affect the hazard at the DCPP.

The NRC developed five alternative interpretations to characterize the Shoreline fault (summarized in Table 4-1) based on the available data. Figure 4-2 shows these five scenarios overlain on Figure 4-17 of the Shoreline Fault Report. Some of these scenarios used combinations of the same segments identified by PG&E. However, the NRC did not consider scenarios in which the segments acted independently. The magnitudes in these five scenarios range from less than M5.9 to M6.9. Considering all available information, the NRC concludes that two deterministic assessments are needed to reasonably assess the potential impact of the Shoreline fault seismicity on the overall DCPP seismic hazard assessment. The first assessment is based on Scenario 1, in which the Shoreline fault is deemed to be a creeping fault and capable of producing smaller magnitude earthquakes up to M5.9. A magnitude M5.9 was selected as a reasonable upper- bound magnitude earthquake on the Shoreline fault that

could occur without producing visible surface rupture. The lack of observable surface rupture is an important characteristic of the Shoreline fault accounted for in the Scenario 1 interpretation. The fault displacement analysis in Appendix C (Figure C-1 and Figure C-2) shows that there is roughly an equal likelihood that an M5.9 earthquake will or will not produce surface rupture based on worldwide empirical data from historical earthquakes and constraints of the 10-12 km width of the seismogenic crust offshore the DCPP. The second assessment considered a maximum magnitude of M6.7 because that represents magnitudes from Scenarios 3 and 4. These two scenarios include a full rupture of the Shoreline fault based on the most defensible interrelations of the Shoreline fault length and fault area.

The NRC did not consider a scenario in which an earthquake on the Shoreline fault continues to rupture onto the Hosgri fault. Large earthquakes from simultaneous rupture on the two faults (i.e., those greater than M7) would produce large surface displacement, which are not evident in the geologic record. The NRC concludes that the lack of significant horizontal displacement across the Shoreline fault rules out the possibility of joint rupture.

4.3.1 Scenario 1: Shoreline Fault is Aseismic

In Scenario 1, the Shoreline fault is interpreted as an essentially aseismic creeping fault with a very small strain (slip rate) budget. This interpretation is based on similarities of the Shoreline fault to other creeping faults in California and the lack of detected horizontal displacement along the fault except what may exist below the 1-to 2-meter resolution of the bathymetry and seismic reflection data. The alignment of microseismicity coupled with the presence of serpentine and possibly talc (Moore and Rymer, 2007) has been observed along segments of several strike-slip faults that creep. These materials have low degrees of friction (i.e., are “slippery”) and talc is also very soft, thereby precluding significant strain energy to accumulate along its surface. Allen et al. (1965) and Allen (1968) were among the first to recognize the creeping sections of the San Andreas fault between Hollister and Cholame. Hanna et al. (1974) showed that creeping sections of the San Andreas are characterized by magnetic anomalies interpreted to be large masses of serpentinite in the subsurface. As noted by Coleman (1971), because serpentinized ultramafic rocks have relatively low densities compared to the overlying strata, faults could provide pathways for upward migration of serpentinite to shallow depths. East of Parkfield, CA, the Table Mountain Serpentinite is considered to be an extruded body of serpentinite that formed from diapiric rise along faults of deeply buried, low-density ultramafic material (Dickenson, 1966). By analogy, the Shoreline fault may also simply be creeping at a low slip rate. Under this latter interpretation, the Shoreline fault would be incapable of generating large earthquakes (M≥5.9).

In the Shoreline Fault Report, PG&E estimates a maximum horizontal slip rate for the Shoreline fault of 0.05 to 0.3 mm/yr, with a preferred upper bound range of 0.2 to 0.3 mm/yr. Because PG&E (2011) did not have sufficient geologic data to support a slip-rate determination, its analyses relied primarily on comparisons to the Hosgri fault, with an estimated slip rate of between 0.5 and 6 mm/yr (preferred rate of 1 to 3 mm/yr; Hall et al., 1994; Hanson et al., 1994, 2004). Based on these comparisons, PG&E estimates that the slip rate for the Shoreline fault is probably at least an order of magnitude lower than that for the Hosgri. Thus, PG&E (2011) estimates the slip rate of the Shoreline fault to range from 0.05 to a “maximum” rate of 0.2 to 0.3 mm/yr. A slip rate near the 0.3 mm/yr upper bound is also supported by PG&E’s analysis of the rate of the relationship between frequency of microearthquakes from Hardebeck (2010) and their magnitude as shown in Figure 4-3 of the Shoreline Fault Report, reproduced here as Figure 4-3. In Figure 4-3 of the Shoreline Fault Report, PG&E estimates the slip rate based on empirical best fits of the microearthquakes, assuming a Characteristic Earthquake model (Youngs and Coppersmith 1985) fit to these data. The types of magnitude recurrence relationships commonly used in seismic hazard analysis are shown in Figure 4-4. PG&E (2011)

tested the best fits of the observed seismicity rate against varied assumptions of a characteristic magnitude earthquake on the Shoreline fault and concluded from these plots that the slip rate is considered to be between 0.05 and 1.0 mm/yr, with the highest weights given to 0.1 and 0.3 mm/yr.

However, these slip rates seem incompatible with the observed geologic record. A slip rate of 0.2 mm/yr would result in 5 m of horizontal slip in the last 25,000 years and 20 m of offset in the last 100,000 years. These displacements should be easily visible in the bathymetric maps, even given the 1- to 2-m resolution of the imagery. In addition, with the exception of apparent offsets of the older geologic strata, there is little if any evidence for any late Quaternary horizontal displacement along the Shoreline fault. At most, the fault could record a few meters of late Quaternary displacement, an amount at or below the 1-2 m resolution of the new bathymetric and geologic data. As shown in Figure 4-5, the area and length of fault rupture scale disproportionately with event magnitude, and larger earthquakes tend to produce surface rupture and increased surface expression, as shown in Figure 4-6. Thus, while 1 to 2 m of slip could mean one or possibly two M ≥ 6.5 characteristic events in the past, the recurrence of surface earthquakes that rupture the surface along the Shoreline fault would clearly leave evidence for such events. This leads to the supposition that, if the Shoreline is assumed to be an active strike-slip fault that can produce large earthquakes, then it is either a very young fault (with only one or two such earthquakes in the recent geologic history) or it is one with an exceedingly low slip rate, such that the repeat times between events is on the order of tens to hundreds of thousands of years and is inconsistent with the rate predicted by the recently observed microearthquakes as shown in Figure 4-3 of the Shoreline Fault Report.

Figure 4-3 in this document is an annotated version of Figure 4-3 in the Shoreline Fault Report. This figure shows the number of earthquakes recorded per year (in the upper left), the cumulative number of earthquakes recorded in each magnitude bin (in the upper right) and the calculated catalog completeness, and the magnitude recurrence curves for various maximum magnitudes and slip rates overlain on the recorded data (in the lower half). However, none of the characteristic magnitude/slip rate combinations shown in Figure 4-3 fit the data when the lack of observed surface displacement is considered. Instead, the current rate of seismicity of small earthquakes and the lack of visible offset would be explained by a combination of a lower characteristic magnitude and lower slip rate. This supports a Shoreline fault model with a smaller M_{max}.

As described above, this interpretation is supported by the recorded seismicity, coupled with the lack of visible offset along the fault. The remaining scenarios (shown in Figure 4-2) ignore the discrepancy related to the lack of surface expression because deterministic analyses do not explicitly consider slip rate, likelihood, and other data tied to the probability of the Scenario Earthquake of interest occurring. The remaining discussion in this Section considers whether a scenario is likely to be plausible, not the likelihood of the event.

4.3.2 Scenario 2: 16-Kilometer-Long Shoreline Fault

In Scenario 2, the Shoreline fault extends from its intersection with the Hosgri fault south-southeast to where the fault is truncated by the San Luis Bay system of faults. The best and most compelling argument for this interpretation is the apparent 5 to 8 m of down-to-the-north offset associated with the San Luis Bay fault where it crosses the trend of the Shoreline fault. This interpretation would therefore include just the north and central segments of the Shoreline fault, as described by PG&E (2011). This interpretation is also supported by the change in the spatial distribution of microearthquakes along the south segment compared to the north and central segments. Only 6 of the 49 relocated earthquakes from Hardebeck (2010) are along the south segment, and those six earthquakes appear to be in two distinct clusters rather

than distributed along the fault. By contrast, the remaining 43 earthquakes are along the north and central segments and are evenly distributed. This scenario presumes that the south segment of the Shoreline fault as described in PG&E (2011) is an older (Tertiary) fault that has not been reactivated in the Quaternary.

4.3.3 Scenario 3: Shoreline Fault Linked to San Luis Bay Fault Zone

In Scenario 3, the north and central segments of the Shoreline fault (~16 km long) rupture in conjunction with rupture on the eastern portion of the San Luis Bay zone of faults (8 km long). This scenario is based on the apparent bending to the east of the south end of the central segment of the Shoreline fault near Rattlesnake Canyon and the differing heights of the MIS5a terrace platform north and south of this area (PG&E, 2011 Plates 1 and I-1c). This scenario makes kinematic sense because 5 to 8 m of late Quaternary north-side-up vertical offset (PG&E, p. I-54) associated with the east-west striking, north-dipping (60°), reverse right-oblique San Luis Bay zone of faults could result in several meters of horizontal slip associated with the N 30° W striking Shoreline fault, an amount near or below our threshold of detection. For this scenario, the north and central segments of the Shoreline fault are modeled as near vertical (90°) with a width of the fault plane of 15 km, and for that portion of the San Luis Bay fault east of the Shoreline fault, it is modeled as a 60° north-dipping fault, giving it a width of 19 km.

4.3.4 Scenario 4: 23-Kilometer-Long Shoreline Fault

In Scenario 4, the Shoreline fault ruptures along the entire fault trace length as mapped by PG&E (2011). The rupture would involve the north segment (8 km long), the central segment (8 km long) and the south segment (7 km long), for a total rupture length of 23 km. This scenario assumes that the Shoreline fault acts independently of other faults and does not rupture with them in combination. In its logic tree, PG&E (2011) considers this independent style of behavior more likely (70 percent probability), as opposed to rupture in combination with other faults (30 percent probability).

The microseismicity detected from 1988 to 2008 spans all three mapped segments of the Shoreline fault. Most of the events have similar right-lateral focal mechanisms. This suggests that all three segments of the fault are in a similar stress-loaded state at this time. Therefore, if the stress state eventually exceeds the critical threshold in one of the three segments to create a surface-rupturing earthquake, it is reasonable to assume that the propagating rupture would dynamically load the adjacent segments to above their critical thresholds, which would permit the rupture to continue onto them. In the judgment of the NRC, the two internal segment boundaries proposed by PG&E for the Shoreline fault are unlikely to stop a surface rupture. Both of these boundaries (between the north and central segments, and central and south segments) are inferred by PG&E to be small fault stepovers (for example, the central/south segment boundary, which is a 0.25-km-wide right, or releasing bend, stepover). Wesnousky (2006) showed that stepovers less than 2 km wide do not stop surface ruptures in most cases, based on an analysis of 22 historic strike-slip ruptures. Therefore, under this scenario, a surface rupture that occurs on any of the three fault segments will likely rupture all the segments, for a total rupture length of 23 km.

4.3.5 Scenario 5: 33-Kilometer-Long Shoreline Fault

In Scenario 5, there is a rupture of the Shoreline fault involving simultaneous rupture of the entire length of the fault mapped by PG&E (2011), plus an additional fault length farther to the southeast. The whole rupture would involve the north segment (8 km long), the central segment (8 km long) and an extended southern segment (17 km long), for a total rupture length of 33 km. This scenario assumes that the south segment of the Shoreline fault does not end beneath the sand sheet where mapped by PG&E (2011), but continues southeast along the same magnetic

lineament for another 10 km, to include the 1913 earthquake epicenter (plus the uncertainty of the epicenter location). PG&E (2011, p. 4–5) stated, "A search of the historical database prior to 1970 and prior to local seismic networks (NCEDC, 2010; McLaren and Savage, 2001) showed two M5 earthquakes that occurred in 1913 and 1916 in the vicinity of the [Shoreline] seismicity lineament in the past 100+ years. Considering the location uncertainty of 10 to 20 km (PG&E, 1988; McLaren and Savage, 2001) for these events, *it is possible that they could have been associated with the south segment of the Shoreline fault zone* or one of the faults in the Southwestern Boundary fault zone" [emphasis added]. The 1913 epicenter is located at 35.1° N, 120.7° W by NCEDC with a 10-km uncertainty; this position lies about 5 km southeast, and along the projection, of the south segment of the Shoreline fault.

In this interpretation, the entire mapped trace of the south segment of the Shoreline fault lies along a magnetic lineament (see Figure 4-2). PG&E (2011, Plate 1) arbitrarily ended the fault at the farthest southeast "pick of faults and fold axes interpreted from shallow seismic survey lines," but the magnetic lineament continues at least another 5 km farther southeast. On Plate 1 of the Shoreline Fault Report, PG&E shows three "picks of faults and fold axes interpreted from shallow seismic survey lines" lying along the projection of the south segment of the Shoreline fault that are not ascribed to any particular fault zone (shown as small yellow squares in Figure 4-7). Two of these "picks" lie at 5.8 km and 6.7 km southeast of the end of the Shoreline fault as mapped by PG&E in the Shoreline Fault Report. A line connecting the two picks trends N 35° W. If that line is projected to the northwest, it comes much closer to the Shoreline fault than to any other fault mapped by PG&E (2011). Under this scenario, the maximum the Shoreline fault can be extended is 13 km southeast of PG&E's current mapped terminus. Otherwise, the fault trace would come onshore, and there is no evidence for an onshore Quaternary fault that can be linked to the Shoreline fault. Thus, the maximum permissible length of the Shoreline fault is 36 km. However, we also note that there has been no clustered microseismicity in the period from 1988 to 2008 along the proposed 10 km extension of the south segment. Therefore, even if the Shoreline fault exists there as an old (Tertiary) fault, there is no evidence it has been reactivated in the Quaternary except for the possibility that the 1913 earthquakes occurred on it. The epicenter of the 1913 earthquake is highly uncertain and could have occurred on several of the Southwestern Boundary zone faults, including the Pecho, Los Berros, or Oceano faults. Therefore, although the scenario has been hypothesized as one representing the maximum permissible length, it is not supported as well as other scenarios by the data.

4.4 PG&E Approach to Characterizing the Shoreline Fault Scenario

PG&E used a weighted logic tree approach to characterize the input to the Shoreline fault DSHA. Although the logic tree used 30 branches for full characterization of the source, the general approach can be understood by considering a few key nodes. First, the tree has two main branches. In one, the Shoreline fault is independent of the San Luis Bay fault, and the scenarios are based on segmented and non-segmented models composed of the north, central, and southern segments of the Shoreline fault, as shown in Figure 3-2. In the second main branch, the central and northern segments of the Shoreline fault rupture with the eastern segments of the San Luis Bay fault. In both main branches, a variety of northern and southern end points are considered, leading to different magnitude ranges. Additionally, a variety of failure plane widths are included, as are various dips for the non-vertical segments. The full logic tree figures and explanation are provided in Section 5 of the Shoreline Fault Report. Only NRC Scenarios 2, 3, and 4 above are found within the PG&E logic tree.

4.5 Conclusions

The complexity of the PG&E approach in considering the probability of various deterministic scenarios, as well as the consideration of which of the five NRC scenarios above should be used to perform its DSHA, highlights the challenges of the deterministic approach. Engineering judgment is required, but the application of engineering judgment may not be well constrained or transparent. In particular, DSHA does not explicitly account for the likelihood of a particular scenario. Commonly, DSHAs assume an upper bound scenario independent of the likelihood of its occurrence. For this DSHA, the NRC assumed that the Shoreline fault is capable and took an approach focused on identifying an interpretation consistent with most or all of the available data. In the end, the NRC performed its DSHA considering two scenario earthquakes: a M5.9 earthquake, representing Scenario 1, and M6.7, representing Scenarios 3 and 4. Scenario 1, which characterizes the Shoreline fault as a creeping fault, is an interpretation that is consistent with the available geologic and seismic data. The NRC staff considers the M6.7 scenarios to yield a reasonable upper bound magnitude based on an appropriately conservative interpretation of all available information.

Table 4-1 Five NRC faulting scenarios for the Shoreline fault.

Scenario	Scenario Description
1	Shoreline fault is aseismic and creeping with a slow slip rate.
2	Shoreline fault extends 16 km from its intersection with the Hosgri fault south-southeast to where the fault is truncated by the San Luis Bay system of faults.
3	Shoreline fault extends 15 km from its intersection with the Hosgri fault south-southeast to where the fault merges with the 8-km-long eastern portion of the San Luis Bay fault, for a total length of 23 km.
4	Shoreline fault extends 23 km and includes all three of the mapped segments (north, central, and south) as mapped by PG&E in the Shoreline Fault Report (PG&E, 2011).
5	Shoreline fault includes the entire length of the fault as mapped by PG&E (2011), plus additional rupture farther to the southeast another 10 km for a total fault length of 33 km.

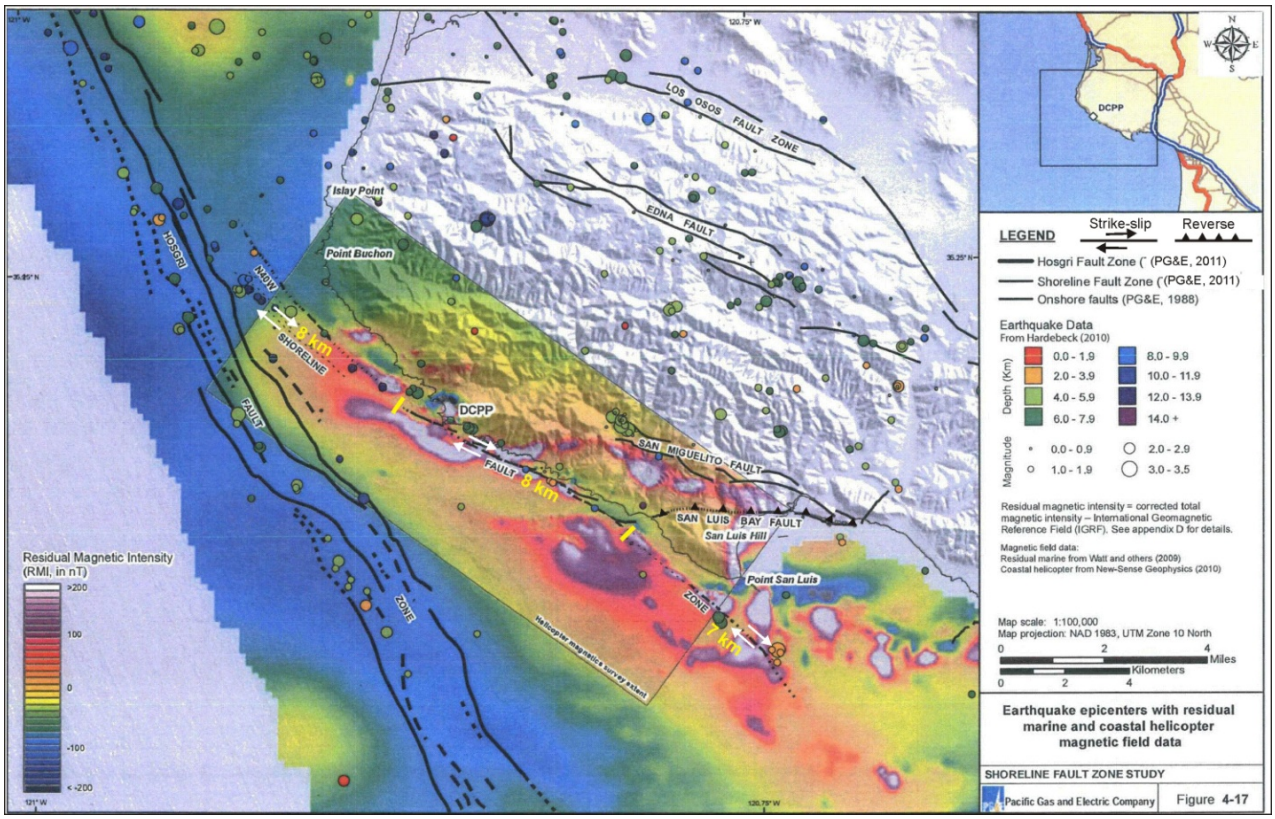

Annotated Figure 4-17 of the Shoreline Fault Report showing the fault segment lengths (north, central, and south) as defined by PG&E. The trace of the San Luis Bay fault was also annotated to show the sense of slip.

Figure 4-1 Segments of the Shoreline fault.

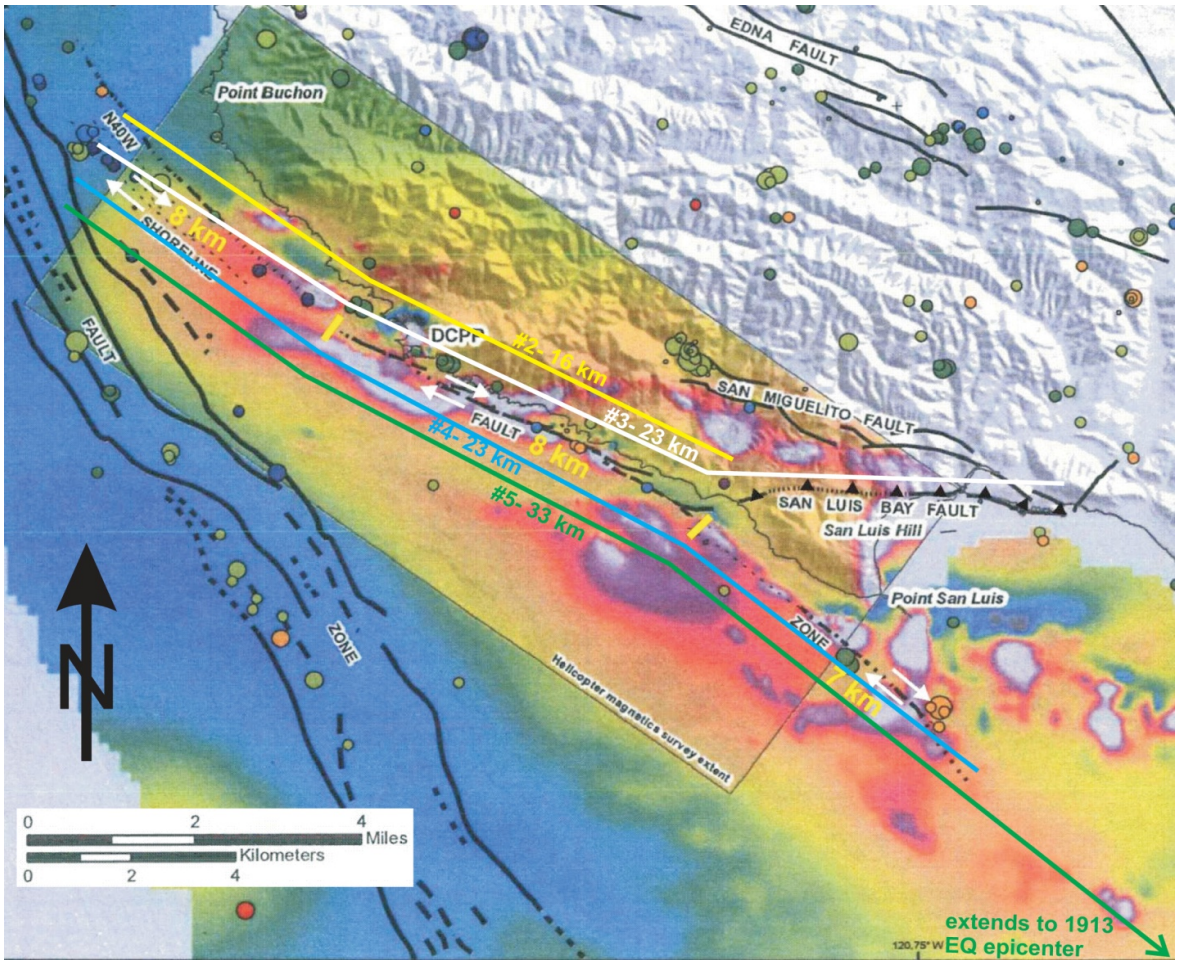

SCENARIO DESCRIPTION
1: Aseismic or creeping with no surface rupture.
2: Rupture of the Shoreline fault, north and central segments (16 km)
3: Rupture of the Shoreline fault, north and central segments, plus the San Luis Bay fault (23 km)
4: Rupture of all three segments of the Shoreline fault (23 km)
5: Rupture of the entire Shoreline fault plus an additional 10 km to the approximate epicenter of the 1913 earthquake, and the SE end of the magnetic lineament.

Note that, for clarity, the four proposed fault models are shown offset NE or SW from the dash-dotted line that delineates the mapped location of the Shoreline fault. The fifth model allows for M < 6 earthquakes to occur anywhere along the fault trace.

Figure 4-2 Lateral extent of characteristic earthquake rupture scenarios considered as viable possibilities in this report.

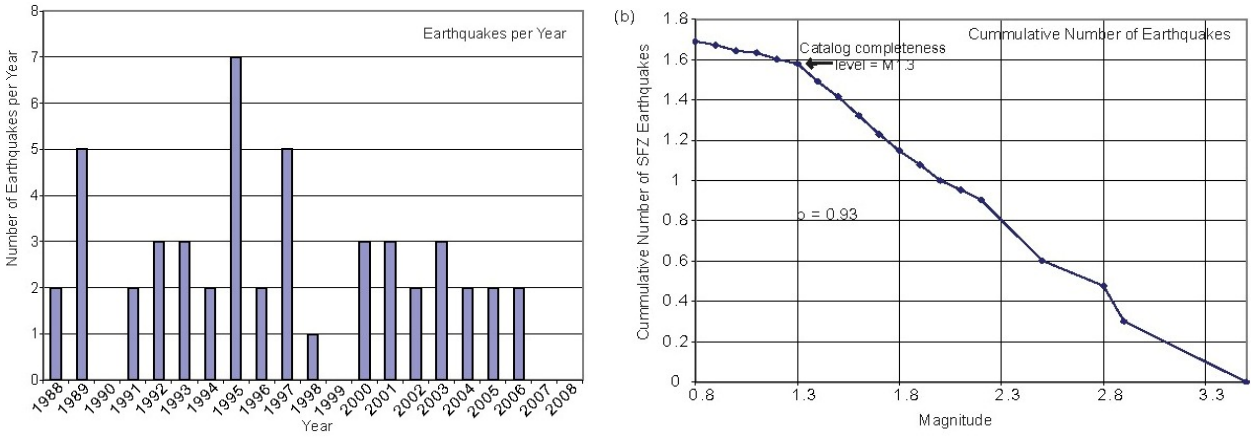

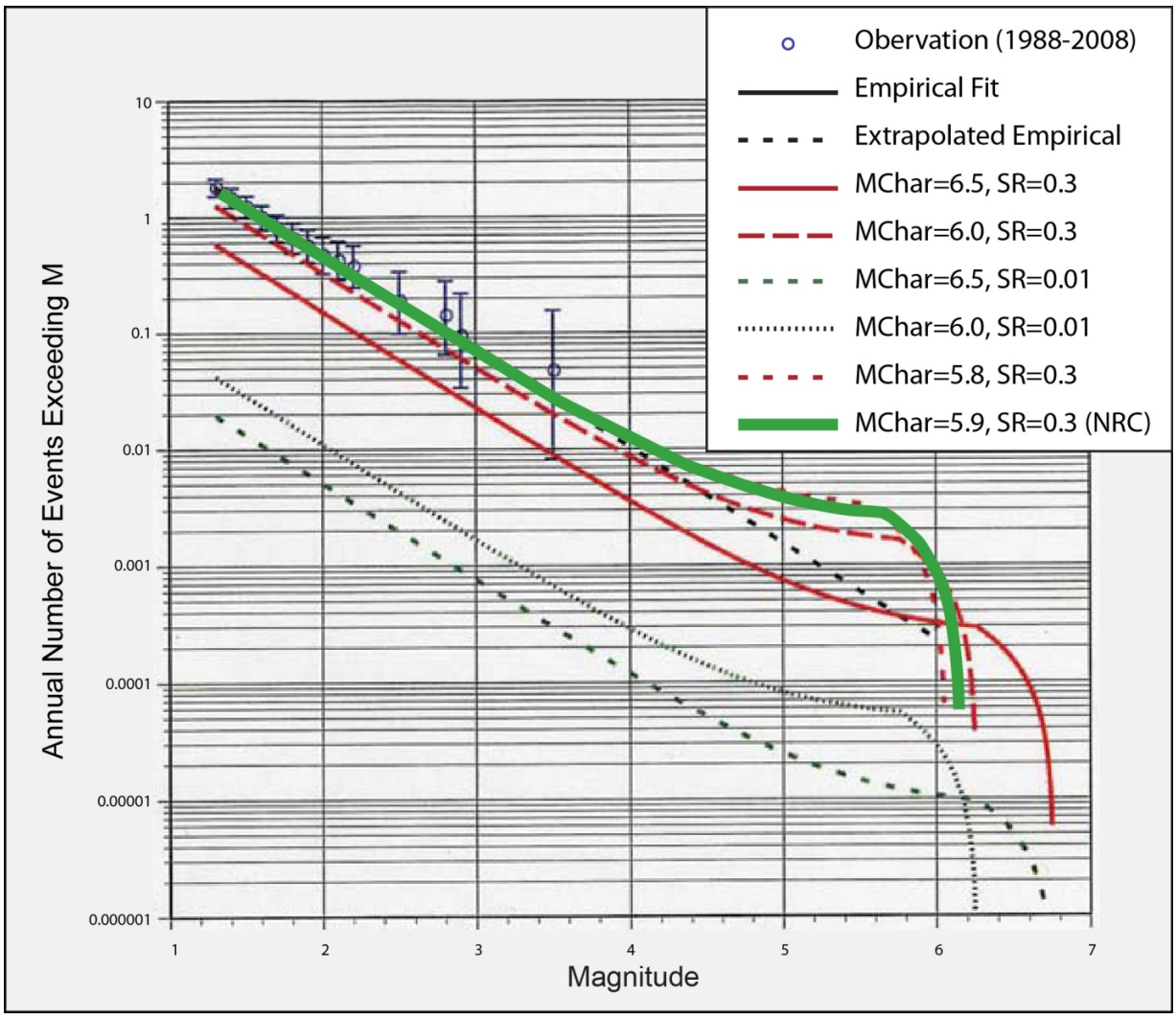

Figure 4-3 Seismicity and recurrence curves for the Shoreline fault (Figure 4-3 of the PG&E Shoreline Fault Report, annotated with the curves appropriate for a creeping fault).

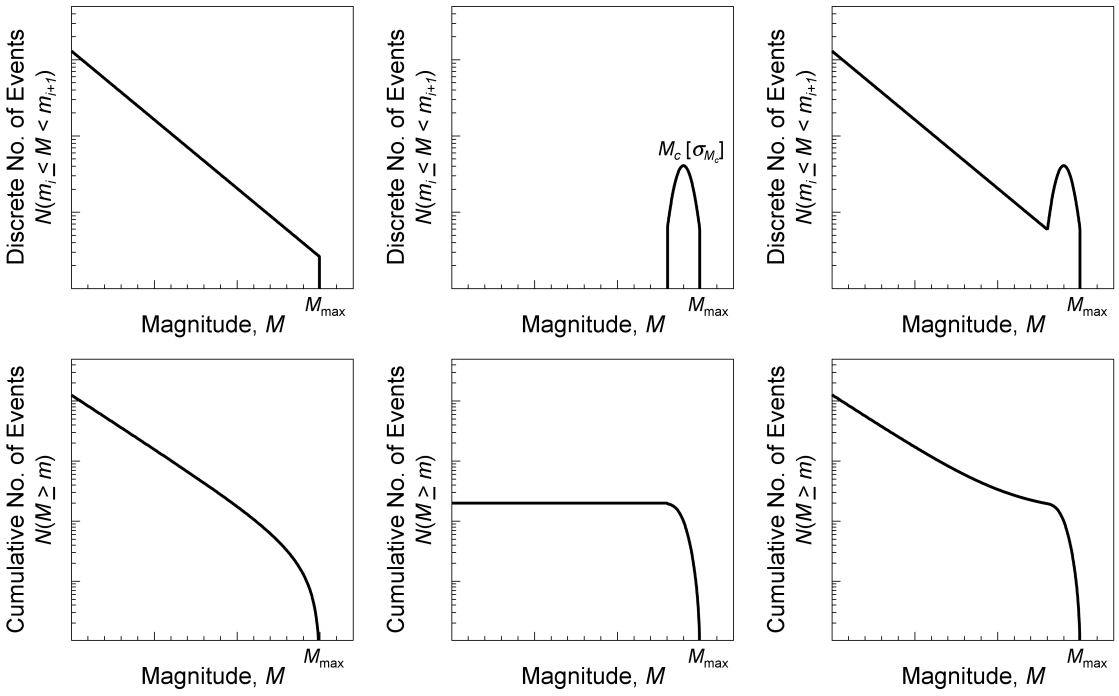

The relationships are shown in non-cumulative (*upper row*) and cumulative (*lower row*) formats. *From left to right*: Gutenberg-Richter model, maximum magnitude model, and characteristic earthquake model (from Bommer and Stafford, 2008).

Figure 4-4 Commonly used forms of magnitude recurrence curves.

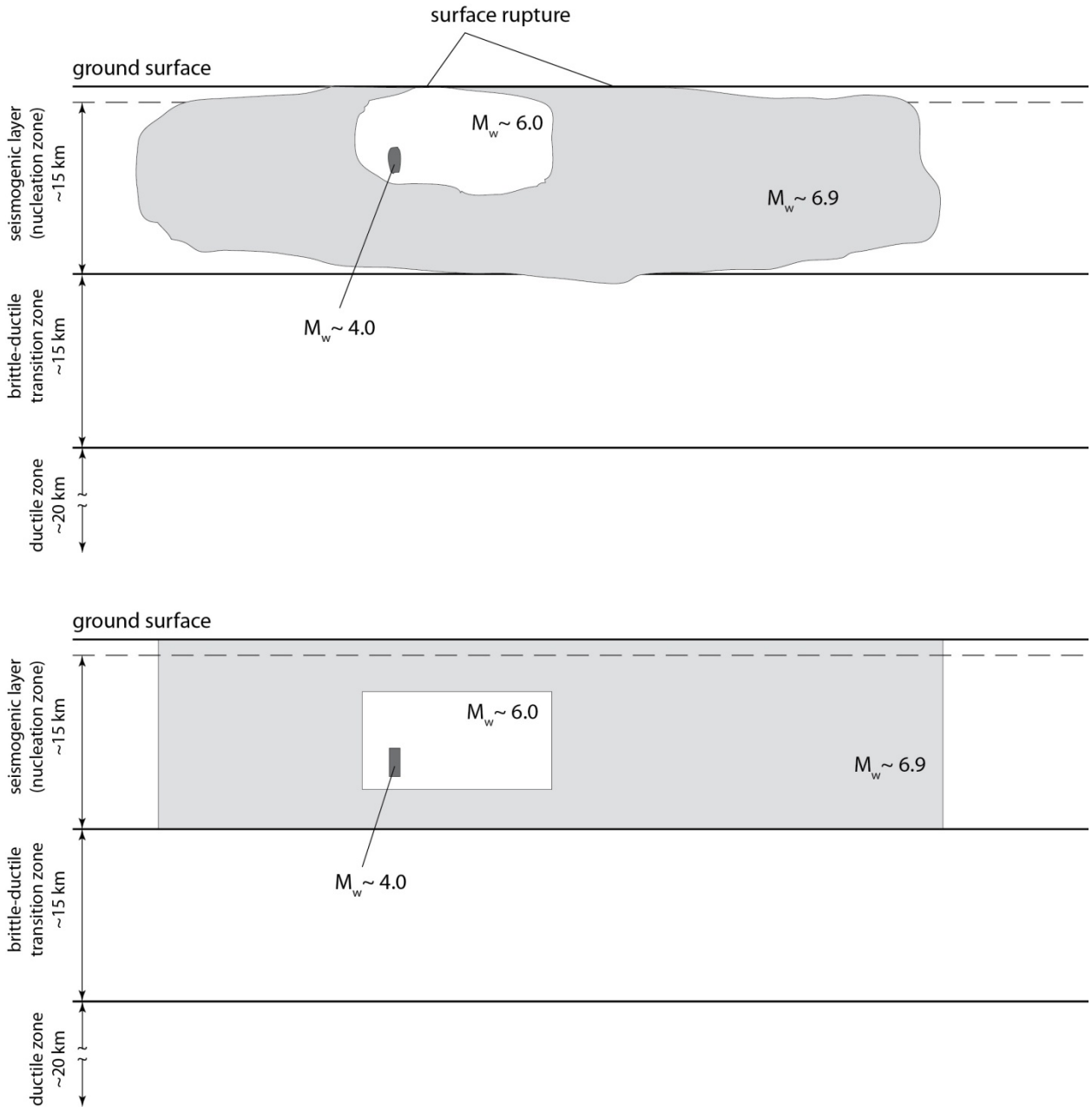

Figure 4-5 Schematic representation of typical rupture planes (above) and idealized models of rupture planes (below) for magnitude 4, 6, and 6.9 earthquakes.

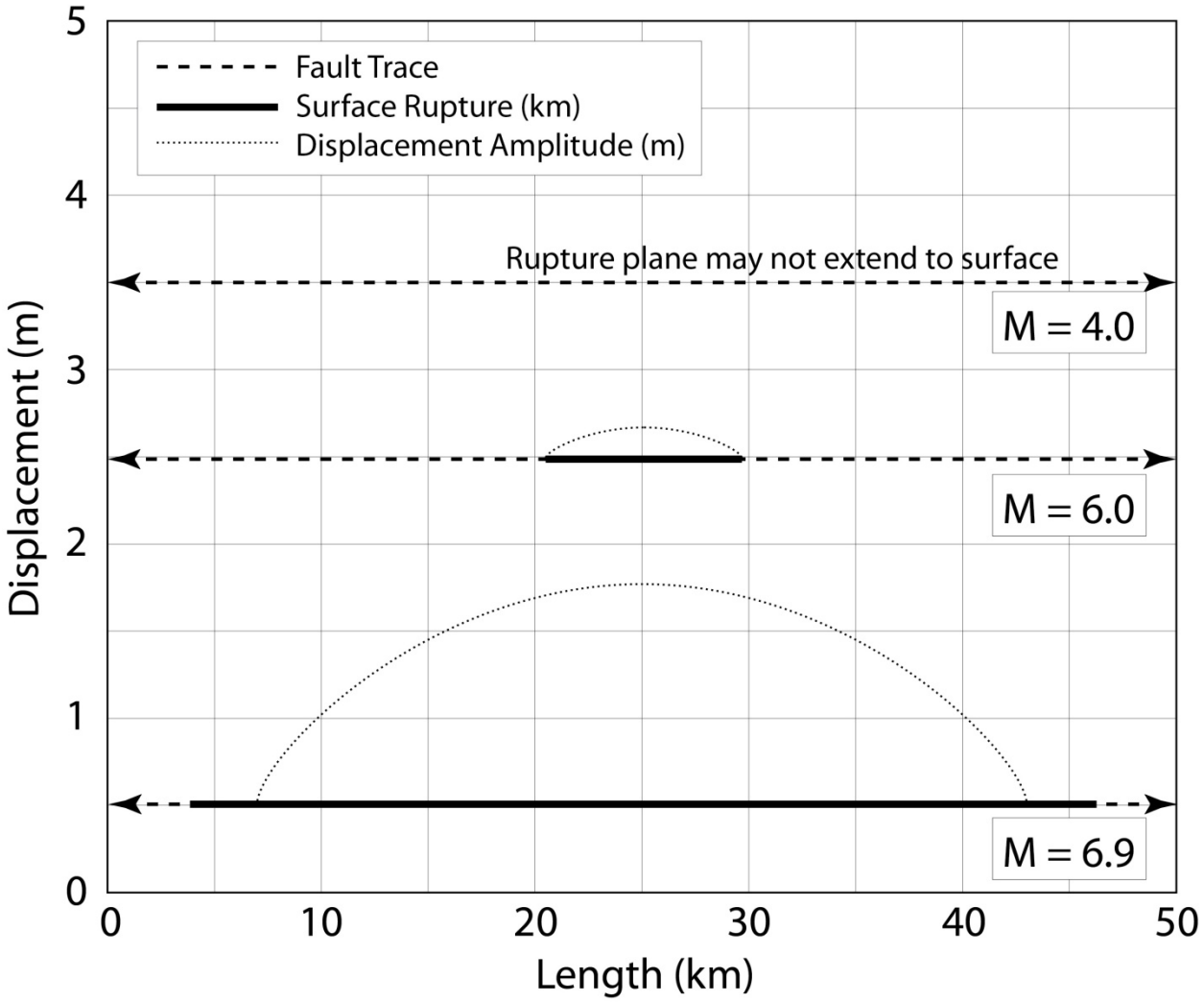

Figure 4-6 Schematic representation of typical surface rupture dimensions for magnitude 4, 6, and 6.9 earthquakes.

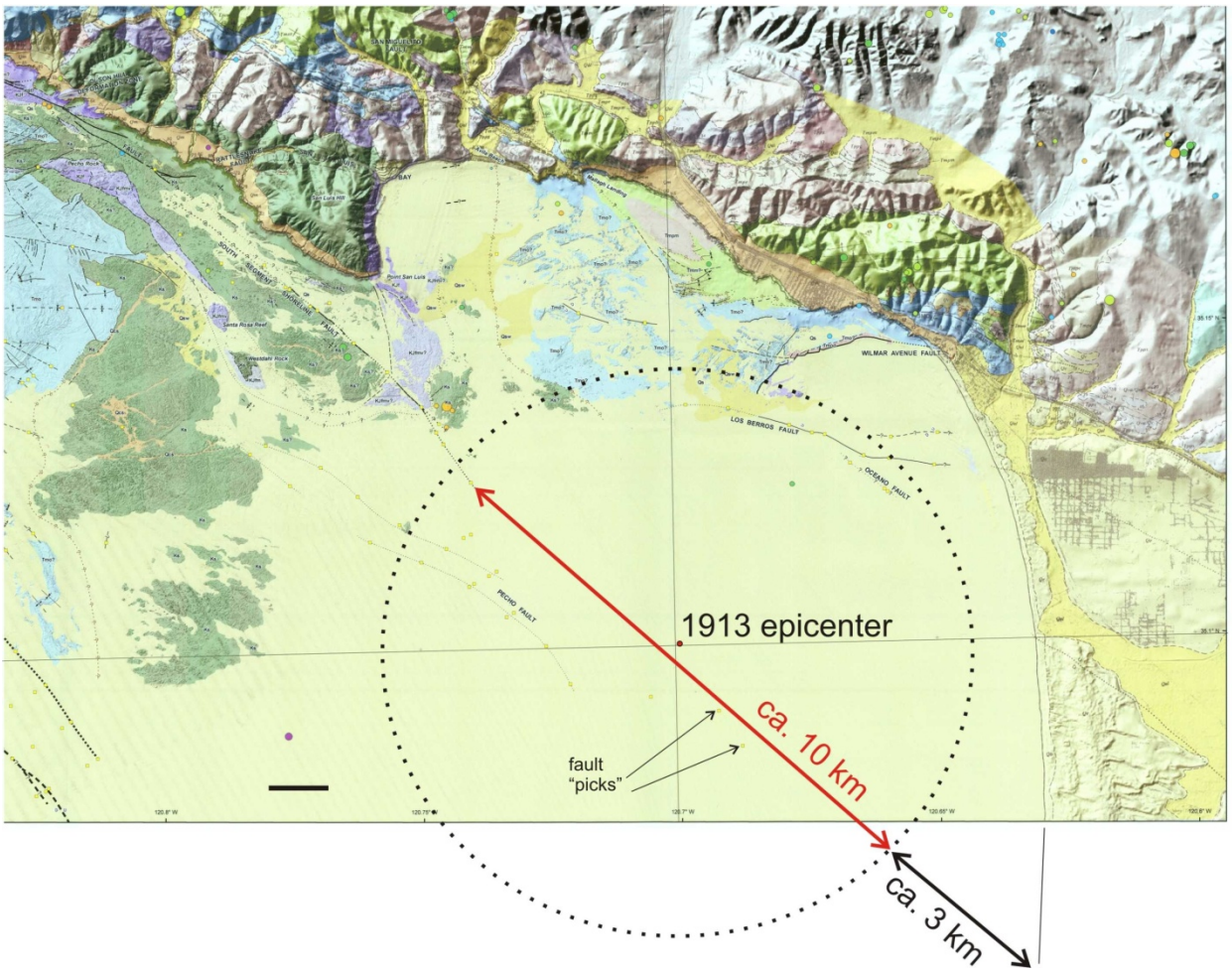

This extension lies on the magnetic lineament that defines PG&E's south segment and continues past the 1913 earthquake epicenter and past two fault "picks" from the deep seismic reflection profiles. The extension terminates at the outside uncertainty radius of the epicenter. If the fault were to continue another 3 km, it would come onshore, but no Quaternary fault is mapped there. This constraint places an upper bound of the length of the Shoreline fault at 36 km (23 km plus 13 km).

Figure 4-7 Map showing the proposed 10-km-long extension of the south segment of the Shoreline fault (red line).

5 Deterministic Seismic Hazard Assessment

5.1 Introduction to Deterministic Seismic Hazard Assessment

There are two approaches that can be used in assessing seismic hazard: deterministic and probabilistic. A DSHA typically considers a single characteristic scenario earthquake and resulting ground motion based on the largest magnitude that can reasonably be considered to occur on the fault (i.e., its maximum magnitude, M_{max}). The preceding Section described the individual earthquake scenarios that the NRC considered to be among the most technically defensible interpretations of the M_{max} earthquake for the Shoreline fault based on the available data sets. This Section describes the NRC staff deterministic assessment of the Shoreline fault.

Even if M_{max} is known, the estimated ground motions are uncertain because of the natural variability of earthquake source, travel path, and local site conditions. For example, the ground motion recordings from similar earthquake scenarios (i.e., similar magnitudes and distances) show significant scatter. As an example, Figure 5-1, shows scatter in the ground motion amplitudes for the 2004 M6.0 Parkfield earthquake as a function of distance from the fault rupture. This natural variability leads to ground motion prediction equations (GMPEs) that have not only a best estimate (median or 50^{th}-percentile) value but also a value of uncertainty defined by a standard deviation (σ), as shown in Figure 5-2. The objective of the present review was to produce an assessment of the recently acquired data and information on the Shoreline fault. As a result, the 84^{th}-percentile (median plus one standard deviation) ground motions resulting from the preferred M5.9 and M6.7 scenario earthquakes on the Shoreline fault that are described in Sections 4.3 and 4.5 are compared to the LTSP and HE ground motions. The HE ground motion response spectrum was also developed as an 84^{th}-percentile deterministic ground motion, as discussed in Section 2.

For the NRC's evaluation, a conservative deterministic approach is used to evaluate whether there is a credible challenge to the plant's licensing basis. The deterministic confirmatory analysis described herein also evaluates the adequacy of PG&E's deterministic assessment of the Shoreline fault. To perform a DSHA, a number of inputs need to be specified. These inputs, which are described in the remainder of this Section based on the data and assessments in Sections 3 and 4, include (1) the GMPEs to be used, (2) scenario maximum magnitude, (3) distance from the rupture plane to the site, (4) type of faulting, (5) near-surface shear wave velocity of the site, (6) depth to hard rock conditions, (7) dip angle of fault plane, and (8) depth to rupture. The following sections discuss each of these inputs and the way they were determined for this assessment.

5.2 Ground Motion Prediction Equations

There are two principal elements in both DSHAs and PSHAs. They are the seismic source characterization (SSC) and the ground motion characterization (GMC) models. In deterministic studies, the source characterization model defines the magnitude and location of one or more scenario earthquakes. For each scenario earthquake, a GMC model is also required to predict the amplitude of the ground motion at the site. The principal components of the GMC model are the GMPEs and their relative weights. The inputs to the GMPEs are parameters that are determined by the SSC model; the outputs are estimates of ground shaking for a specific earthquake scenario, both in terms of best estimates and uncertainty.

In active tectonic areas, these equations are generally empirically-based relationships developed from large sets of recorded earthquakes. GMPEs estimate ground motions that would occur at a site as a result of a specific earthquake scenario. They can provide information on both the most probable and the possible range of shaking that could occur at a particular site, based on the range of earthquake motions recorded in similar scenarios in the past (see Figure 5-2). As noted above, the 84th-percentile ground motion is used in the present analysis for comparison to the LTSP and HE response spectra.

The attributes of the Shoreline fault needed for input to the GMPEs are described in the following subsections. Because the GMPEs were developed using a limited dataset from a specific tectonic environment, care must be taken in choosing the appropriate GMPEs to use in any particular case. PG&E selected the recently developed set of GMPEs referred to as the Next Generation Attenuation (NGA) models[3] in its DSHA (PG&E, 2011). These GMPEs were developed for shallow crustal interplate earthquakes (such as those that occur in coastal California) during the recent NGA project managed by the Pacific Earthquake Engineering Center at the University of California, Berkeley. The details of the NGA GMPEs are documented in a special edition of the professional journal *Earthquake Spectra* published in February 2008.

5.2.1 PG&E Approach

All five of the NGA GMPEs were weighted equally in the evaluation performed by PG&E. These specific relationships were those developed by Abrahamson and Silva (2008), Chiou and Youngs (2008), Campbell and Bozorgnia (2008), Idriss (2008), and Boore and Atkinson (2008). PG&E noted that current practice assumes that epistemic uncertainty in the GMPEs is captured by including multiple models (five in this case). The process that was used in the development of the NGA models was collaborative and involved a significant amount of interaction and exchange of ideas among the developers. None the less, the level of epistemic (or knowledge-based) uncertainty could be underestimated. To compensate, PG&E added additional epistemic uncertainty in the median[4] ground motion models in its assessment following the methodology of Youngs (2009).

Although all of the GMPEs discussed above are still considered state-of-the-art, two additional site-specific ground motion modeling corrections are also included in the PG&E report. The first of these is a correction to adjust the median ground motion prediction from a generic site condition to one that is appropriate for the DCPP site. This correction is discussed in Section 5.7 and Appendix B. The second potential modification is called the single station sigma (σ_{ss}) correction.

5.2.2 NRC GMPE Approach

To perform its assessment, the NRC staff also principally relied on the NGA GMPEs, as these relationships used the most complete, consistently processed, and well-documented database currently available. The NRC chose to use four of the NGA relationships. Idriss (2008) was not used, as it does not contain predictive equations for all the spectral periods required for this assessment and is based on broad V_{S30} ranges. The NRC staff added the relationship of Graizer and Kalkan (2007, 2009) to address the potential underestimation of epistemic uncertainty noted above. This relationship used the same database as the NGA GMPEs but

---

[3] GMPEs were formerly known as “attenuation relationships.”

[4] Note that the median values predicted by the GMPE are used for this comparison to recorded data. However, in a DSHA, the higher 84th-percentile values are used to account for variability in the ground motions for a particular scenario.

was developed independently and used a unique prediction approach. All five of the GMPEs were equally weighted in the NRC assessment. Table 5-1 and Table 5-2 summarize all parameters for the five GMPEs (including those for options not used) and provide the values of the parameters used in this assessment.

Using the input parameters in Table 5-1 and Table 5-2, the NRC staff performed deterministic analyses using the GMPE relationships discussed above. Additional discussions of the inputs to the DSHA are provided in the sections that follow.

5.3 Type of Faulting Mechanism

In the past, seismologists have recognized that the faulting mechanism (e.g., strike-slip, normal, reverse, or oblique faulting, see Figure 3-1) has a statistically significant effect on observed ground motions during earthquakes. As a result, the GMPEs used in this study have all incorporated faulting mechanism as a first-order parameter. The available information on the Shoreline fault indicates a fault with a dominant strike-slip orientation (i.e., minimal reverse or normal components), and so this was the focal mechanism used in the DSHA performed by NRC staff.

A strike-slip orientation is indicated by both the focal mechanisms of recorded earthquakes on the potential fault and the physical orientation of the fault as determined by a 3D plot of the recorded earthquakes. Figure 3-9, Figure 3-10, and Figure 5-3 show the hypocentral locations of recorded earthquakes on cross section projections along and across the fault. These cross sections indicate a vertical orientation, which is only associated with a strike-slip faulting mechanism. Figure 3-11 shows the focal mechanisms of recorded earthquakes along the fault through the use of seismic “beach ball” graphs for each recorded earthquake. It can be seen that both the individual and composite (average) orientation of the recorded earthquakes have had a dominantly near-vertical orientation.

The strike-slip faulting mechanism simplified the analysis because the fault orientation parameters associated with a dipping fault are not used for the present analysis. RIL 09-001 noted that a small amount of oblique motion may become evident as additional data were obtained. However, the NRC staff identified no evidence of oblique motion or an inclined orientation in the data subsequently collected and processed.

PG&E also used a strike-slip mechanism with a weight of 1.0 in their logic trees, as indicated in Figure 5.3 of the PG&E Shoreline Fault Report.

5.4 Distance and Fault Orientation

Parameters related to distance from the fault to DCPP are also required as input to the GMPEs used for the analysis. Based on the available information, particularly the hypocenter relocations coupled with the MBES and magnetic data, the best estimate of distance at the surface is 0.6 km. This was the lower bound of the range (of 0.6 km to 1.4 km) that the NRC staff used in the preliminary study in RIL 09-001.

The various distance parameters used by the GMPEs, as shown in Figure 5-4 can sometimes be challenging to determine if complex geometries exist between the fault plane and the site. As discussed above and in Section 3, the recorded seismicity of the Shoreline fault indicates a vertical fault, which (coupled with the conservative assumption that the fault ruptures to the surface) greatly simplifies the development of the distance and fault orientation parameters. Given a vertical fault configuration with surface rupture, the distance parameters r_{JB} and r_x would

be the same as the closest distance from the site to the rupture plane, r_{rup}. PG&E also modeled the Shoreline fault as a vertical fault and used a distance of 600 m for all distance measures.

5.5 Maximum Magnitude

5.5.1 NRC Approach

The determination of maximum magnitude (M_{max}) is challenging in DSHA because the data available allow for multiple technically valid interpretations, although the evidence more strongly favors some interpretations. The approach described in Section 3 focused on developing M_{max} scenarios that were the maximum plausible or credible given the available data. Estimates of M_{max} for the five scenarios described in Section 3 are provided in Table 5-3 (using fault trace length) and Table 5-4 (using fault area). These estimates are based on the relationships developed by Wells and Coppersmith (1994) and Hanks and Bakun (2002). The relationships that apply to the potential Shoreline fault are the Wells and Coppersmith (1994) equation for strike-slip earthquakes:

$$M = (1.02 \pm 0.03) logA + (3.98 \pm 0.07) \quad \text{Equation 5.1}$$

and the Hanks and Bakun (2002) relationship (for A ≤ 537 km^2):

$$M = logA + 3.98 \pm 0.03 \quad \text{Equation 5.2}$$

The parameter *A* is the area of the rupture plane in km^2 in both relationships. As a clear upper limit, the NRC concludes that M_{max} cannot be larger than M6.9 because events of this size clearly would produce observable evidence of surface deformation. There is no evidence of major seafloor surface rupture above the threshold of detection on the bathymetric images, which is 1 to 2 m. Therefore, no earthquake larger than that associated with a rupture of 1 to 1.5 m could have occurred in the late Quaternary (ca. 75 ka). According to the strike-slip fault analysis of Wells and Coppersmith (1994), a maximum displacement of 1 m correlates to an earthquake of M6.8 and a maximum displacement of 1.5 m correlates to an earthquake of M6.9. As described in Scenario 5 (Section 4.3), the magnetic anomaly that the south segment of the fault follows, continues southeast at least another 5 km, and the 1913 earthquake, which PG&E speculated might have been on the Shoreline fault, increases the trace length to 33 km. According to Wells and Coppersmith (1994), a surface rupture 33 km long correlates to an earthquake of M6.9. Any fault length greater than 33 km, and thus capable of generating a larger earthquake, would have to extend onshore on the opposite side of the bay where evidence of faulting would be seen. These two lines of field evidence suggest that M_{max} cannot exceed M6.9. While this line of reasoning is informative and provides a clear upper boundary for M_{max}, use of this scenario is not supported by the data, and the NRC staff determined that using M6.9 in a DSHA is speculative and not supported by the currently available observations.

It is the judgment of the NRC staff that a more realistic, though still highly conservative, upper bound is M6.7 which is the M_{max} that results from Scenarios 3 and 4 as described in Section 4. This is the highest magnitude that is still reasonably consistent with the data. Analyses were also performed using the M5.9 earthquake, which is the largest magnitude the staff assigned to Scenario 1, and one that is also well supported by the data. By using these two magnitudes (i.e, M5.9 and M6.7), the NRC staff assessment provides a reasonable representation of the range of maximum magnitudes that resulted from the evaluation described in Section 4.3. The

two values were not weighted but rather were reviewed jointly to gain insights. The M6.7 scenario earthquake was used as a "best estimate" for purposes of assessing the safety of the DCPP.

A best estimate of M_{max} of 6.4 was used in the 2009 NRC preliminary analysis detailed in RIL 09-001, and a magnitude range of 6.25 to 6.85 was analyzed. Therefore, the range of values used in the current assessment is similar to those used in the earlier, preliminary review but is somewhat lower, due to a reduction in uncertainty because of the more complete and mature dataset now available.

5.5.2 PG&E Approach

To determine M_{max} for its DSHA, PG&E coupled the logic tree discussed in Section 5 of its Shoreline Fault Report with Wells and Coppersmith (1994) and Hanks and Bakun (2002), the same area-to-magnitude relationships used by the NRC staff. PG&E gave these relationships weights of 0.3 and 0.7, respectively. The standard error term was also applied. As a result, PG&E used a value of M6.5 in its DSHA because this value represented the 90^{th} fractile of the mean characteristic magnitude from the logic tree.

The value of M_{max} used in the NRC deterministic assessment is conservative relative to the PG&E DSHA value (M6.7 vs. 6.5). Given the intended purpose of this assessment (to evaluate if a credible challenge to the plant licensing basis exists), the NRC staff concludes the conservative M_{max} value of 6.7 is appropriate in the DSHA. However, Staff notes that this single value would not be appropriate for use as a "best-estimate" in a PSHA, in which the full range of alternatives are considered.

5.6 Assessment of Regional and Site Properties

To assess potential ground motions at a site, three general elements should be considered: the seismic source (the fault), the large-scale path through which the waves travel (the crustal model), and site geologic materials, which includes the basement rock and the near-surface materials. Most of the information in the earlier sections relates to the regional tectonic setting and the source parameters of the Shoreline fault. The GMPEs address the regional propagation of waves from the source to the site. The techniques for incorporating the effect of the geologic materials that underlie the site are equally important to the assessment of seismic hazard because of their amplification or de-amplification of seismic waves that enter the site. For soil sites, GMPEs can incorporate the surficial site properties directly, or the shear wave velocity at an appropriate (rock) horizon can be used coupled with other classical geotechnical site response techniques. For rock sites, such as DCPP, both the near-surface and basement rock properties may be considered and incorporated in the analyses. The NRC included the effect of both the near-surface and basement rock properties in its assessment.

5.6.1 Introduction to Shear Wave Velocity, V_S

A principal parameter used in assessing site response is shear wave velocity (V_S), which is the velocity at which shear waves travel through geologic materials. In addition to being a direct measure of an important property, V_S also acts as a general proxy for the stiffness of geologic materials and is used to place materials into categories such as "rock" or "soil." Shear wave velocity is used as a first-order parameter in the GMPEs because the stiffness of geologic materials underlying a site is important in predicting ground motions at the surface. A V_S profile is used to determine V_{S30}, the average shear wave velocity in the top 30 m (approximately 100 feet) of a site. The shear wave velocity profile may also be used to obtain the parameter noted as $Z_{1.0}$, the depth to where a shear wave velocity of 1,000 m/s is reached (where the

depth is expressed in meters). $Z_{2.5}$ is a similar parameter for 2,500 m/s that is used to address effects associated with geologic basins, which can have significant effects on incoming ground motions.

5.6.2 Shear Wave Velocity Properties under Containment in RIL 09-001

For the preliminary review discussed in RIL 09-001, the NRC staff determined input shear wave velocity profiles under the containment structure of the DCPP, using Figure 5-3 and Figure 5-5 of the Diablo Canyon LTSP Report (which were based on the original 1970s data). These figures, with additional annotation by the NRC staff, are provided as Figure 5-5 and Figure 5-6 in this document.

Typically, shear wave velocity profiles are recorded in the free field. During construction, the excavation and construction processes may affect the V_S properties. For this study, the NRC staff assumed that a compensated foundation exists (i.e., the weight of the structure is approximately equal to the weight of material removed) and that the V_S profile preconstruction can be used for the post-construction values.

Using Figure 5-6 and accounting for the foundation depth, in the 2009 study, the staff determined that the best estimate of V_{S30} at the site was 1,100 m/s and the best estimate of $Z_{1.0}$ was 0 m, as shown in Table 5-5. The upper and lower bound values used in the parametric study in RIL 09-001 are also shown in the table. Information to directly determine $Z_{2.5}$ was not available. As a result, the staff used the estimation techniques described in Campbell and Bozorgnia (2007).

The equations provided (where all depths are in km) are as follows:

$$Z_{2.5} = 0.519 + 3.595Z_{1.0} \qquad \sigma_Z = 0.711 \qquad \text{Equation 5.3}$$

or

$$Z_{2.5} = 0.636 + 1.549Z_{1.5} \qquad \sigma_Z = 0.864 \qquad \text{Equation 5.4}$$

Figure 5-6 shows that $Z_{1.5}$ (the depth to 1.5 km/s) is 40 m in the best-estimate profile. Because higher values of $Z_{2.5}$ are conservative and, functionally, any value between 1.0 km and 3.0 km is treated the same in the GMPE, the default value of 2 km provided by Campbell and Bozorgnia (2007) was used.

5.6.3 Comparisons of Shear Wave Velocity Properties from 1978 and 2010 Site Investigations

The NRC's results from the parametric study described in RIL 09-001 indicated that the site characteristics (V_{S30}) represented the single biggest source of uncertainty in the results of the study. Therefore, at the NRC staff's request, PG&E subsequently provided the NRC with updated digital V_S data that were collected for the design of the DCPP independent spent fuel storage installation (ISFSI) in 2010, which is shown in Figure 5-7. The ISFSI is located approximately 400 m away from the power block, and with a significant elevation difference, but it is seated on the same rock layer as the power block. The relative locations are shown in Figure 5-8 and can also be seen in Figure 3-6.

Since the original DCPP site investigation in 1978, methods and equipment used for measuring shear-wave velocities have improved significantly. Therefore, when the ISFSI was being licensed, the NRC staff requested that a new down-hole test be conducted at the DCPP ISFSI

for determining V_{S30} in order to minimize the uncertainty in the ground motion assessment. Four borings were drilled in 1998: two borings each at two different locations. Borings 98BA-1 and 98BA-4 were drilled adjacent to each other at one site. The other two 1998 borings (98BA-2 and 98BA-3) were drilled at the ISFSI pads adjacent to each other. Both 98BA-2 and 98BA-3 were cored, but 98BA-2 had to be abandoned before reaching target depth when the drill casing broke off. Down-hole tests were conducted for borings 98BA-1, 98BA-4, and 98BA-3.

Using the ISFSI data, the NRC performed a review comparing the shear-wave velocity profiles obtained for the DCPP in 1978 to those of the DCPP ISFSI profiles collected in 2010, as shown in Figure 5-7. The objective of the analysis was to develop a best estimate of V_{S30} from the data obtained in 2010 using current methods and state-of-the-art equipment, and then to compare the results of the new study against the results of the 1978 study, which the NRC staff used in the preliminary analysis described in RIL 09-001.

Although the data were collected at different locations, the results of the NRC review show that the V_{S30} values obtained in 2010 agree well with those from 1978. The 1978 down-hole survey that PG&E conducted for the powerblock resulted in a V_{S30} value of 1,212 m/s. ISFSI Borings 98BA-1 and 4 were averaged, resulting in a V_{S30} value of 1,228 m/s and 98BA-3 resulted in a V_{S30} of 1,215 m/s. As a result of this review, a value of 1,200 m/s was used in the NRC DSHA, which is slightly higher than the estimate of 1,100 m/s used by the NRC staff in RIL 09-001. The same $Z_{1.0}$, and $Z_{2.5}$ values were used in this new study. These values are summarized in Table 5-5.

5.7 Incorporation of Site Properties

5.7.1 Introduction and Discussion of the PG&E Approach

As noted above in Section 5.6, the geologic materials underlying a site have a significant effect on amplification and de-amplification of seismic waves as they approach the surface. The V_{S30} parameter is, by definition, a measure of the material properties in the top 30 m of geologic materials, which often have a significant impact on the response. However, the materials below 30 m are also important, particularly for rock sites that do not have any overlying soil cover. Kappa (κ_0) is an upper crustal site ground motion attenuation parameter that accounts for the overall damping in the basement rock immediately beneath a site. The properties and behavior of the upper few hundreds of meters of the crust has been shown to produce as much as 50% or more of the total attenuation of the high-frequency portion of the ground motion spectrum (Abercrombie, 1997; Anderson and Hough, 1984). The value of kappa influences the shape of the ground motion spectrum observed at a given site. High values of kappa result in enhanced attenuation of the high-frequency portion of the spectrum.

Kappa is a site-specific property that can be determined by either using seismograms recorded at the site of interest or from correlations with other site properties such as V_{S30}. Generally, the harder the rock (i.e., the higher the V_{S30}), the lower the κ_0 value; however, this is not universally true. Kappa values of <0.01 to 0.02 s have been observed or estimated for hard rock sites (i.e., V_{S30} values greater than 1,100 m/s). However, considerable scatter in these estimates has been documented (VanHoutte et al., 2011, Douglas et al., 2006, Silva, 1999).

GMPEs are developed from statistical regression of a database of seismograms recorded on sites with different geologic properties. As such, the limitations of the regressions must be considered. Generally, the rock underlying the DCPP is harder than in a typical interplate region, and so it is harder than the rock under the majority of the seismic stations from which the earthquake recordings were collected for the NGA GMPE development project. The average

V_{S30} parameter for the database of earthquake recordings used in the NGA GMPE development project is less than 400 m/s. Only a very small percentage of the recordings in that dataset are from sites with V_{S30} values of 900 m/s or higher. Of the 3551 recordings in the NGA-West PEER data base (http://peer.berkeley.edu/smcat/) available at the time of the development of the GMPEs, there are only 51 recordings with sites defined with V_{S30} >= 900 m/s. This is less than 1.4% of the data base. There are only 15 records with V_{S30} >=1,200 m/s (less than one-half of one-percent). Of these, only 11 are actually measured values from close to 30 m in depth (the rest are "inferred"). As noted in Section 5.6.3, the measured V_{S30} value for DCPP is approximately 1,200 m/s. Hence, applying a V_{S30} of 1,200 m/s directly in the GMPEs increases uncertainty, as this value is outside the range well constrained by the observational data.

A significant amount of work went into the development of the V_{S30} amplification factors for the NGA GMPEs because of the well-recognized importance of near-surface site response on observed ground motions (Chiou et al., 2008; Walling et al, 2008). As noted above, sites with V_{S30} values of 900 m/s or higher are rare in the current observational database and so ground motions predicted at hard rock sites are extrapolated resulting in additional uncertainty. For very hard rock sites, an alternative technique to the direct application of high V_{S30} in the GMPEs is to estimate ground motions for a soft-rock site condition where the data constraints are more robust and then to adjust these ground motion values based on the relative amplification (or de-amplification) as estimated using site response analyses. This latter technique, analogous to commonly used techniques for soil response, was employed by PG&E in the Shoreline Fault Report.

As part of the NGA project, Silva (2008) (further documented in Walling et al., 2008) conducted a study to develop frequency-dependent amplification factors using the equivalent linear method to constrain nonlinear soil response for use in the NGA GMPEs. A broad range of site conditions (V_{S30} between 160 and 900 m/s and variable soil depths) were used to directly determine V_{S30} amplification values in that study. One of the target V_{S30} values used in the study was 760 m/s. The input rock motion in the Silva (2008) study assumed a particular near-surface shear wave velocity (1,130 m/s) and kappa value (κ_0=0.04 sec). Hence, the resulting amplification values are relative to the assumed input rock conditions of V_{S30} of 1,130 m/s and κ_0 of 0.04 sec.

In the Shoreline Fault Report, PG&E estimated ground motions for a reference site condition of 760 m/s and then applied the shear-wave velocity correction factors from the Silva (2008) study. These correction or amplification factors (contained in Table 5-6 of this report) can be used with computed median ground motion estimates for a soft-rock site to develop appropriate ground motion estimates for a site with hard rock conditions (1,130 m/s, for example) following:

$$S_{a,1130}(T) = S_{a,760}(T) \cdot \exp[a_1(T)] \qquad \text{Equation 5.5}$$

where $S_{a,760}(T)$ is the median term from the GMPE computed assuming V_{S30} equal to 760 m/s and $a_1(T)$ is the amplification term (Table 5-6). After the site response correction is made to the median ground motion estimate, the 84th-percentile value is obtained by multiplying the median by $\exp(\sigma)$.

The Silva (2008) study estimated an average κ_0 value of 0.04 s for generic California soft-rock sites contained in the NGA database. The analysis conducted by PG&E (2011) estimated a site-specific κ_0 value of 0.045 s using a single recording from the 2003 M3.9 earthquake that occurred approximately 4 km from DCPP in Deer Canyon (described in Appendix L of the Shoreline Fault Report). The similarities in this κ_0 value and the assumed basement rock velocities were used by PG&E as justification for application of the correction factors of Silva

(2008) in the Shoreline Fault Report. PG&E did not use the direct application of V_{S30} in the GMPEs in its analyses.

5.7.2 NRC Assessment and Incorporation of Site Response

The NRC staff recognizes that it is possible to simply input the observed V_{S30} values for a hard rock site, such as the DCPP site, directly into the selected GMPEs to estimate spectral accelerations ($S_a(T)$). However, the NRC concluded that this approach has serious limitations. Because the ground motions estimated using the V_{S30} directly in GMPEs are heavily influenced by data from sites with lower shear wave velocities (through the regression process), it is reasonable to conclude that some bias may be introduced in the results for sites with high V_{S30}. Specifically, the resulting spectral accelerations and hence the shape of the response spectrum may not be representative of the ground motions at the site of interest. As a result, the NRC staff concluded that the shear-wave velocity correction approach taken by PG&E, which uses site-specific observations, is the most appropriate methodology for estimating the potential ground motions at the DCPP.

To develop additional insight, the NRC staff compared ground motions observed at DCPP to those recorded at Point Buchon (the closest seismograph site to DCPP sited on rock) and to the ground motions predicted by one of the five GMPEs described in Section 5.2. Figure 5-9 compares the ground motions from the Point Buchon and DCPP sites for the 2003 M6.5 San Simeon earthquake and Figure 5-10 provides a similar comparison for the 2004 M6.0 Parkfield earthquake. DCPP and Point Buchon are located at almost identical distances from each of these two earthquakes. The Point Buchon site is considered a "soft-rock" site and has a lower near-surface velocity (~515 m/s) than does DCPP (~1,200 m/s). Both Figure 5-9 and Figure 5-10 illustrate the significantly lower ground motion amplitudes for high spectral frequencies observed at DCPP relative to both Point Buchon and to the median GMPE results of Graizer and Kalkan (2009) obtained using a V_{S30} of 1,200 m/s directly in the equation. Because of the increased high-frequency ground motions observed in the Point Buchon recordings (which is a softer rock) relative to the DCPP recordings at virtually the same distance, the NRC staff concluded this difference in relative spectral amplitudes at high frequencies is a function of the DCPP site conditions and not a characteristic of the earthquake source(s).

Figure 5-11 and Figure 5-12 present comparisons of the same DCPP recordings and the median ground motion prediction results of Graizer and Kalkan (2009) for two cases. One incorporates the shear-wave velocity based site response correction factors of Silva (2008) assumed for the site presented in Table 5-6 and described in Section 5.7.1, while the other uses V_{S30} directly in the GMPE. It can be seen that, in this instance, the site response based correction factors provide better agreement between the observations and the median[5] estimates, particularly for the high-frequency portion of the spectrum.

The near-surface shear wave velocities at the DCPP site are relatively high (~1,200 m/s). There are few ground motion recordings available to constrain the GMPEs in this velocity range. As described above, the approach taken by PG&E in the Shoreline Fault report was to estimate ground motions for a V_{S30} value where sufficient data exists (760 m/s in this case) and then apply correction factors to the median GMPE results to render them applicable to the higher velocity conditions of the DCPP site. The NRC staff considers this approach to be reasonable. However, the applicability of the specific correction factors applied requires additional discussion and justification.

---

[5] Note that the median values predicted by the GMPE are used for this comparison to recorded data. However, in a DSHA, the higher 84th-percentile values are used to account for variability in the ground motions for a particular scenario.

In the view of the NRC staff, the applicability of these correction factors for the DCPP site is determined by two issues. First, the development of the factors utilized a simple seismological model that assumed a specific value of 0.04 s for the kappa (κ_0) factor. Is the κ_0 value used by Silva (2008) appropriate for the DCPP site? Using the 1,200 m/s V_{S30} value for the DCPP site in the published kappa-shear wave velocity correlations suggests a κ_0 value of 0.01-0.03 s (Van Houtte et al., 2011). As noted above, PG&E estimated a value of 0.045 s for kappa at the DCPP site based on a single recording of a relatively small earthquake. Based on the similarity in kappa values used in the Silva (2008) study (0.04 sec) and that estimated for the DCPP site, PG&E concluded the Silva (2008) factors could be applied directly. NRC staff note that one source of the uncertainty in the kappa estimated for a site based on a specific recording is a result of the inherent tradeoff between the true kappa and the stress drop of the earthquake (Boore et al., 1992).

Second, PG&E (by incorporating the Silva (2008) results) used an approach that utilized a generic velocity profile with randomization of the near-surface velocity structure applied to develop the amplification factors. While this may be an acceptable approach for sites with little or no available data, NRC staff feels adequate data exists at DCPP to develop site-specific amplification factors. Further, the base rock velocity condition used in the Silva (2008) study (V_S =1,130 m/s) differed slightly from the 1,200 m/s documented in Section 5.6.3 for the DCPP site.

Based on these two issues, the NRC staff used the available data and developed an independent set of DCPP-specific correction factors for use in the present assessment. The development of these factors is described more completely in Appendix B: . Two slightly different approaches were employed. The first used DCPP velocity profiles and a time series-based response analysis to produce correction factors (ratios between DCPP-specific and generic 760 m/s response spectra) that would be applied to the median GMPE results using the process described in 5.7.1. The second approach used a response analysis based on the use of random vibration theory (RVT) to develop the correction factors (Silva et al., 1997 and McGuire et al., 2001). The resulting correction factors are compared to the factors employed by PG&E in Figure 5-13 and summarized in Table 5-7. The results are generally similar, with the NRC results being conservative relative to the PG&E results at nearly all spectral frequencies.

5.8 Deterministic Results for the Baseline Case

A series of 84th-percentile deterministic ground motion response spectra were calculated using M5.9 and M6.7 earthquake scenarios with the five GMPEs discussed in Section 5.2, the suite of input parameters that are summarized in Table 5-1 and Table 5-2 and the site correction factors shown in Table 5-7. The deterministic analysis results are compared to the LTSP and HE ground motion response spectra in Figure 5-14. The results for the NRC scenarios with the DCPP response correction factors applied are consistent with or below the LTSP and Hosgi spectral values at all frequencies.

When performing a seismic hazard assessment, appropriately accounting for both epistemic and aleatory uncertainty is important. Epistemic, or model uncertainty, results from a less-than-perfect knowledge of the phenomenon to be modeled. Aleatory variability, which is sometimes called aleatory uncertainty, is the inherent randomness in nature. The relative importance of these uncertainties for this assessment are illustrated in Figure 5-15, Figure 5-16 and Figure 5-17. Figure 5-15 compares the 84th-percentile results from each of the five GMPEs used in this assessment for the M6.7 scenario and Figure 5-16 does the same for the M5.9 scenario. The spread in GMPEs is representative of the epistemic uncertainty in the GMPEs, which tends to be higher in the magnitude-distance ranges with sparse available seismological data (such as

large magnitudes at short distances). Generally, the GMPEs are the largest source of uncertainty in the ground motion values produced in seismic hazard analyses. Figure 5-17 shows a comparison of the predicted median and 84th-percentile spectra for the M5.9 and M6.7 scenario earthquakes occurring on the Shoreline fault. Both the median and the 84th-percentile ground motions are shown to provide insight into the aleatory variability of ground motions for each of the two scenarios. Note that there is a smaller difference between the two magnitudes than between the median and 84th-percentile motion for each of the magnitudes. This is partly due to the inherent natural variability in ground motions for a single earthquake, as shown in Figure 5-1 and partly because of the very close distance to the fault. In both cases, the ground motion is heavily dominated by the portion of the fault closest to the site and the additional rupture length of fault further away contributes increasingly less to the hazard at the site.

In summary, based on the results shown in these figures, the NRC staff's assessment is that the 84th-percentile deterministic seismic-loading levels predicted for the Shoreline fault produce ground motions that are at or below those levels for which the plant was evaluated previously and demonstrated to have reasonable assurance of safety. The uncertainty in the DSHA is dominated by the uncertainty in site response and the aleatory variability in the ground motion predictions for a given magnitude. Taking the results of the deterministic analyses as a whole and the current level of uncertainty, the Shoreline fault is very unlikely to produce ground motions that exceed those for which the plant has already been analyzed.

5.9 Single Station Sigma Correction

In the past, uncertainty in GMPEs was addressed through the use of a single term, σ. This parameter accounts for both the epistemic (model) uncertainty and the aleatory (natural) variability. More recently, an effort was made to separate the uncertainty into its component parts, including the uncertainty that comes from the seismic source, the path through which the waves travel in the crust, and the site response. If high-quality data from a modern seismographic network are available, some of the uncertainty for a specific location can be reduced. The single-station-sigma, σ_{ss}, adjustment has the potential to remove uncertainty in the application of the GMPEs by determining a station term from a set of earthquakes recorded at the site.

The single-station-sigma adjustment represents advancement in the field of engineering seismology and could be a useful approach in the assessment of seismic hazard at NPPs that install a modern seismographic system, such as that at DCPP. The single-station-sigma correction applied by PG&E was developed based on data from two earthquakes. Generally a larger number of earthquakes would be needed to develop confidence in the correction factor. This correction was applied by PG&E but was not required for the confirmatory analysis that the NRC conducted. Nevertheless, the analysis performed by PG&E provides a strong proof-of-concept. The NRC staff recognizes the importance of the Central California Seismic Network (CCSN), because it has provided the data required for development and application of the site-specific amplification correction and for the single-station sigma correction for the DCPP site.

5.10 Regional Tectonics and Other Faults of Interest

Although this RIL focuses on the Shoreline fault specifically, PG&E's Shoreline Fault Report also discussed and analyzed several other regional faults of interest. While the faults in the DCPP region were originally investigated in the 1970s, during the mid-to-late 1980s, a significant additional effort went into characterizing the regional faults specifically for the DSHA

and PSHA performed as part the LTSP, as described in the final LTSP report (PG&E, 1988 and 1991). The discussions of the regional faults in the Shoreline Fault Report provide an update of that earlier information based on the new data.

As discussed in Section 2, the LTSP study in the 1980s determined that the Hosgri seismic zone remained the dominant seismic source. Based on the new information provided in the Shoreline Fault Report, PG&E demonstrates that the Hosgri fault continues to be the dominant seismic source for all structural frequencies of interest (see Figure 5-18 through Figure 5-20). Figure 5-18 through Figure 5-20 demonstrate that the identification and characterization of the Shoreline fault has not substantially altered existing conclusions regarding the seismic hazard estimates at the DCPP site.

The HE ground motion response spectrum was developed using a specific deterministic scenario (i.e., M7.5 at 5 km) and the GMPEs that existed in the 1970s. Since that time, GMPEs have improved based on the acquisition of new data. Current GMPEs now predict amplitudes of ground motion for the HE scenario that are lower than the HE response spectrum. However, it is important to understand that the HE ground motion response spectrum, which is part of the licensing basis, does not change. Once ground motion response spectra are developed through a seismic hazard analyses and incorporated into licensing, they are defined only in terms of ground motions and do not remain tied to the faults and scenarios from which they were derived.

Based on NRC's evaluation of the information in the Shoreline Fault Report, none of the local faults is capable of producing ground motions that challenge the licensing basis of the plant in a deterministic framework. Within a probabilistic framework, the relative importance of each of the regional faults to the seismic hazard at the DCPP site, as well as the overall hazard, will be estimated through the SSHAC Level 3 PSHA study currently underway for the DCPP (see Section 6).

5.11 Summary of Deterministic Seismic Hazard Assessment

This Section discusses various aspects of DSHA, including the parameters used in the NRC staff's analysis and the results. The key information in this Section can be summarized as follows:

- Based on the scenarios in Section 4, the NRC staff performed a DSHA for two different magnitude earthquakes, each assumed to occur 600 m from DCPP on a vertical strike-slip fault. These earthquake scenarios, with magnitudes M5.9 and M6.7, were chosen to represent the scenarios developed in Section 4 that are most consistent with the available data.
- Due to the availability of appropriate data at the DCPP site, NRC staff developed site-specific amplification factors for use in the present assessment.
- The ground motion spectra resulting from the NRC staff's DSHA are at or below the HE and LTSP ground motion spectra for which the plant was evaluated previously and demonstrated to have reasonable assurance of safety. Therefore, the Shoreline fault, as characterized by the NRC review, does not challenge the current licensing basis.
- Contained within the PG&E analyses are new concepts that address site-specific information and uncertainty. Corrections for hard rock damping, near-surface amplification, and single-station-sigma, σ_{ss}, were applied by PG&E. The NRC staff developed and applied the amplification correction factor as well, supported by an

evaluation of earthquakes recorded at DCPP. The analyses by PG&E served as a useful proof-of-concept and the use of both near-surface amplification and σ_{ss} correction factors should be encouraged and further developed.

Table 5-1 Parameters for the NGA models and parameter values used in this study.

Input Parameter	Parameters used in GMPEs				Parameter Values Used in This Study
	AS 08	BA 08	CB 08	CY 08	
Moment Magnitude	M	M	M	M	Magnitudes 5.9 and 6.7 were analyzed
Depth to top of rupture (km)	Z_{TOR}		Z_{TOR}	Z_{TOR}	Assumed to be 0 km (surface rupture)
Reverse style-of-faulting	F_{RV}	RS	F_{RV}	F_{RV}	Strike slip assumed; flag not applied
Normal style-of-faulting	F_{NM}	NS	F_{NM}	F_{NM}	Strike slip assumed; flag not applied
Strike-slip style-of-faulting		SS			Strike slip flag applied
Unspecified style-of-faulting		US			Strike slip assumed; flag not applied
Aftershock flag				AS	Main shock desired; flag not applied
Dip (degrees)	δ^a		δ^a	δ^a	Not used for vertical strike slip faults
Down-dip rupture width (km)	W^a				Not applied. Used for hanging-wall scaling only.
Closest distance to the rupture plane (km)	r_{rup}		r_{rup}	r_{rup}	Best estimate of 0.6 km
Horizontal distance to the surface projection of the rupture (km)	r_{JB}	r_{JB}	r_{JB}	r_{JB}	For BA08 assumed to be same as r_{rup} based on vertical faulting. Not applied to other models as only used for hanging wall scaling.
Horizontal distance to the top edge of the rupture measured perpendicular to strike (km)	r_x			r_x	Not applied. Used for hanging-wall scaling only.
Hanging wall flag	F_{NM}			F_{NM}	Not applied, due to assumption of vertical strike-slip faulting
Average shear wave velocity in the top 30 m (m/s)	V_{S30}	V_{S30}	V_{S30}	V_{S30}	Best estimate of 1,200 m/s
Depth to V_S=1.0 km/s (km)	$Z_{1.0}$			$Z_{1.0}$	Best estimate of 0 m
Depth to V_S=2.5 km/s (km)			$Z_{2.5}$		Default value of 2 km was used, based on recommendations in Campbell and Bozorgnia (2007)
Rock motion PGA for non-linear site response				Y_{ref}	Non-linear site response is not required because the shear wave velocity exceeds the rock limit

Table 5-2 Parameters for the GMPE of Graizer and Kalkan (2007, 2009).

Input Parameter	Parameters Used in GMPE	Parameter Values Used in This Study
Moment Magnitude	M	Magnitudes 5.9 and 6.7 were analyzed
Style of Faulting	F	Strike-slip assumed
Basin Effects	C	Not used for DCPP, due to location on hard rock
Closest distance to the rupture plane (km)	r	Best estimate of 0.6 km
Average shear-wave velocity in the top 30 m (m/s)	V_{S30}	Best estimate of 1,200 m/s

Table 5-3 Magnitude results for the Shoreline fault based on different scenarios and rupture lengths.

Scenario	Surface Rupture Length (km)	M_{max}
1	N/A*	≤ 5.9
2	16	6.5
3	23	6.7
4	23	6.7
5	33	6.9

Analyses are based on Wells and Coppersmith (1994). Calculated values are for mean M_{max}. One standard deviation about this mean is approximately ± 0.3 magnitude units.

*Scenario is for low-magnitude, non-surface-rupturing event.

Table 5-4 Magnitude results for the Shoreline fault based on different scenarios and rupture areas.

Scenario	Surface Rupture Area (km^2)	M_{max}	
		Wells & Coppersmith (1994)	Hanks & Bakun (2002)
1	N/A*	≤ 5.9	≤ 5.9
2	240 (16 × 15 km)	6.4	6.4
3	350 (23 × <15 km)†	6.6	6.5
4	345 (23 × 15 km)	6.6	6.5
5	495 (33 × 15 km)	6.7	6.7

Analyses based on Wells and Coppersmith (1994) and Hanks and Bakun (2002). A single down-dip rupture of 15 km is assumed.

† Rupture area is similar to that of Scenario 4, due to the intersection of the vertical Shoreline fault with the 60° north-dipping San Luis Bay fault. Calculated values are for mean M_{max}. One standard deviation about this mean is approximately ± 0.2–0.3 magnitude units.

*Scenario is for low-magnitude, non-surface-rupturing events.

Table 5-5 Shear wave velocity parameters used in this document and in RIL 09-001 as determined from the PG&E Final Report of the LTSP (1988).

	V_{S30}	$Z_{1.0}$	$Z_{2.5}$
Best Estimate for This Study	1,200 m/s	0 m	2 km
Best Estimate RIL 09-001	1,100 m/s	0 m	2 km
Lower Bound RIL 09-001	800 m/s	40 m	2 km
Upper Bound RIL 09-001	1,600 m/s	0 m	2 km

Table 5-6 Site correction factors (a_1) for adjusting GMPEs from 760 m/s to 1,100 and 1,200 m/s applied by PG&E [from Silva (2008)].

Period	Frequency (Hz)	a_1 for V_{s30}=1200 m/s	a_1 for V_{s30}=1100 m/s
0.01	100.00	-0.35	-0.28
0.02	50.00	-0.35	-0.29
0.03	33.33	-0.35	-0.28
0.05	20.00	-0.26	-0.21
0.075	13.33	-0.26	-0.19
0.10	10.00	-0.27	-0.26
0.15	6.67	-0.29	-0.33
0.20	5.00	-0.31	-0.21
0.25	4.00	-0.34	-0.28
0.30	3.33	-0.37	-0.36
0.40	2.50	-0.4	-0.37
0.50	2.00	-0.42	-0.44
0.75	1.33	-0.42	-0.34
1.0	1.00	-0.36	-0.22
1.5	0.67	-0.27	-0.17
2.0	0.50	-0.21	-0.28
3.0	0.33	-0.130	-0.12
4.0	0.25	-0.080	-0.07
5.0	0.20	-0.045	-0.04
10.0	0.1	0	0

Table 5-7 Site correction factors (a_1) for adjusting GMPEs from 760 m/s to 1,200 m/s based on NRC Analysis.

Period	Frequency (Hz)	Amplification Factor	a_1 for V_{s30}=1200 m/s
0.01	100	0.814	-0.206
0.02	50.00	0.819	-0.199
0.03	33.33	0.830	-0.186
0.04	25.0	0.829	-0.188
0.05	20.00	0.830	-0.186
0.075	13.33	0.820	-0.198
0.10	10.00	0.794	-0.231
0.15	6.67	0.752	-0.284
0.20	5.00	0.723	-0.324
0.25	4.00	0.733	-0.311
0.30	3.33	0.748	-0.29
0.40	2.50	0.818	-0.201
0.50	2.00	0.864	-0.146
0.75	1.33	0.931	-0.071
1.0	1.00	0.955	-0.046
1.5	0.67	0.977	-0.023
2.0	0.50	0.986	-0.14
3.0	0.33	0.992	-0.008
4.0	0.25	0.995	-0.005
5.0	0.20	0.995	-0.005
7.5	0.13	0.999	0
10.0	0.1	1.030	0.003

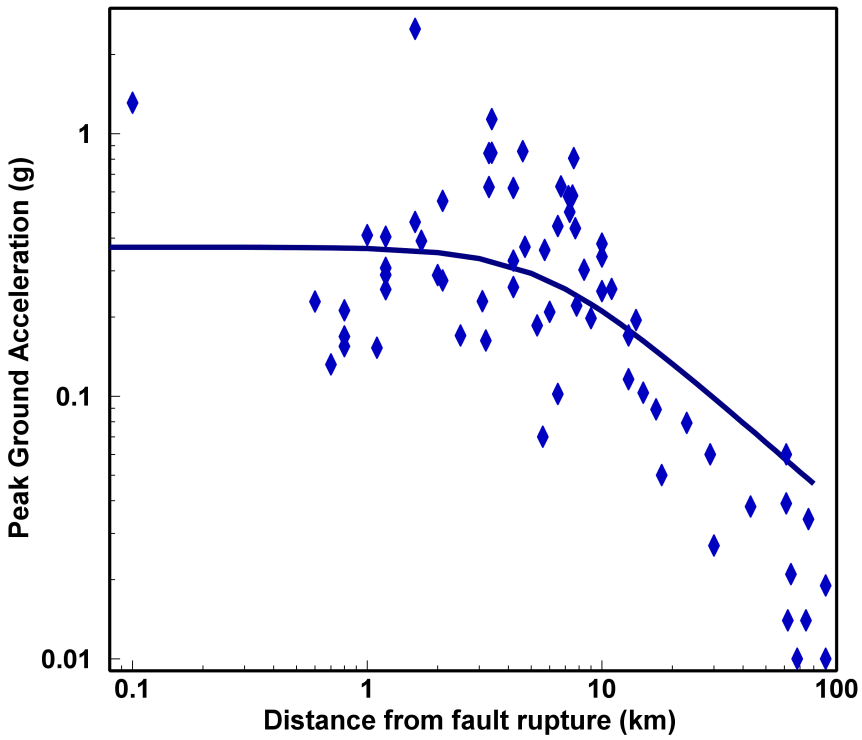

Figure 5-1 **PGA values recorded on soil sites from the 2004 M6.0 Parkfield, CA earthquake compared with the median prediction of the western U.S. GMPE of Boore et al. (1997) (Figure B-11, of NUREG-2117).**

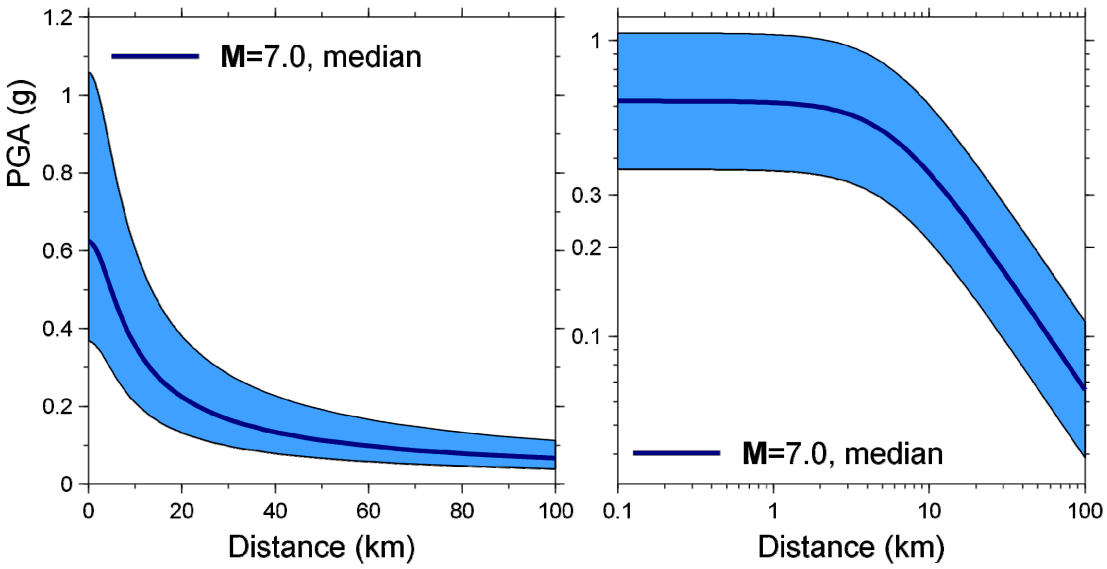

Figure 5-2 **Predicted PGA values for soft soil sites at different distances (r_{JB}) for a M7.0 earthquake based on the Western U.S. GMPE of Boore et al. (1997). The solid line represents median values, and the shaded area indicates the range from 16th to 84th-percentile values; the plots are identical except the left is on linear axes and the right on logarithmic (from Bommer and Boore, 2004).**

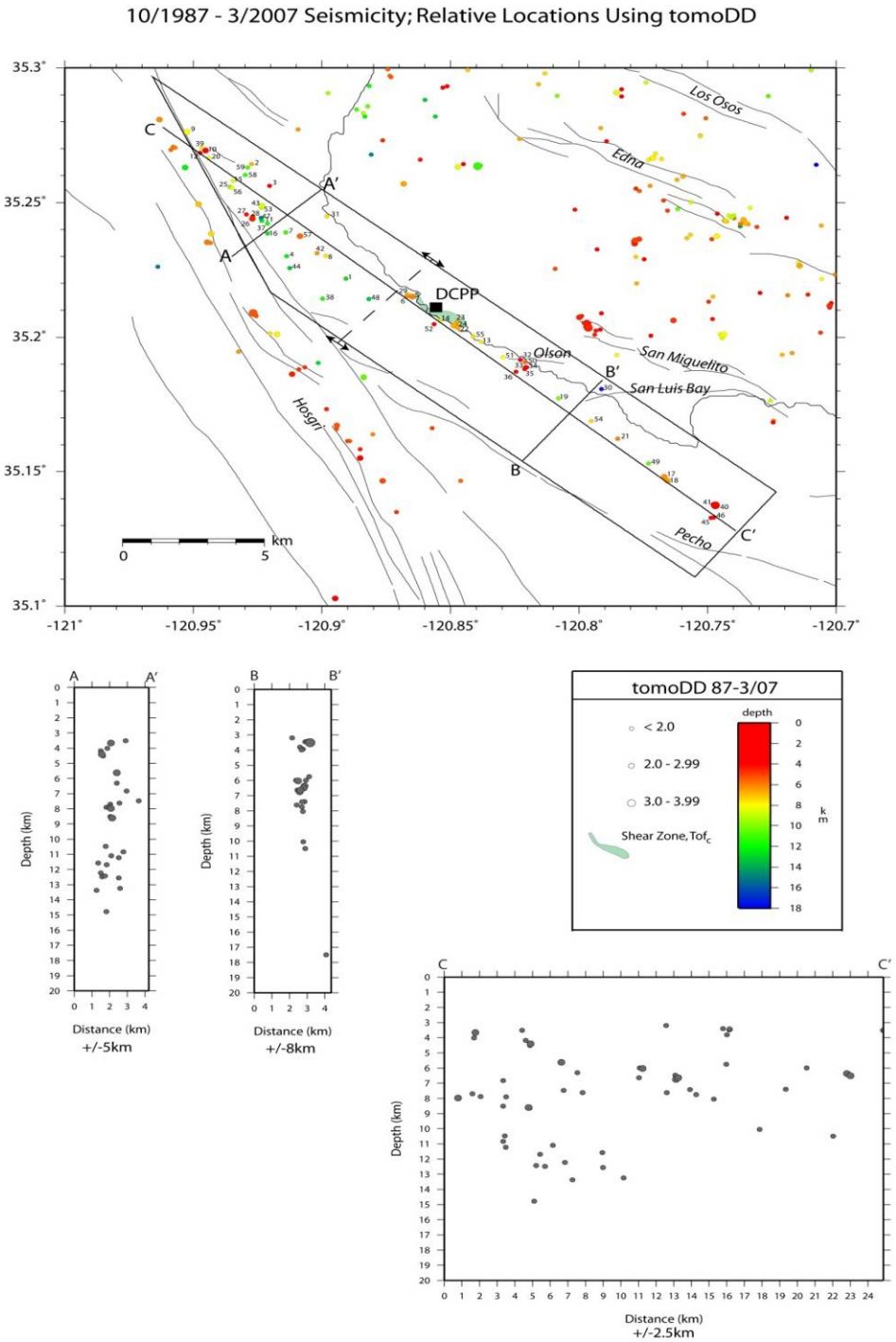

Figure 5-3 Seismicity in vicinity of DCPP, figures and underlying data from the PG&E CRADA (Hardebeck, 2010).

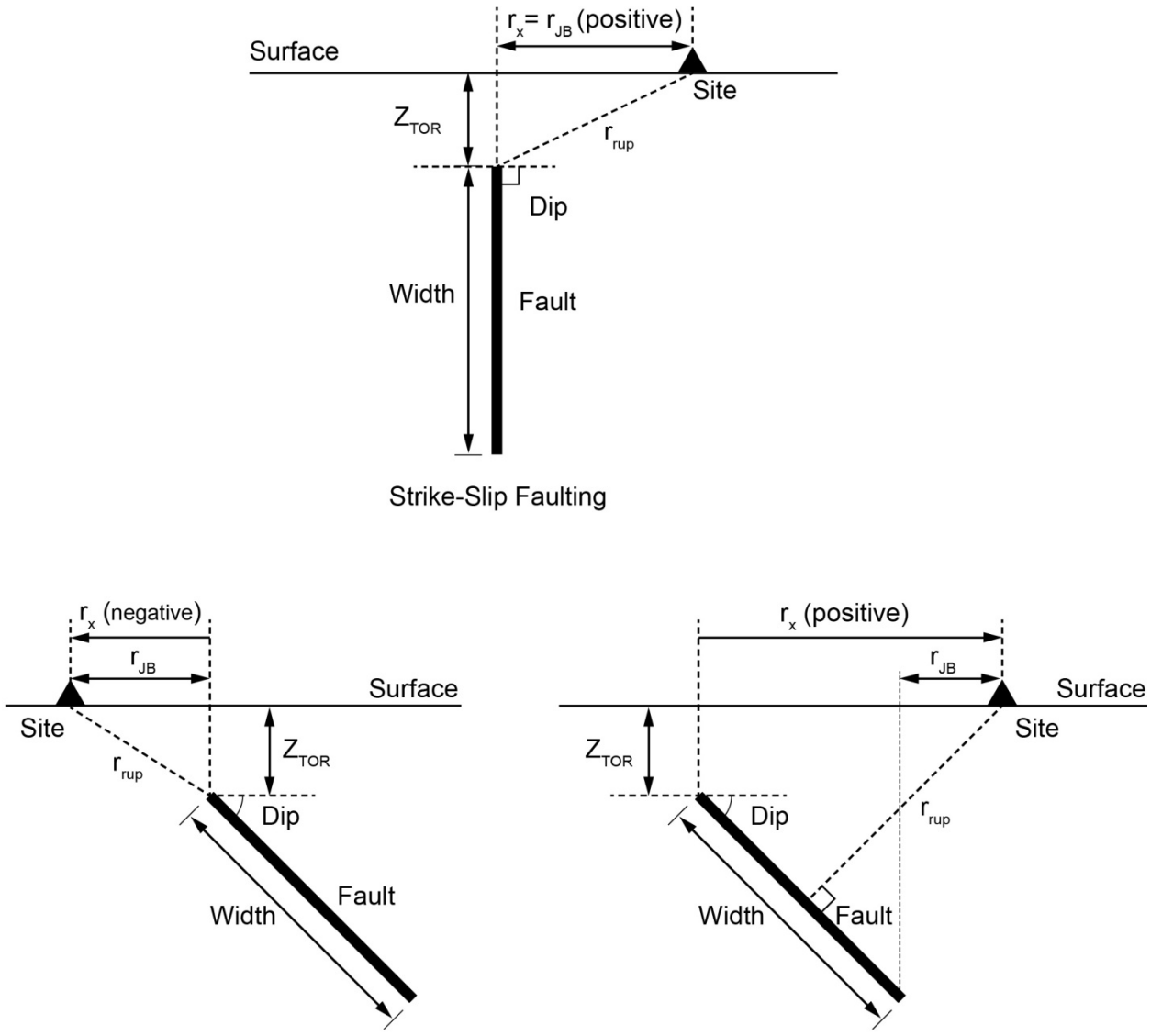

Figure 5-4 Definitions of distance between a site and the source of an Earthquake (Abrahamson and Shedlock, 1997).

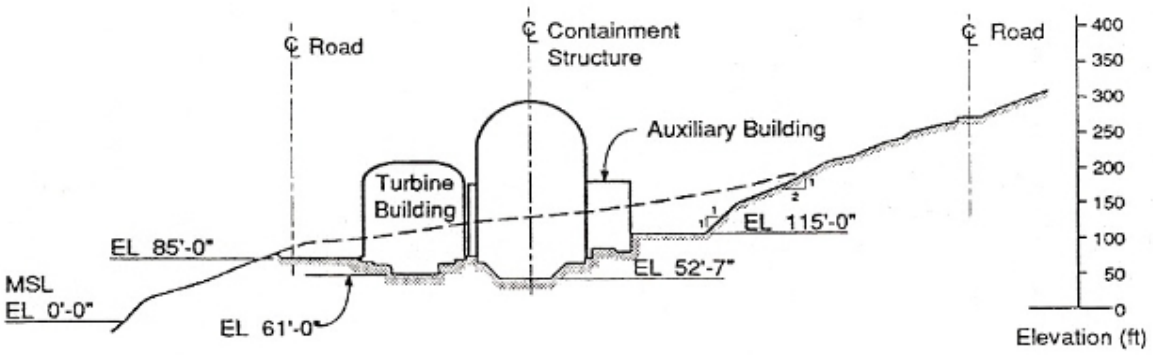

Figure 5-5 Cross section of DCPP (Figure 5-3 in DCPP LTSP Report).

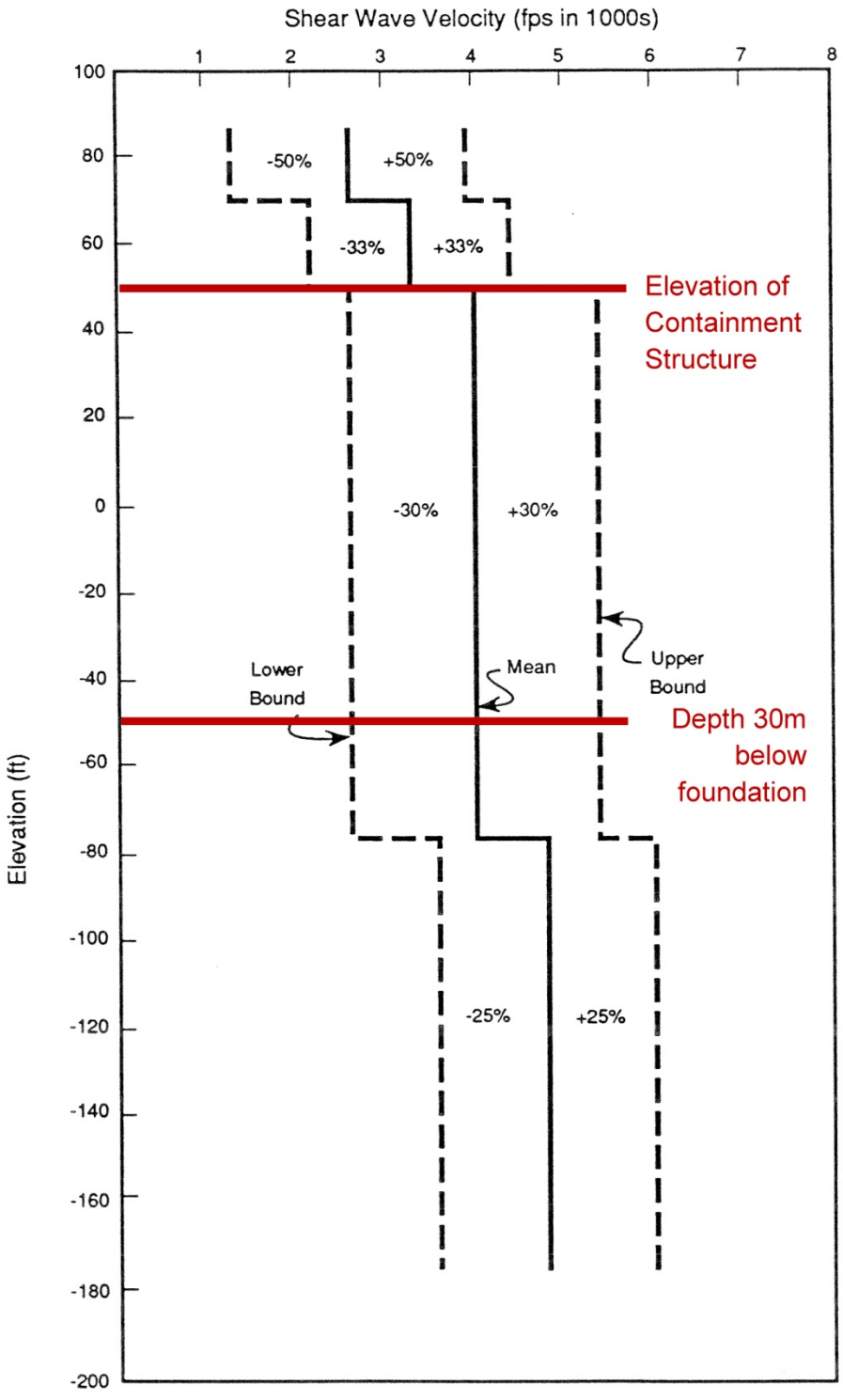

Figure 5-6 Shear wave velocity profiles from 1978 downhole measurements (Figure 5-5 in DCPP LTSP Report, with annotation by the NRC Staff (from RIL 09-001)).

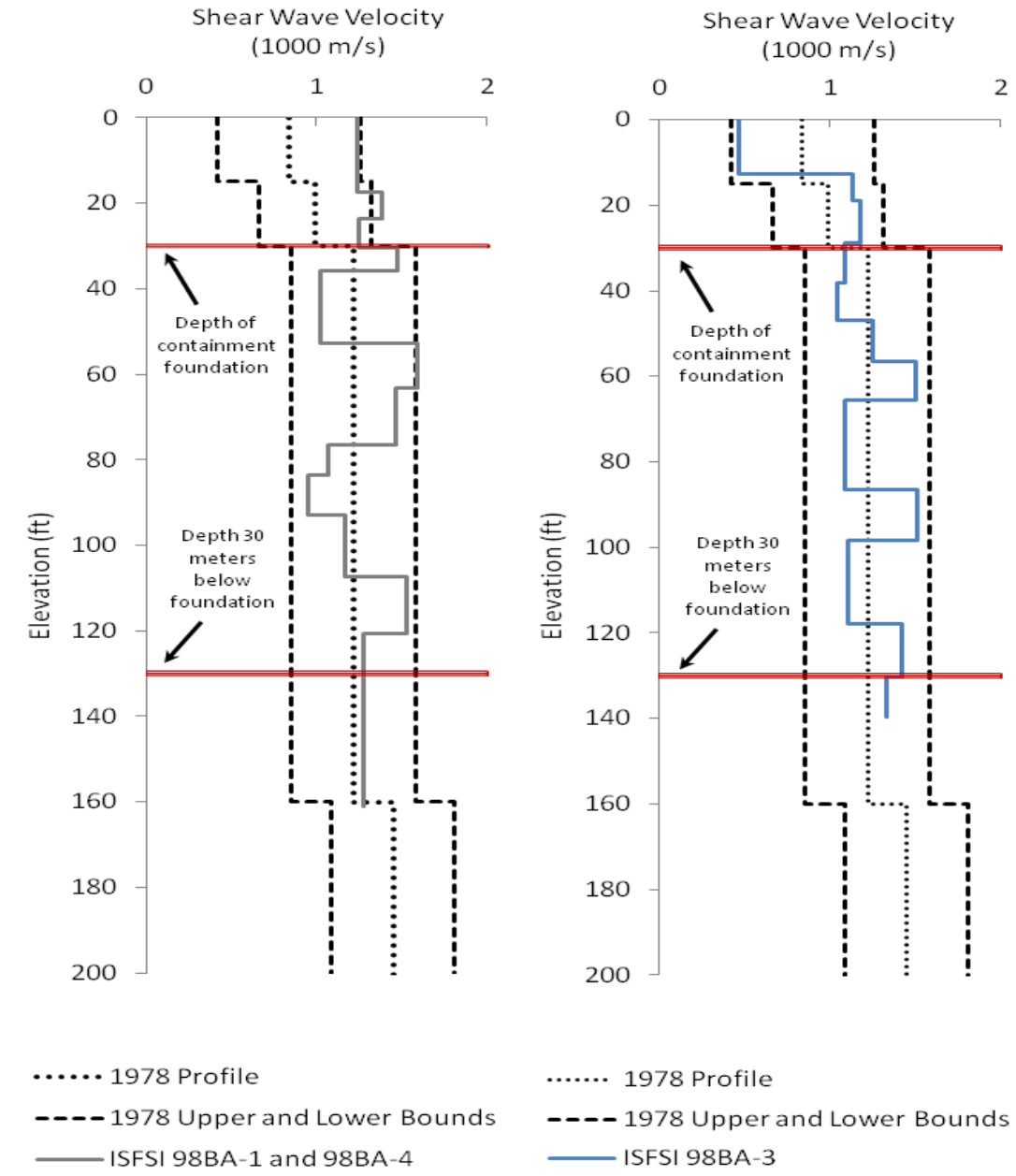

Figure 5-7 Comparison of 2010 DCPP ISFSI velocity profiles to that of the 1978 velocity profile.

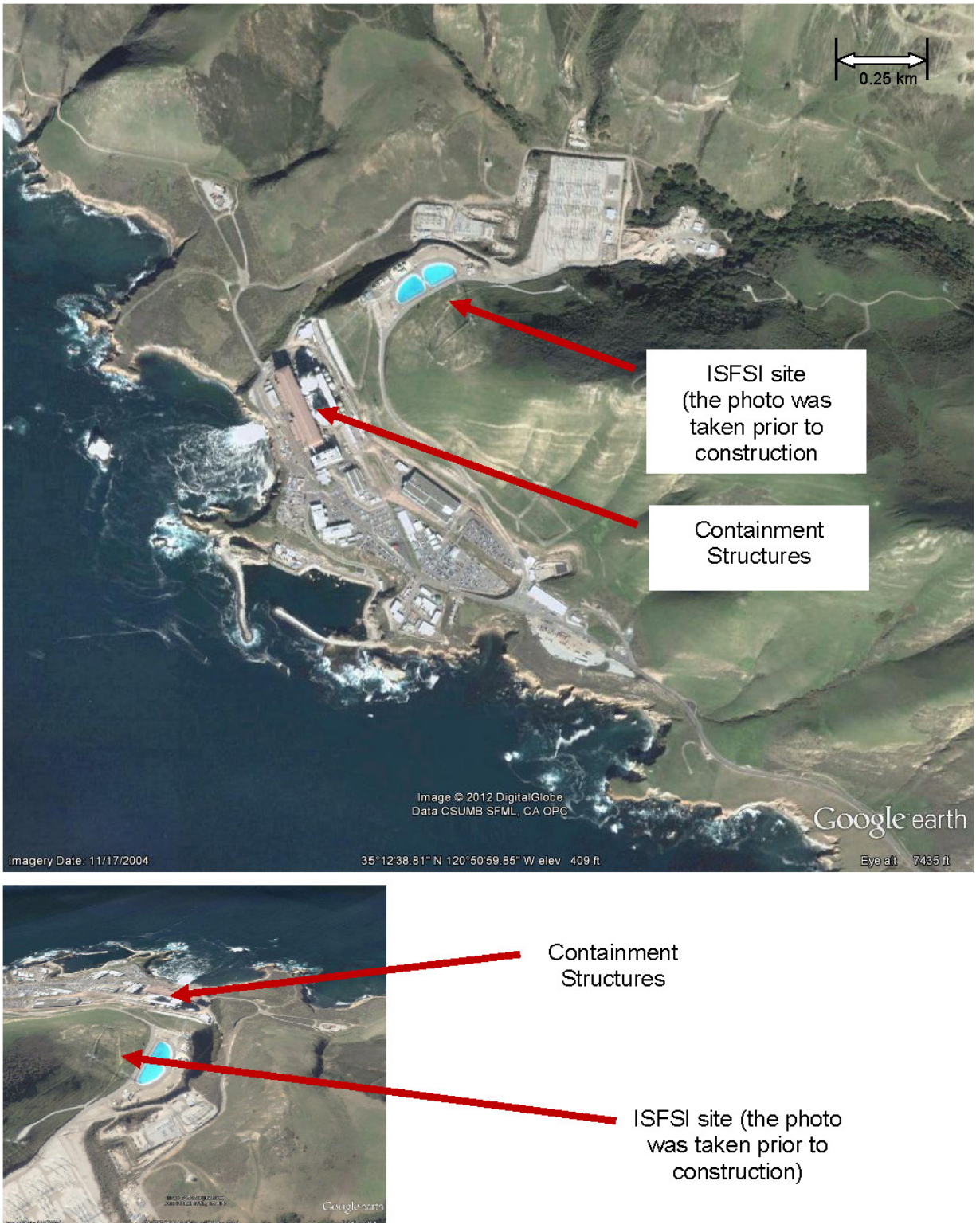

Figure 5-8 Location of the ISFSI in relation to the power block.

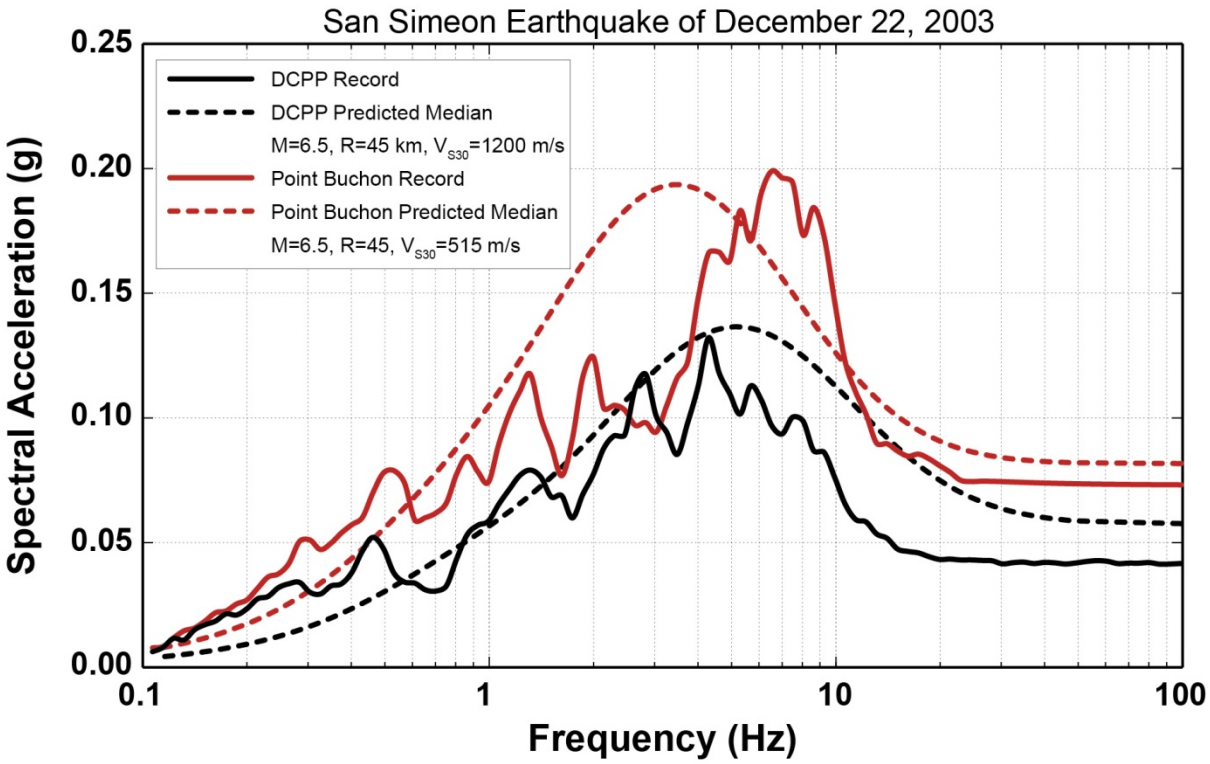

Figure 5-9 Comparison of the 2003 San Simeon earthquake records at DCPP and Point Buchon with median motions predicted by Graizer and Kalkan (2009) using V_{S30} of 1,200 m/s directly in the GMPE.

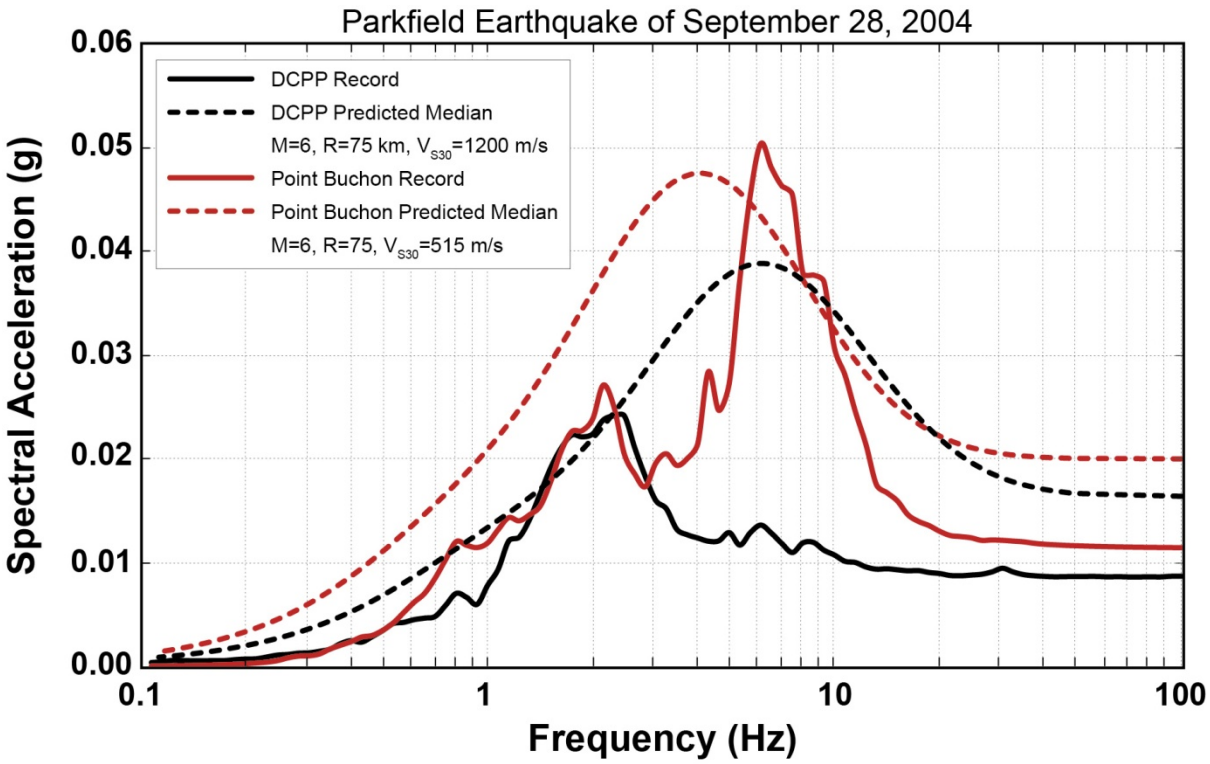

Figure 5-10 **Comparison of the 2004 Parkfield earthquake records at DCPP and Point Buchon with median motions predicted by Graizer and Kalkan (2009) using V_{S30} of 1,200 m/s directly in the GMPE.**

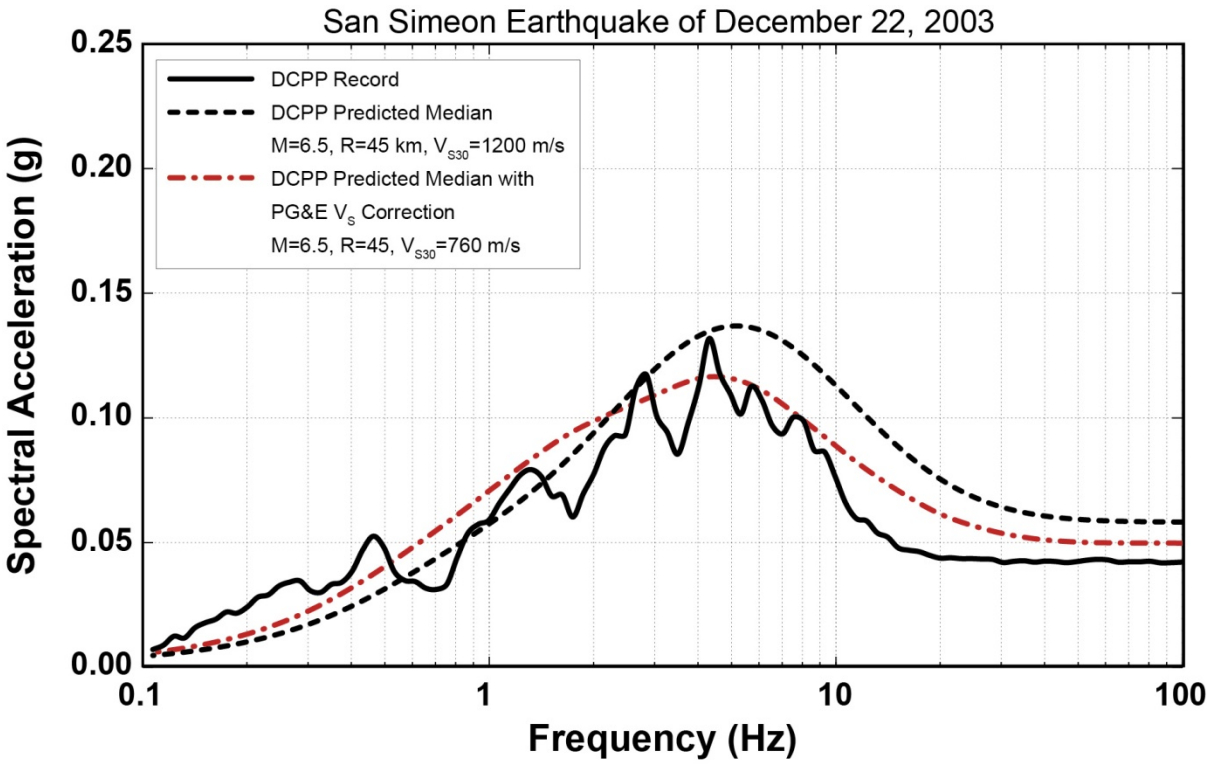

Figure 5-11 Comparison of recording from 2003 San Simeon Earthquake at DCPP with predicted median ground motions from Graizer and Kalkan (2009) with and without site response correction factors of Silva (2008).

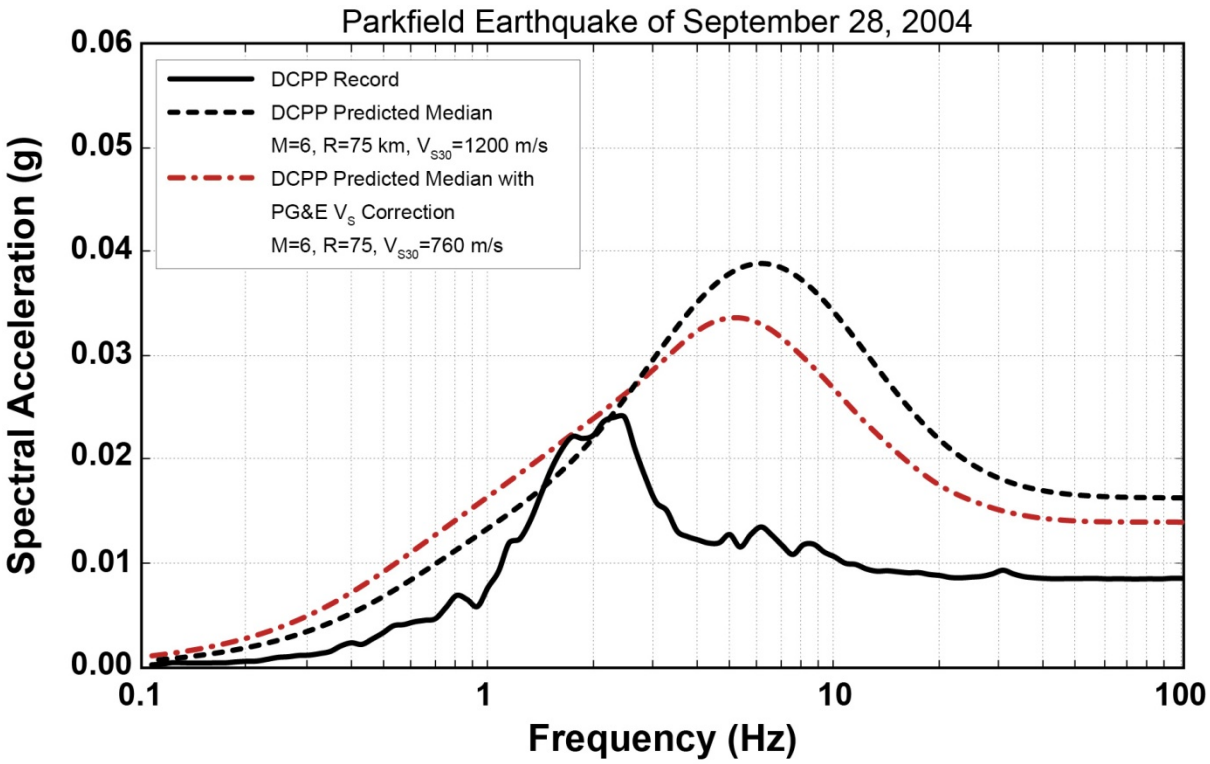

Figure 5-12 Comparison of recording from 2004 Parkfield Earthquake at DCPP with predicted median ground motions from Graizer and Kalkan (2009) with and without site response correction factors of Silva (2008).

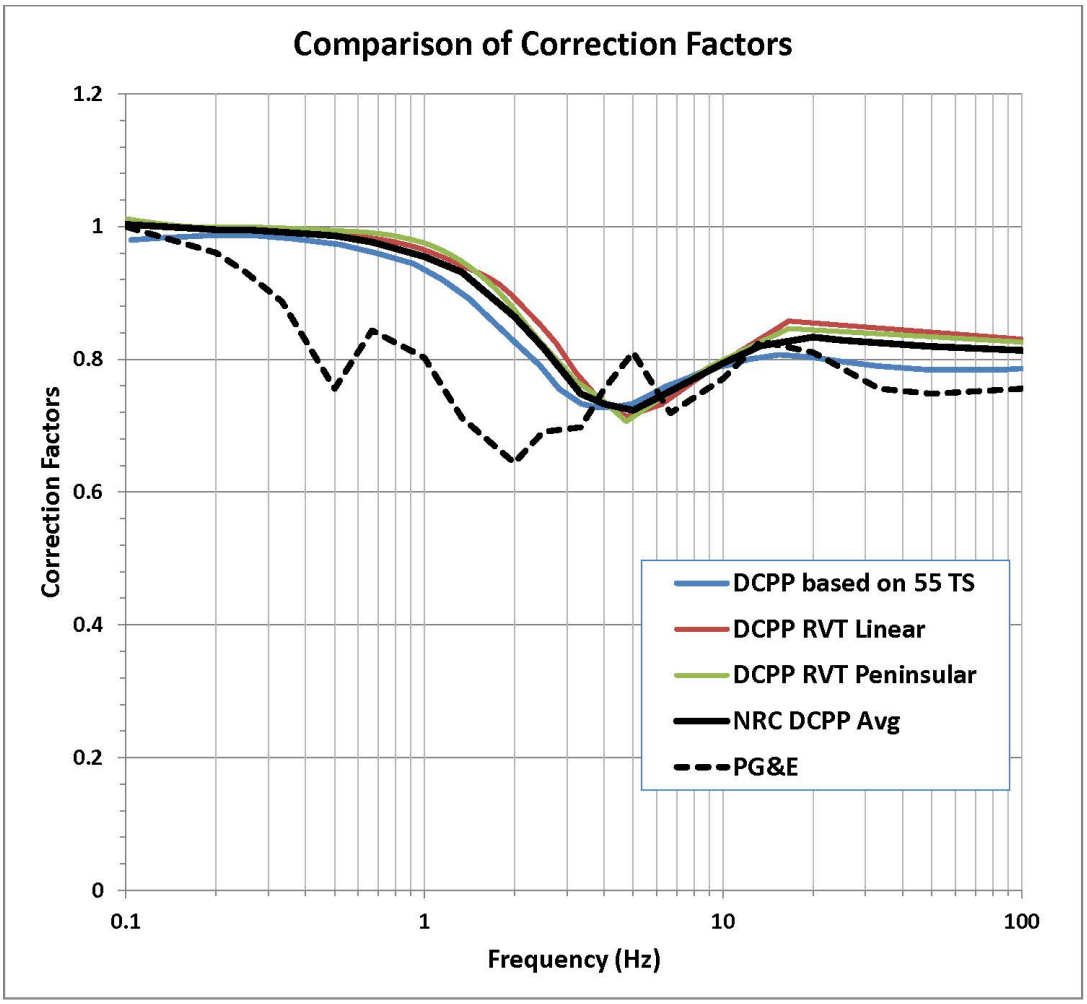

Figure 5-13 Comparison of correction factors developed by NRC using DCPP specific velocity profile with time series (TS) and random vibration theory (RVT) approaches to the factors used by PG&E from Silva (2008). The heavy black line is the average of the three NRC results and was used in the present assessment.

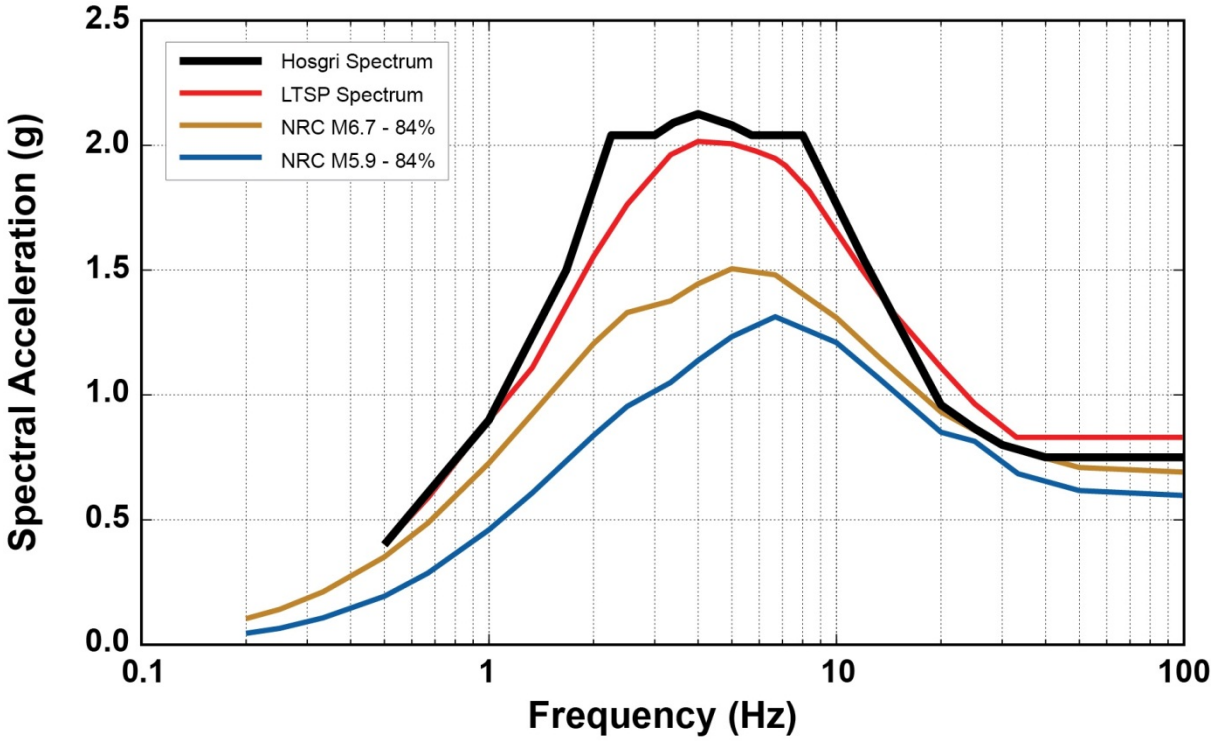

Figure 5-14 Comparison of results of 84th-percentile ground motions for magnitude 5.9 and 6.7 earthquakes on the Shoreline fault to Hosgri and LTSP spectra. Results developed using NRC correction factors.

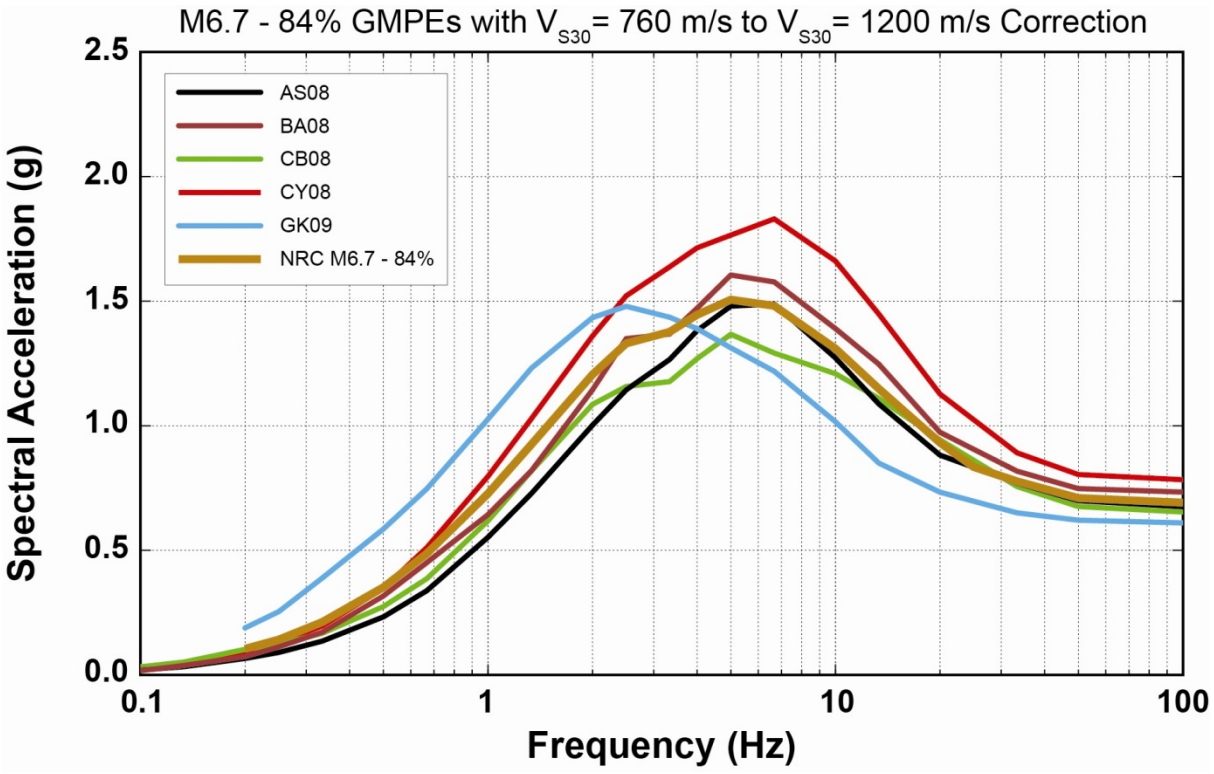

Figure 5-15 84th-percentile ground motions for the five GMPEs used in NRC analyses for a M6.7 scenario earthquake on the Shoreline fault.

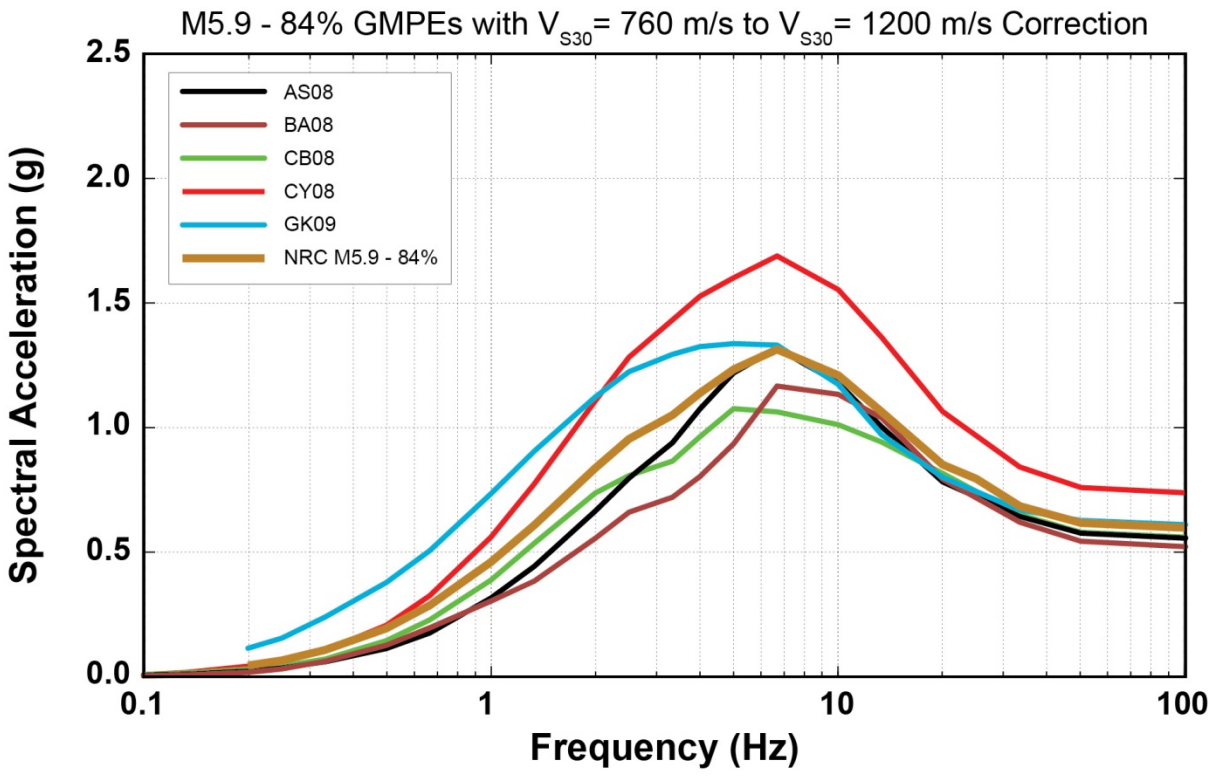

Figure 5-16 84th-percentile ground motions for the five GMPEs used in NRC analyses for a M5.9 scenario earthquake on the Shoreline fault.

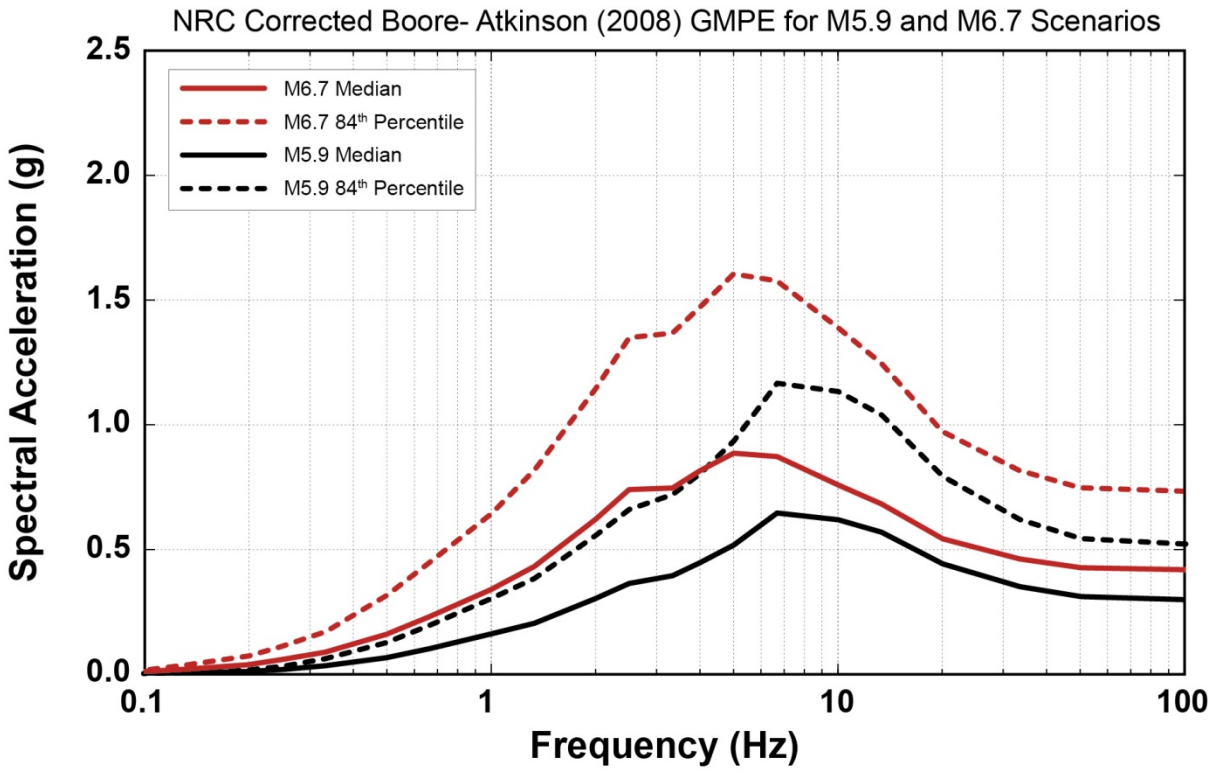

Figure 5-17 Comparison of median and 84th-percentile ground motions for the M5.9 and M6.7 scenario earthquakes on the Shoreline fault for Boore-Atkinson 2008 GMPE.

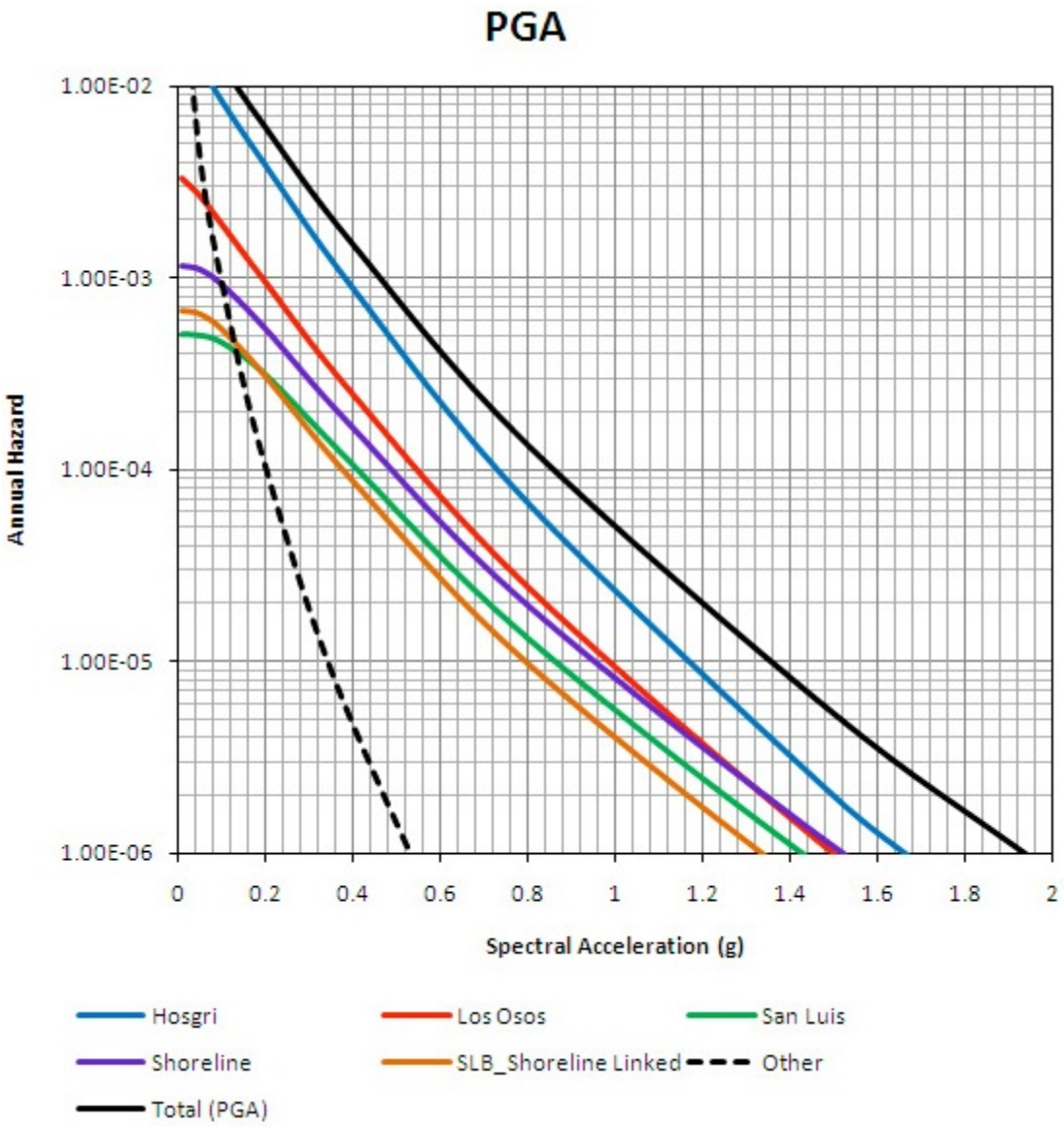

Figure 5-18 Contribution to seismic hazard by seismic source for PGA (Figure 6-20 (a) of the PG&E Shoreline Fault Report).

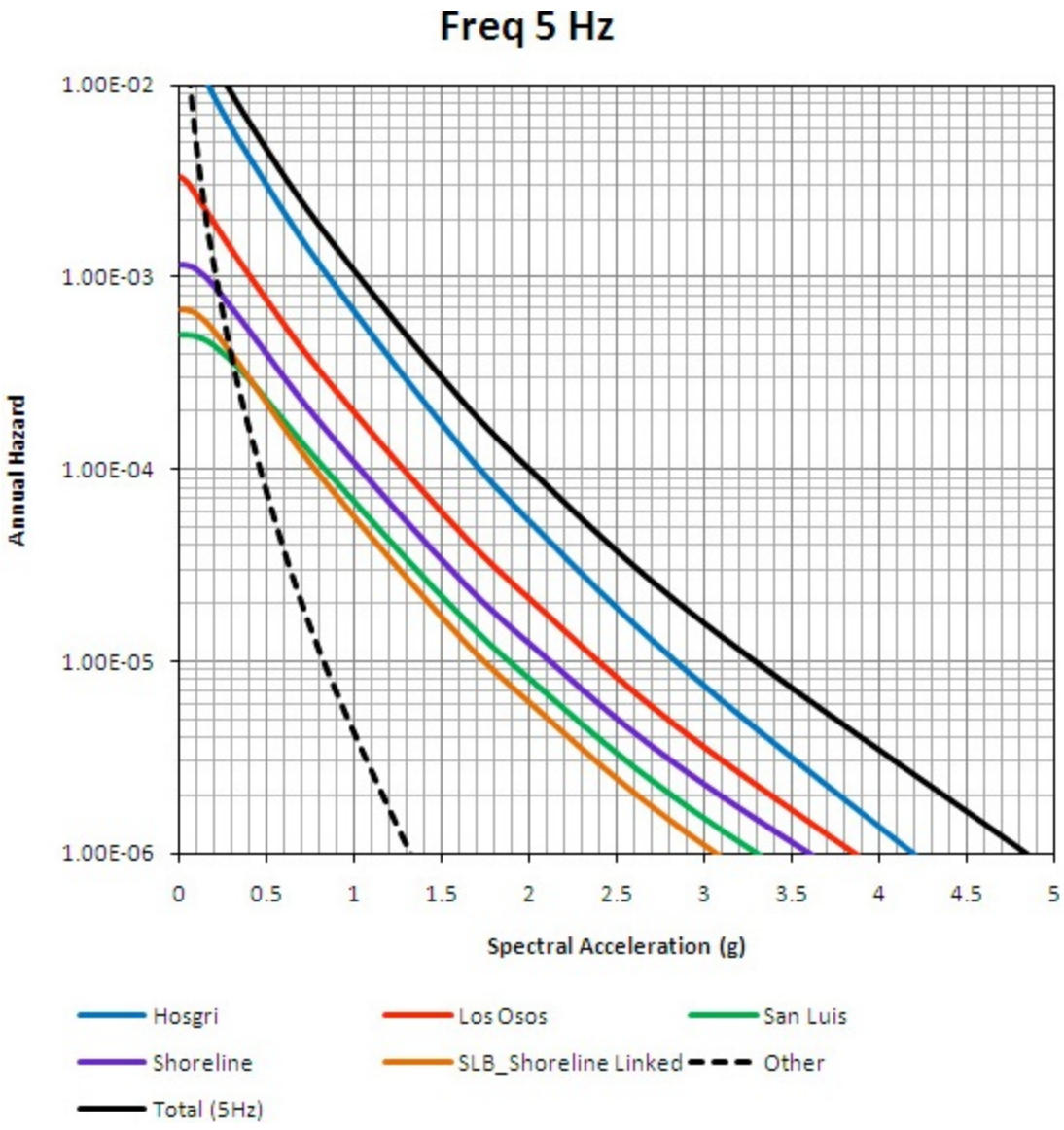

Figure 5-19 Contribution to seismic hazard by seismic source for 5 Hz (Figure 6-20 (b) of the PG&E Shoreline Fault Report).

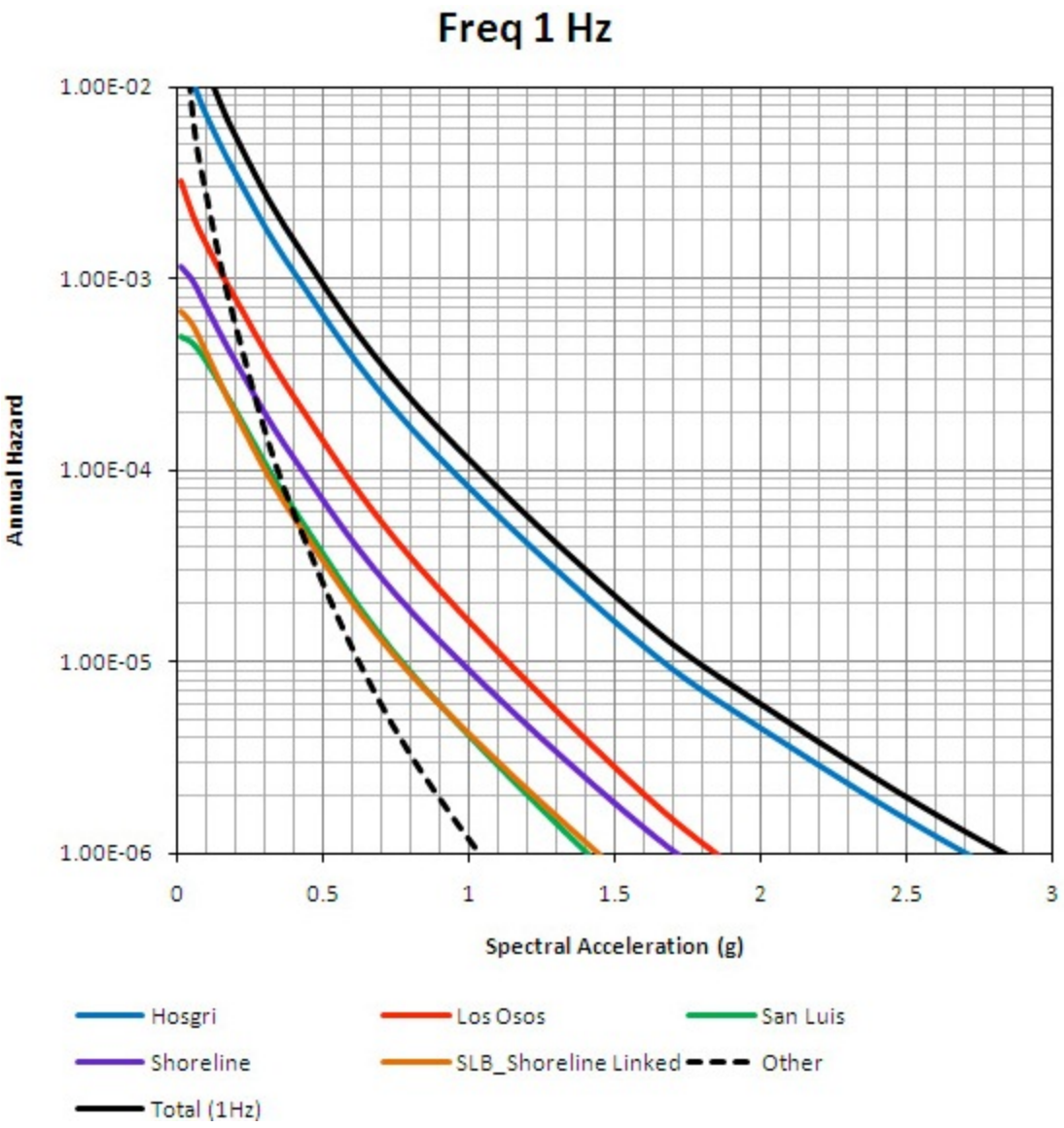

Figure 5-20 Contribution to seismic hazard by seismic source for 1 Hz (Figure 6-20 (c) of the PG&E Shoreline Fault Report).

6 Probabilistic Seismic Hazard Assessment

6.1 Probabilistic and Deterministic Assessments

The goal of the deterministic seismic hazard assessment (DSHA) is to evaluate the potential ground motion at the DCPP from a single earthquake scenario, one that can be used to simply assess the potential hazard from that fault source or as a way to compare hazard results among a set of discrete deterministic evaluations. The seismic hazard evaluation for the Shoreline fault described in Chapter 5 is based on such a deterministic approach, in which each of the evaluated scenarios considers a specific set of seismic source and ground motion parameters. While these deterministic analyses are informed by the historical record, they do not explicitly consider how likely the specific scenarios are, or how frequently they may occur.

In standard DSHA, the seismic source and ground motion parameters are (1) ground motion prediction relationships, (2) earthquake magnitude, (3) distance from the rupture plane to the site, (4) type of faulting, (5) shear wave velocity of the soils and bedrock beneath the site, (6) depth to rupture, (7) dip angle of the fault plane, and (8) statistical level of ground motion uncertainty applied to derive the hazard spectrum (e.g., median, mean, 84^{th}-percentile). In the analyses provided in Section 5, NRC Staff evaluated two deterministic scenarios. Both scenarios used a site-to-source distance of 0.6 km and the same suite of ground motion prediction equations. The final hazard spectra for both scenarios were calculated at one standard deviation above the median values (84^{th}-percentile). Both scenarios were based on vertical strike-slip faults in which the ruptures were modeled to occur at the earth's surface. The only difference between the two scenarios was earthquake magnitude, M5.9 for one scenario and M6.7 for the other scenario. The Shoreline fault DSHA results from these two scenarios were also compared to the existing 84^{th}-percentile Hosgri fault spectrum (Figure 5-14). The Hosgri spectrum is based on a magnitude M7.5, located 5 km from the DCPP, but using an older generation of ground motion prediction relationships.

As noted earlier, the approach used in both the licensing of new reactors, and described in the 10 CFR 50.54(f) Request for Information Letter focused on operating reactors, is a probabilistic seismic hazard assessment (PSHA), developed through a systematic SSHAC Level 3 or Level 4 process. A PSHA differs from a DSHA in that it incorporates multiple earthquake scenarios, including the frequency of occurrence of those scenarios, and includes a quantitative assessment of the uncertainty into a single analysis. The goal of the PSHA is to capture the center, body, and range of the seismic hazard values as accurately as possible from all possible earthquake scenarios including the uncertainties associated with the PSHA inputs. The best estimate median ground motions from the PSHA thereby represent the "center" of the distribution of all plausible scenarios. The "body" and "range" are essentially the shape and extrema of the ground motion distributions, respectively. Currently applicable regulations under 10 CFR 100.23(d)(1), "Determination of the Safe Shutdown Earthquake Ground Motion," require that the uncertainty inherent in estimates of the safe shutdown earthquake be addressed through an appropriate analysis, such as a PSHA.

The uncertainty in a PSHA can be due to the variability of input parameters reflecting the precision or accuracy of data, the reliability of supporting models, or the uncertainty among the technical experts reflecting differences in approach or expert judgment. The complexity of the physical processes that generate earthquakes and the consequent ground shaking, coupled with the limited data available for seismic source and ground motion characterization result in a situation where multiple technically defensible interpretations are valid. This was apparent in

the discussions in Section 4, where several equally defensible earthquake scenarios for the Shoreline fault were derived from the same geologic and geophysical information. As a result, incorporating a significant level of expert judgment in developing source characterization and ground motion models for seismic hazard assessment studies is unavoidable. For critical facilities such as nuclear power plants, the judgment of multiple experts is therefore needed to capture the full range of technically defensible interpretations. The Senior Seismic Hazard Assessment Committee (SSHAC) process, which is detailed in NUREG/CR-6372 and NUREG-2117, provides a transparent method of structured expert interaction that is entirely focused on meeting this need. Additional discussion on this process is continued in Appendix A.

A PSHA is often described as a "frequency" based approach (e.g., Bommer, 2002) in that the resulting hazard curves estimate the frequency of exceeding different levels of ground motion. In one sense, a PSHA can be considered an accumulation of multiple DSHA calculations in which all seismic sources, ground motion attenuation models, and associated statistical uncertainty are included. In addition, PSHA also incorporates two additional and important seismic source characteristics that are not part of a DHSA. These are the likelihood that the earthquake source will generate large earthquakes and the recurrence rate of those earthquakes on the seismic source. Consider the case of two faults equally distant from the site. Based simply on fault length, both faults are deemed capable of generating equally large magnitude earthquakes. Nonetheless, geologic or seismologic evidence indicates that one fault has a high likelihood of producing these large earthquakes and at a predictable recurrence rate while the other fault has less evidence of past seismicity and a significantly lower recurrence rate. In the DSHA, both faults may be judged to contribute equally to the seismic hazard because the DSHA is based only on maximum magnitude and source-to-site distance. In the PSHA, however, the likelihood of earthquake activity and the fault's recurrence rate are included in the analysis. As a result, active fault sources which are considered more likely to generate large magnitude earthquakes will dominate in the PSHA. Additional geological, geophysical, or seismological information can be used to evaluate and constrain recurrence rates or slip rates. In addition, the recurrence rate of earthquakes on a particular fault and/or in a region can also be constrained by information on the tectonic slip rate "budget" in that region. This concept is discussed in more detail in Appendix D.

6.2 Current and Updated PG&E Probabilistic Seismic Hazard Assessments

The Shoreline Fault Report presents a PSHA performed by PG&E, including a discussion of how the Shoreline fault is incorporated into PG&E's PSHA model. Based on the PSHA provided in the Shoreline Fault Report (see Figure 6-20a-c in PG&E, 2011), PG&E concludes that the Hosgri fault is the main contribution to the total hazard. Two factors contribute to this conclusion. First, the Hosgri is deemed capable of producing up to M7.5, larger than the maximum magnitude of other faults in the vicinity of the DCPP. Second and more importantly, the Hosgri has a slip rate that is up to an order of magnitude greater than other faults near the DCPP, so its activity rate or recurrence rate of large earthquakes is higher than any of the other faults in the vicinity of the DCPP. In 2011, PG&E initiated a more comprehensive study to replace its current PSHA model using the SSHAC Level 3 process. Because this existing PSHA model will be superseded in the next few years, the NRC Staff did not perform a confirmatory analysis of the PSHA provided by PG&E in the Shoreline Fault Report.

For this updated PSHA, PG&E is implementing a SSHAC Level 3 process. The SSHAC Level 3 process includes at least three formal workshops designed to assess all available information,

debate alterative interpretations of those data, and provide feedback to the evaluator experts on preliminary models. Appendix A provides an overview and summary of the SSHAC Level 3 process based on NUREG-2117. In the case of the DCPP SSHAC Level 3 study, the first workshop, on available data, was held November 29 to December 2, 2011. The workshop presentations can be viewed on the PG&E Web site at:

http://www.pge.com/mybusiness/edusafety/systemworks/dcpp/SSHAC/workshops/index.shtml.

The remaining workshops are planned to take place in 2012 and 2013.

To meet the objectives of a SSHAC Level 3 study, the updated PG&E SSHAC PSHA should consider all known seismic sources that could generate earthquake ground motions at the DCPP, including the Shoreline fault. Characterization of the Shoreline fault by the evaluator experts in the PSHA should incorporate the full range of technically permissible interpretations of this fault, including estimates of the uncertainty of each interpretation and statistical uncertainty of each of the underlying source characteristics, such as magnitude, site-to-source distance, and recurrence rate.

6.3 Application of PSHA Results

The PSHA results are an important input to plant-specific seismic risk analyses. However, it is important to note that in modern seismic engineering, meeting acceptable risk targets comes from choosing a low annual rate of exceedance in the ground motion from the PSHA (i.e., a very rare ground motion) and then incorporating appropriate seismic resistance into the design, not by adding conservatisms to the ground motion prediction. As shown schematically in Figure 6-1, seismic risk analysis for nuclear facilities requires probabilistic characterization of both the earthquake loading (through the PSHA) and a quantification of the plant-level fragility (noted as the “Mean Core Damage Fragility Curve” in the figure). The plant-level fragility is developed through a Seismic Probabilistic Risk Assessment (SPRA), which is a technique for quantification of the seismic robustness of the plant as a result of its specific design and structures, systems, and components. Therefore, the SSHAC Level 3 PSHA study currently underway for the DCPP site should be designed and conducted to use the newly accumulated dataset to develop a state-of-the-art assessment of hazard to be used as a fundamental input to a new SPRA analysis. The SPRA will provide an updated assessment of seismic risk of the DCPP facility consistent with the intent of the 10 CFR 50.54(f) Request for Information Letter. Although the DCPP plant is already designed and constructed, the SPRA results can be used to determine which structures, systems, and components are most important within a risk context.

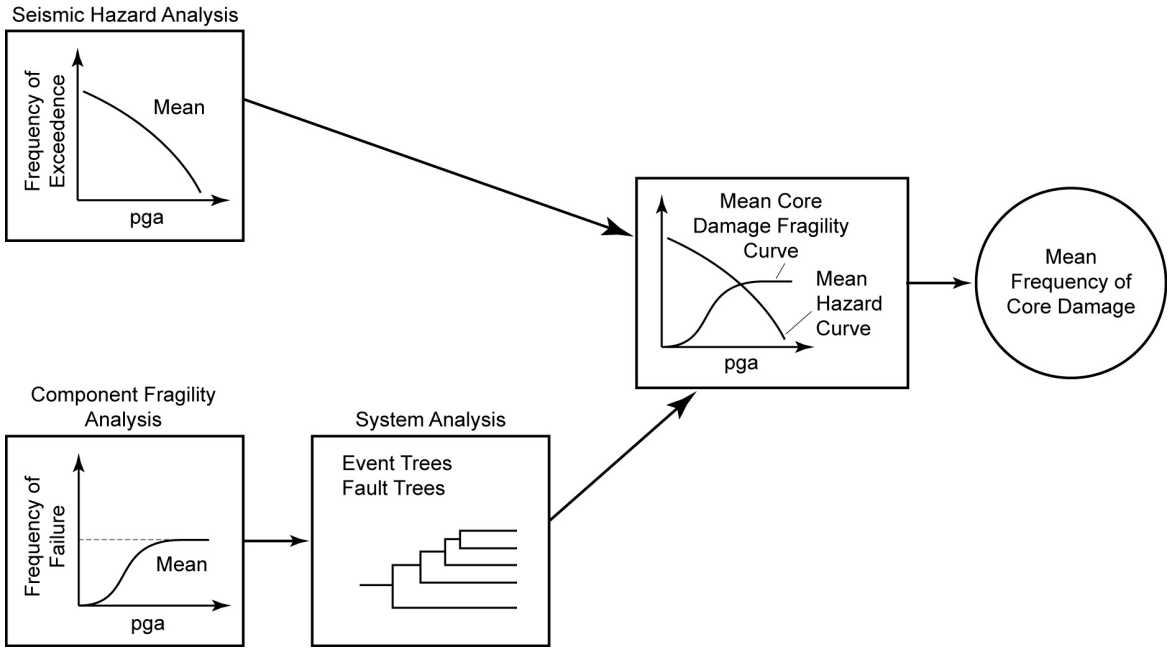

The box entitled “System Analysis” indicates event trees or fault trees, which are diagrams that illustrate the links between different structures, systems, and components, and how the performance of one of these affects the next in the sequence. Although these visually have the appearance of logic trees they are quite different in meaning and application.

Figure 6-1 Overview of seismic probabilistic risk assessment methodology ((Kennedy, 1999), annotated as Figure B-1 in NUREG-2117)

7 Secondary Fault Displacement

7.1 Introduction to Secondary Fault Displacement

When faults rupture during an earthquake, they have the potential to cause not only primary rupture of geologic materials on the fault but also secondary effects related to secondary rupture or permanent offset of the geologic materials in the vicinity of the fault. Ground-surface displacements associated with large earthquakes are often found in the area near the causative fault. Secondary surface rupture may also occur away from the primary fault trace. Although the amplitude of secondary displacements from these secondary ruptures are much smaller than the displacements that occur on the main trace of the ruptured fault—and decrease with distance from the main fault—they can potentially pose danger to the structures or infrastructure in their immediate vicinity.

The main trace of the Shoreline fault is located offshore about 600 m from the power block of the DCPP facility (Figure 1-1). As a result, the threat of direct rupture of the main fault under the facility is negligible. However, there is a need to assess the risk to the DCPP resulting from a secondary rupture associated with an earthquake on the main Shoreline fault trace.

The question of secondary displacements was discussed in RIL 09-001, p. 10:

> The precise location of the fault and the near-surface properties are important for determining the potential for surface rupture to impact the site. The closest postulated distance of the fault to the site is approximately half a kilometer. Based on the NRC staff's current understanding of the fault orientation, surface rupture under the facility is highly unlikely. Although the fault rupture is unlikely to occur directly under the plant, it may cause displacements in the near field. PG&E noted that ancient faulting at the site may show some deformations as a result of either the direct rupture or the ongoing stress accumulation in the rock. The action plan provided by PG&E details a path to acquire the data needed to appropriately address the issue.

In response to NRC staff concerns expressed during a public meeting on January 5, 2010, PG&E issued Letter No. DCL-10-019 to the NRC on February 26, 2010. Enclosure 1 of this letter, "Evaluation of Secondary Fault Rupture Hazard from the Shoreline Fault" (PG&E, 2010), details calculations that PG&E performed to assess the potential impact of secondary rupture displacements on the calculated annual probability of core damage at the DCPP.

As stated by PG&E and the NRC staff at the January 2010 public meeting, the only safety-related structures, systems, or components that could be sensitive to small secondary displacements are eight Dresser couplings situated along the auxiliary salt water pipes. The auxiliary salt water pipes are located in the weaker rock unit called Unit C of the Obispo Formation (PG&E, 2009). The purpose of the PG&E calculation, as explained in the provided report (PG&E, 2010), was to estimate the probability that the secondary surface rupture will occur at any one of the eight couplings during an earthquake along the Shoreline fault zone. PG&E used two earthquake scenarios in its hazard calculations: (1) a magnitude 6 event caused by the rupture of the entire central segment of the Shoreline fault and (2) a magnitude 6.25 event that would result if both the central and southern segments ruptured together.

The NRC staff performed a confirmatory analysis to evaluate the secondary fault rupture hazard and resulting potential effect to the annual probability of core damage associated with the Shoreline fault zone.

The NRC staff used these two events in its confirmatory analyses as a point of comparison with PG&E. NRC staff also analyzed the risk from a magnitude 6.7 scenario earthquake consistent with the hazard analyses performed in Section 5. Other specific details differed between the PG&E and NRC assessments.

The results of the analyses are discussed below. In addition, Appendix B: provides the details of the analyses in depth, with the goal of allowing the mathematically inclined lay person to review the full approach used in the assessment.

7.2 General Approach to Confirmatory Analysis

The NRC staff performed its confirmatory analyses using the probabilistic method of Petersen et al. (2004), which is the same general analysis technique that PG&E used. However, the NRC staff used results from a more recent regression analysis by Petersen et al. (2011). The Petersen et al. (2004, 2011) method is based on an empirical relationship between earthquake ruptures on main faults that have come all the way to the surface (primary surface rupture) and the occurrence of secondary surface rupture at a nearby location. Their empirical data were recorded for strike-slip earthquakes around the world. To use the method, it must first be determined how often earthquakes of certain magnitudes occur on the main fault of interest. Based on this, it can be determined how often earthquakes occur that rupture the surface (not all earthquake fault ruptures reach the surface, as shown in Figure 4-6) and the likelihood of a surface rupture occurring on any particular part of the main fault. Next, probabilistic relationships (often expressed as probability density functions) can be used to determine the likelihood of a secondary rupture occurring at a specific nearby location and with a specific amplitude of displacement. Displacement values of 1 centimeter (cm) and 2 cm are used in this case, because they are amplitudes of displacement that piping can tolerate.

This method to assess the potential for secondary faulting is newer than methods to assess other types of seismic effects; therefore, the details are not as standardized. As such, different assumptions and approaches to parameters could be used. Additionally, because a risk assessment specifically addressing this issue has not been developed, a set of assumptions had to be made to translate the results of the analyses into risk to the plant, in terms of core damage frequency (CDF). The NRC staff's complete approach is discussed in detail in Appendix C.

7.3 Results of Analysis of Secondary Rupture

As noted, the PG&E calculation of hazard from secondary rupture due to an earthquake on the Shoreline fault was repeated by the NRC staff as part of the confirmatory analyses. The NRC staff repeated PG&E's calculations but also performed the analyses using a magnitude of 6.7 and a distance of 300 m. Other assumptions and parameters also differed from those used by PG&E in some cases. The NRC and PG&E results are listed in Table 7-1.

As a result of differences in the assumptions and analysis approach, the NRC's calculated values of annual probability of exceedance are about a factor of 6 larger than the M6 earthquake scenario and about 4 times larger than the M6.25 rupture scenario earthquake. Although the highest results calculated by the NRC staff (for a larger magnitude at a shorter

distance) are about an order of magnitude higher than PG&E's highest values, the conclusion regarding risk to the plant that was reached by the NRC staff is the same. Specifically, the hazard from secondary rupture at the location of couplings has negligible impact on the seismic CDF at DCPP. The seismic CDF at DCPP is 3.8×10^{-5}, approximately 2 orders of magnitude larger than the hazard from a secondary rupture associated with the Shoreline fault at DCPP. Moreover, to compare the probability of occurrence of displacements (of 1 cm and 2 cm) with core damage, one needs to make two highly conservative assumptions: (1) that the displacement calculated always leads to operational failure of a Dresser coupling and (2) that the failure of a Dresser coupling leads directly to core damage. Since these results are highly conservative; the actual impact to CDF of the DCPP is likely to be far lower. In summary, the risk from secondary fault displacement is negligible.

Table 7-1 Hazard from secondary Shoreline Fault rupture at DCPP

$\overline{m}_{\text{char}}$	Fault Dimensions		Slip Rate (mm/yr)	Annual Probability of Exceedance					
				PG&E Distance=600 m		NRC Distance=600 m		NRC Distance=300 m	
	Width (km)	Length (km)		1 cm	2 cm	1 cm	2 cm	1 cm	2 cm
PG&E Scenarios									
6.00	10	8	0.01	2.6×10^{-10}	1.4×10^{-10}	1.5×10^{-9}	7.9×10^{-10}	3.2×10^{-9}	1.7×10^{-9}
6.25	12	14	0.01	6.0×10^{-10}	3.5×10^{-10}	2.6×10^{-9}	1.6×10^{-9}	5.4×10^{-9}	3.3×10^{-9}
6.00	10	8	0.30	7.8×10^{-9}	4.1×10^{-9}	4.6×10^{-8}	2.4×10^{-8}	9.5×10^{-8}	5.1×10^{-8}
6.25	12	14	0.30	1.8×10^{-8}	1.1×10^{-8}	7.9×10^{-8}	4.7×10^{-8}	1.6×10^{-7}	9.8×10^{-8}
NRC Scenario									
6.70	15	33	0.30			9.9×10^{-8}	7.0×10^{-8}	2.0×10^{-7}	1.4×10^{-7}

8 Conclusions

Conclusions related to the data and analyses are provided throughout this report. However, a few key conclusions warrant repeating.

1. The Shoreline fault was discovered from relocated microearthquakes in 2008. Further data collection confirmed the existence of the Shoreline fault as a potential seismic source.
2. The geologic and geophysical information, including geologic mapping and the earthquake database, can be used to develop reasonable interpretations of fault geometry, activity, maximum magnitude, and proximity of earthquakes to the DCPP.
3. Geologic evidence for recent surface fault displacement along the Shoreline fault is not evident in the newly acquired data.
4. The NRC's conservative estimate for the potential ground motions from the Shoreline fault are bounded by the ground motions for which the DCPP has been previously analyzed and shown to have adequate safety margin (i.e., the HE and LTSP ground motion response spectra). This analysis confirms the earlier conclusions of RIL 09-001.
5. The NRC also analyzed the risk to the DCPP from a secondary surface fault rupture associated with the Shoreline fault and found that the risk to the DCPP is insignificant.
6. The Shoreline fault has a low slip rate that is estimated to be an order of magnitude less than the Hosgri fault, which implies that its overall contribution to the hazard is relatively limited. An understanding of the relative importance of the Shoreline fault to the hazard at DCPP is best demonstrated from a PSHA, which considers the likelihood of earthquake activity from all the seismic sources.
7. Evaluation of the current dataset indicates that it is sufficient to move forward with the SSHAC Level 3 PSHA.

9 References

Abercrombie, R., “Near-surface attenuation and site-effects from comparison of surface and deep borehole recordings”, *Bull. Seismol. Soc. Amer*., 87, p. 731-744, 1997.

Abrahamson, N.A. and K.M. Shedlock, “Overview of ground motion attenuation relations,” *Seismological Research Letters,* Vol. 68, No. 1, 9–23, 1997.

Abrahamson, N.A. and W. Silva, “Summary of the Abrahamson and Silva NGA Ground-Motion Relations,” *Earthquake Spectra*, Vol. 24, No. 1, 2008.

Allen, C.R., “The Tectonic Environments of Seismically Active and Inactive Areas Along the San Andreas Fault System,” Proceeding of Conference on Geologic Problems of San Andreas Fault System, W.R. Dickinson and A. Grantz, eds., Stanford University Publications in the Geological Sciences, Vol. 11, p. 70–82, 1968.

Allen, C.R., et al., “Relationship Between Seismicity and Geologic Structure in the Southern California Region,” *Bull. Seismol. Soc. Amer.*, Vol. 55, p. 753–797, 1965.

Anderson, J. G., and S. E. Hough, “A Model for the Shape of the Fourier Amplitude Spectrum of Acceleration at High-Frequencies,” *Bull. Seismol. Soc. Amer*., 74, p. 1969-1993, 1984.

Bommer, J.J. and D.M. Boore, “Engineering Seismology,” *Encyclopedia of Geology*, Academic Press, Vol. 1, p. 499–514, 2004.

Bommer, J.J. and P.J. Stafford, “Seismic Hazard and Earthquake Actions,” *Seismic Design of Buildings to Eurocode 8*, A.Y. Elghazouli *ed*., Taylor and Francis, p. 6-46. 2008.

Boore, D.M. and G.M. Atkinson, “Ground-Motion Prediction Equations for the Average Horizontal Component of PGA, PGV, and 5%-Damped PSA and Spectral Periods between 0.01 and 10.0S,” *Earthquake Spectra*, Vol. 24, No. 1, 2008.

Boore, D.M., W.B. Joyner, and T.E. Fumal, “Equations for Estimating Horizontal Response Spectra and Peak Acceleration from Western North American Earthquakes: A Summary of Recent Work,” *Seismological Research Letters*, Vol. 68, p. 128–153, 1997.

Boore, D. M., W. B. Joyner, and L. Wennerberg. “Fitting the Stochastic ω-2 Source Model to Observed Response Spectra in Western North America: Trade-offs between $\Delta\sigma$ and κ,” *Bull. Seismol. Soc. Amer.*, 82, p. 1956–1963, 1992.

Campbell, K. and Y. Bozorgnia, “Campbell-Bozorgnia NGA Ground Motion Relations for the Geometric Mean Horizontal Component of Peak and Spectral Ground Motion Parameters,” *PEER Center Report 2007/02*, Pacific Earthquake Engineering Research Center, University of California, Berkeley, 2007.

Campbell, K. and Y. Bozorgnia, “NGA Ground Motion Model for the Geometric Mean Horizontal Component of PGA, PGV, PGD, and 5% Damped Linear Elastic Response Spectra for Periods Ranging from 0.01 to 10s,” *Earthquake Spectra*, Vol. 24, No. 1, 2008.

Chiou, B., et al., “NGA Project Strong-Motion Database,” *Earthquake Spectra*, Vol. 24, No. 1, 2008.

Chiou, B. and R. Youngs, “An NGA Model for the Average Horizontal Component of Peak Ground Motion and Response Spectra,” *Earthquake Spectra*, Vol. 24, No. 1, 2008.

Coleman, R.G., “Petrologic and Geophysical Nature of Serpentinites,” *Geological Society of America Bulletin*, Vol. 82, p. 897–918, 1971.

Dickenson, W.R., “Table Mountain Serpentinite Extrusion in California Coast Ranges,” *Geological Society of America Bulletin*, Vol. 77, p. 451–472, 1966.

Douglas, J., H. Bungum, and F. Scherbaum, “Ground-motion Prediction Equations for Southern Spain and Southern Norway Obtained Using the Composite Hybrid Model Perspective”, J. Earthq. Eng. 10, p. 33–72, 2006.

Goldfinger, C., “Chapter 2B—Sub-Aqueous Paleoseismology,” J.P. McCalpin, ed., *Paleoseismology*, 2nd Edition, Elsevier Academic Press, Missouri, p. 119–170, 2009.

Graizer, V. and E. Kalkan, “Ground Motion Attenuation Model for Peak Horizontal Acceleration from Shallow Crustal Earthquakes,” *Earthquake Spectra*, Vol. 23, No. 3, p. 585–613, 2007.

Graizer, V. and E. Kalkan, “Prediction of Response Spectral Acceleration Ordinates Based on PGA Attenuation,” *Earthquake Spectra*, Vol. 25, No. 1, p. 39–69, 2009.

Hall, C.A., Jr., “Geologic Map of the Morrow Bay South and Port San Luis Quadrangles, San Luis Obispo County, California,” *U.S. Geological Survey Miscellaneous Field Studies Map MF-511, Scale 1:24,000*, 1973.

Hall, T., T.D. Hunt, and P.R. Vaughan, “Holocene Behavior of the San Simeon Fault Zone, South-Central Coastal California,” *Seismotectonics of the Central California Coast Ranges,*” I.B. Alterman, R.B. McMullen, L.S. Cluff, and D.B. Slemmons, eds., Geological Society of America Special Paper 292, p. 167–189, 1994.

Hanks, T.C. and W.H. Bakun, “A Bilinear Source-Scaling Model for M–log A Observations of Continental Earthquakes,” *Bull. Seismol. Soc. Amer.*, Vol. 92, No. 5, p. 1,841–1,846, 2002.

Hanna, W.F., S.H. Burch, and T.W. Dibblee, Jr., “Gravity, Magnetics, and Geology of the San Andreas Fault Area Near Gholame, California,” U.S. Geological Survey Professional Paper 646-C, 1974.

Hanson, K.L., et al., “Style and Rate of Quaternary Deformation of the Hosgri Fault Zone, Offshore South-Central California,” *Evolution of Sedimentary Basins/Offshore Oil and Gas Investigations—Santa Maria Province*, M.A. Keller, ed., *U.S. Geological Survey Bulletin 1995-BB*, 2004.

Hanson, K.L., et. al., “Correlation, Ages, and Uplift Rates of Quaternary Marine Terraces, South-Central California,” *Seismotectonics of the Central California Coast Range,* I.B. Alterman, R.B. McMullen, L.S. Cluff, and D.B. Slemmons, eds., Geological Society of America Special Paper 292, p. 45–72, 1994.

Hardebeck, J.L., “Seismotectonics and Fault Structure of the California Central Coast,” *Bull. Seismol. Soc. Amer.,* Vol. 100, p. 1,031–1,050, 2010.

Hardebeck, J.L. and P.M. Shearer, “A New Method for Determining First-Motion Focal Mechanisms,” *Bull. Seismol. Soc. Amer.*, Vol. 92, p. 2,264–2,276, 2002.

Hardebeck, J.L., H. Zhang, and C.H. Thurber, “Determination of the Geometry of the Shoreline and Hosgri Faults, Near Point Buchon, California, from Seismicity Relocations,” The Eastern Section 2011 83rd Annual Meeting of the Seismological Society of America, Little Rock, AK, October 16–18, 2011, El Cerrito, CA, Seismological Society of America, http://www.seismosoc.org/meetings/showabstract.php?recid=67722011, 2011.

Idriss, I.M., “An NGA Empirical Model for Estimating the Horizontal Spectral Values Generated By Shallow Crustal Earthquakes,” Earthquake Spectra 24, p. 217-242, 2008.

Kennedy, R.P. “Overview of methods for seismic PRA and margin analysis including recent innovations”. Proceedings of the OECD-NEA Workshop on Seismic Risk, August 10-12, Tokyo, Japan, 1999.

Langenheim, V.E., R.C. Jachens, and K. Moussaoui, “Aeromagnetic Survey Map of the Central California Coast Ranges,” U.S. Geological Survey Open File Report 2009-1044, http://pubs.usgs.gov/of/2009/1044/, 2009.

Lettis, W.R. and N.T. Hall, “Los Osos Fault Zone, San Luis Obispo County, California,” *Seismotectonics of the Central California Coast Ranges,* I.B. Alterman, R.B. McMullen, L.S. Cluff, and D.B. Slemmons, eds., Geological Society of America Special Paper 292, p. 73–102, 1994.

Lettis, W.R., et al, “Quaternary Tectonic Setting of South-Central Coastal California,” *U.S. Geological Survey Bulletin 1995-AA*, http://pubs.usgs.gov/bul/l995/aa, 2004.

McGuire, R. K., W. J. Silva, and C. Constantino, Technical basis for revision of regulatory guidance on design ground motions: hazard and risk-consistent ground motion spectra guidelines, NUREG/CR- 6728, prepared for U.S. Nuclear Regulatory Commission, Office of Nuclear Regulatory Research, Division of Engineering Technology, 2001.

McLaren, M.K. and W.U. Savage, “Seismicity of South-Central Coastal California, October 1987 through January 1997,” *Bull. Seismol. Soc. Amer.*, Vol. 91, p. 1,629–1,658, 2001.

Morre, D.E. and M.J. Rymer, “Talc-Bearing Serpentinite and the Creeping Section of the San Andreas Fault,” *Nature*, Vol. 448, p. 795–797, 2007.

Pacific Gas & Electric Company, “Final Report of the Diablo Canyon Long-Term Seismic Program, Report to the U.S. NRC,” Agencywide Documents and Access Management System (ADAMS) Accession No. ML8803160246, U.S. Nuclear Regulatory Commission Docket Nos. 50-275 and 50-323, San Francisco, CA, 1988.

Pacific Gas & Electric Company, “Addendum to the 1988 Final Report of the Diablo Canyon Long-Term Seismic Program,” U.S. Nuclear Regulatory Commission Docket No. 50-275 and No. 50-323, San Francisco, CA, February 1991.

Pacific Gas & Electric Company, “PG&E Letter No. DCL-91-091 Benefits and Insights of the Long-Term Seismic Program,” April 17, 1991, Docket No. 50-275, OL-DPR-80 and Docket No. 50-323, OL-DPR-82, ADAMS Accession No. ML9104300253, 1991a.

Pacific Gas & Electric Company, “PG&E Letter No. DCL-91-143 Long-Term Seismic Program—Implementation of the Results of the Program,” May 29, 1991, U.S. Nuclear Regulatory Commission, Docket No. 50-275, OL-DPR-80, and Docket No. 50-323, OL-DPR-82, ADAMS Accession No. ML9106070210, 1991b.

Pacific Gas & Electric Company, “Calculation 17-107, Rev 0, Postulated Ground Deformation Shoreline Fault Auxiliary Salt Water Buried Piping Stress Analysis,” August 3, 2009.

Pacific Gas & Electric Company, “Progress Report: Shoreline Fault Zone, Central Coastal California,” U.S. Nuclear Regulatory Commission, Docket Nos. 50-275 and 50-323, PG&E Letter No. DCL-10-003, January 13, 2010, ADAMS Accession No. ML100190142, 2010.

Pacific Gas & Electric Company, “Report on the Analysis of the Shoreline Fault Zone, Central Coastal California, Report to the U.S. Nuclear Regulatory Commission,” ADAMS Accession No. ML110140431, 2011.

Petersen, M., et al., “Evaluating Fault Rupture Hazard for Strike-Slip Earthquakes,” Geotechnical Engineering for Transportation Projects (GSP 126), *ASCE Proceedings of GeoTrans 2004*, p. 787–796, 2004.

Petersen, M., et al., “Fault Displacement Hazard for Strike-Slip Faults,” *Bull. Seismol. Soc. Amer.*, Vol. 101, p. 80–825, 2011.

Schwartz, D.P. and K.J. Coppersmith, “Fault Behavior and Characteristic Earthquake: Examples from Wasatch and San Andreas Faults,” *J Geophys Res*, Vol. 89, p. 5,681–5,698, 1984.

Silva, W., R. B. Darragh, N. Gregor, G. Martin, N. Abrahamson, and C. Kircher, “Reassessment of site coefficients and near-fault factors for building code provisions”, Technical Report Program Element II: 98-HQ-GR-1010, Pacific Engineering and Analysis., El Cerrito, California USA, 1998.

Silva, W. J., N. A. Abrahamson, G. Toro, and C. Costantino, Description and Validation of the Stochastic Ground Motion Model, Brookhaven National Laboratory, Upton, N.Y., 1997.

Sliter, R.W., et al., “High-Resolution Seismic Reflection and Marine Magnetic Data Along the Hosgri Fault Zone, Central California,” U.S. Geological Survey Open File Report 2009-1100, Ver. 1.1, http://pubs.usgs.gov/of/2009/1 100, 2009.

U.S. Nuclear Regulatory Commission, “Safety Evaluation Report Related to the Operation of Diablo Canyon Nuclear Power Plant, Units 1 and 2,” NUREG-0675, Supplement No. 7, May 26, 1978.

U.S. Nuclear Regulatory Commission, “Safety Evaluation Report Related to the Operation of Diablo Canyon Nuclear Power Plant, Units 1 and 2,” NUREG-0675, Supplement No. 34, ADAMS Accession No. 9106120065, June 6, 1991.

U.S. Nuclear Regulatory Commission, “Recommendations for Probabilistic Seismic Hazard Analysis: Guidance on Uncertainty and Use of Experts,” NUREG/CR-6372, Washington, DC, 1997.

U.S. Nuclear Regulatory Commission, “A Performance-Based Approach to Define the Site-Specific Earthquake Ground Motion,” Regulatory Guide 1.208, Washington, DC, March 2007.

U.S. Nuclear Regulatory Commission, Research Information Letter 09-001, “Preliminary Deterministic Analysis of Seismic Hazard at Diablo Canyon Nuclear Power Plant from Newly Discovered ‘Shoreline Fault,’” Washington, DC, 2009.

U.S. Nuclear Regulatory Commission, “Practical Implementation Guidelines for SSHAC Level 3 and 4 Hazard Studies,” NUREG-2117, Washington, DC, 2012.

U.S. Nuclear Regulatory Commission, “Request for Information Pursuant to Title 10 of the *Code of Federal Regulations* 50.54(f) Regarding Recommendations 2.1, 2.3, and 9.3, of the Near-Term Task Force Review of Insights from the Fukushima Dai-ichi Accident,” ADAMS Accession No. ML12056A046, Washington, DC, 2012.

Van Houtte, C., S. Drouet, and F. Cotton, “Analysis of the Origins of Kappa to Compute Hard Rock to Rock Adjustment Factors,” *Bull. Seismol. Soc. Amer.*, 101, p. 2926-2941, 2011.

Waldhauser, F. and Ellsworth, W.L., “A Double-Difference Earthquake Location Algorithm; Method and Application to the Northern Hayward Fault, California,” *Bull. Seismol. Soc. Amer.*, Vol. 90, p. 1,353–1,368, 2000.

Walling, M., W. Silva, and N.A. Abrahamson, “Non-Linear Site Amplification Factors for Constraining the NGA Models,” *Earthquake Spectra*, Vol. 24, No. 1, 2008.

Watt, J.T., et al., “Geologic Mapping in the Central California Coastal Zone: Integrating Geology, Geophysics, and Geomorphology,” *Geological Society of America Abstracts with Program,* Vol. 41, No. 7, 2009.

Wells, D. and K.J. Coppersmith, “Empirical Relationships among Magnitude, Rupture Length, Rupture Width, Rupture Area, and Surface Displacement,” *Bull. Seismol. Soc. Amer.*, Vol. 84, No. 4, p. 974–1002, August 1994.

Wesnousky, S.G., “Predicting the Endpoints of Earthquake Ruptures,” *Nature,* Vol. 444, p. 358–360, 2006.

Youngs, R.R, “Epistemic Uncertainty in the NGA Models, Appendix D and Appendix G in Round Motion Models for the Pacific Northwest, Report to BC Hydro,” 2009.

Youngs, R.R. and K. Coppersmith, “Implications of Fault Slip Rates and Earthquake Recurrence Models to Probabilistic Seismic Hazard Estimates,” *Bull. Seismol. Soc. Amer.*, Vol. 75, p. 939–964, 1985.

Youngs, R.R., et al., “A Methodology for Probabilistic Fault Displacement Hazard Analysis (PFDHA),” *Earthquake Spectra,* Vol. 19, p. 191–219, 2003.

Zhang, H. and C.H. Thurber, “Double-Difference Tomography: The Method and Its Application to the Hayward Fault, California,” *Bull. Seismol. Soc. Amer.*, Vol. 93, p. 1,875–1,889, 2003.

Appendix A: Overview and Summary of the Senior Seismic Hazard Analysis Committee Guidelines

Appendix A is provided to provide background information for those readers of this report who do not have knowledge of how seismic analyses are carried out. This appendix describes one aspect of seismic analyses; that being the Senior Seismic Hazard Analysis Committee (SSHAC) process.

A.1 History, Current Guidance, and Objectives of the Senior Seismic Hazard Analysis Committee Process

The complexity of tectonic environments, coupled with the limitations in the data available for seismic source and ground motion characterization make the use of a significant level of expert judgment in seismic hazard assessment studies unavoidable. For critical facilities such as nuclear power plants, the judgments of multiple experts are required to capture the complete distribution of technically defensible interpretations (TDIs) of the available earth science data. However, in the early days of seismic hazard analyses, guidance for the appropriate use of experts did not exist and studies were conducted using different approaches.

In order to develop more standardized protocols, in the mid-1990s, the U.S. Nuclear Regulatory Commission (NRC), the U.S. Department of Energy, and the Electric Power Research Institute sponsored a study to develop recommendations for how studies incorporating the use of expert assessments should be conducted in the future. The Senior Seismic Hazard Analysis Committee (SSHAC) developed a structured, multilevel assessment process (the "SSHAC process") described in NUREG/CR-6372, "Recommendations for Probabilistic Seismic Hazard Analysis: Guidance on Uncertainty and Use of Experts," issued in 1997, that has since been used for numerous natural hazard studies. The SSHAC process provides a transparent method of structured expert interaction entirely focused on capturing the center, body, and range (CBR) of the full suite of TDIs that the available data permit. The goal is not to determine the single *best* interpretation; rather, it is to develop and integrate all TDIs. This approach leads to greater assurance that the "true" hazard at a site is captured within the breadth of the PSHA results.

NRC Regulatory Guide 1.208, "A Performance-Based Approach to Define the Site-Specific Earthquake Ground Motion," issued in March 2007, recommends the process for the development of new models to be used in probabilistic seismic hazard analyses (PSHAs). More recently, in 2012, the NRC developed NUREG-2117, "Practical Implementation Guidelines for SSHAC Level 3 and 4 Hazard Studies," after studying the experience and knowledge gained in the application of the original guidance in several studies conducted during the last 15 years. NUREG-2117 provides additional practical implementation guidelines consistent with the framework of NUREG/CR-6372, which is more general and high level in nature. NUREG-2117 also provides a much more extensive discussion of the Level 3 process, while NUREG/CR-6372 generally focused on the Level 4 approach. Much of the information in this section comes from NUREG-2117, and the reader is referred to that document if a more in-depth understanding is desired.

A.2 Epistemic and Aleatory Uncertainty

Regulations under Title 10 of the *Code of Federal Regulations* (10 CFR) 100.23(d)(1), "Determination of the Safe Shutdown Earthquake Ground Motion," require that uncertainty inherent in estimates of the Safe Shutdown Earthquake be addressed through an appropriate analysis, such as a PSHA. In a PSHA, uncertainty is generally separated into two categories, aleatory variability and epistemic uncertainty. Aleatory variability comes from the inherent randomness in natural processes (e.g., the hypocentral depth of any particular earthquake on

the Hosgri fault). Epistemic uncertainty is modeling uncertainty and comes either from our imperfect knowledge of the earth's systems or from a necessity to use simplified models for computational efficiency. An example of epistemic uncertainty is the spread of results of median ground motion prediction equation (GMPE) models for the same scenario. Aleatory variability is typically accounted for in a PSHA by using a probability distribution to express the randomness of the parameter. An integration process over the parameter is then used. Epistemic (modeling or interpretation) uncertainty requires expert judgment and the use of logic trees.

The complexity of the processes that generate earthquakes and the consequent ground shaking, and the invariably limited data available for seismic source and ground motion characterization (GMC), universally result in a range of TDIs of a complete set of earth science data for a site. This was apparent in the discussions in Section 4. This leads to many of the greatest challenges in seismic source characterization (SSC) and GMC model development. The fact that there is almost never a unique and unambiguous model for any component of the hazard input models reflects our generally imperfect knowledge of earthquake processes and of the factors influencing the shaking hazard at a specific location. This is the heart of epistemic uncertainty.

In theory, epistemic uncertainty can be reduced through the acquisition of additional data and improved understanding of the physical processes involved in earthquake generation and seismic wave propagation. However, in practice, a significant degree of epistemic uncertainty will always be associated with the SSC and GMC models developed for both deterministic seismic hazard analysis (DSHA) and PSHA, and expert judgment is required to infer both the most defensible and the most likely technical interpretations and their associated epistemic uncertainties. The tool most commonly used to incorporate epistemic uncertainty in current PSHA practice is the logic tree in which alternative parameter values are placed on different branches and assigned weights. The weights reflect the relative merit of each alternative value in the view of the analyst team. As described below, development of a complete PSHA model (in the form of a logic tree) that captures the CBR of TDIs is the goal of the SSC and GMC development processes in the NRC guidelines. Logic trees allow for transparency in both the models used and the weights given to each model. Examples of logic trees can be seen in a number of figures in Section 5 of the Shoreline Fault Report.

A.3 Overview of the Senior Seismic Hazard Analysis Committee Level 3 Process

An overview of the SSHAC Level 3 process is shown in Figure A-1, which is annotated to also show the status of the Diablo Canyon Power Plant (DCPP) project at the time of this writing. To capture the CBR of the TDIs of the available data, models, and methods, the SSHAC process encompasses two principal activities described as *evaluation* and *integration.* The fundamental goal of the SSHAC Level 3 process is to properly carry out and completely document the activities of evaluation and integration, defined as follows:

> *Evaluation:* The consideration of the complete set of data, models, and methods proposed by the larger technical community that are relevant to the hazard analysis.
>
> *Integration:* Representing the CBR of TDIs in light of the evaluation process (i.e., informed by the assessment of existing data, models, and methods).

The *evaluation* process starts by the Technical Integrator (TI) team (participant roles are discussed in Section A.4) identifying (with input from resource and proponent experts) the available body of hazard-relevant data, models, and methods—including all those previously produced by the technical community—to the extent possible. This body of existing knowledge is supplemented by new data gathered for the study, such as the data collected in the U.S. Geological Survey (USGS)-PG&E research program. The first workshop (workshops are discussed in Section A.5) assists with the identification of hazard-relevant data, models, and methods. The TI team then evaluates these data, models, and methods and documents both the process by which this evaluation was undertaken and the technical bases for all decisions made regarding the quality and usefulness of these data, models, and methods. This evaluation process explicitly includes interaction with, and among, members of the technical community. The expert interaction includes subjecting data, models, and methods to technical challenge and defense. Workshop #2 provides a forum for proponents of alternative viewpoints to debate the merits of their models. The successful execution of the evaluation is confirmed by the concurrence of the Participatory Peer Review Panel (PPRP) that the TI team has provided adequate technical bases for its conclusions about the quality and usefulness of the data, models, and methods, and has adhered to the SSHAC assessment process. The PPRP will also provide guidance on meeting the objective of considering all of the views and models existing in the technical community.

Informed by this evaluation process, the TI team then performs an *integration* process that may include incorporating existing models and methods, developing new methods, and building new models. The objective of this integration process is to capture the CBR of TDIs of the available data, models, and methods. The technical bases for the weights on different models in the final distribution, as well as the exclusion of any models and methods proposed by the technical community, need to be justified in the documentation. Workshop #3 provides an opportunity for the experts to review hazard-related feedback on their preliminary models and to receive comments on their models from the PPRP. To conclude the project satisfactorily, the PPRP will also need to confirm that the SSHAC assessment process was adhered to throughout and that all technical assessments were sufficiently justified and documented.

A.4 Participants in a Senior Seismic Hazard Analysis Committee Level 3 Process

Central to the success of the SSHAC process is the clear definition of the different roles that experts play and how they interact in the process. In the following section, each of the different expert roles is described in terms of the role of the individual or group in the process and the responsibilities that the individual or group assumes in the project.

A.4.1 Resource Expert

The *role* of a resource expert is to present data, models, and methods in an impartial manner. The expert is expected to present his or her understanding of a particular dataset, including how the data were obtained, or to present a model or a method with its limitations and caveats. In all cases, a resource expert is expected to make the presentation without any interpretation in terms of hazard input. The main responsibility of a resource expert is to share his or her technical knowledge in an impartial way in presentations to the evaluator experts. The resource expert is also expected to respond candidly and impartially to questions posed by the evaluator experts. The necessary attributes of a resource expert are knowledge and impartiality.

A.4.2 Proponent Expert

The role and responsibility of a proponent expert is to advocate a specific model, method, or parameter for use in the hazard analysis. Experts will advocate models within the forum of a formal workshop where they may be invited to present a model, which will usually be their own, either because the model has been published, is widely known, and is therefore considered a credible option, or because the model is controversial. In some cases, a proponent may be invited to present a relatively new model, which may not have even been published at that stage, if it is thought that the model is directly relevant to the hazard analysis and is credible. The proponent is required to justify this assertion, to demonstrate the technical basis for the model, and to defend the model in the face of technical challenge. The proponent is also charged with making full disclosure about the model in this process, including all underlying assumptions. A proponent expert has full responsibility for the material that he or she presents but does not participate in any way in the weighting of alternative hypotheses or in the ownership of the hazard models.

A.4.3 Evaluator Expert

The evaluator expert plays the most important role in a SSHAC process. The role and responsibility of the evaluator expert is to identify and objectively examine available data and diverse models, challenge their technical bases and underlying assumptions, and—where possible—test the models against observations. The process of evaluation includes identifying the issues and the applicable data, interacting among the experts (i.e., challenging other evaluators and proponent experts, interrogating resource experts) and finally considering and weighing alternative models and proponent viewpoints. In Level 3 studies, evaluators and integrators are the same people, but these labels refer to distinct roles played at different stages of the project. In a Level 3 project, the evaluator executes this responsibility as part of a team and, therefore, must interact openly and constructively with the other members of the team.

A.4.4 Technical Integrator

Integration is the process by which evaluations of candidate models are brought together in a single logic tree that reflects the CBR of the TDI. The role of the TI is linked with the role of evaluator (discussed above). Explicitly, in Level 3 studies, evaluator experts adopt the role of integrators during the second phase of their assessments when they develop a model that reflects their understanding of the range of TDIs. In a Level 3 study, interactions with other evaluators in the project also contribute to a successful integration process, as does a TI team with a mix of backgrounds, specialties, and experience levels.

The responsibility of a TI is to construct a model for input to a PSHA that captures the CBR of the TDI and to provide complete and clear justifications of the technical bases for all elements of the model, including the reasons for excluding or down-weighting any data, models, or methods. The model is in the form of a logic tree using existing or new models and assigning branch weights so they reflect the understanding of the broader community distribution. TIs in Level 3 studies will always be members of a team, and they have the responsibility to challenge the technical basis of assessments made by the other evaluators and to subject their own assessments to the same challenge.

The main attributes of a TI are the ability to objectively evaluate the views of others in developing models and expressions of uncertainty and to deeply appreciate the influences of different models and parameters on hazard results. The TI also needs to be able to produce

large volumes of clear and complete documentation on schedule as well as critically review all contributed documentation from evaluators and others.

A.4.5 Participatory Peer Review Panel

The PPRP is a key and indispensable element of a SSHAC Level 3 study. Within a SSHAC study, the PPRP is the only peer review team with a formal standing. Following the issuance of the final PSHA report, the PPRP must concur that the project has conformed to the requirements of the specified study level and that all technical assessments have been adequately defended and documented. Because the PPRP will be composed of experienced specialists in the field of seismic hazard assessment, this approval should carry considerable weight and can be expected to increase regulatory assurance.

The PPRP fulfills two parallel roles, the first being technical review. This means that the PPRP is charged with ensuring that the full range of data, models, and methods has been duly considered in the assessment and also that all technical decisions are adequately justified and documented. The second role of the PPRP is process review, which means ensuring that the project conforms to the requirements of the selected SSHAC process level. Collectively, these two roles imply oversight to ensure that the integration is performed appropriately. Membership of the PPRP is always on an individual basis and not as an affiliate of any organization.

The responsibility of the PPRP is to provide clear and timely feedback to the project to ensure that any technical or process deficiencies are identified at the earliest possible stage so that they can be corrected. In terms of technical review, a key responsibility of the PPRP is to highlight any data, models, methods or proponents views that have not been considered. Beyond completeness, it is not within the remit of the PPRP to judge the weighting of the logic trees in detail but rather to judge the justification provided for the models, included or excluded, and for the weights applied to the logic tree branches.

The PPRP has the clear responsibility to be present at all the formal workshops as observers and to subsequently submit a consensus report containing comments, questions, and suggestions. Some confusion exists about this specific point because of the use of the word “participatory” that was introduced to distinguish this type of review from late-stage review. It has since been suggested that a more appropriate adjective might be “continual” (Hanks et al., 2009) to make it clear that the PPRP does not participate in the technical assessments.

The *attributes* of the PPRP can be defined both for individuals and in collective terms for all of the members of the panel as a group. A key requirement is for each member of the group to have an understanding of and commitment to the principles of the SSHAC process. In addition, the members of the panel must collectively cover all technical aspects of building SSC and GMC models and of conducting a PSHA. The requirements for technical expertise are particularly emphasized for a Level 3 study.

A.5 Workshops in the Senior Seismic Hazard Analysis Committee Level 3 Process

NUREG-2117 discusses a number of important and required steps in a SSHAC Level 3 process. Among the most critical are the three required workshops. The structured, facilitated workshops are the hallmark of a SSHAC Level 3 process and provide opportunities for key interactions to occur; for models and interpretations to be presented, debated, and defended; and for sponsors, reviewers, and regulators to observe the progress being made on the study.

As will be noted further below, however, they are *not* the place where models are developed and technical assessments are made. That occurs between the workshops in technical working meetings.

Each workshop has a specific focus and goal, and each requires that particular work activities be conducted before its occurrence and that certain work activities occur afterward. The ground rules for the workshops are generally established and presented at the beginning of each workshop so that the attendees understand and can fulfill their particular roles.

A.5.1 Workshop #1: Significant Issues and Available Data

The goals of Workshop #1 are (1) to identify the technical issues of highest significance to the hazard analysis and (2) to identify the available data and information that will be needed to address those issues. The workshop should begin with a clear definition of the goals of the workshop, an explanation of the process that will be followed, and a definition of the roles of all those who attend. First and foremost, the workshops are held to provide information to assist the TI Leads and the evaluator experts in their technical assessments. Therefore, it is essential that they be given ample opportunity to ask questions and to thoroughly understand what is being presented. All other workshop attendees are "observers" except as their participation is required. At the first workshop, resource experts are asked to present and discuss their databases. Questions following each presentation should first come from the evaluator experts, not from other resource experts or other workshop attendees. However, it is strongly suggested that a short period of time be set aside at the end of each day for any of the observers at the workshop, including the PPRP and any regulatory or State observers present, to make statements or to pose questions.

Prior to Workshop #1, the TI Leads should conduct preliminary hazard studies and sensitivity studies to assist in identifying hazard-significant issues based on available data. The sensitivity analyses should be presented and discussed at the workshop, and they can be supplemented with considerations of hazard sensitivity at other sites and the issues that have generally been shown to be important, based on experience. The purpose of identifying the hazard-significant issues first is to provide a basis for focusing and prioritizing the database development efforts. This part of the workshop should end with a listing of the hazard-significant issues and a listing of the types of data that can best address the issues.

The second part of Workshop #1 focuses on the data available to address the hazard-significant issues identified in the first part of the workshop. The discussions of the available data should be through a series of presentations by resource experts who have developed specific datasets. Data resource experts should come from a wide range of affiliations and aspects of the technical community. The goal of this part of the workshop is to assist the TI members in identifying the data and information that should be made part of the project database and in understanding the attributes of the available datasets (e.g., the precision, limitations) to the extent possible. During the course of the data identification process, the evaluator experts may identify data gaps that can be filled with new data collection efforts within the time and resource constraints of the project. If data collection activities are contemplated or have been initiated at the time of the workshop, they should be described in detail at this workshop.

One concern that often emerges in the first workshop is the tendency for the resource experts to move from merely a presentation of available data into discussions of their interpretations of the data and the models that they have developed from it. In most earth science problems, no clear-cut boundary exists between what we call "data" and what we call "interpretations." The forum for hearing and debating alternative interpretations of the data is Workshop #2. So the TI

Leads generally make every effort to limit the discussions at Workshop #1 to the available data, acknowledging that some discussion of data interpretations will inevitably occur.

In the case of the DCPP SSHAC Level 3 study, Workshop #1 was held November 29 to December 2, 2011. The workshop presentations can be viewed on the PG&E Web site at http://www.pge.com/mybusiness/edusafety/systemworks/dcpp/SSHAC/workshops/index.shtml.

A.5.2 Workshop #2: Alternative Interpretations

The goals of Workshop #2, "Alternative Interpretations," are (1) to present, discuss, and debate alternative viewpoints on key technical issues, (2) to identify the technical bases for the alternative hypotheses and to discuss the associated uncertainties, and (3) to provide a basis for the subsequent development of preliminary hazard models that consider these alternative viewpoints. The workshop also provides an opportunity to review the progress being made on the database development and to elicit additional input, as needed, about this activity.

A key attribute of this workshop is the discussion and debate of the merits of alternative models and viewpoints on key technical issues. Proponents and resource experts should present their interpretations and the data supporting them. Presentations of alternative viewpoints on the same topic should be juxtaposed, if possible, and facilitated discussion should occur with a focus on implications of the inputs to the hazard analysis (not just on scientific viability) and on uncertainties (e.g., which conceptual models would capture the range of interpretations and the relative credibility of the alternatives). Because not all proponents of alternative viewpoints may be able to attend the workshop, interpretations made by individuals who may not be present should be identified and discussed. This will help ensure that all viewpoints are ultimately considered. If feasible, the TI should present those viewpoints at the workshop so that an opportunity exists to present, challenge, and defend them.

In the spirit of capturing the spectrum of thinking across the entire technical community, a goal of this workshop is to provide an effective forum for the exchange of ideas. More importantly for the SSHAC process, the workshop provides a unique opportunity for the evaluator experts to begin their consideration of the range of models and methods held by the larger technical community. Therefore, they should strive to not only understand the alternative interpretations, but also the degree to which each hypothesis is supported by the available data. The proponent experts should be asked to be prepared to discuss the uncertainties in their interpretations, the strengths and weaknesses in their arguments, and their view of the degree of support that their interpretations have within the larger technical community. It is often useful for the TI to provide presenters with a list of questions developed by the TI specifically for each presenter in order to focus each presentation on areas of interest to model development. A role of the TI should be to provide support, as needed, to proponents to ensure that interpretations are not judged on the basis of presentation skills. Proponent experts should be encouraged to interact among themselves within the structure facilitated by the TI Lead.

A.5.3 Workshop #3: Feedback

Following Workshop #2, the evaluator experts develop their preliminary models. Based on these models, preliminary calculations and sensitivity analyses are conducted. The goal of Workshop #3, "Feedback," is to present and discuss the preliminary models and calculations in a forum that provides the opportunity for feedback to the evaluators. Feedback is given in the form of hazard results and sensitivity analyses to shed light on the most important technical issues. Feedback is also provided at this workshop by participation of the PPRP members and

by allowing them to ask questions about the preliminary SSC and GMC models. Feedback provided at this workshop will ensure that no significant issues have been overlooked and will allow the evaluators to understand the relative importance of their models, uncertainties, and assessments of weights. This information will provide a basis for the finalization of the models following the workshop.

Workshop #3 consists of two parts: (1) the evaluators presenting their preliminary models, with particular emphasis on the way in which alternative viewpoints and uncertainties have been incorporated, and (2) sensitivity analyses and hazard calculations that provide insight into the preliminary models. In the discussions of the preliminary models, the technical bases for the assessments and weights should be described to allow for a discussion of the implications and constraints provided by the available data. In a Level 3 study, the entire TI Team will have been involved in the development of the preliminary model, and it is not expected that individual members of the team will question aspects of the model. Rather, the PPRP will be expected to question and probe aspects of the preliminary model to understand the manner in which the views of the larger technical community have been considered and the range of technically defensible interpretations included. In the second part of the workshop, the presentation of the sensitivity analyses and preliminary hazard calculations provide a way to focus discussion on those issues with the greatest hazard significance, including the largest contributors to uncertainty. In turn, this will serve to focus the assessments performed after the workshop on those technical issues of most importance to the hazard results. It is important to include not only hazard calculations and associated sensitivity analyses but also sensitivity analyses that will provide insight into the models themselves. For example, the effect of various components (branches of the logic tree) of the SSC model on the assessments of maximum earthquake magnitudes and earthquake recurrence rates could be examined. Likewise, the relative contribution that the epistemic uncertainty and aleatory variability in a particular element of the model make to an intermediate output can be explored. These feedback calculations are not intended to provide a basis for artificially truncating or otherwise limiting the models that the evaluators developed. Rather, they are intended to provide a basis for prioritizing the activities associated with developing the final models. Developing and using feedback during the integration (model-building) process is an important characteristic of a SSHAC Level 3 process.

A.5.4 Documentation Requirements

The original SSHAC report (NUREG/CR-6372) devotes Section 7 to recommendations on documentation. Those recommendations are further enhanced in NUREG-2117. The project documentation is the fundamental basis for the reader to understand (1) what process was used in the hazard analysis, (2) what data were available and used in the evaluation process, (3) how the data, models, and methods of the larger technical community were considered, (4) the elements of the models and their technical bases, (5) how the models capture the CBR of TDIs, and (6) the hazard results and instructions for their use. The draft report is subject to review by the sponsors and other groups but especially by the PPRP.

A.6 Appendix A References

Hanks, T.C. and W.H. Bakun, “A Bilinear Source-Scaling Model for M–log A Observations of Continental Earthquakes,” *Bull. Seismol. Soc. Amer.*, Vol. 92, No. 5, p. 1,841–1,846, 2002.

Hanks, T.C., N.A. Abrahamson, D.M. Boore, K.J. Coppersmith and N.E. Knepprath (2009). Implementation of the SSHAC Guidelines for Level 3 and 4 PSHAs – Experience gained from actual applications. *Open-File Report 2009-1093*, US Geological Survey, Reston VA.

Pacific Gas & Electric Company, “Report on the Analysis of the Shoreline Fault Zone, Central Coastal California, Report to the U.S. Nuclear Regulatory Commission,” ADAMS Accession No. ML110140431, 2011.

U.S. Nuclear Regulatory Commission, “Recommendations for Probabilistic Seismic Hazard Analysis: Guidance on Uncertainty and Use of Experts,” NUREG/CR-6372, Washington, DC, 1997.

U.S. Nuclear Regulatory Commission, “A Performance-Based Approach to Define the Site-Specific Earthquake Ground Motion,” Regulatory Guide 1.208, Washington, DC, March 2007.

U.S. Nuclear Regulatory Commission, “Practical Implementation Guidelines for SSHAC Level 3 and 4 Hazard Studies,” NUREG-2117, Washington, DC, 2012.

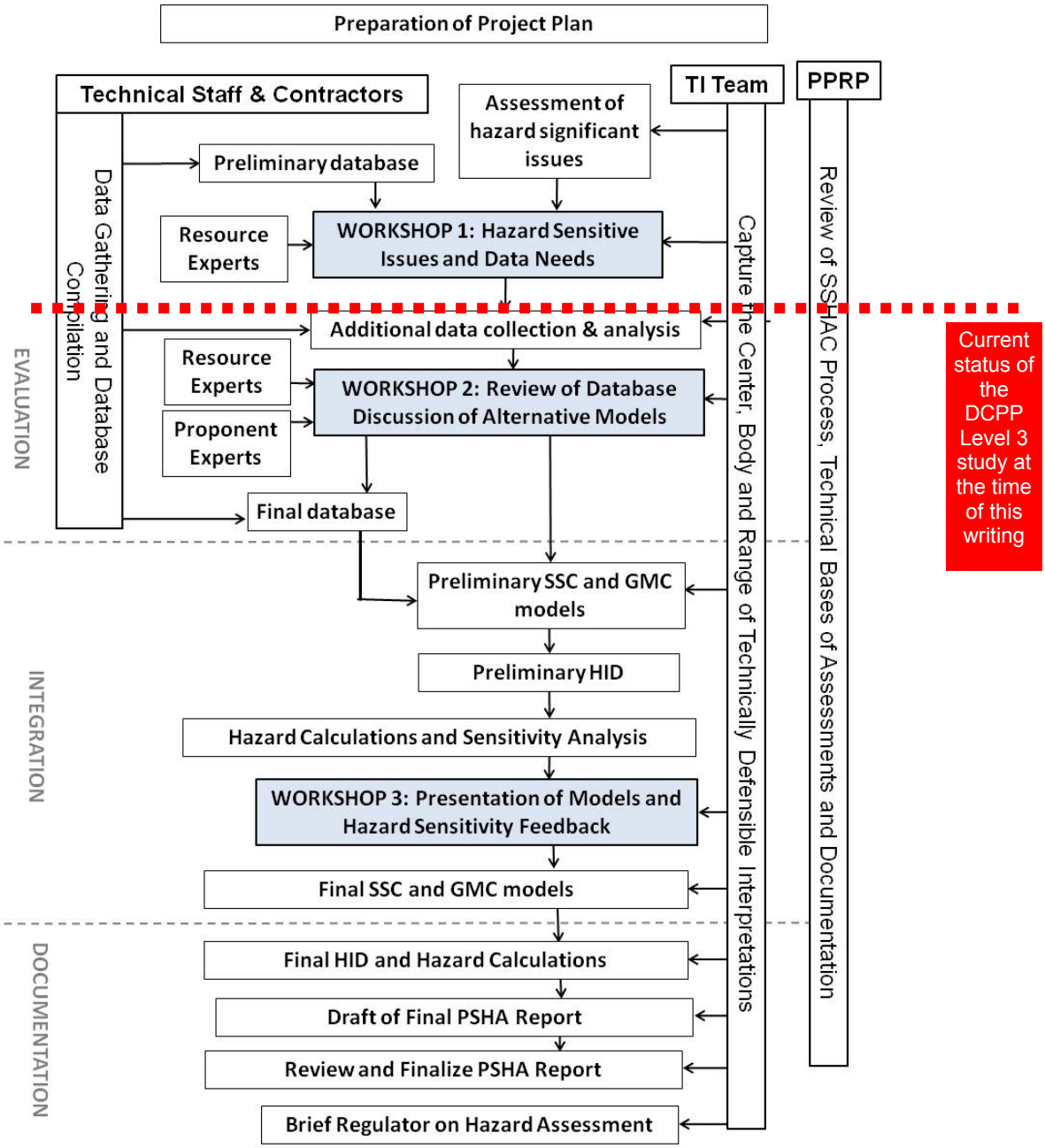

Figure A-1 Diagram illustrating the various participants and activities within a SSHAC Level 3 process (Figure 4-1 of NUREG-2117 annotated with status of DCPP SSHAC Level 3 Study). The beginning of the project occurs at the top of the diagram, and time progresses toward the bottom. The activities associated with evaluation, integration, and documentation are shown. HID is the hazard input document that contains only a description of the model for the PSHA analyst.

Appendix B: NRC Assessment of DCPP Site Correction Factors

B.1 NRC Assessment of DCPP Site Correction Factors

As discussed in Section 5.6 of this report, the near-surface shear wave velocities measured at the DCNPP site are approximately 1200 m/s. In typical seismic engineering applications, the near-surface shear-wave velocity (or its proxy, V_{S30}) is used as a direct input parameter in the GMPEs to estimate ground motion amplitudes. However, the lack of a significant amount of empirical ground motion data recorded at sites with near-surface velocities greater than 900 m/s renders direct application of these GMPEs questionable using this approach. To overcome this issue, an alternative approach was utilized by PG&E in the Shoreline Fault Report that estimated median ground motions for a V_{S30} value that was well constrained by empirical observations (760 m/s in this case) and then developed correction factors that are applied to make the median values appropriate for the site velocity of interest (as described in Section 5.7). This Appendix documents and describes the staff assessment of the development of the correction factors that were used by PG&E as well as the development of an independent set of factors by the NRC staff.

B.2 Correction Factors Applied in the Shoreline Fault Report

The PG&E approach to the development of site response correction factors based on near-surface shear wave velocity was to utilize a set of generic correction factors that had been developed for possible use with the NGA GMPEs (Silva, 2008). Additional discussion on the development of these factors is contained in Walling et al. (2008). That study developed correction factors using a number of generic velocity profiles. Two of these velocity profiles were similar to the shear-wave velocity conditions inferred for the DCPP site. These factors were applied by PG&E and are contained in Table 5.6 of the present report. In the view of the NRC staff, the applicability of these factors for the DCPP site is determined by several factors. First, the development of the factors utilized a simple seismological model that assumed a specific value of 0.04 s for the kappa (κ_0) factor. Kappa is used to represent the high-frequency attenuation of seismic waves by the near-surface geologic materials (Anderson and Hough, 1984, Boore, 2003). A relevant question that the staff needed to answer is the following: Is the κ_0 value used by Silva (2008) appropriate for the DCPP site? PG&E estimated a value of 0.045 s for kappa based on a single recording of a relatively small earthquake (the Deer Canyon earthquake) at the DCPP site (described in Appendix L of the Shoreline Fault Report). Based on the similarity in kappa values used in the Silva (2008) study (0.04 sec) and that estimated for the Deer Canyon earthquake (0.045 sec), PG&E concluded the Silva (2008) factors could be applied directly to the DCPP site.

A second issue that impacts the applicability of the Silva (2008) factors is the use of a generic velocity profile and a randomization procedure used in the Silva study. That set of factors was developed for use at generic sites with limited or poorly known velocity structure.

B.3 NRC Staff Evaluation and Development of Alternative Correction Factors

The staff identified three sets of recordings that could be used to develop an estimate of κ_0 at the DCPP site. The first is the 2003 Deer Canyon recording used by PG&E in the Shoreline Fault report. In addition, recordings from the 2004 Parkfield and 2003 San Simeon earthquakes at the DCPP were made available to the staff by PG&E.

B.3.1 Methodology to Estimate Kappa

The methodology used by NRC staff to estimate kappa at the DCPP site relied on a widely used, simple seismological model to represent earthquake source, propagation path and site characteristics (Boore, 2003 and references therein). The ground motions recorded at a given site from an earthquake can be represented in the frequency domain as:

$$Y(M_0, R, f) = E(M_0, f) \cdot P(R, f) \cdot G(f).$$

Where $Y(M_0,R,f)$ is the recorded ground motion Fourier amplitude spectrum, $E(M_0,f)$ is the seismic source spectrum, $P(R,f)$ represents the propagation path effects, and $G(f)$ represents the modification due to site effects. In this equation M_0 is the seismic moment of the earthquake, R is the distance from the source to the site, and f is frequency. The seismic moment and the earthquake magnitude are related through the definition of the moment magnitude, M (Hanks and Kanamori, 1979):

$$\text{Log } M_0 = 1.5M + 16.05.$$

The $P(R, f)$ term accounts for path effects, geometrical spreading and anelastic attenuation and can be expressed as:

$$P(R,f) = S(R)\, exp((-\pi f R)/(Q(f)V_S)).$$

Where $S(R)$ is the geometrical spreading function, $Q(f)$ is the seismic quality factor, and V_S is the shear-wave velocity in the upper crust.

The $G(f)$ term accounts for upper crustal amplification and diminution:

$$G(f) = A(f) \cdot D(f).$$

Where $A(f)$ is the amplification function relative to source depth velocity conditions ($A(f) = (Zsource/Zavg)^{0.5}$), where Z is the product of density and velocity (ρV_S) and $D(f)$ represents the frequency-dependent diminution term ($D(f) = exp(-\pi\kappa_0 f)$).

The approach developed by Anderson and Hough (1984) to estimate κ_0 utilizes a fit to the slope of the observed earthquake Fourier spectrum in log-linear space corrected for geometric spreading, anelastic attenuation and crustal amplification. A second approach involves fitting the simple seismological model described above to the entire response spectrum which involves assumptions not only for geometric spreading, anelastic attenuation and crustal amplification but for earthquake magnitude and stress drop. Both of these approaches were used by NRC staff to judge the applicability of the ~0.04 s kappa valued suggested by PG&E for the Deer Canyon earthquake recording.

To perform the necessary corrections for crustal amplification, the NRC staff used the measured near-surface shear-wave velocity profile from the DCPP site combined with the generic central California velocity profile used by Boore (2003) and Silva (2008) to develop a site-specific $A(f)$ function. The shear-wave velocity profile and resulting $A(f)$ function adopted for this assessment are shown in Figure B-1. Since the generic central California upper crustal velocity model has been successfully applied to the analysis of both the Parkfield and San Simeon events (Liu et al. 2006, Dreger et al., 2005) in the literature, the $A(f)$ function will be utilized in the analysis of all three of the subject earthquakes.

The corrections for path effects ($P(f)$, above) will be numerically different for each of the subject earthquakes, but rely on a consistent set of assumptions for this assessment. The geometrical spreading function for central California (Assatourinis and Atkinson (2007)) is assumed to be represented by:

$Z(R) = 1/R$ for R<= 40 km, and $(1/40)(40/R)^{0.5}$ for R>40 km.

Where R is the source-site distance. For the present assessment the following values for distances between DCPP and the earthquake source were assumed: Deer Canyon earthquake: 7.8 km, San Simeon earthquake: 50 km, and Parkfield earthquake: 85 km (V. Graizer, pers.comm, N. Abrahamson, pers.comm.).The crustal anelastic attenuation function requires specification of a model for the seismic quality factor Q, this model for central California is assumed to be $Q(f) = 150\ f^{0.5}$ (Mena et al., 2006).

The fits to the slope of the acceleration Fourier amplitude spectra (the Anderson and Hough method described above) recorded at DCPP for each of the three earthquakes considered are shown in Figure B-2 and Figure B-3. The frequency range chosen for the fitting process was determined by a visual assessment of the signal-to-noise ratio at high frequency and of the estimated corner frequency of the seismic source on the low-frequency end of the spectrum. The average of the results for the three events suggests a kappa value of 0.04 s is reasonable.

The second method that was used to estimate kappa (or at least understand the limitations of estimating kappa) relied on calculating a geometric mean structural response spectrum with measured ground motions from an event, and then identifying a kappa value that produces a best fitting response spectrum. This process again relies on the simple seismological model and the assumptions described above. In addition, the process requires specification of magnitude and stress drop. To perform these comparisons the NRC staff relied on published magnitude values for the San Simeon and Parkfield events (Hardebeck et al. 2004; Harris and Arrowsmith, 2006) and a documented estimate for the Deer Canyon event (V. Graizer, pers. comm.) The stress drop for each of the events was varied along with the kappa value to produce a theoretical spectrum that best matched the observed spectrum in a least squares sense over the frequency range of interest. Figure B-4 illustrates the trade-off between kappa and stress drop in producing a “best-fitting” response spectrum. Examples for the San Simeon and Deer Canyon response spectrum are shown in Figure B-5. Consistent with the “Anderson and Hough” method of estimating kappa, this method again suggests a value of 0.04 s to be reasonable and consistent with the limited observations.

B.3.2 Development of DCPP Site Specific Crustal Amplification Functions

The PG&E Shoreline fault report applied the generic shear-wave velocity site response correction factors of Silva (2008) and Walling et al. (2008). This approach utilized a generic velocity structure that was assumed to extend from mid-crustal depths to the ground surface. The NRC staff recognizes this approach to be appropriate for sites where very limited shear-wave velocity information is available or where site-specific estimates are not required. In an attempt to evaluate the applicability of the generic correction factors, as well as make the results as specific to the DCPP site as possible, NRC staff developed independent correction factors using DCPP-specific near-surface velocity profiles (Figure B-6). Two slightly different approaches were employed. The first used DCPP velocity profiles and a time series-based response analysis to produce correction factors (ratios between DCPP-specific and generic 760 m/s response spectra) that would be applied to the median GMPE results. The second approach used a response analysis based on the use of random vibration theory (RVT) to develop the correction factors (Silva et al., 1997 and McGuire et al., 2001).

The time-history-based response analysis identified and used a series of 55 time histories. The source for all of the recordings was the NGA-West/PEER database (http://peer.berkeley.edu/smcat/). Forty-five of these recordings are from earthquakes of magnitudes between 6.25 and 7 and rupture distances less than 25 km (Northridge, San

Fernando, Gazli, Friuli, Imperial Valley, and Loma Prieta events primarily). Ten of the records are from the M7.4 Chi-Chi Taiwan earthquake. In aggregate these records are felt to be representative of the magnitudes and distances that are most important to seismic hazards at the DCPP site as indicated from the PSHA conducted by PG&E (Sections 6.8 and 6.9 of the Shoreline Fault Report). Hence, the use of these records, in conjunction with the DCPP velocity profile, will result in the development of correction factors that are as appropriate as possible for this site. A subset of 27 time histories is plotted in Figure B-7 to illustrate the variability in spectral characteristics and amplitudes encompassed by the selected time histories. Depth dependent modulus degradation and damping curves were used in the equivalent linear response analyses.

The RVT-based analysis utilizes a single input response spectrum to perform the response analysis. Two assumptions regarding the behavior of the near-surface materials at higher ground motion levels were used in the RVT assessment. In one case, depth dependent modulus degradation and damping curves were applied (the Peninsular Ranges curves of Silva, 2008 (see Walling et al., 2008)). In the second case, linear behavior of the near-surface materials was assumed. Some randomization to the velocities (but not depths) in the upper 80 m of the profile was applied in the RVT-based analysis.

Figure B-8 compares the resulting correction factors for the time-series (TS) based approach and the RVT-based approach to those used by PG&E in the Shoreline Fault report. The results obtained using the TS and RVT approaches do not differ significantly from each other in this case. Since these two approaches represent two different, but both plausible, methodologies to perform this assessment, the NRC staff simply computed the arithmetic average of the three results to use in the deterministic analysis (shown as the heavy black line in Figure B-8). The correction factors used by PG&E in the Shoreline Fault Report are also shown in Figure B-8 as the dashed black line. As can be seen in Figure B-8, the NRC results are conservative relative to the PG&E results at virtually all frequencies.

B.4 Site Response Summary

The near-surface shear wave velocities at the DCPP site are relatively high (~1200 m/s). There are few ground motion recordings available to constrain the GMPEs in this velocity range. The approach taken by PG&E in the Shoreline Fault Report was to estimate ground motions for a V_{S30} value where sufficient data exists (760 m/s in this case) and then apply correction factors to the median GMPE results to render them applicable to the higher velocity conditions of the DCPP site. The NRC staff considers this approach to be reasonable and has performed a similar assessment in this RIL.

The NRC evaluated the kappa value assumed by PG&E in the response analysis of Silva (2008) using several earthquake recordings from the DCPP site. The NRC staff evaluation concluded that the kappa value assumed by PG&E was in fact, reasonable and consistent with the available data. However, the NRC staff believes that a defensible basis and adequate data exists to develop site-specific correction factors for the DCPP site. The DCPP-specific correction factors developed by the NRC staff are conservative relative to the generic factors proposed by PG&E in the Shoreline Fault Report at virtually all spectral frequencies. The NRC staff used this more conservative set of correction factors in the deterministic evaluation discussed in Section 5.8 of the RIL. These correction factors are applied to the median ground motion estimates, the 84th-percentile values are obtained by multiplying the median by exp(σ).

The assessment presented in this report should not be viewed as a substitute for a more detailed site-specific response analysis that should be undertaken in the course of performing the PSHA in response to the 10 CFR 50.54(f) letter.

B.5 Appendix B References

Assatourians, K., and G. M. Atkinson, "Modeling Variable-Stress Distribution with the Stochastic Finite-Fault technique," *Bull. Seismol. Soc. Amer.*, 97, p. 1935-1949, 2007.

Anderson, J. G., and S. E. Hough, "A Model for the Shape of the Fourier Amplitude Spectrum of Acceleration at High-Frequencies," *Bull. Seismol. Soc. Amer.*, 74, p. 1969-1993, 1984.

Boore, D. M., "Simulation of Ground Motions Using the Stochastic Method," Pure and Applied Geophys., p. 635-676, 2003.

Dreger, D. S., L. Gee, P. Lombard, M. H. Murray, and B. Romanowicz, "Rapid Finite-Source Analysis and Near-Fault Ground Motions: Application to the 2003 M 6.5 San Simeon and 2004 M 6.0 Parkfield Earthquakes," *Seismol. Res. Lett.*, 76, p.40-48, 2005.

Hanks, T. C., and H. Kanamori, "A Moment Magnitude Scale," *Jour. Geophys. Res.,* 84, p. 2348-2350, 1979.

Hardebeck, J. L., J. Boatwright, D. Dreger, R. Goel, V. Grazier, K. Hudnut, C. Ji, L. Jones, J. Langbein, J. Lin, E. Roeloffs, R. Simpson, K. Stark, R. Stein, and J. Tinsley, "Preliminary Report on the 22 December 2003, M6.5 San Simeon, California, Earthquake," *Seism. Res. Lett.* 75**,** p. 155–172, 2004.

Harris, R. A., and J. R. Arrowsmith, "Introduction to the Special Issue on the 2004 Parkfield Earthquake and the Parkfield Earthquake Prediction Experiment," *Bull. Seismol. Soc. Amer.*, 96, p. S1-S10, 2006.

McGuire, R. K., W. J. Silva, and C. Constantino, Technical basis for revision of regulatory guidance on design ground motions: hazard and risk-consistent ground motion spectra guidelines, NUREG/CR- 6728, prepared for U.S. Nuclear Regulatory Commission, Office of Nuclear Regulatory Research, Division of Engineering Technology, 2001.

Mena, B. E. Durukal, and M. Erdik, "Effectiveness of Hybrid Green's Function Method in the Simulation of Near-Field Strong Motion: An Application to the 2004 Parkfield Earthquake," *Bull. Seismol. Soc. Amer.*, 96, p. S183-S205, 2006.

Liu, P., S. Custodio, and R. J. Archuleta. Kinematic inversion of the 2004 M 6.0 Parkfield earthquake including an approximation to site effects, *Bull. Seism. Soc. Am.* **96,** no. 4B, S143–S158, 2006.

Silva, W. J., Site Response Simulations for the NGA Project, Report prepared for the Pacific Engineering Center, Pacific Engineering and Analysis Corp., 2008.

Silva, W. J., N. A. Abrahamson, G. Toro, and C. Costantino, Description and Validation of the Stochastic Ground Motion Model, Brookhaven National Laboratory, Upton, N.Y., 1997.

Walling, M., W. Silva, and N.A. Abrahamson, "Non-Linear Site Amplification Factors for Constraining the NGA Models," *Earthquake Spectra*, Vol. 24, No. 1, 2008.

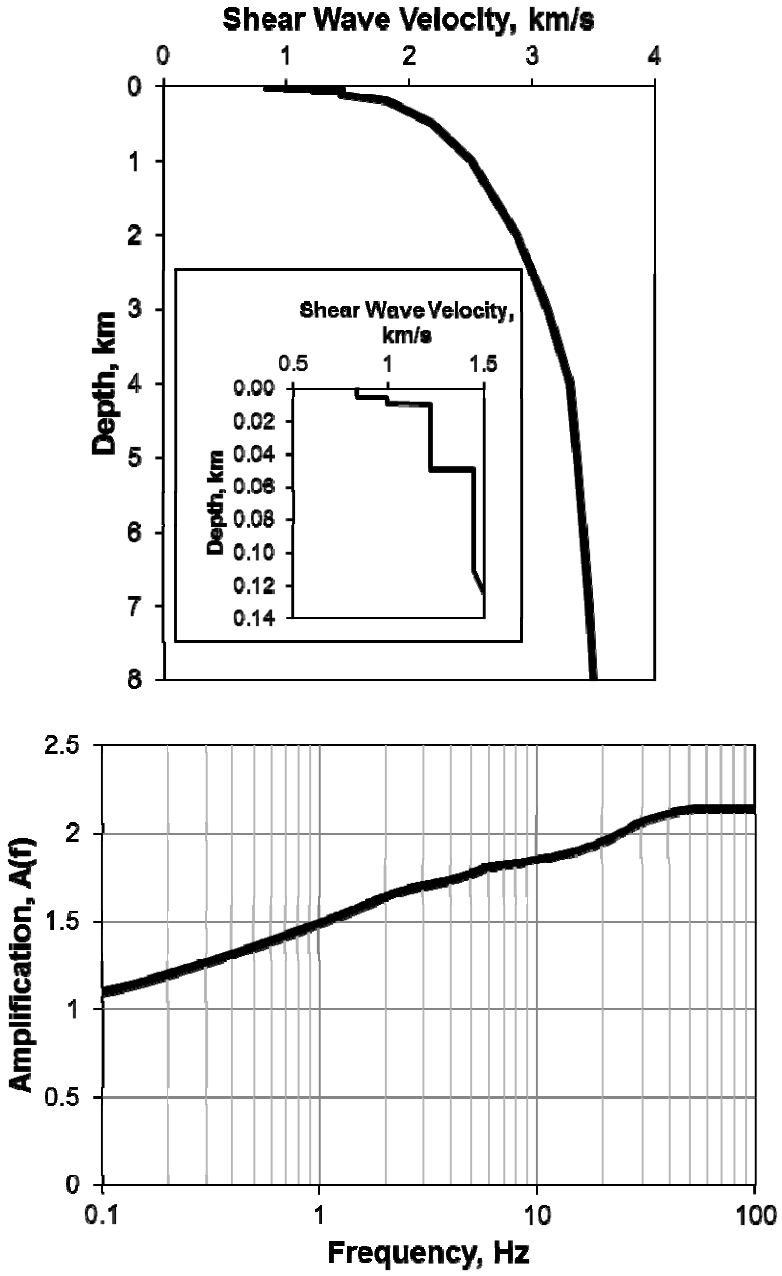

Figure B-1 The DCPP shear-wave velocity profile is shown as an inset on the generic central California shear-wave velocity model (upper panel). Illustration of upper crustal amplification function ($A(f) = (Zsource/Zavg(R))^{0.5}$) for the Diablo Canyon site (lower panel) computed from profile in upper panel.

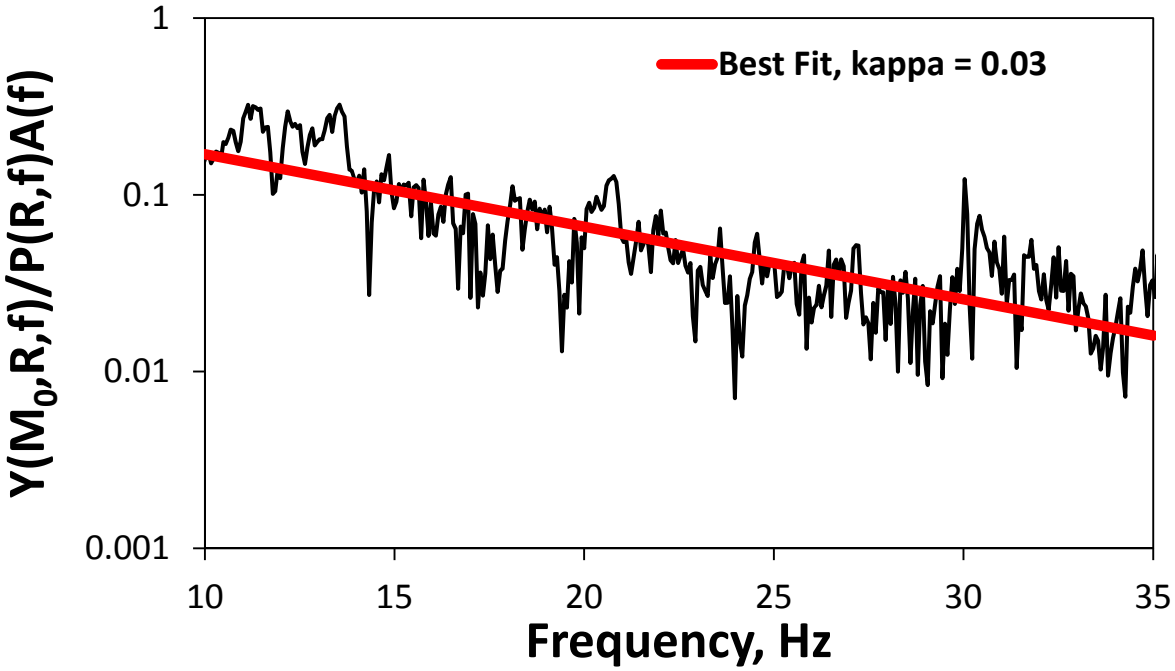

Figure B-2 **Fit to the acceleration Fourier amplitude spectrum of the 2003 Deer Canyon event recorded at the DCPP. Linear best fit kappa value of 0.03 s.**

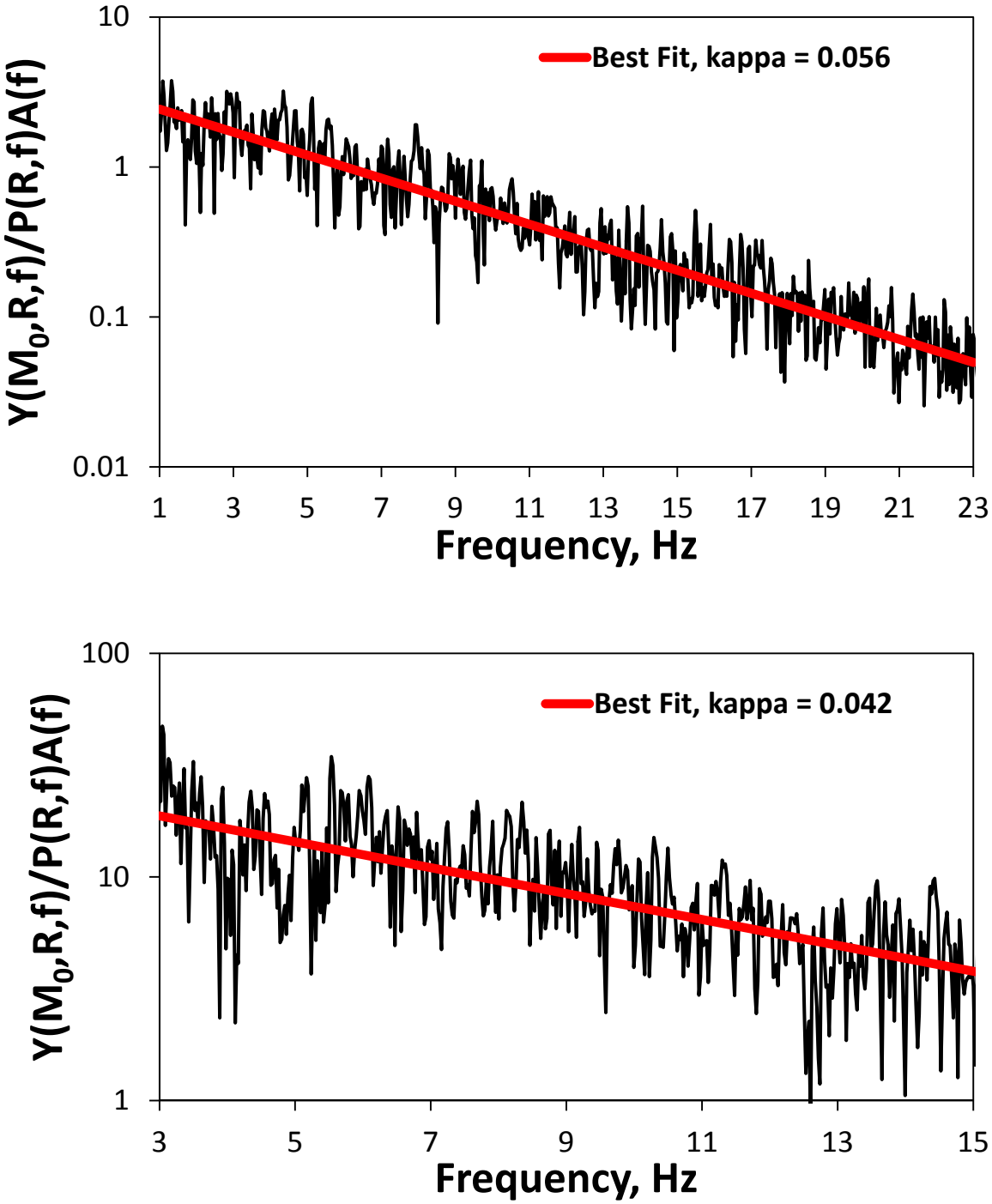

Figure B-3 **Fits to the acceleration Fourier amplitude spectra of the 2003 San Simeon (top) and 2004 Parkfield (bottom) earthquakes recorded at the DCPP. Linear best fit kappa value of 0.056 and 0.042 s, respectively.**

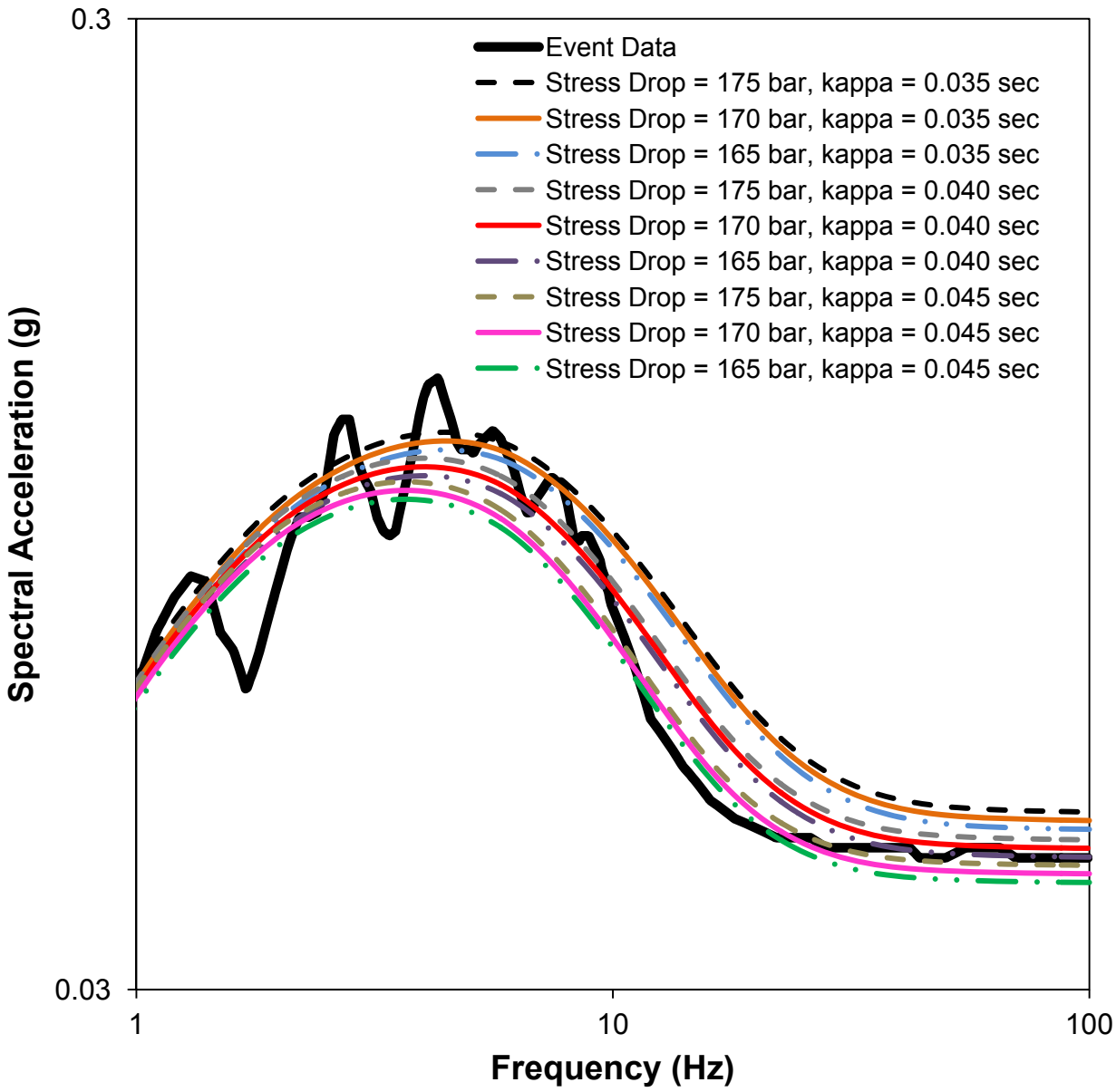

Figure B-4 Illustration of tradeoff between stress drop and kappa for M 6.5 2003 San Simeon earthquake recorded at DCPP. Kappa value of 0.04 s and stress drop of 170 bars produce best fitting (root mean square error) spectral estimates.

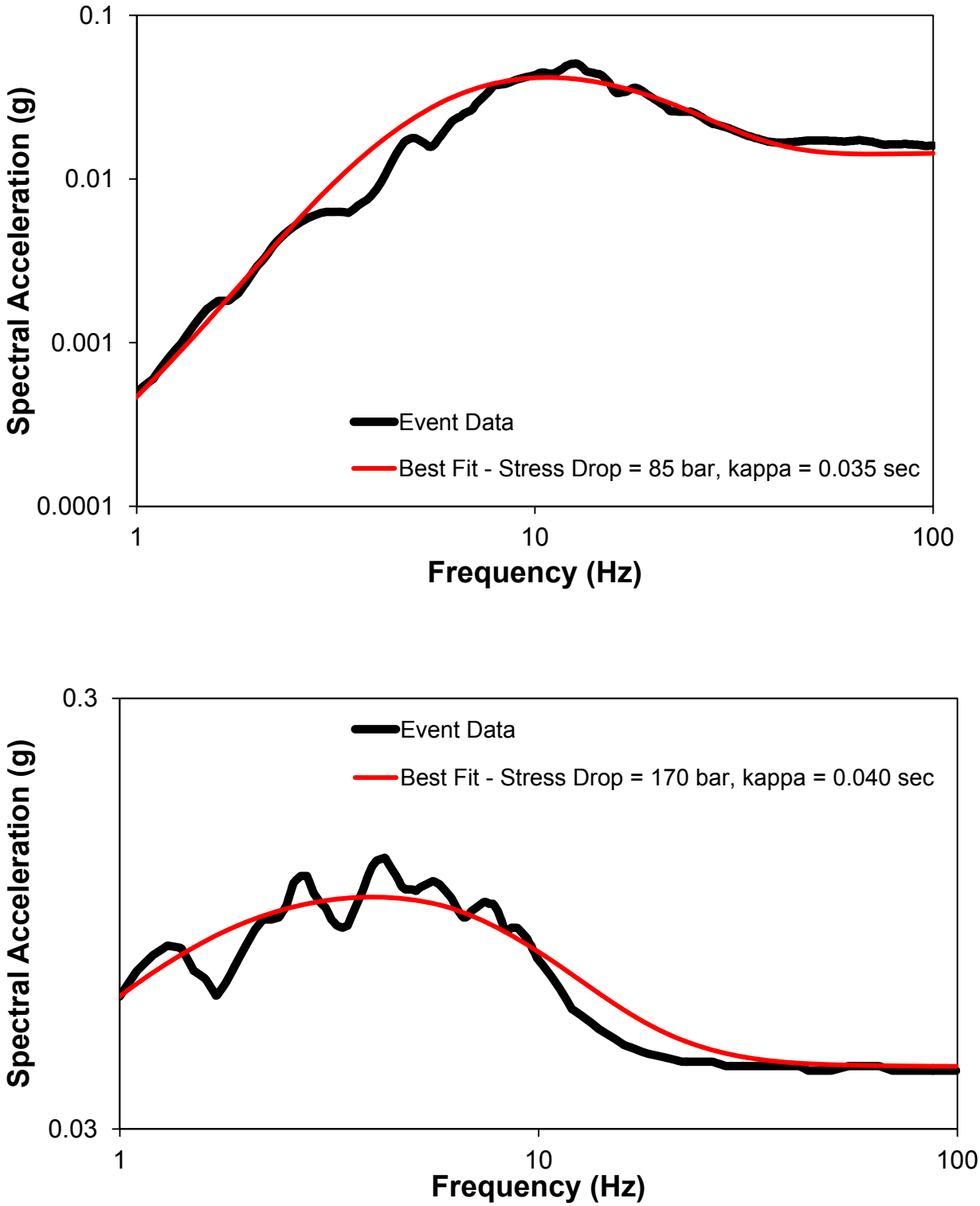

Figure B-5 Best fitting response spectral results for the Deer Canyon (top) and San Simeon (bottom) earthquakes in red, compared to observed recordings from DCPP in black.

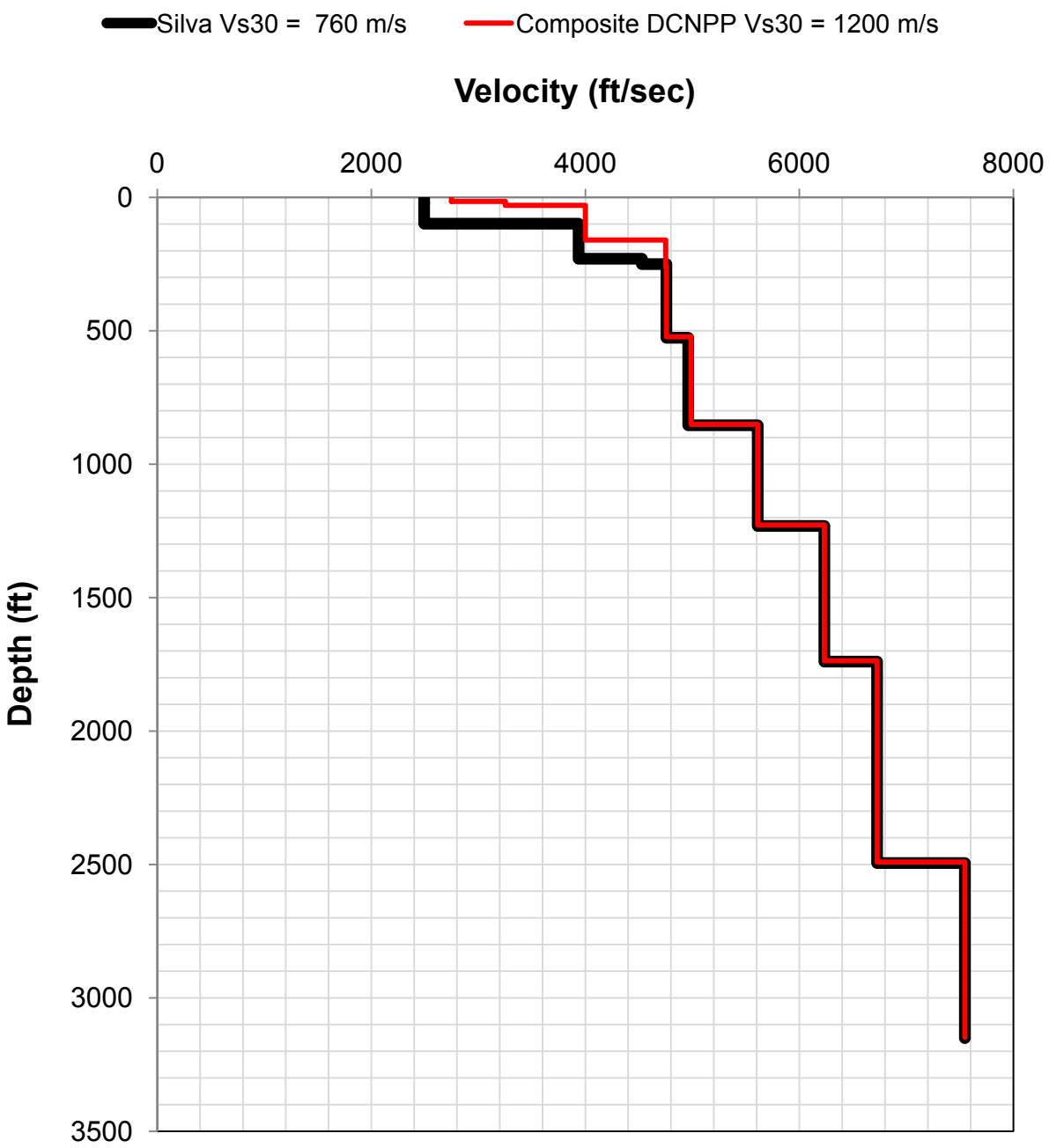

Figure B-6 Shear-wave velocity profiles used in the time history based approach to developing DCPP-specific amplification functions. The red line indicates the DCPP shear-wave velocity profile used and the blue line the generic 760 m/s profile of Silva (2008). The profiles are identical below 80 m (262 ft).

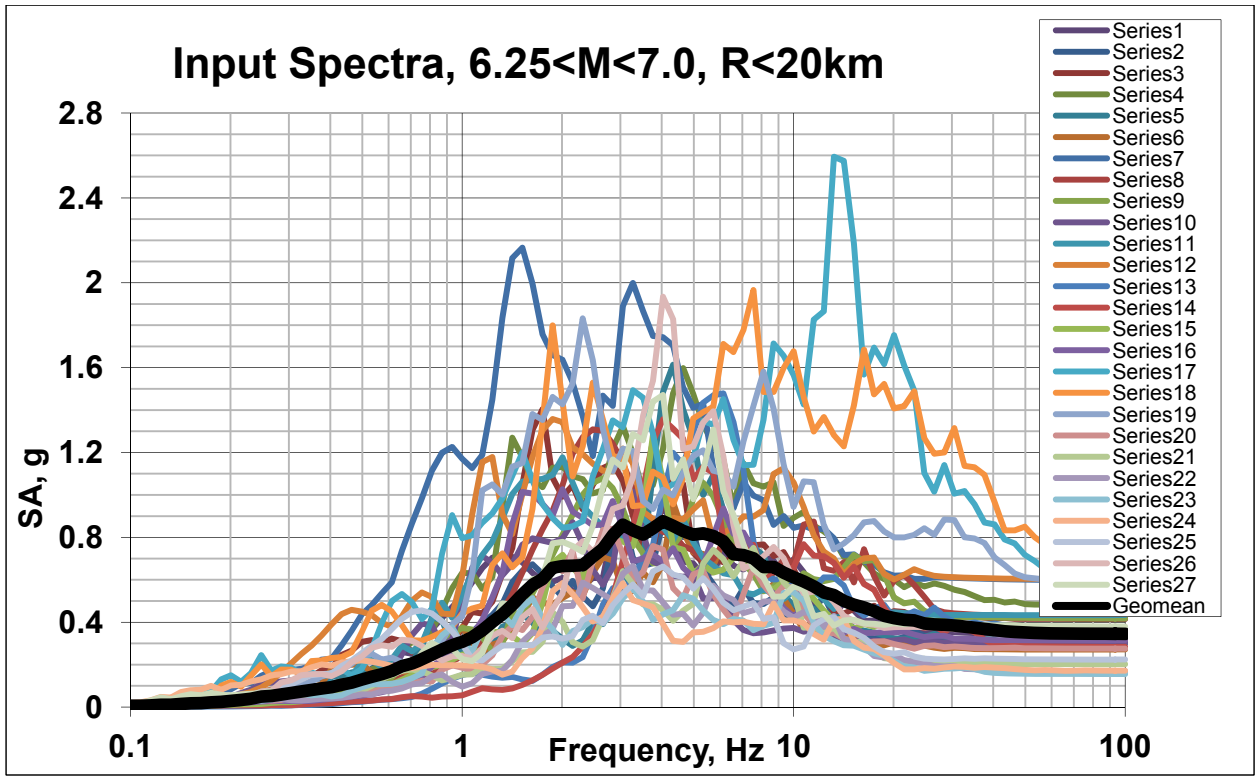

Figure B-7 **Subset of 27 of the 55 time histories used in the time series-based response analysis. Events are from the Northridge, Imperial Valley, San Fernando, Gazli, and Friuli earthquakes. The geometric mean of the records is indicated by the heavy black line.**

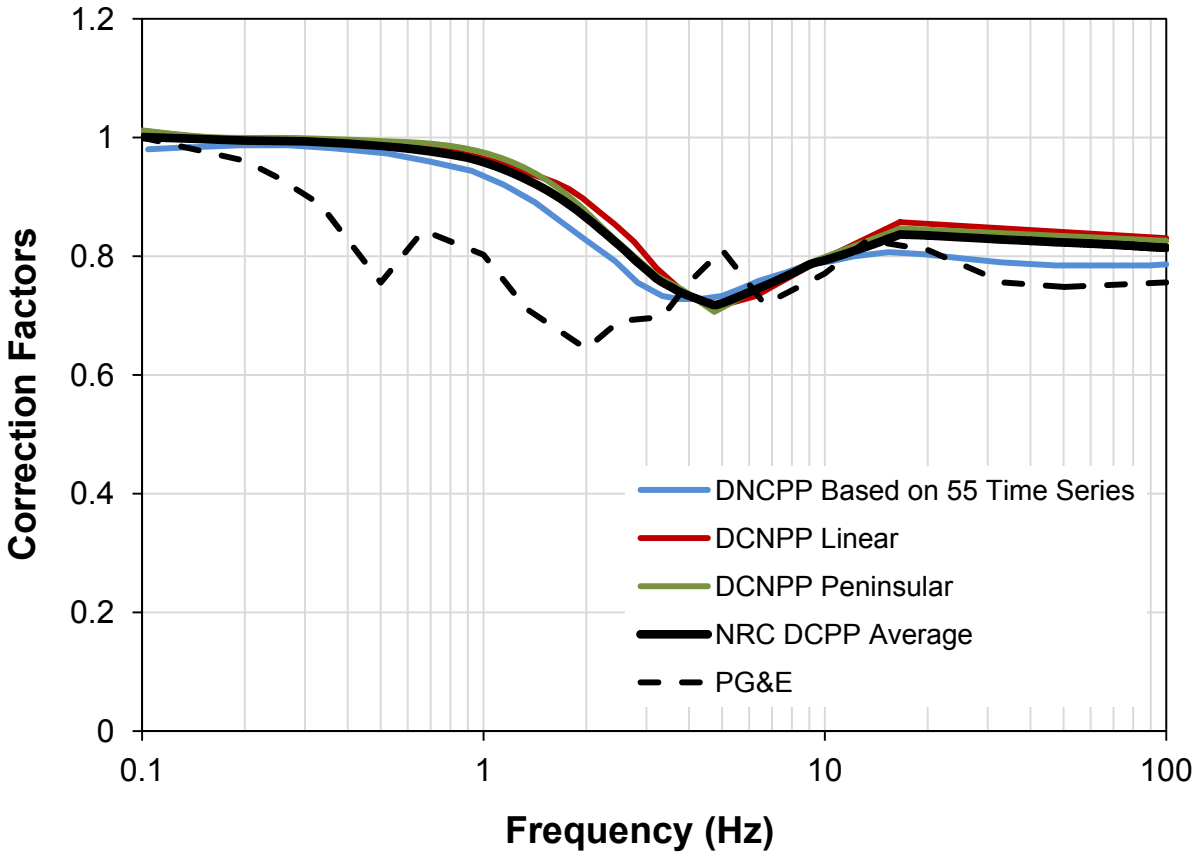

Figure B-8 Comparison of correction factors developed by NRC staff to those applied by PG&E (black dashed line). The heavy black line is the arithmetic mean of the correction factors developed by the NRC using the time-series (TS) method (shown in blue) and the RVT method (shown in red and green). The average of those three curves (solid black curve) was used by the NRC staff in the deterministic evaluation

Appendix C: Details of the Analysis to Assess the Risk from Secondary Fault Deformation

C.1 Introduction to Secondary Fault Displacement

When faults rupture during an earthquake, they have the potential to cause not only primary rupture of geologic materials on the fault but also secondary effects related to secondary rupture or permanent offset of the geologic materials in the vicinity of the fault. Ground-surface displacements associated with large earthquakes can cause damage to structures and lifelines that are built on or cross the causative faults. Figure C-1(a) shows a schematic of strain accumulation and Figure C-1(b) shows the fault displacement or offset at the location of a strike-slip fault over time (plan view). The straight line labeled "Fault Trace" represents the surface projection of a vertical fault that is the interface between two blocks of the earth's crust that are forced to move in opposite directions by tectonic forces (*F,-F*). This leads to regional stresses and tectonic strains over time. During an earthquake, permanent offset occurs around the location of the fault, as shown in Figure C-1(b).

During large earthquakes, secondary surface rupture may also occur away from the primary fault trace. Although the amplitude of secondary displacements from these secondary ruptures are much smaller than the displacements that occur on the main trace of the ruptured fault—and decrease with distance from the main fault—they can pose danger to the structures or infrastructure in their immediate vicinity. The main trace of the Shoreline fault is located offshore about 600 meters from the power block of the DCPP and, as a result, the threat of direct rupture of the main fault under the facility is negligible. Therefore, any hazard with regard to damage to the DCPP resulting from rupture-related displacement comes from the potential for a secondary rupture associated with a rupture on the main Shoreline fault trace.

The analyses performed by PG&E, described in Enclosure 1 of PG&E Letter No. DCL-10-019 to the NRC on February 26, 2010, "Evaluation of Secondary Fault Rupture Hazard from the Shoreline Fault" (PG&E, 2010), details calculations performed by PG&E to assess the potential impact of secondary rupture displacements to the calculated annual probability of core damage at the DCPP As stated by PG&E at the January 2010 public meeting, the only safety-related structures, systems, or components that could be sensitive to small secondary displacements are eight Dresser couplings situated along the auxiliary salt water pipes located in the weaker rock unit called Unit C of the Obispo Formation (PG&E, 2009). The purpose of the PG&E calculation, as explained in the provided report (PG&E, 2010), was to estimate the probability that the secondary surface rupture will occur at any one of the eight couplings during an earthquake along the Shoreline fault. The confirmatory analyses described briefly in Section 7 and in more detail herein evaluate the secondary fault rupture hazard and resulting potential impact to the annual probability of core damage associated with the Shoreline fault.

PG&E used two earthquake scenarios in these hazard calculations: (1) a M6 event caused by rupture of the entire central segment of the Shoreline fault and (2) a M6.25 event that would result if both the central and southern segments ruptured together. The NRC staff also used these two events in its confirmatory analyses as a point of comparison with PG&E. However, the NRC also analyzed the risk from a M6.7 scenario earthquakes consistent with the hazard analyses performed in Section 5.

C.2 General Approach to Confirmatory Analysis

The confirmatory analyses were performed using the probabilistic method of Petersen et al. (2004), which is the same general analysis technique used by PG&E. However, the NRC staff has used regression results from a more recent regression analysis by Petersen et al. (2011) of nearly the same empirical dataset as in the 2004 study. The goal of regression analysis is to determine the equation that provides a best fit to a set of data or observations. This method to assess the potential for secondary faulting is newer than methods to assess other types of seismic effects; therefore, the details are not as standardized. As such, different assumptions and approaches to parameters could be used. Additionally, because a risk assessment that looks specifically at this issue is not available, a set of assumptions has to be made to translate the results of the analyses into risk to the plant, in terms of core damage frequency. Therefore, the remainder of this Section discusses in detail the complete approach taken by the NRC staff.

As described in the following sections, the Petersen et al. (2004, 2011) method is based on an empirical relationship between earthquake ruptures on main faults that have come all the way to the surface (primary surface rupture) and the occurrence of secondary surface rupture at a nearby location. Their empirical data were recorded for strike-slip earthquakes around the world. To use the method, it must first be determined how often earthquakes of certain magnitudes occur on the main fault of interest. Based on this, it can be determined how often earthquakes occur that rupture the surface (not all earthquake fault ruptures reach the surface) and the likelihood of a surface rupture occurring on any particular part of the main fault. Next, probabilistic relationships (expressed as probability density functions) can be used to determine the likelihood of a secondary rupture occurring at a specific nearby location and with specific amplitude of displacement (1 cm and 2 cm in this case). The displacement values of 1 cm and 2 cm are used in this case, because they are amplitudes of displacement that piping are known to tolerate. These displacements are called d_0 in the subsequent analyses.

C.3 Methodology of Petersen et al. (2011)

C.3.1 Secondary Rupture Hazard Assessment Algorithm

According to Petersen et al. (2004, 2011), for an earthquake of magnitude m that ruptures a main fault to the surface, the probability that a secondary displacement d (i.e., displacement away from the main fault rupture) within a square footprint $(z \times z)$ at location (l, r) (see Figure C-2) exceeds value d_0 (1 cm and 2 cm) is given by the following:

$$\lambda(d \geq d_\circ) = \alpha \int_m f_M(m) \int_s f_S(s) \int_r f_R(r) P[sr \neq 0|m] P[d \neq 0|l, r, m, z, s, sr \neq 0] P[d \geq d_\circ|l, r, m, d \neq 0] dr ds dm \quad \text{Equation C-1}$$

where:

$\boldsymbol{\alpha}$ is the earthquake activity rate defined as the ratio of the rate of total accumulated moment $\dot{M}_0$ to the average moment-release per earthquake $\bar{M}_0$. For a fault, this activity rate parameter balances the strain energy accumulating on the fault over time with the energy released through earthquakes on the fault.[1] In a region, an associated approach can be

[1] This is a mathematical description of the moment balancing technique discussed qualitatively in Appendix D.

used to ensure that the strain energy accumulating in a region as a result of the relative motion of tectonic plates (such as the North American and Pacific plates) is balanced with the energy released in the form of earthquakes.

$\boldsymbol{f_M(m)}$ is the probability density function (pdf) describing the magnitude-frequency distribution along a fault. This describes the *relative* occurrence rates of earthquakes of different magnitudes. Because it is expressed as a pdf (which has a total probability of 1.0), this information must be combined with rate information (α) to get the actual frequency of earthquakes of a particular magnitude.

$\boldsymbol{f_S(s)}$ is the pdf characterizing the probability of rupture at a specific location, s, along the fault (Figure C-2), given that an earthquake has occurred.

$\boldsymbol{f_R(r)}$ is the pdf characterizing the distribution of perpendicular distances from the site (l, r) (Figure C-2) to all potential ruptures. Because some faults always rupture along the exact same trace while others move around in a seismic zone, this parameter was developed to account for the aleatory variability (randomness) of the location of the rupture away from (and parallel to) the center of the main trace or seismic zone.

$\boldsymbol{P[sr \neq 0|m]}$ is the probability of the occurrence of surface rupture for an earthquake of magnitude m. This parameter accounts for the fact that not all earthquakes rupture to the surface and that the probability that an earthquake causes surface rupture increases as a function of the magnitude of the earthquake.

$\boldsymbol{P[d \neq 0|l, r, m, z, s, sr \neq 0]}$ is the probability that, for a magnitude m earthquake occurring on the main fault, there is a non-zero displacement or dislocation d at a location away from the main fault (l, r) within a footprint of the size $z \times z$ (Figure C-2).

$\boldsymbol{P[d \geq d_\circ|l, r, m, d \neq 0]}$ is the probability that, for a magnitude m event, the secondary displacement or dislocation d at location (l, r) exceeds some value d_0, given that some non-zero displacement occurs at that location (as determined by the equation above).

C.3.2 Magnitude-Frequency Probability Density Function

The pdf $f_M(m)$ describes the relative occurrence rates of earthquakes of different magnitudes along a fault. In general, it is expressed mathematically using an exponential form (e.g., the truncated exponential model), which describes the decrease in the number of earthquakes above some magnitude (m) that occurs as that magnitude increases. Although this model works well for a regional model with faults of varying dimensions, it does not fully represent earthquake distribution on any single fault. This is because individual faults often release most of the accumulated stress through the same size (characteristic) earthquakes with a relatively narrow range of magnitudes (one-half unit) near the maximum (Schwartz and Coppersmith, 1984).

A fully characteristic earthquake model assumes a uniform distribution of earthquakes with a range of magnitudes around the “characteristic” magnitude that is typically the “maximum magnitude” calculated using the dimensions of the potential rupture area on the fault. However, this model does not account for small or moderate earthquakes on the fault. Therefore, to represent the earthquake magnitude distributions that most often actually occur on faults more realistically, composite models have been introduced. These models combine a truncated exponential distribution for smaller earthquakes and uniform distribution around the “characteristic” magnitude for larger earthquakes.

For this study, the characteristic-earthquake (composite) model of Youngs and Coppersmith (1985) is used to describe $f_M(m)$ for earthquakes on the Shoreline fault. This composite model uses an exponential magnitude-frequency distribution for magnitudes below the maximum magnitude (m_{max}) and a uniform distribution for a range of one-half magnitude unit above m_{max}. The amplitude of the uniform distribution is calculated as the amplitude of the exponential density function at one magnitude unit below m_{max}, that is, $f_M(m_{\text{max}} - 1)$.

For consistency, the NRC staff adopted the convention that PG&E used to describe the magnitude range of characteristic earthquakes on the Shoreline fault (i.e., characteristic earthquakes with one-half magnitude range above m_{max} ($m_{\text{max}} \leq m_{\text{char}} \leq m_{\text{max}} + 0.5$), with a mean $\overline{m}_{\text{char}} = m_{\text{max}} + 0.25$. Therefore, this composite model has an exponential distribution $f_M(m)$ for the magnitude range of $m_0 \leq m \leq \overline{m}_{\text{char}} - 0.25$ and a uniform distribution $f_M(\overline{m}_{\text{char}} - 1.25)$ for $\overline{m}_{\text{char}} - 0.25 < m \leq \overline{m}_{\text{char}} + 0.25$. Figure C-3 displays this magnitude-frequency distribution graphically for $6.0 \leq m_{\text{char}} \leq 6.5$. Here, m_0 is the smallest magnitude earthquake that can occur on the fault and $\overline{m}_{\text{char}}$ is the mean magnitude of characteristic earthquakes that can occur on the fault.

The truncated exponential model of Youngs and Coppersmith (1985) in the magnitude range (m_0, m_{max}) is given by:

for $m_0 \leq m \leq m_{\text{max}}$

$$f_M(m) = \frac{\beta e^{-\beta(m-m_0)}}{1 - e^{-\beta(m_{\text{max}}-m_0)}} \qquad \text{Equation C-2}$$

For the Shoreline fault, the composite model assumed above becomes:

for $m_0 \leq m \leq \overline{m}_{\text{char}} - 0.25$

$$f_M(m) = \gamma \frac{\beta e^{-\beta(m-m_0)}}{1 - e^{-\beta(\overline{m}_{\text{char}}-m_0-0.25)}} \qquad \text{Equation C-3}$$

and for $\overline{m}_{\text{char}} - 0.25 < m \leq \overline{m}_{\text{char}} + 0.25$

$$f_M(m) = \gamma \frac{\beta e^{-\beta(\overline{m}_{\text{char}}-m_0-1.25)}}{1 - e^{-\beta(\overline{m}_{\text{char}}-m_0-0.25)}} \qquad \text{Equation C-4}$$

Figure C-3 schematically demonstrates the relative relationship between magnitudes of earthquakes on a fault and the frequency of earthquakes of those magnitudes (on a semi-natural log scale) given a characteristic earthquake model (Youngs and Coppersmith, 1985). Here, the normalization factor γ is introduced to ensure that the sum of the probability density function $f_M(m)$ over the range of all possible magnitudes (i.e., the area under the curve in Figure C-4) is equal to 1.0. β is the product of the b-value and $\ln(10)$. The b-value is the slope of Gutenberg-Richter magnitude-frequency distribution ($\log_{10} f_M(m)$ vs. m). It describes the change in the distribution of earthquakes above a given magnitude. For example, on a given fault, it describes the rate at which the number of earthquakes with magnitudes greater than m drops as m becomes larger. For the Shoreline fault, a b-value of 0.8 ($\beta = 1.842$) was used. This value is widely used for the magnitude-frequency distribution for northern California (Bolt, 1993). However, the earthquake hazard in this analysis is not sensitive to the b-value. Calculations repeated for b-values of 0.8, 1.0, and 1.2 showed negligible effect on the hazard.

The factor γ is determined to allow for normalization of the magnitude-frequency distribution in Equations C-3 and C-4 (i.e., to ensure that the area under the curve in Figure C-3 integrates to one):

$$1 = \int_{m_0}^{\overline{m}_{\text{char}}+0.25} f_M(m)dm,$$

or,

$$1 = \gamma \int_{m_0}^{\overline{m}_{\text{char}}-0.25} \frac{\beta e^{-\beta(m-m_0)}}{1-e^{-\beta(\overline{m}_{\text{char}}-m_0-0.25)}} dm + \gamma \frac{\beta e^{-\beta(\overline{m}_{\text{char}}-m_0-1.25)}}{1-e^{-\beta(\overline{m}_{\text{char}}-m_0-0.25)}} \times 0.5 \qquad \text{Equation C-5}$$

The value of the integral in Equation C-5 is unity. Therefore:

$$\frac{1}{\gamma} - 1 = \frac{\beta e^{-\beta(\overline{m}_{\text{char}}-m_0-1.25)}}{1-e^{-\beta(\overline{m}_{\text{char}}-m_0-0.25)}} \times 0.5 \qquad \text{Equation C-6}$$

Assuming

$$c_2 \equiv \frac{1}{2} \frac{\beta e^{-\beta(\overline{m}_{\text{char}}-m_0-1.25)}}{1-e^{-\beta(\overline{m}_{\text{char}}-m_0-0.25)}} \qquad \text{Equation C-7}$$

then,

$$\gamma = \frac{1}{1+c_2} \qquad \text{Equation C-8}$$

C.3.3 Activity Rate

The activity rate $\alpha\ (m \geq m_0)$ describes the rate of earthquakes with magnitudes greater than m_0 occurring on a given fault. It is defined as the rate of the total accumulated seismic moment, $\dot{M}_{\text{o}} = \mu AS$, normalized by the mean moment released per earthquake, $\overline{M}_{\text{o}}$:

$$\alpha\ (m \geq m_0) = \frac{\dot{M}_{\text{o}}}{\overline{M}_{\text{o}}}$$

The total accumulated seismic moment for a fault with a seismically active area A and an average slip rate S, is defined as (Brune 1968):

$$\dot{M}_{\text{o}} = \mu AS$$

where, μ is the shear modulus of the Earth's crust. The mean moment released per earthquake for a fault with earthquake magnitude probability density function $f_M(m)$ is given by:

$$\overline{M}_{\text{o}} = \int_m f_M\,(m) M_{\text{o}}(m) dm$$

Here, the moment $M_{\text{o}}(m)$ is related to magnitude m by the Hanks and Kanamori (1979) moment-magnitude relationship:

$$M_{\text{o}}(m) = 10^{1.5m+16.05}$$

Therefore, for the Shoreline fault with a magnitude recurrence relationship shown in Figure C-3, the rate of occurrence earthquakes with magnitudes larger than m_0 is:

$$\alpha\ (m \geq m_0) = \frac{\mu AS}{\int_{m_0}^{\overline{m}_{\text{char}}+0.25} f_M\ (m) M_{\text{o}}(m) dm}$$

The activity rate for the occurrence of earthquakes with magnitudes larger than $m_{\min}$ is obtained by scaling the activity rate $\alpha\ (m > m_0)$:

$$\alpha\ (m \geq m_{\min}) = \alpha\ (m \geq m_0) \int_{m_{\min}}^{\overline{m}_{\text{char}}+0.25} f_M\ (m) dm \qquad \text{Equation C-9}$$

C.3.4 Distance-from-Surface-Rupture Probability Density Function

The pdf, $f_R(r)$, characterizes the perpendicular distance from the site (l, r) to all potential ruptures. For the Shoreline fault, it is assumed that the surface rupture always passes at the closest distance r_{min} from the DCPP as determined by seismological and geophysical data (distances of 300 and 600 meters are used). Therefore, the distribution function $f_R(r)$ is equal to a constant for $r = r_{\text{min}}$, and equal to 0 for all other values of r. This behavior of $f_R(r)$ is represented by the δ-function:

$$f_R(r) = \delta(r - r_{\text{min}}) \qquad \text{Equation C-10}$$

Hence, because the hazard is independent of s and $f_R(r)$ has a non-zero value only at r_{min}, Equation C-1 becomes:

$$\lambda(d \geq d_\circ) = \alpha \int_{m_0}^{\overline{m}_{\text{char}}-0.25} f_M\ (m) P[sr \neq 0|m] P[d \neq 0|l, r_{\text{min}}, m, z, sr \neq 0] P[d \geq d_\circ|l, r_{\text{min}}, m, d \neq 0] dm \qquad \text{Equation C-11}$$

C.3.5 Conditional Probability for Surface Rupture

Not all earthquakes rupture to the surface and the probability of surface fault rupture increases with earthquake size. The probability $P[sr \neq 0|m]$ for having surface rupture as a function of magnitude, m, is given by the empirical expression (Youngs et al., 2003):

$$P[sr \neq 0|m] = \frac{e^{u(m)}}{1 + e^{u(m)}} \qquad \text{Equation C-12}$$

Where,

$$u(m) = a + bm$$

Parameters a and b are estimated empirically from the regression of seismic data recorded worldwide (Wells and Coppersmith, 1994). Substituting the values $a = -12.51, b = 2.053$ (Youngs et al., 2003; Wells and Coppersmith, 1994), Equation C-12 is rewritten as:

$$P[sr \neq 0|m] = \frac{1}{2}(\tanh(m - 6.1) + 1)$$ Equation C-13

Equation C-13 provides an estimate of the probability of surface rupture as a function of magnitude based on data from 276 worldwide earthquakes. However, PG&E asserts that, because of the varying seismogenic thicknesses associated with these 276 earthquakes, the probability estimates implied by Equation C-13 do not necessarily apply to the Shoreline fault. The assumed width of 10 km for the central segment and 12 km for the central and southern segments limit the magnitudes for which the rupture does not reach the free surface. Therefore, since the earthquake magnitude is proportional to the area of the fault, if the potential rupture area for a given magnitude earthquake on the fault exceeds the area of the fault, the rupture has to break all the way to the surface. This is a conservative approach that the NRC staff implemented in the confirmatory analyses.

To develop a more conservative model describing the conditional probability of surface rupture specific to the Shoreline fault, PG&E used the empirical model of Wells and Coppersmith (1994) for estimating rupture area (RA) from the magnitude of the strike-slip earthquakes:

$$\log RA = -3.42 + 0.9\,m, \qquad \sigma = 0.22$$ Equation C-14

In this equation, the value of $\log RA$ obtained for an earthquake of magnitude m represents the mean value of a normal (Gaussian) distribution for $\log RA$ with the standard deviation $\sigma = 0.22$.

PG&E used two scenario earthquakes with magnitudes 6.6 and 6.8 to constrain its model. These earthquakes, because of their size, have a very high probability of rupturing the entire width of the fault (i.e., rupture reaches the surface).

To illustrate how these magnitudes were chosen, consider an earthquake that ruptures both the central and southern segments of the Shoreline fault. Assuming a width of 12 km and a length of 15.2 km for the two segments, the combined rupture area RA becomes 182 km^2. Assuming that log(182)=2.26 represents the mean value (μ) of $\log RA$ in Equation C-14, then the magnitude at which the surface-rupture probability is 97.7 percent ($\log RA \leq \mu + 2\sigma$) (Figure C-4) is calculated:

$$m = \frac{\mu + 2\sigma + 3.42}{0.9}$$
$$= \frac{2.26 + 2 \times 0.22 + 3.42}{0.9}$$
$$= 6.8$$

Similarly, the surface rupture probability for a magnitude 6.6 earthquake on the central segment (10 km $\times$ 12 km) is 0.977. Using these two constraints ($m = 6.8,\ P = 0.977$) and ($m = 6.6,\ P = 0.977$), along with a third constraint provided by the Wells and Coppersmith (1993) model for $m = 5.75$ (Figure C-5), the surface rupture probability model developed by PG&E (2010) for the Shoreline fault becomes:

for $m \geq 5$

$$P[sr \neq 0|m] = \frac{1}{2}\left(\tanh\left(2.5\ (m - 5.9)\right) + 1\right)$$ Equation C-15

and for $m < 5$

$$P[sr \neq 0|m] = 0 \qquad \text{Equation C-16}$$

C.3.6 Conditional Probability for Secondary Rupture

C.3.6.1 PG&E Approach

The conditional probability for secondary rupture, $P[d \neq 0|l, r_{\text{min}}, m, z, sr \neq 0]$, is the probability for non-zero secondary displacement (d) within a square footprint $(z \times z)$ at location (l, r_{min}) for a magnitude (m) event. Petersen et al. (2004) investigated the frequency of secondary rupture within a 50×50 m^2 cell as a function of distance from the main fault trace for nine strike-slip earthquakes worldwide (Figure C-6). The data are widely scattered. To estimate the probability of secondary rupture from an earthquake on the Shoreline fault, PG&E used the lower range of this distribution (red curve in Figure C-6). The reason given for this assumption is that the Petersen et al. (2004) data are from more spatially complex strike-slip faults, whereas the section of the Shoreline fault near the DCPP is relatively straight and uniform and therefore is less likely to cause a secondary rupture. Although PG&E's argument in support of its assumption is reasonable, the NRC staff used a more conservative curve based on Petersen et al. (2011) for use in the confirmatory analyses discussed in the next section.

The Shoreline fault is about 600 meters from the power block at DCPP. Using the red curve, the probability of secondary rupture in a 50×50 m^2 footprint at a distance of 600 meters (given that surface rupture has occurred on the main trace) is 0.0052. This is slightly larger than the value 0.004 that PG&E originally assumed based on the same figure.

C.3.6.2 NRC Approach

Since PG&E's hazard analyses, Petersen et al. (2011) have carried out new regression analyses on a set of empirical data for secondary (distributed) rupture associated with strike-slip earthquakes. The pool of data consists of eight strike-slip earthquakes, five in California (1968 M6.5 Borrego Mountain, 1979 M6.5 Imperial Valley, 1987 M6.5 Superstition Hills, 1992 M7.3 Landers, 1999 M7.1 Hector Mine), two in Turkey (1999 M7.6 Izmit, 1999 M7.1 Duzce), and one in Japan (1995 M6.9 Kobe). This dataset is very similar to the dataset used in Petersen et al. 2004. However, to limit the dataset to strike-slip earthquakes, data from the 1971 San Fernando earthquake (thrust faulting) were replaced with data from the 1999 Duzce, Turkey, earthquake (strike-slip faulting).

Based on the above dataset, and assuming the power function $P(z) = b(z)r^{a(z)}$, Petersen et al. (2011) calculated the probability P for a rupture to occur in a given cell $(z \times z)$ at a distance r from the principal fault. The parameters $a(z)$ and b(z) were determined from the empirical data. For a 50×50 m^2 cell, a and b are -0.90, and 0.99, respectively. Figure C-7 shows a plot of this rupture probability as a function of the distance from the 50×50 m^2 cell to the main fault trace.

Therefore, at a distance of 600 meters from the principal fault, the probability that a secondary-fault displacement passes through a 50-m $\times$ 50-m cell area varies between 0.0027 and 0.027 (16$^{\text{th}}$- and 84$^{\text{th}}$-percentile), with a median of 0.0085. The median is about a factor of two larger than the PG&E assumption.

Assuming a secondary rupture in a 50×50 m^2 cell that contains the eight Dresser couplings, the probability that a 50-meter rupture cuts through one of the couplings (each of which is 0.30 m long) is 0.049 (8×0.30 m per 50 m), as shown schematically in Figure C-8. Therefore the probability that there is a secondary rupture, and that it cuts through at least one coupling, will have a range of $(1.3 \times 10^{-4}, 1.3 \times 10^{-3})$ with the median:

$$P[d \neq 0 | l, r_{\text{min}} = 600 \text{ m}, m, z = 50 \text{ m}, sr \neq 0] = 0.0085 \times 0.049 = 4.2 \times 10^{-4}$$

Although the Shoreline fault is 600 meters from the power block, the NRC also repeated the analyses for a distance of 300 meters to account for the closest distance to the intake structure as shown in Figure C-9.

C.3.7 Probability for Secondary Displacement Exceeding the Conditional Probability for Secondary Rupture

Once the probability of some displacement occurring at the location of one of the Dresser couplings has been assessed, it is necessary to calculate the likelihood of various amplitudes of displacements (such as shown in Figure C-1b). Petersen et al. (2004) show a histogram of the distribution of the ratio of secondary dislocation d to the maximum dislocation (fault offset) on the main fault trace D_{max} (Figure C-10). PG&E used this distribution in its hazard analyses. By fitting a Gaussian form to this distribution, it calculated the following mean and standard deviation:

$$\mu_{\log(d/D_{\text{max}})} = -1.587$$

$$\sigma_{\log(d/D_{\text{max}})} = 0.537$$

The blue curve is the Gaussian fit to this distribution by PG&E. The red curve shows the Petersen et al. (2011) regression results for the distribution of the ratio of secondary rupture to the average displacement on the principal trace as used by the NRC.

The recent regression analyses of Petersen et al. (2011) uses the average displacement (D_{ave}) along the principal fault trace to model the distribution of the secondary fault displacement (d) instead of the maximum displacement (D_{max}) used in their 2004 study. However, as shown in Figure C-11 (solid and dashed red curves), this use of different parameters (D_{ave} vs D_{max}) does not significantly alter the shape of the distribution.

The red curve in Figure C-11 represents the distribution of $\log(d/D_{\text{ave}})$ at a distance of 600 meters from the principal fault. Its median and the standard deviation are as follows:

$$\mu_{\log(d/D_{\text{ave}})} = -1.365$$

$$\sigma_{\log(d/D_{\text{ave}})} = 0.507$$

Although both d and D_{ave} are dependent on magnitude m, their ratio is not. Therefore, for a given strike-slip earthquake of magnitude m, the median value of the secondary dislocation can be written as the average displacement on the main trace multiplied by the ratio $\log(d/D_{\text{ave}})$ given in Figure C-10.

$$d(m) = D_{\text{ave}}(m) \times \frac{d}{D_{\text{ave}}}$$

or,

$$\log d(m) = \log D_{\text{ave}}(m) + \log(d/D_{\text{ave}}) \qquad \text{Equation C-17}$$

$$\sigma_{\log d(m)} = \sqrt{\sigma^2_{\log D_{\text{ave}}} + \sigma^2_{\log(d/D_{\text{ave}})}} \qquad \text{Equation C-18}$$

Here the median and variance for the maximum displacement on a strike-slip fault, $D_{\text{max}}(m)$ and $\sigma_{\log D_{\text{max}}}$, are obtained from the empirical relation of Wells and Coppersmith (1994):

$$\log D_{\text{ave}}(m) = -6.32 + 0.90\, m, \qquad \sigma_{\log D_{\text{ave}}} = 0.28 \qquad \text{Equation C-19}$$

Figure C-11 shows an example of the lognormal distributions for d/D_{ave}, $D_{\text{ave}}(m)$, and $d(m)$ for an $m = 6.25$ strike-slip earthquake.

The probability of the observed displacement exceeding a displacement of interest for an earthquake of magnitude m (and assuming some displacement occurs) $P[d \geq d_0|m, d \neq 0]$ is represented as the shaded area in Figure C-11 and is calculated by evaluating the following integral:

$$P[d \geq d_0|m, d \neq 0] = \frac{1}{\sqrt{2\pi}\,\sigma_{\log d(m)}} \int_{\log d_0}^{+\infty} e^{-\frac{\left(\log d(m) - \left(\log(D_{\text{ave}}(m)) + \log\left(\frac{d}{D_{\text{ave}}}\right)\right)\right)^2}{2\sigma^2_{\log d(m)}}} \delta(\log d(m))$$

This distribution is inferred from the combination of the lognormal distributions for the average displacement on the principal trace and the ratio of the secondary displacement to the average displacement on the principal trace. The red dashed curve, representing PG&E's approach based on the maximum displacement on the principal fault, is shown for comparison. The shaded area represents the probability that during a M6.25 earthquake, the secondary displacement at a distance of 600 meters from the principal trace exceeds d_0 =2 cm.

This is equivalent to calculating the complement to the normal cumulative distribution function $\Phi[\log(d_0)|m]$, that is:

$$P[d \geq d_0|m, d \neq 0] = 1 - \Phi[\log(d_0)|m] \qquad \text{Equation C-20}$$

where,

$$\Phi[\log(d_0)|m] = \frac{1}{\sqrt{2\pi}\,\sigma_{\log d(m)}} \int_{-\infty}^{\log d_0} e^{-\frac{(\log d(m) - (\log D_{\text{ave}}(m) + \log(d/D_{\text{ave}})))^2}{2\sigma^2_{\log d(m)}}} \delta(\log d\,(m))$$

The above integral is equivalent to the standard normal cumulative distribution function ($mean = 0$, and $sd = 1$), $\Phi[t_0|m]$ (Equation C-21), through the following change of variables:

$$t \equiv \frac{\log d - (\log D_{\text{ave}}(m) + \log(d/D_{\text{ave}}))}{\sigma_{\log d(m)}}$$

$$\Phi[t_0|m] = \frac{1}{\sqrt{2\pi}} \int_{-\infty}^{t_0} e^{-\frac{t^2}{2}}\, dt \qquad \text{Equation C-21}$$

Therefore,

$$P[d \geq d_0|m, d \neq 0] = 1 - \Phi\left[\frac{\log d_0 - (\log D_{\text{ave}}(m) + \log(d/D_{\text{ave}}))}{\sigma_{\log d(m)}}|m\right] \qquad \text{Equation C-22}$$

which is the approach described in PG&E (2010) and shown graphically in Figure C-12.

Now that all of the terms in the integrand of Equation C-11 have been determined, the hazard can be calculated. Because it is assumed that there is no surface rupture for Shoreline fault earthquakes smaller than magnitude 5 ($P[sr \neq 0|m < 5] = 0$), the lower limit of the integral in Equation C-11 becomes 5:

$$\lambda(d \geq d_0) = \alpha \int_5^{\overline{m}_{\text{char}}-0.25} f_M\ (m) P[sr \neq 0|m] P[d \neq 0|l, r_{\text{min}}, m, z, sr \neq 0] P[d \geq d_0|l, r_{\text{min}}, m, d \neq 0] dm \qquad \text{Equation C-23}$$

Table C-1 lists the equations and the numbers for substitution into Equation C-23 for hazard calculations.

C.4 Comparison of Approaches and Results of Analysis of Secondary Rupture

The PG&E calculation of hazard from secondary rupture due to an earthquake on the Shoreline fault was repeated by the NRC staff as part of the confirmatory analyses. The NRC staff also performed the analyses using assumptions and parameters that differed from those PG&E used in some cases. In addition to the use of a different curve (Petersen et al., 2011) for the frequency of occurrence of secondary rupture as a function of distance from the main trace (as described in Section C.3.6), the NRC staff used only one magnitude distribution whereas PG&E used two. PG&E used one characteristic earthquake model for $m \geq 0$ to calculate the activity rate α (number of earthquakes per year with $m \geq 0$). This distribution is identical to the one that the NRC staff used (both dashed and solid lines in Figure C-3). PG&E also used a second distribution to calculate the hazard associated with secondary fault rupture at the site of couplings. The second distribution represents only the $m \geq 5$ events likely to have surface rupture (solid lines in Figure C-3). However, introduction of the second distribution is not necessary, because the conditional probability $P[sr \neq 0|m]$ (Equations C-15 and C-16) in the integrand of Equation C-11 ensures that only events with $m \geq 5$ contribute to the hazard calculations. The NRC staff also used an additional scenario earthquake of magnitude 6.7.

The NRC and PG&E results for the different tectonic assumptions are listed in Table C-2. The NRC's calculated values of annual probability of exceedance are about a factor of 6 larger for the central segment individual rupture scenario earthquakes and about 4 times larger for the

central and southern segments joint rupture scenario earthquakes. The differences in calculated results are caused by the following:

1. Different approaches to estimate the probability of a secondary rupture at a distance of 600 meters. PG&E used Figure C-6 (Petersen et al. 2004) to estimate the probability, whereas the NRC staff used the regression analysis of Petersen et al. (2011). The value estimated by the NRC staff is 0.0085, which is about 2 times larger than the 0.004 PG&E reported (Section C.3.6).

2. Incorrect calculation of the activity rate α of earthquakes with magnitudes larger than 5 in the Matlab code provided by PG&E. They use the probability density function $\beta e^{-\beta(m-m_0)}$ (Gutenberg-Richter model) to scale the activity rate for $m \geq 5$ earthquakes that contribute to secondary fault displacements, that is:

$$\alpha(m \geq m_{\min}) = \alpha(m \geq m_0) \int_{m_{\min}}^{\infty} \beta e^{-\beta(m-m_0)} dm$$

$$= \alpha(m \geq m_0) \times e^{-\beta(m_{\min}-m_0)}$$

$$= \alpha(m \geq m_0) \times 10^{-b(m_{\min}-m_0)}$$

or

$$\alpha(m \geq 5) = \alpha(m \geq 0) \times 10^{-0.8(5-0)}$$

$$= \alpha(m \geq 0) \times 10^{-4}.$$

However, this activity-rate scaling is for an exponential distribution, not the composite (characteristic earthquake) model used in this study (Figure C-3). The correct activity rate for events larger than magnitude five should be calculated using Equation C-9. That is:

$$\alpha(m \geq 5) = \alpha(m \geq 0) \int_{5}^{\overline{m}_{\text{char}}+0.25} f_M(m) dm.$$

For example, from the above equation, for a Shoreline fault scenario earthquake with $\overline{m}_{\text{char}} = 6.00$:

$$\alpha(m \geq 5) = \alpha(m \geq 0) \times 2.21 \times 10^{-4},$$

and for $\overline{m}_{\text{char}} = 6.25$:

$$\alpha(m \geq 5) = \alpha(m \geq 0) \times 1.76 \times 10^{-4}.$$

The PG&E hazard calculations assume that the Dresser couplings are at a distance of 600 meters from the main trace of the Shoreline fault. However, it is the understanding of the NRC staff that these couplings could be as close as 300 meters to the main trace. Therefore, the NRC staff calculated the hazard associated with secondary rupture at this distance, as well.

The dependence of hazard (Equation C-11) on distance from the principal fault trace (r_{min}) comes from the dependence of $P[d \neq 0 | l, r_{\text{min}}, m, z, sr \neq 0]$, the conditional probability for secondary rupture, and $P[d \geq d_0 | l, r_{\text{min}}, m, d \neq 0]$, the conditional probability for the secondary

displacement exceeding a given value d_0, on r_{min} (Sections C.3.6 and C.3.7). Figure C-7 shows a plot of $P[d \neq 0 | l, r_{\text{min}}, m, z = 50, sr \neq 0]$ for a 50×50 m^2 cell as a function of r_{min}. From this plot, the median probability at 300 meters is 1.6×10^{-2}, with a range of 5.0×10^{-3} to 5.0×10^{-2}. This rupture probability is about a factor of two larger than the probability at 600 meters.

The dependence of $P[d \geq d_\circ | l, r_{\text{min}}, m, d \neq 0]$ on distance comes from the dependence of $\log(d/D_{\text{ave}})$ distribution on r_{min}. Figure C-13 shows the distribution of $\log(d/D_{\text{ave}})$ at distances of 300 and 600 meters from the principal fault trace (Petersen et al., 2011). The distribution at 300 meters is almost identical to that at 600 meters, indicating that, at intermediate distances, the distribution is not a strong function of distance. Therefore, the dependence of the secondary fault rupture hazard on distance is mainly because of the dependence of the secondary rupture probability on distance. Since the median rupture probability at 300 meters is about twice that at 600 meters, it is expected that the average hazard at 300 meters would be about two times higher (Table C-2). The distributions are identical in shape except for a slight shift along the horizontal axis as shown in Figure C-13. The shaded area shows that the error (ratio of the green area to orange) in interchanging the distributions is very small.

C.5 Summary of Analysis of Secondary Rupture

The results of the analyses are shown in Table C-2. Although the results the NRC staff calculated are about an order of magnitude higher than the numbers PG&E provided, the conclusion on risk to the plant was the same. Specifically, the hazard from secondary rupture at the location of couplings has negligible impact on the seismic core damage frequency (CDF) at DCPP. The seismic CDF at DCPP is 3.8×10^{-5}, more than two orders of magnitude larger than the hazard from a secondary rupture at DCPP. Moreover, to compare the probability of occurrence of displacements (of 1 cm and 2 cm) with core damage, two highly conservative assumptions were made: (1) the displacement calculated always leads to operational failure of a Dresser coupling and (2) the failure of a Dresser coupling leads directly to core damage. Therefore, the actual impact to CDF of the DCPP is likely to be far lower. In summary, the risk from the failure mechanism analyzed is negligible.

C.6 Appendix C References

Bolt, B.A., *Earthquakes*, W.H. Freeman and Company, New York, p. 173, 1993.

Brune, J. N., "Seismic Moment, Seismicity and Rate of Slip along Major Fault Zones," *Jour. Geophys. Res.,* Vol. 73, pp 777-784, 1968.

Hanks, T.C. and H. Kanamori, “A Moment-Magnitude Scale,” *Jour. Geophys. Res.,* Vol. 84, p. 2,348–2,350, 1979.

Pacific Gas & Electric Company, “Calculation 17-107, Rev 0, Postulated Ground Deformation Shoreline Fault Auxiliary Salt Water Buried Piping Stress Analysis,” August 3, 2009.

Pacific Gas & Electric Company, “Progress Report: Shoreline Fault Zone, Central Coastal California,” U.S. Nuclear Regulatory Commission, Docket Nos. 50-275 and 50-323, PG&E Letter No. DCL-10-003, January 13, 2010, ADAMS Accession No. ML100190142, 2010.

Petersen, M., et al., “Evaluating Fault Rupture Hazard for Strike-Slip Earthquakes,” Geotechnical Engineering for Transportation Projects (GSP 126), *ASCE Proceedings of GeoTrans 2004*, p. 787–796, 2004.

Petersen, M., et al., “Fault Displacement Hazard for Strike-Slip Faults,” *Bull. Seismol. Soc. Amer.*, Vol. 101, p. 80–825, 2011.

Schwartz, D.P. and K.J. Coppersmith, “Fault Behavior and Characteristic Earthquake: Examples from Wasatch and San Andreas Faults,” *Jour. Geophys. Res.*, Vol. 89, p. 5,681-5,698, 1984.

Wells, D. and K.J. Coppersmith, “New Empirical Relationships among Magnitude, Rupture Length, Rupture Width, Rupture Area, and Surface Displacement,” *Bull. Seismol. Soc. Amer.*, Vol. 84, No. 4, p. 974–1002, August 1994.

Wells, D. L. and K.J. Coppersmith, “Likelihood of Surface Rupture as a Function of Magnitude (abstract),” *Seismol. Res. Lett.*, Vol. 64, No. 1, p. 54, 1993.

Youngs, R.R. and K. Coppersmith, “Implications of Fault Slip Rates and Earthquake Recurrence Models to Probabilistic Seismic Hazard Estimates,” *Bull. Seismol. Soc. Amer.*, Vol. 75, p. 939–964, 1985.

Youngs, R.R., et al., “A Methodology for Probabilistic Fault Displacement Hazard Analysis (PFDHA),” *Earthquake Spectra,* Vol. 19, p. 191-219, 2003.

Table C-1 Integrand of Equation C-23

Terms in Equation C-23	Substitution
α	Eq. C-9
$f_M(m)$	Eqs. C-3, C-4
$P[sr \neq 0 \mid m]$	Eq. C-15, C-16
$P[d \neq 0 \mid l, r_{\min}, m, z, sr \neq 0]$	4.2×10^{-4}
$P[d \geq d_0 \mid m, d \neq 0]$	Eq. C-22

Table C-2 Hazard from secondary Shoreline Fault rupture at DCPP

$\overline{m}_{\text{char}}$	Fault Dimensions		Slip Rate (mm/yr)	Annual Probability of Exceedance					
	Width (km)	Length (km)		PG&E Distance=600 m		NRC Distance=600 m		NRC Distance=300 m	
				1 cm	2 cm	1 cm	2 cm	1 cm	2 cm
PG&E Scenarios									
6.00	10	8	0.01	2.6×10^{-10}	1.4×10^{-10}	1.5×10^{-9}	7.9×10^{-10}	3.2×10^{-9}	1.7×10^{-9}
6.25	12	14	0.01	6.0×10^{-10}	3.5×10^{-10}	2.6×10^{-9}	1.6×10^{-9}	5.4×10^{-9}	3.3×10^{-9}
6.00	10	8	0.30	7.8×10^{-9}	4.1×10^{-9}	4.6×10^{-8}	2.4×10^{-8}	9.5×10^{-8}	5.1×10^{-8}
6.25	12	14	0.30	1.8×10^{-8}	1.1×10^{-8}	7.9×10^{-8}	4.7×10^{-8}	1.6×10^{-7}	9.8×10^{-8}
NRC Scenario									
6.70	15	33	0.30			9.9×10^{-8}	7.0×10^{-8}	2.0×10^{-7}	1.4×10^{-7}

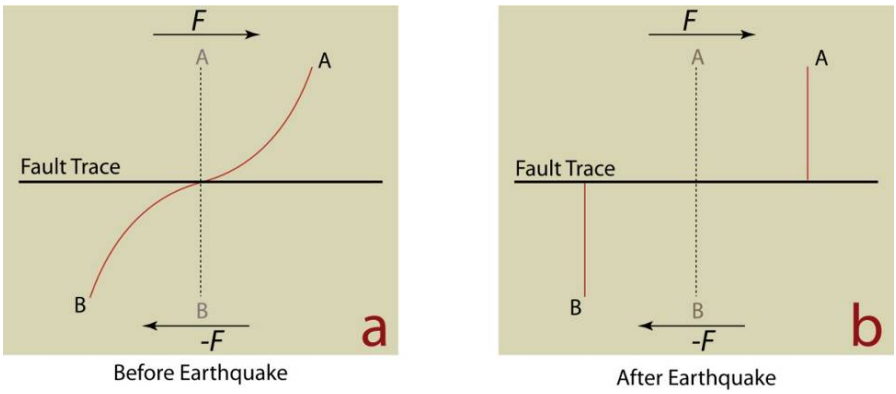

Figure C-1 A simplified schematic representation of permanent fault offset during a strike-slip earthquake

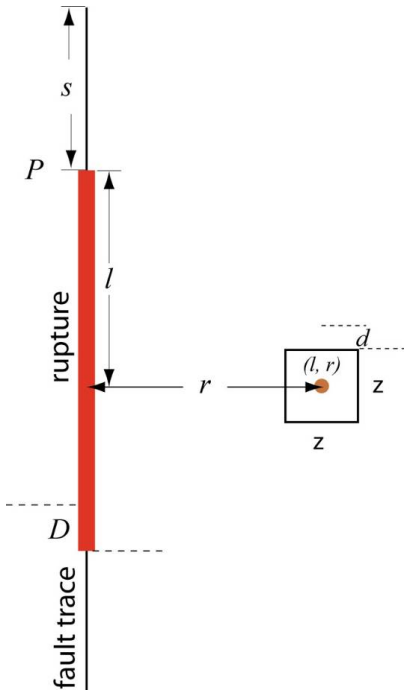

Figure C-2 Visual description of parameters for determination of the probability of secondary displacement (d) within a square footprint ($z \times z$) at location (l,r) due to displacement D on the ruptured segment of the fault (red line)

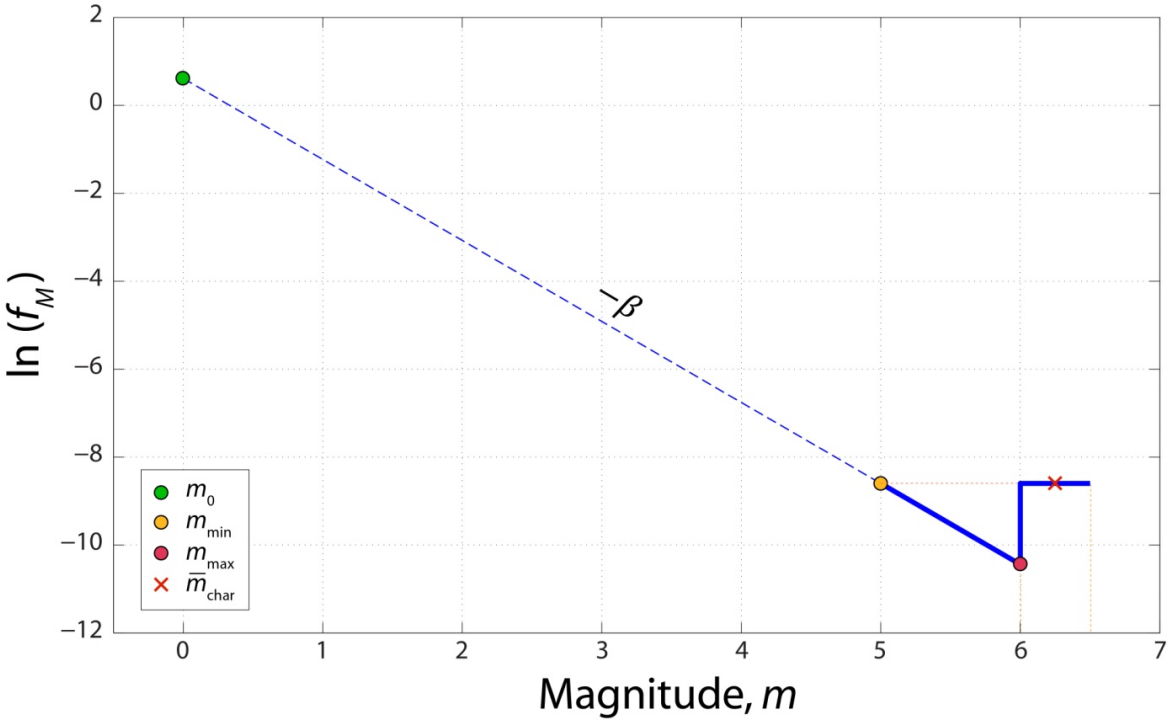

Figure C-3 **A graphical display of the magnitude-frequency distribution for the Shoreline fault based on the characteristic earthquake model of Youngs and Coppersmith (1985) for the magnitude range $0 \leq m \leq 6.5$.**

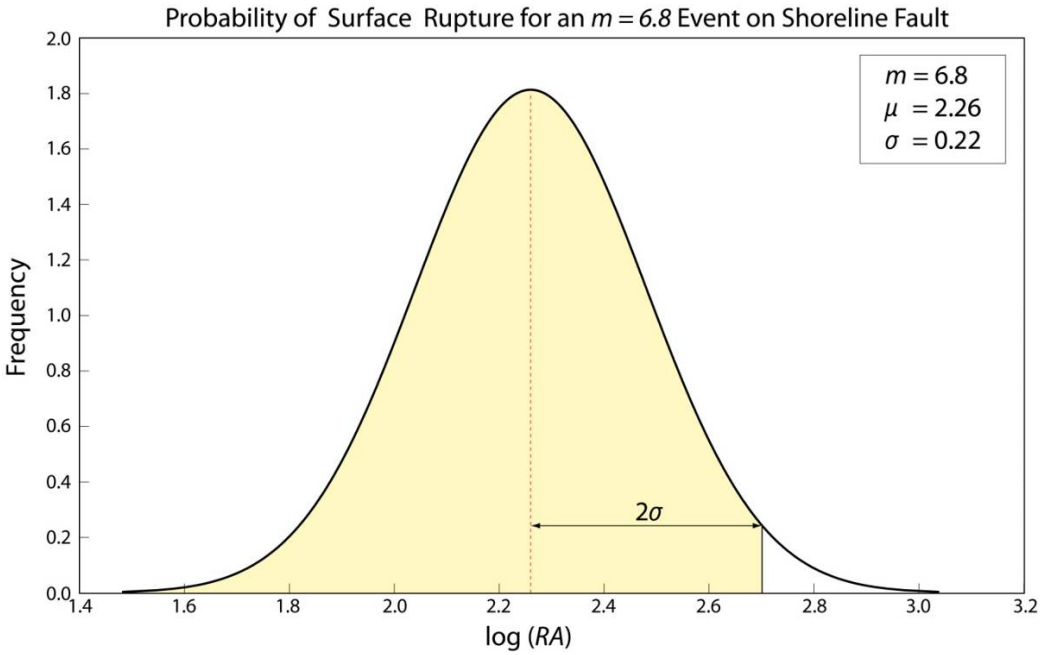

Figure C-4 **The 97.7% probability (area of the shaded region) that surface rupture occurs during a magnitude 6.8 event on the central and southern segments of the Shoreline fault.**

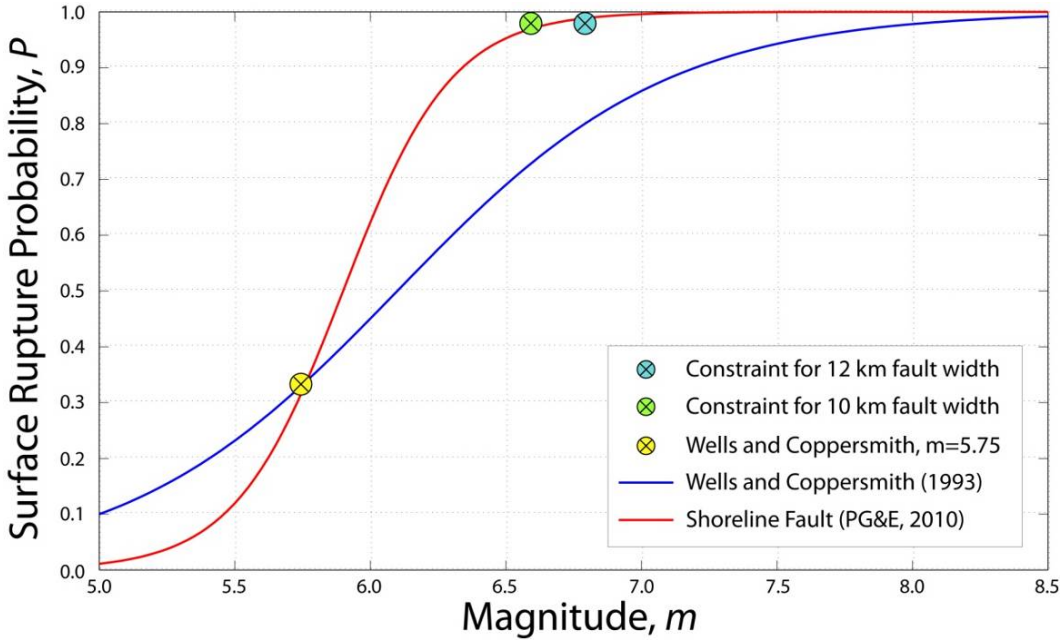

Figure C-5 Probability of surface rupture obtained from the empirical data (Wells and Coppersmith, 1993) (blue curve) and for the Shoreline fault developed by PG&E (red curve).

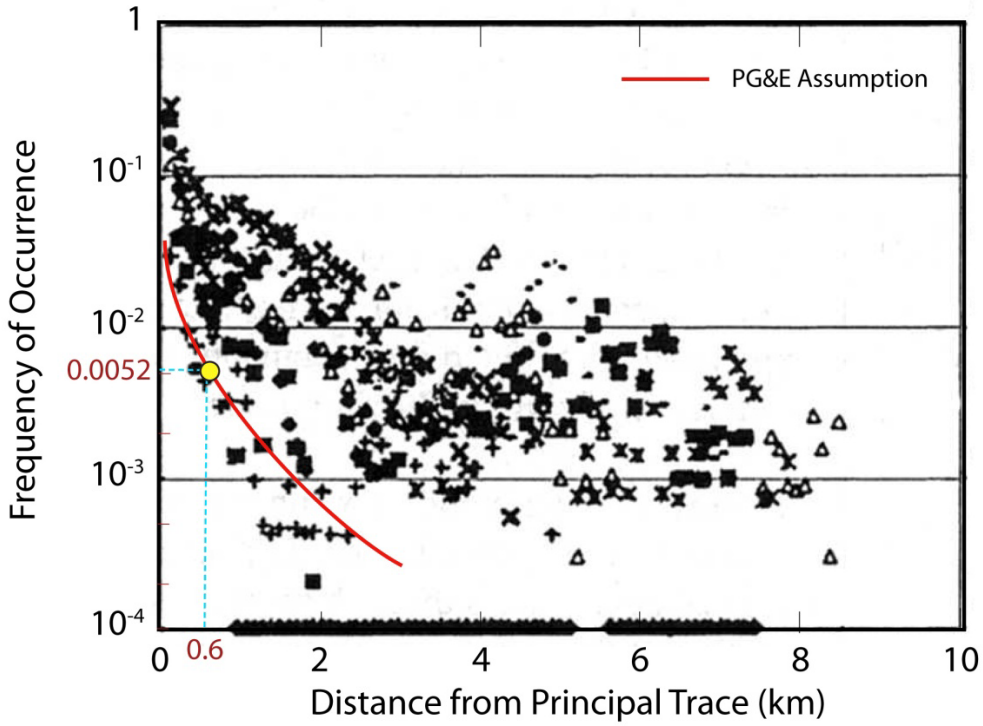

Figure C-6 Figure 4 of Petersen et al. (2004) showing the frequency of secondary surface rupture within a 50 × 50 m^2 footprint as a function of distance from the principal trace, shown with an overlay of the PG&E and NRC assumptions.

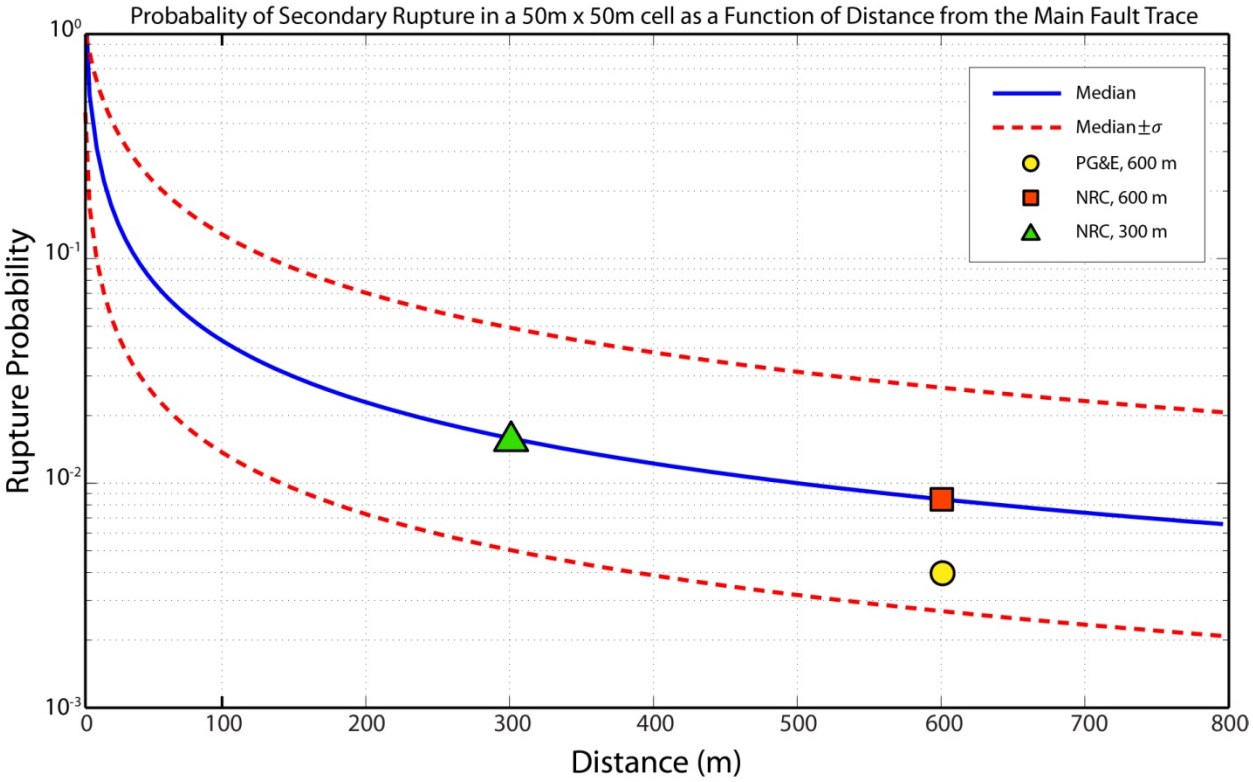

Figure C-7 A plot of secondary rupture probability as a function of distance from the principal fault trace within a 50×50 m^2 cell.

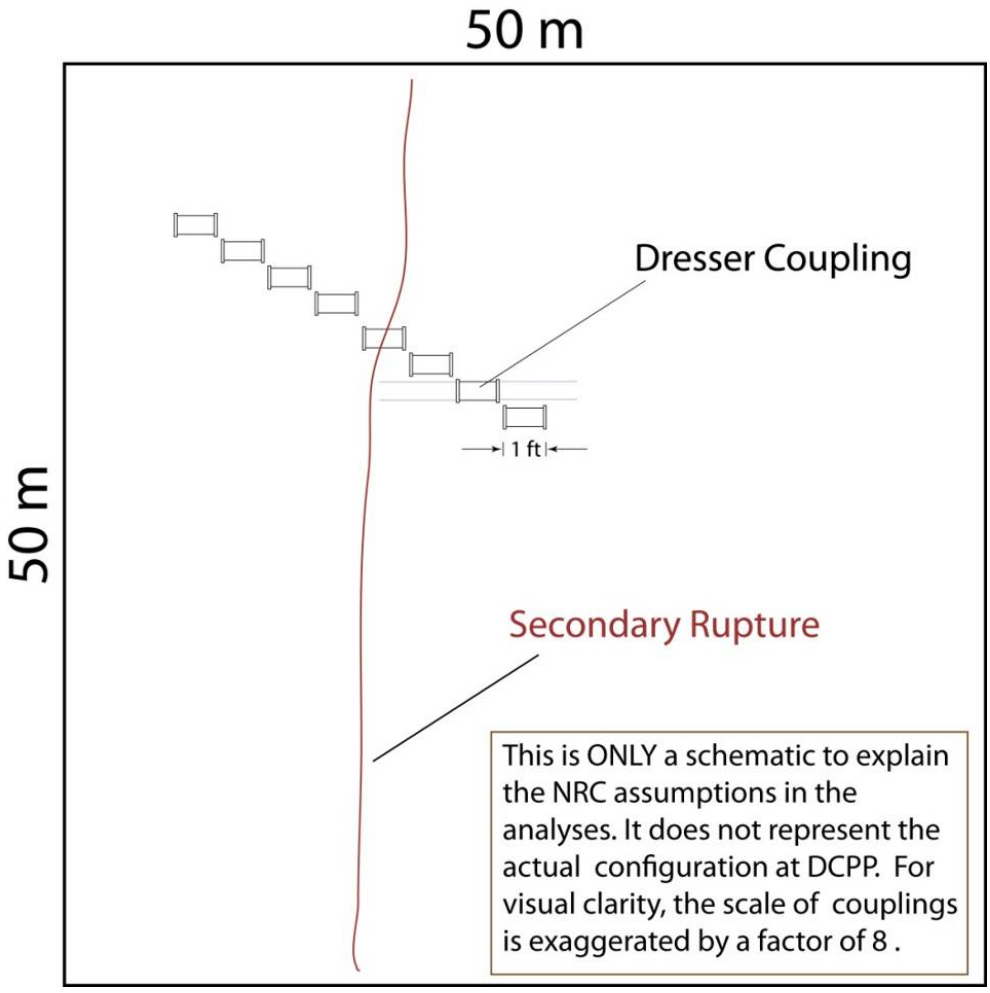

Figure C-8 General schematic diagram illustrating the final calculation in the determination of conditional probability for secondary rupture.

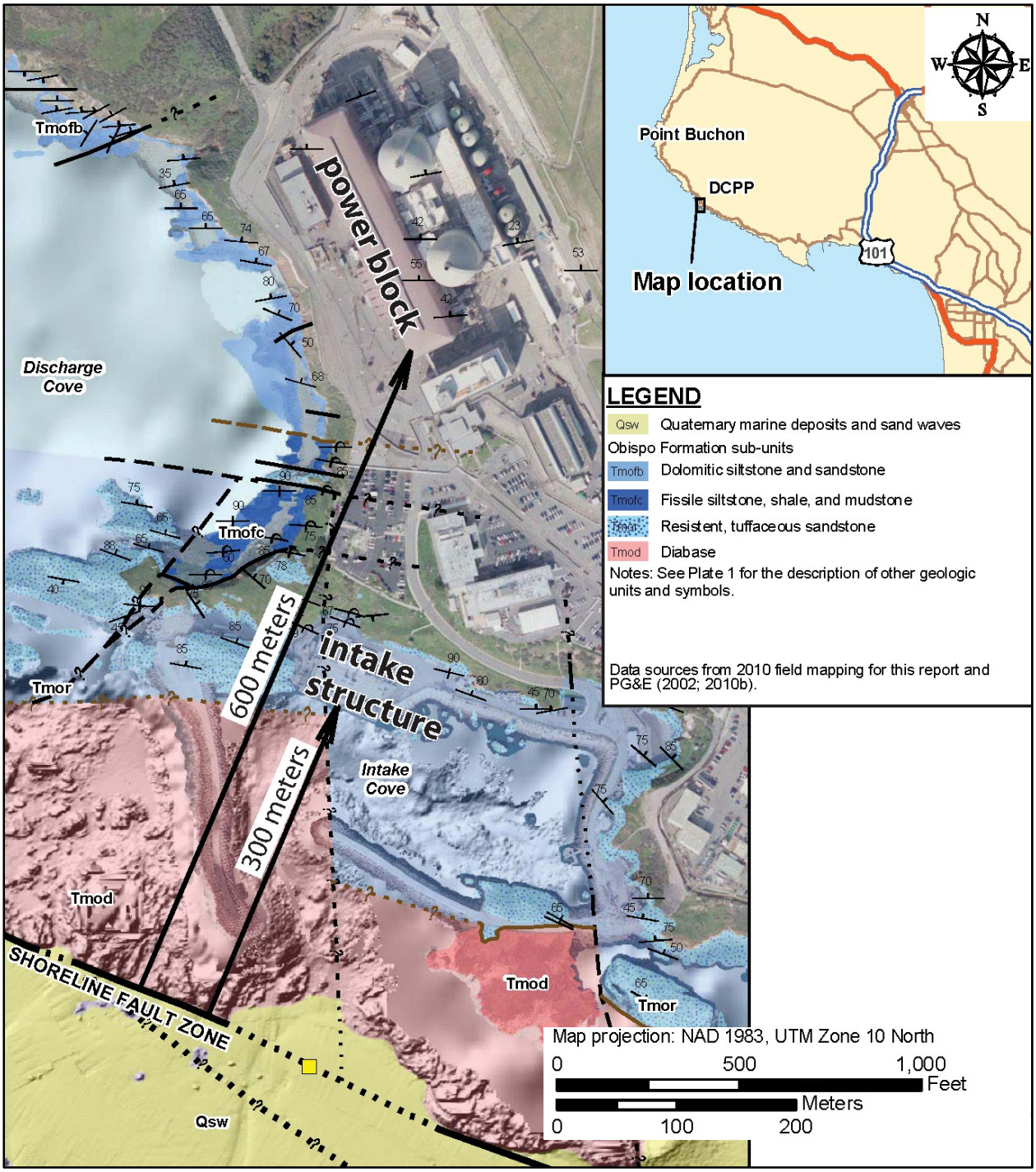

Figure C-9 Distance of Shoreline fault from intake structure and power block.

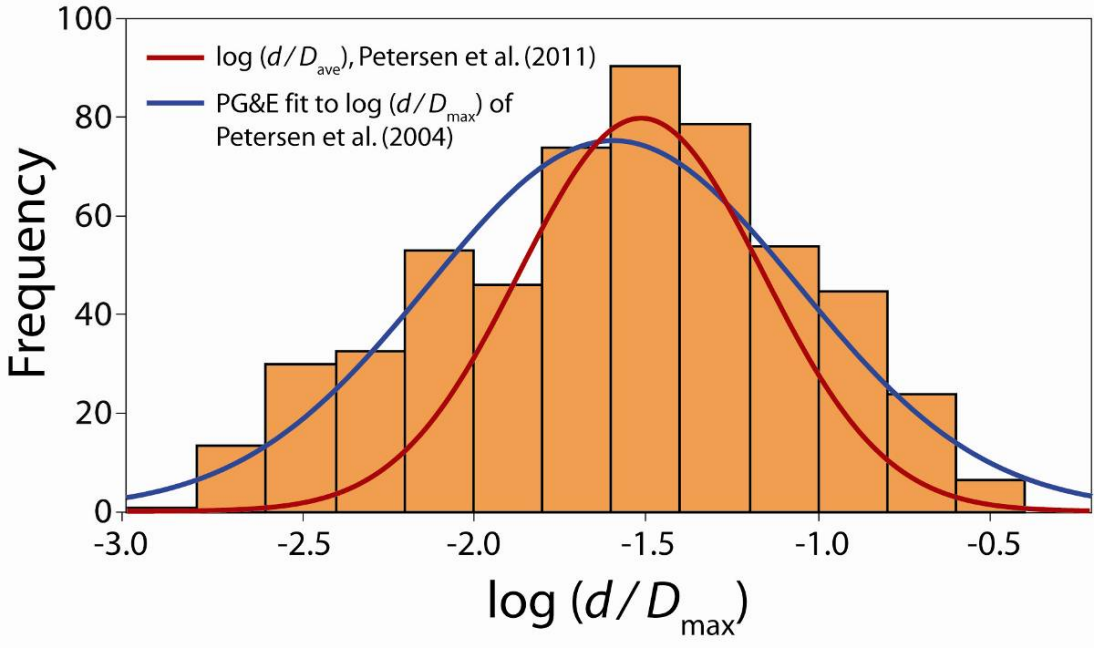

Figure C-10 Histogram provided in Figure 6 in Petersen et al. (2004) showing the distribution of the ratio of the secondary rupture to the maximum displacement on the principal trace overlain with curve used by PG&E (in blue) and NRC (in red), from Petersen et al. (2011).

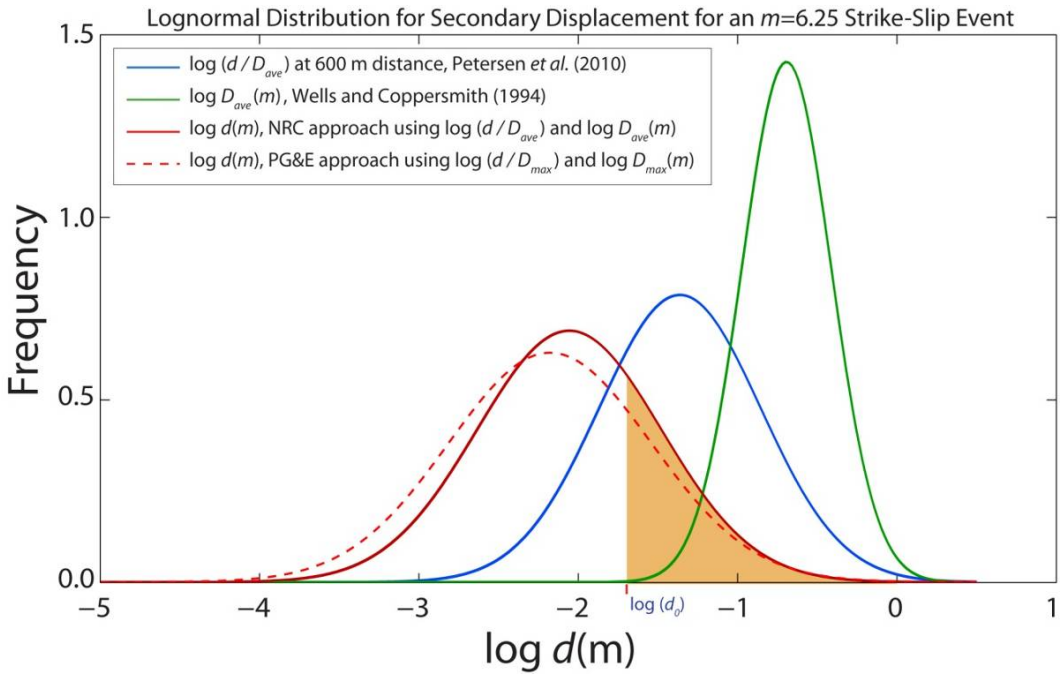

Figure C-11 An example of the lognormal distribution for secondary rupture associated with a magnitude 6.25 strike-slip earthquake (shown here in red).

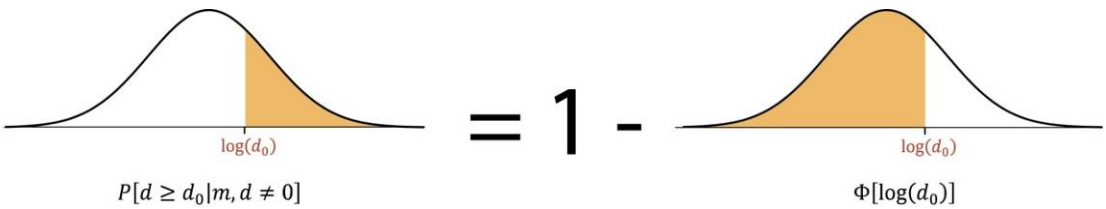

Figure C-12 Graphical representation of Equation C-20.

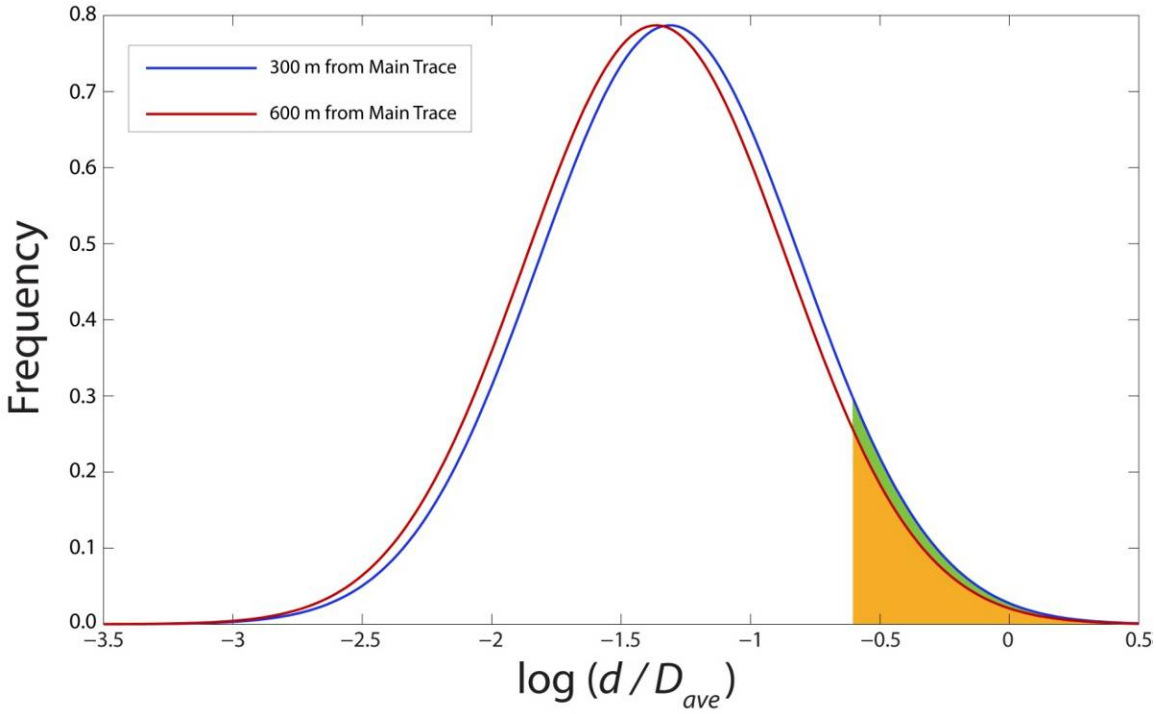

Figure C-13 Plots of the distribution of the ratio of secondary rupture to the average displacement on the principal trace at 300 meters and 600 meters from the principal fault trace (Petersen et al., 2011).

Appendix D: Seismic Moment Balancing, Slip Rate Budgets, and Background Seismicity Models

D.1 Seismic Moment Balancing, Slip Rate Budgets, and Background Seismicity Models

One of the fundamental components of the PSHA is the seismic source characterization (SSC), which defines and then weights the suite of alternative seismic source models in the PSHA logic tree framework. When developing SSC models where the regional deformation can be reasonably well determined (such as at along tectonic plate boundaries), some important techniques for constraining and developing the model are available to the analyst. Two of these techniques, slip rate budget and seismic moment balancing, are presented here because they are especially useful for understanding the seismic hazard at DCPP, and are likely to be an important point of discussion in the PG&E SSHAC Level 3 study.

D.1.1 Slip Rate Budgets

In the context of faulting and seismicity, the concept of fault slip rate is the rate at which two opposing sides of a fault move past one another. For active faults, the slip rate is often an average rate that is determined by dividing the accumulated fault displacement (as measured by the relative offset of a geologic or geomorphic feature that was once juxtaposed across the fault) by an estimate of the period of geologic time over which the fault slip occurred. The accumulated fault displacement across the fault could be the result of steady incremental creep or one or more larger episodic fault ruptures caused by earthquakes.

Along tectonic plate boundaries, the relative motions of the tectonic plates are the principal driving force generating fault slip. In the case of central California, the driving tectonic forces arise from the northwestward motion of the Pacific Plate relative to the Sierran Microplate and the North American continent; these two plates are moving horizontally past each other at a rate of approximately 39 mm/yr. It is the interaction of these tectonic plates that gives rise to seismicity in the region of the DCPP. Because this tectonic plate interaction is driving the deformation in central California, this 39 mm/yr rate constrains the slip rate of the faults within the plate margin such that the vector sum of fault slip rates for all the faults within the plate margin cannot exceed the overall plate motion rate of 39 mm/yr. In this way, the relative motion of the tectonic plates provides the PSHA analysts with a maximum regional slip rate budget that needs to be portioned among all the faults within the plate boundary. The regional slip rate is a maximum because, in most cases the interaction between the plates is not perfectly coupled (i.e., the plates themselves deform) and because some fraction of the plate tectonic deformation is accommodated by other aseismic geologic features such as fractures or folds. Thus, the total regional tectonic strain rate as a predictor of earthquake activity clearly provides an upper bound. In reality, the total strain budget is used up by both seismic and aseismic processes. Creeping faults, like model of the Shoreline fault in Scenario 1, allow deformation (slip) without significant seismicity.

Consider Figure D-1, which shows the relative motion of the Pacific Plate and the Sierran Microplate. This plate motion is accommodated by a series of largely northwest-trending strike-slip faults situated between the stable parts of each plate. If a line is drawn from a stable location in the center of one plate to a stable location in the center of the adjacent plate (as shown in Figure D-1), the vector sum of the slip rate of all the faults that the line crosses must be less than or equal the rate at which the ends of the line are moving relative to each other.

A fault's slip rate is an important parameter because it determines the rate at which strain energy is being accumulated and released. The slip rate, therefore, also determines the amount of seismic energy (seismic moment) that a fault can release in earthquakes over time.

For this reason, significant effort is often placed on determining fault slip rates. One traditional technique is to evaluate recent fault slip events as recorded by offset soils strata and other near surface geologic features exposed in trenches dug perpendicular to a fault trace. Trench studies are helpful for determining both the average slip rate of a fault and the behavior it exhibits in terms of earthquake recurrence. Slip rates can also be determined through geodetic (global-positioning-system-based) studies, in which a fault slip rate is interpreted from very precise geolocation measurements of fixed measurement stations (called monuments) across the fault. Depending on the fault slip rate, this approach may require instrumentation to be in place for years or even decades in order to record sufficient fault displacement to render the interpretation statistically meaningful. Other approaches to estimating fault slip rates include detailed geomorphic or geophysical investigation to detect and quantify relative offset of "markers," such as displaced stream drainages or bifurcated gravity or magnetic anomalies.

As noted, the regional horizontal slip rate budget for the plate boundary near the DCPP is 39 mm/yr. The San Andreas Fault, which is well east of the DCPP, accounts for approximately 75 percent of the slip rate budget between the Pacific and Sierran plates. This means that the reaming 25 percent or about 9.75 mm/yr of northwest horizontal motion is the maximum available slip rate budget available for the remaining faults with the plate boundary. It is important to note here that nearly all of the remaining slip rate budget can be accounted for by slip on the known faults in the region. Thus, it is highly unlikely that a strike-slip fault capable of producing frequent, large earthquakes remains undetected in the region. Some readers may point to the discovery of the Shoreline fault as contrary to this statement. However, as noted in Chapter 4, a careful review of the offshore data did not reveal horizontal displacements across the Shoreline fault, at least within the 1-2 m resolution of the data. Based on this observation the NRC Staff concluded that the fault must have a very low slip rate.

Just as there is a slip rate budget in the horizontal plane, there is a similar constraint in the vertical direction wherein the kinematic movements of the overall region that result from movement on various dip-slip faults must conform within the overall rate of uplift. As discussed in Section 3.4, the technique of using marine terrace data coupled with the chronology of sea-level stands, was used to develop an estimate of the uplift rate of the DCPP region. However, the regional vertical uplift rate is not as well constrained as the horizontal slip rate budget. Dipping faults, such as the Los Osos, that cause vertical deformation are important to DCPP and have relatively higher uncertainty in terms of their dip angle and slip rate.

D.1.2 Seismic Moment Balancing

The accumulation and expenditure of seismic energy must also be in balance, at least over periods of extended geologic time. Plate tectonic forces and movements lead to the accumulation of strain energy in geologic materials. Once the strain exceeds the strength of the rock, some portion of the accumulated energy is released and propagates outward as seismic waves during earthquakes. Seismic moment is a quantitative parameter that relates to the energy released in a particular earthquake and is the key parameter used to determine the magnitude of that earthquake. It is a product of the area of the actual rupture plane, the relative movement of the two sides of the fault (i.e., the slip), and the strength of the rock. Because the strength of rock is often fairly uniform in a region, each magnitude earthquake can be scaled to a specific amount of slip and a discrete rupture area.

For a fault, the accumulated moment on a fault should be balanced by the seismic moment release associated with the earthquakes that occur on the fault over a certain time. Magnitude recurrence relationships, such as those shown in Figure 4-3, display the annual rate of earthquakes of varying magnitudes that occur on a fault. Each of the magnitude recurrence

curves, therefore, also represents the annual release of seismic moment. The total annual seismic moment release can be determined by summing up the earthquakes represented by the curve, accounting for their annual rate of recurrence. Moment balancing is the process of assuring that the annual rate of moment release of a fault (represented by the magnitude recurrence curve) is balanced by the seismic moment accumulating on the fault as determined by the slip rate. Section C.3.3 provides a more detailed discussion of the relationship between the rate of the earthquakes, earthquake magnitudes, accumulated seismic moment, and the mean moment released per earthquake on that fault.

Figure 4-3 shows an example of how recorded seismicity on a fault can be used to determine the magnitude recurrence curve in the small magnitude range. Using small magnitude earthquake data, coupled with the slip rate on the fault, and assuming a magnitude recurrence relationship (e.g., the Gutenberg-Richter or characteristic earthquake models shown in Figure 4-4), a maximum magnitude for the fault can be determined.

A common misconception in seismic hazard studies is that assigning relatively large maximum magnitudes to faults is a conservative way to capture the remaining uncertainty in the fault characterization assessment. However, in a PSHA, an assumption of a large maximum magnitude often leads to a lower hazard because, when considered in light of the slip rate or seismic moment budgets, this approach constrains the rate at which earthquakes occur. As shown in Figure 4-5 and Figure 4-6, seismic moment and seismic slip are both expended to a disproportionately greater degree in large earthquakes than in small ones.

D.1.3 Considerations in Using a Slip Rate Budget and Moment Balancing

The regional slip rate budget and moment balancing on each fault can be used to develop and constrain properties assigned to the faults in the SSC model. The overall regional slip rate can be partitioned among each of the faults. The slip rate for each fault should be consistent with the seismic moment expended by each fault, as represented in the fault's magnitude recurrence curve. The magnitude recurrence curve for each fault should also be consistent with any other data available for the fault, such as the seismological catalog and the maximum magnitude assigned.

Because the overall regional slip rate budget can be determined within some level of uncertainty, the slip rate assigned to one source in a model must, necessarily, reduce the amount remaining to be assigned to other sources. Therefore, it is important to assign slip rates (and their associated uncertainties) with care and with a goal of accuracy and consistency. A distribution of slip rates consistent with the data is typically developed for the logic tree. If the overall slip budget is assumed, assigning conservatively large slip rates on some fault sources necessitates underestimating slip rates on the remaining sources. In a similar way, assigning conservative maximum magnitudes as a way to account for uncertainty can actually reduce the seismic hazard predicted by inaccurately apportioning seismic moment release to larger but much more infrequentbig earthquakes.

In some regions, the recorded or historical seismicity cannot be conclusively assigned to known fault sources. In these cases, this unaccounted for seismicity is incorporated into the PSHA model as "background seismicity." The earthquakes that are now assigned to the Shoreline fault were previously part of the background sources in PG&E's PSHA model. The improved hypocenter locations from Hardebeck (2010) benefitted the PSHA model by more accurately assigning the small earthquakes to a known fault source.

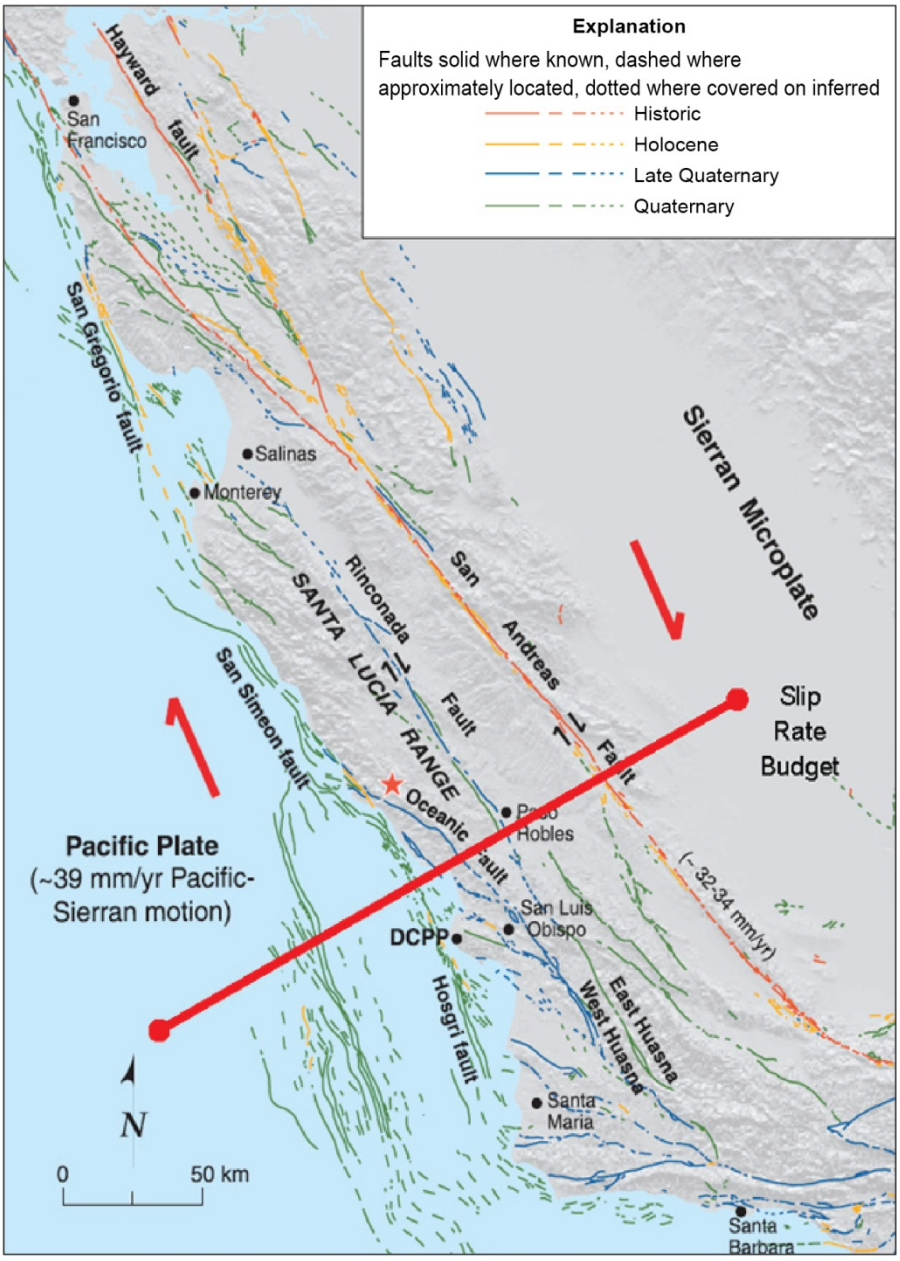

Figure D-1 Diagram illustrating the relative plate motions and the relative motions of major fault systems (base figure from Unruh presentation at the DCPP SSHAC WS#1, annotated for this report)